# University of Cincinnati

**Date: 7/10/2015**

**I, Derek A Marucci , hereby submit this original work as part of the requirements for the degree of Master of Science in Civil Engineering.**

It is entitled:

**Evaluation of the Seismic Performance of Steel Moment Frames with Partially-Restrained Connections**

Student's name: **Derek A Marucci**

This work and its defense approved by:

**Committee chair: James Swanson, Ph.D.**

**Committee member: Thomas M. Burns, Ph.D.**

**Committee member: Gian Rassati, Ph.D.**

19601

# Evaluation of the Seismic Performance of Steel Moment Frames with Partially-Restrained Connections

Master's Thesis

Submitted to the Graduate School of the University of Cincinnati
in partial fulfillment of the requirements for the degree of

Master of Science in Civil Engineering

Department of Civil and Architectural Engineering and Construction Management
College of Engineering and Applied Science
University of Cincinnati

July 2015

By:
Derek Anthony Marucci, EIT
Bachelor of Science in Civil Engineering
Trine University, 2011

Committee Chair: James A. Swanson, Ph.D.

Committee Members:
Gian Andrea Rassati, Ph.D.
Thomas M. Burns, Ph.D.

## Abstract

Previous earthquakes have revealed seismic performance issues associated with fully-restrained (FR) welded beam-to-column connections in steel moment frames. Past research has indicated that bolted partially-restrained (PR) connections can serve as viable alternatives for beam-to-column connections to resist lateral loads. This paper addresses the seismic behavior of special moment frames (SMFs) incorporating PR connections. A series of archetypical buildings are modeled in OpenSees using varying levels of stiffness, strength, and strain hardening in the PR beam-to-column connections. Incremental dynamic analyses (IDAs) are performed on the PR archetypes and the results are compared to a typical building archetype constructed with conventional FR connections. The models are subjected to incrementally larger time histories until the frames fail. Maximum interstory drifts, maximum total roof drifts and maximum base shears are recorded for each model throughout the analyses. The PR archetypes are designed and constructed to engage all of the frames in each principal direction to act as the seismic force resisting system (SFRS) whereas the FR archetype is constructed to engage only the perimeter frames as the SFRS. The PR archetypes are modelled to represent a global building stiffness equivalent to the global building stiffness of the conventional FR archetype. The PR connections are modeled with trilinear moment-rotation characteristics using rotational springs. The advantages of using PR frames include smaller member sizes and increased redundancy in the SFRS compared to conventional FR framing. Since most PR connections are of the bolted type, they generally cost less and are easier to assemble. The results of this study reveal that buildings constructed with PR connections that meet or exceed minimal levels of stiffness and strength have very similar seismic performance compared to buildings constructed with FR connections. The recommendation is made to accept PR connections for prequalification in SMFs.

## Acknowledgements

This thesis would not have been possible without the contributions and efforts from several important individuals. First, I would like to thank my advisor, Dr. James A. Swanson, for his resolute guidance and support throughout this entire project. His leadership as my mentor and my instructor has contributed greatly to my growth as a student and a professional. Second, I would like to thank Dr. Gian A. Rassati for his essential service on my committee. His contributions as my instructor and educator have enabled me to achieve my goals and success in graduate school. I would also like to thank my third committee member, Dr. Thomas M. Burns, for his service and contributions. Dr. Burns constantly provided suggestions and much needed encouragement and support throughout this research project. I am forever grateful for the dedication and commitment that these individuals devoted to me.

Furthermore, I would like to thank my good friend and colleague Mathias Kozma-Thomas for his input and assistance throughout my graduate school career. Also, I am forever grateful for Greg Sizemore for his leadership and encouragement that supported me in the final stages of my graduate studies. Their involvement and support were essential in making my success in graduate school a reality. Additionally, I am grateful for the technical help and support I received from Jonathan Corey for his assistance in running my models and processing my data. I would also like to thank my colleagues Richard Kennedy, Trey Just, Philip Niekamp, Chris Hahnel, Martin Butler, Frida Pettersson, Steve Mitchell, and Murtuza Abbas for their companionship and support throughout my graduate studies.

Lastly, I'd like to thank my family for their unyielding love and support throughout my academic career. Without their care and investment over the years, both financially and emotionally, I would not be where I am today.

## Table of Contents

## List of Tables

## List of Figures

# Chapter 1: Introduction

Steel frame construction is commonly used as the structural support system in many buildings to resist gravity and lateral loads. Steel buildings typically incorporate the use of either braced frames, moment-resisting frames or shear walls to serve as the seismic force resisting system (SFRS) to resist lateral loads produced during earthquakes. Steel moment-resisting frames are often times the SFRS preferred by building owners and architects because they employ long uninterrupted spans that provide open building layouts, allowing for greater flexibility in the design and use of a building.

A key component in the stiffness and ductility of moment-resisting frames is the connection between the beams and columns. In the past, welded steel moment-resisting frames were identified as having superior seismic performance and were considered by engineers to be the most ductile systems. Fully-restrained (FR) welded steel moment connections, such as the one illustrated in Figure 1-1, were frequently the connection type of choice for steel moment-resisting frames up until the 1994 Northridge and 1995 Kobe earthquakes. These events revealed that the welded connections did not perform with the ductility anticipated, with a number of frames experiencing brittle fractures in their beam-to-column connections (FEMA, 2000).

The above occurrences resulted in a renewed interest in the use of partially-restrained (PR) connections in the seismic design of steel moment-resisting frames. Three organizations including the Structural Engineers Association of California (SEAOC), the Applied Technology Council (ATC), and California Universities for Research in Earthquake Engineering (CUREE), united together to form the SAC Joint Venture. In a cooperative agreement with the Federal Emergency Management Agency (FEMA), the SAC Joint Venture initiated the SAC Steel Project in an effort to understand the seismic performance of steel moment-frame buildings and to develop reliable

seismic design criteria for such structures (FEMA, 2000). Research conducted in these previous investigative efforts has demonstrated that PR connections are a viable alternative to FR connections in providing sufficient ductility and performance. However, the American Institute of Steel Construction (AISC) limits the use of PR connections in steel moment-resisting frames. Under current AISC seismic provisions (AISC 341), PR connections are not eligible for prequalification in special moment frames (SMFs).

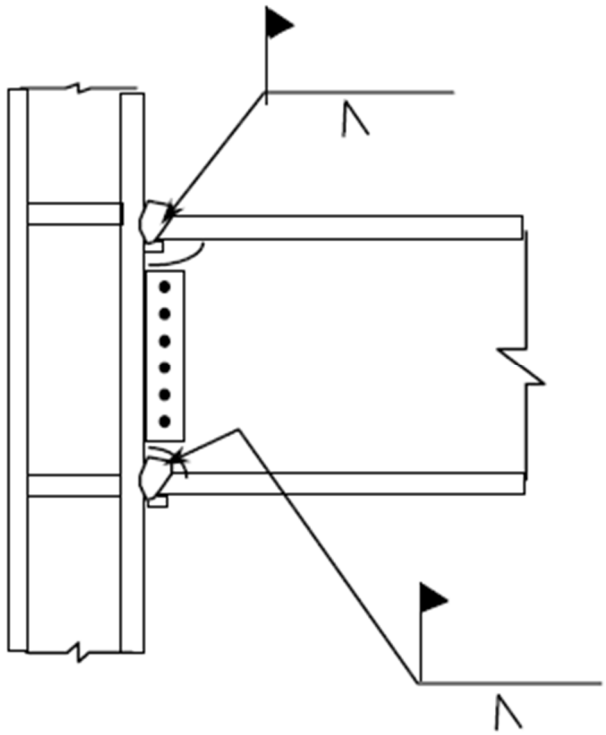

*Figure 1-1: Typical Pre-Northridge Welded Connection (FEMA, 2000)*

The goal of this research is to show that PR connections should be eligible for prequalification in SMFs. Specifically, this thesis aims to demonstrate that special moment frames designed with PR connections can have comparable strength, stiffness, and stability to special moment frames with FR connections. Five different classes of steel moment frames based on five levels of connection stiffness were modeled with PR connections using three levels of connection

strength and two levels of strain hardening moment. Previous research work conducted under the SAC Steel Project was utilized and expanded upon in the undertaking of this study.

Chapter 2 provides a background on moment-resisting frames and moment connections and the previous research investigating the implementation of PR connections. Chapter 3 details the methodology and approaches used to accomplish the goals and objectives of this study. Chapter 4 describes the analytical modeling methodology and procedures used to construct the frame models and perform the analyses. Chapter 5 presents the results of the analytical analyses produced during this study. A summary of the work performed and the conclusions are provided in Chapter 6. The final chapter discusses recommendations for future analytical and experimental studies. Appendices with supplementary information are provided.

# Chapter 2: Background

## 2.1 Partially-Restrained and Fully-Restrained Moment Connections

The AISC Specification for Structural Steel Buildings (ANSI/AISC 360, 2010), herein referred to as the Specification, classifies beam-to-column connections as either simple connections or moment connections. Simple connections are intended to transfer negligible moment by allowing uninhibited relative rotation between the connected beam and column. Moment connections are classified as either FR or PR. FR connections are capable of transferring bending moment between the beam and column with negligible rotation between the connected members. PR connections transfer bending moment between the beam and column without negligible rotation between the connected members (ANSI/AISC 360, 2010).

Moment connections are primarily characterized by their moment-rotation curves, which effectively represent a connection's strength, stiffness, and ductility. The fundamental difference between the two types of moment connections and simple connections is the connection stiffness. The stiffness of a connection is classified by the value of the secant stiffness, $K_s$, defined in Equation 2-1 (ANSI/AISC 360-10).

$$K_S = \frac{M_S}{\theta_S} \qquad \text{(Eq. 2-1)}$$

where:

$M_S$ = moment at service loads, kip-in. (N-mm)

$\theta_S$ = rotation at service loads, rad.

The parameters used to establish the criteria for defining connection classifications are the bending rigidity ($EI$) and length ($L$) of the connected beam. When the value of $K_S \geq 20EI/L$, the connection is classified as FR, and when the value of $K_S \leq 2EI/L$, the connection is classified as simple. These

classifications of the moment-rotation response of a connection are illustrated in Figure 2-1, duplicated from the Specification. Connections with stiffnesses between these two values are classified as PR (ANSI/AISC 360, 2010).

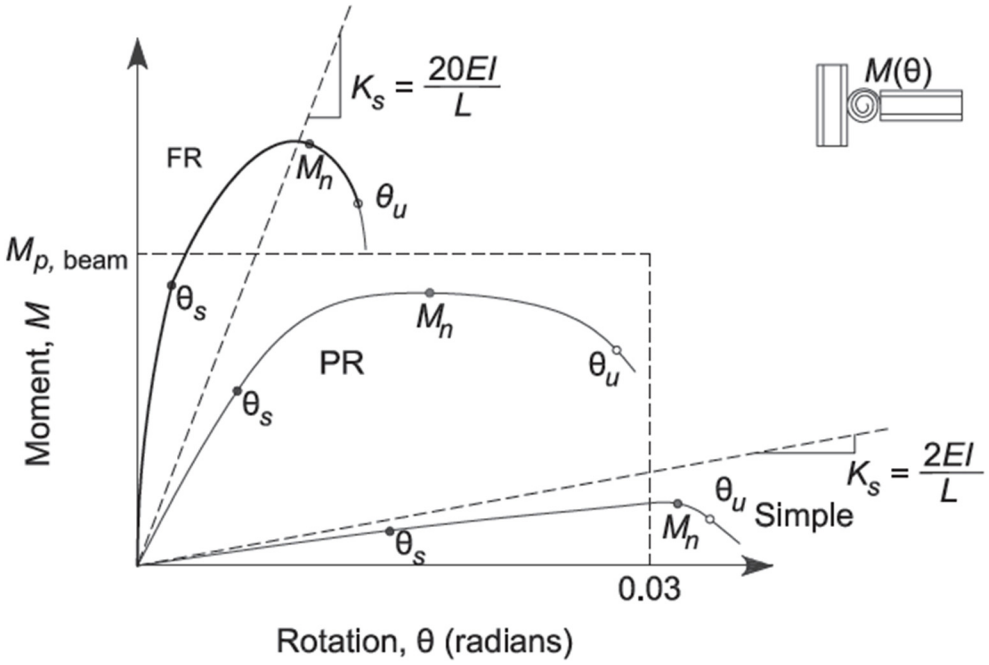


*Figure 2-1: Classification of Moment-Rotation Response of FR, PR, and Simple Connections (ANSI/AISC 360, 2010)*

The type of connections used will determine how they are modeled in the analysis of a structural system. FR connections are often idealized as fixed while simple connections are often idealized as pinned. These idealizations simplify the modeling and analysis of a structure using such connections. However, in the analysis of structures that use PR connections, connection stiffness and strength need to be accounted for. In the past, the analyses of structures with PR connections were arduous and time consuming due to the limited abilities of computers. However, with the advancement of computer technology and structural analysis software, structures with PR

connections can be effectively modeled and analyzed to accurately determine their seismic response and behavior.

## 2.2 Steel Moment Frames

Steel moment-resisting frames resist lateral forces through flexure in the beams and columns that generate bending moments and shear forces in the members and connections. Lateral displacements of a moment-resisting frame result from member and connection rotation. Therefore, member sizes and connection configurations with adequate rigidity are selected and designed to provide moment-resisting frames with the strength and stiffness required to resist the anticipated lateral loads imposed on them. During a seismic event, steel moment frames are subjected to cyclic loading, which requires them to dissipate energy. The goal of modern codes and standards is to design steel moment-resisting frames with sufficient ductility to enable them to withstand large inelastic deformations and thus dissipate energy. The main source of energy dissipation is most often designed to occur in the form of a plastic hinge in the beam adjacent to the connection to the column.

The AISC Seismic Provisions for Structural Steel Buildings (ANSI/AISC 341, 2010), herein referred to as the Seismic Provisions, establishes three different types of moment-frame systems that possess varying levels of ductility. Ordinary moment frames (OMFs) are designed with the most basic detailing requirements and provide minimal inelastic deformation capacity in their members and connections. Intermediate moment frames (IMFs) are designed with more stringent detailing requirements and contain elements that provide moderate inelastic deformation capacity. SMFs require the highest degree of detailing and contain elements that can withstand significant inelastic deformation (ANSI/AISC 341, 2010).

Each moment frame type requires the connections to achieve specific levels of strength, stiffness, and ductility. The Seismic Provisions explicitly approve the use of both FR and PR connection types in OMFs and provides the strength qualifications required for these two connection types. For IMFs and SMFs, however, the Seismic Provisions specify the connection strength, stiffness, and ductility requirements without explicitly mandating which type(s) of connections are approved. The connections in IMFs are required to accommodate story drift angles of at least 0.02 radians while the connections in SMFs are required to accommodate story drift angles of at least 0.04 radians. The connections in both frame types are required to maintain a flexural resistance of at least 80% of the plastic moment strength of the connected beam at the aforementioned respected minimum story drift angles (ANSI/AISC 341, 2010).

Before a beam-to-column moment connection can be used in an IMF or SMF, it must meet prequalification requirements ensuring its compliance with the performance criteria for each of the frame types. Chapter K of the Seismic Provisions specifies the minimum requirements that must be met in order to ensure that a connection can sufficiently provide the required performance on a consistent and reliable basis. This involves using connection performance data from laboratory tests and analytical studies to effectively evaluate the performance and limits of a connection. In lieu of conducting prequalification tests for the connections used in IMFs and SMFs, engineers can use connections designed in accordance with the AISC Prequalified Connections for Special and Intermediate Steel Moment Frames for Seismic Applications (ANSI/AISC 358, 2011), hereafter referred to as the Prequalified Connections Specification. The six moment connections provided in the Prequalified Connections Specification satisfy the prequalification requirements in the Seismic Provisions. However, each of the six connection types are considered FR (ANSI/AISC 358, 2011). There are no PR connection types provided in the Prequalified

Connections Specification. This circumstance is the primary incentive for the current study to demonstrate if PR connections can be eligible for prequalification in SMFs.

### 2.3 Partially-Restrained Connections in Steel Moment Frames

Failures of FR welded steel moment frame connections in the Northridge and Kobe earthquakes sparked a renewed interest in the use of PR connections in high seismic regions. Two analytical studies investigated the seismic performance and feasibility of framing systems having PR connections as part of the FEMA/SAC Phase II Steel Project. The first study considers two of the nine SAC buildings that are redesigned with PR connections and different beam and column sections. The second study considers all nine SAC buildings that are modeled with PR connections with varying levels of stiffness and strength in place of the FR welded connections.

#### 2.3.1 Maison Study

The first study looks at the influence of PR connection design on the beam and column design of a frame and also investigates the impact that such a design scheme has on the dynamic properties of a building. This study, administered by Bruce Maison, developed modified versions of the 3-story SAC building in Los Angeles and the 9-story SAC building in Seattle. The layout of the modified buildings, including the building footprints, column spacing, story heights, and live loads were the same as those in the original designs. PR connections were used at every beam-to-column joint and the members were modified so that each of the frames in the NS and EW directions were of the PR type. The computer analysis program PC-ANSR was used to model and analyze both the modified PR versions of the frames and the original FR frames (Maison and Kasai, 2000).

The LA 3-story building used a combination of composite PR connections and top-and-seat angle connections while the 9-story Seattle building used stiffer T-stub connections. These

PR connections were modeled using rotational springs connecting the girder and column ends. The buildings were designed for lateral loads similar to those used for FR buildings to allow for a direct comparison of the frames. Inelastic static pushover analyses and dynamic analyses were conducted on the PR frame models as well as their FR frame counterparts. The dynamic analyses included three suites of earthquake records for each building based on their geographic location. The three suites consisted of 20 earthquake records representing intensities of 2%, 10%, and 50% probability of exceedance in 50 years (2/50 set, 10/50 set, 50/50 set) (Maison and Kasai, 2000).

The static pushover analyses demonstrated the effects of PR connection design on the global response of moment-resisting frames. The pushover curves in Figure 2-2 reveal that both PR buildings had deteriorated strengths when compared to their base case designs using FR connections. The 3-story PR building acquired about two thirds of the strength of its FR counterpart, and the 9-story PR building only acquired about half of the strength of its FR counterpart. The graphs in Figure 2-2 also show that, when compared to their FR frame equivalents, the 3-story PR building exhibited a reduced elastic stiffness while the 9-story PR building exhibited an equivalent elastic stiffness (FEMA, 2000).

The dynamic properties of the frames can be interpreted from the results produced during the time history analyses. As illustrated in Figure 2-3, the PR 3-story LA frame had slightly larger median drifts for the 10/50 and 2/50 intensity levels compared to the FR frame; however, both frames had equal median drifts for the 50/50 intensity level. The drifts for the PR 9-story Seattle frame, however, were actually slightly less at most levels than the FR frame for both the 10/50 and 2/50 intensity levels. The elastic stiffness of the structure appeared to counteract the

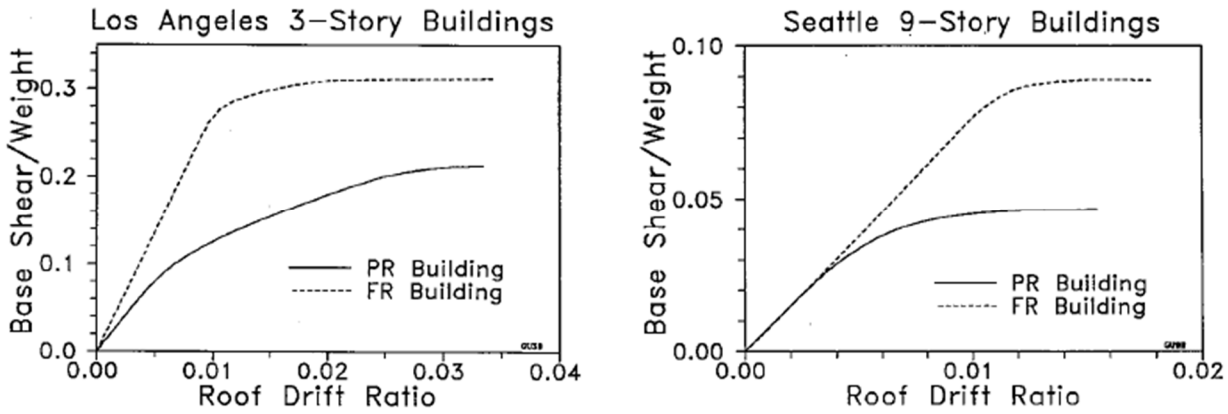


*Figure 2-2: Global Pushover Curves for 3 and 9-Story Buildings (FEMA, 2000)*

structure's reduced strength resulting in slightly improved dynamic performance (Maison and Kasai, 2000).

Both PR structures had more redundancy than their FR equivalents, with the 3-story LA and 9-story Seattle structures having about 5 times and 4 times the number of moment resisting connections respectively. These larger numbers of moment resisting connections gave the PR buildings similar seismic performance to the corresponding FR buildings. The girder and column steel weight for the 3-story PR structure was less than its FR equivalent, but the opposite was true for the 9-story structure. The primary conclusion from this study was that stronger and stiffer PR connections should be used to further enhance the seismic performance of PR buildings (Maison and Kasai, 2000).

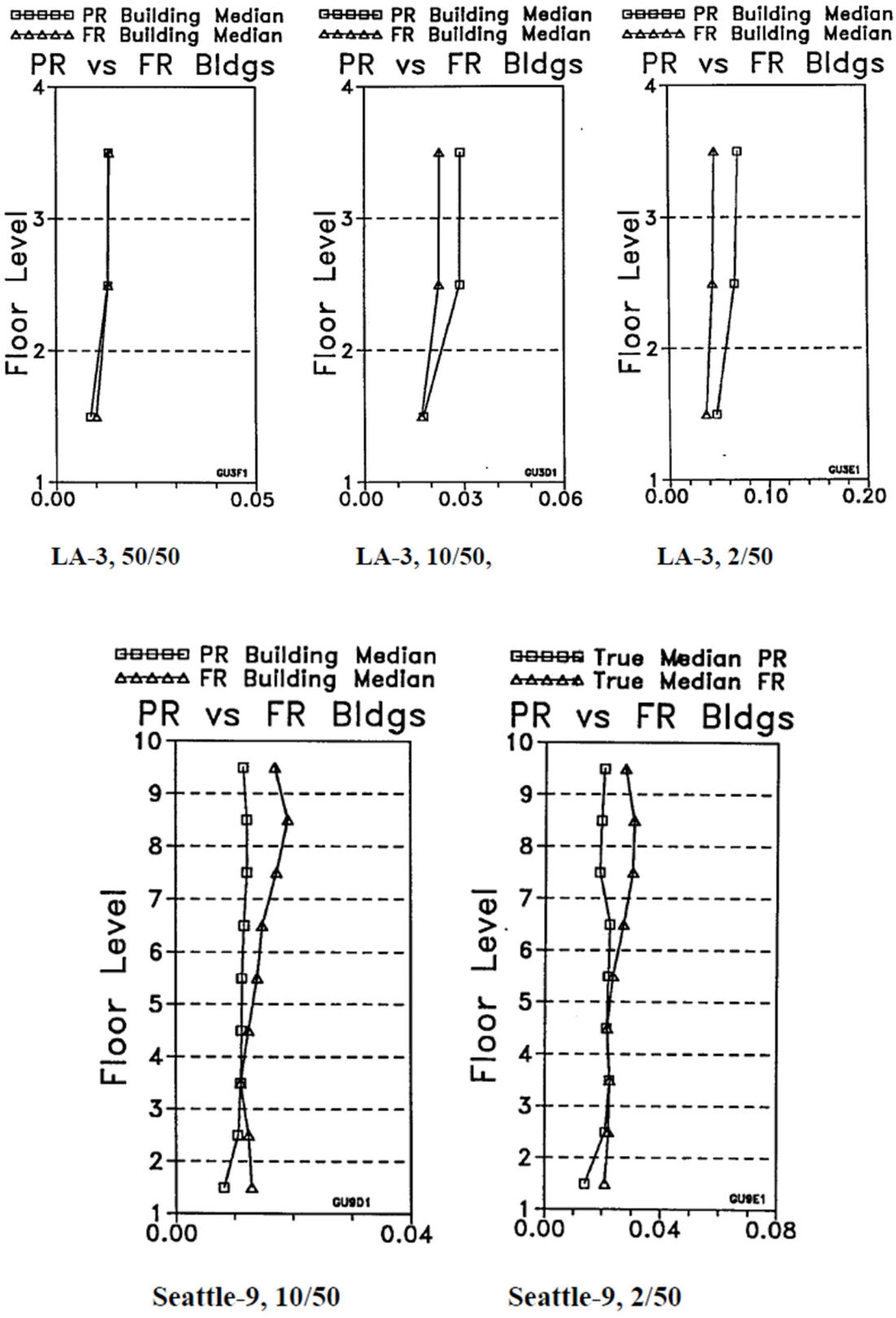


*Figure 2-3: Median Story Drifts for 3 and 9-Story Structures (FEMA, 2000)*

### 2.3.2 Kasai Study

The second study looks at the effects of PR connection stiffness and strength on the seismic performance of steel moment-resisting frames. Headed by Kazuhiko Kasai, this study considers the nine SAC buildings consisting of 3, 9, and 20 story designs for three different seismic zones in Los Angeles (LA), Seattle, and Boston. In each design, the FR welded connections in the SFRS were replaced with PR connections while the beams and columns were kept the same as those used in the original designs. All gravity framing remained unchanged making the beam-to-column connections in the SFRS the only difference between the PR models and the FR models (Kasai et al., 2000).

For each original FR-connected model, eighteen PR-connected models were created with bilinear moment-rotation characteristics having the following properties: three PR connection stiffnesses, $K_c$, of $30EI/L$, $10EI/L$, and $5EI/L$, where $E$, $I$, and $L$ are the beam properties; three PR connection yield moments, $M_{cy}$, of $1.0M_p$, $0.66M_p$, and $0.33M_p$, where $M_p$ is the plastic moment strength of the connected beam; and two strain hardening moments, $M_{ch}$, of $1.4M_{cy}$ and $1.1M_{cy}$ at a rotation of 0.03 radians. Today, the PR connection stiffness of $30EI/L$ would be considered FR, but this study was conducted prior to the development of the three current AISC connection types defined by connection stiffness. Corresponding to the previous study, the connection properties were modeled using rotational spring elements connecting the girder and column ends. In addition, each of the original FR connected models were replicated using the following connection properties in the rotational spring elements: $K_c = 300EI/L$, $M_{cy} = 1.0M_p$, and a connection strain hardening stiffness simulating the 3% strain hardening of the yielded beam (Kasai et al., 2000).

This study conducted inelastic static pushover analyses and dynamic analyses on each of the frame models. The dynamic analyses included 20 ground motions with 10% probability of

exceedance in 50 years (10/50 set) and 20 ground motions with 2% probability of exceedance in 50 years (2/50 set). A total of 180 static pushover analyses (171 PR frames and 9 FR frames) and 7,200 dynamic analyses (171PRx40 + 9FRx40) were conducted. The same computer program used in Maison and Kasai (2000), PC-ANSR, was also used in this study to perform the analyses and record the responses of the frames (Kasai et al., 2000).

The results of the pushover analyses revealed that connection stiffness, yield strength, and post-yield stiffness all impacted the responses of the frames. The PR frames with $K_c = 30EI/L$ had almost an identical lateral stiffness to the FR frames. With the current AISC defined connection types, a PR connection with a stiffness of $30EI/L$ would be an FR connection. Therefore, the pushover results of a PR building constructed with this connection stiffness should match the pushover results of the FR building. The remaining results showed that as the connection stiffness decreased, the PR frames experienced a disproportionate decrease in lateral stiffness. The variation in connection stiffness had less of an impact on the responses of the frames than the connection yield strength and post-yield stiffness. The pushover curves from the LA buildings are shown in Figure 2-4 illustrating the direct influence of connection yield strength and post-yield stiffness on frame behavior. As the yield strength of the connections decreased, the global yield strength of the PR frames decreased proportionally (Kasai et al., 2000). The graphs in Figure 2-4 also reveal that the PR frames have more rounded pushover curves than the FR frames which have mostly a bilinear response. The PR frames with connection yield strengths greater than $0.33M_p$ consistently reached their maximum strengths at larger drift levels than the FR frames, indicating that the PR frames will enter negative stiffness at larger drifts than the FR frames (FEMA, 2000).

The dynamic analyses results reinforced the findings from the pushover analyses on the greater significance of connection yield strength and post-yield stiffness. The median values of

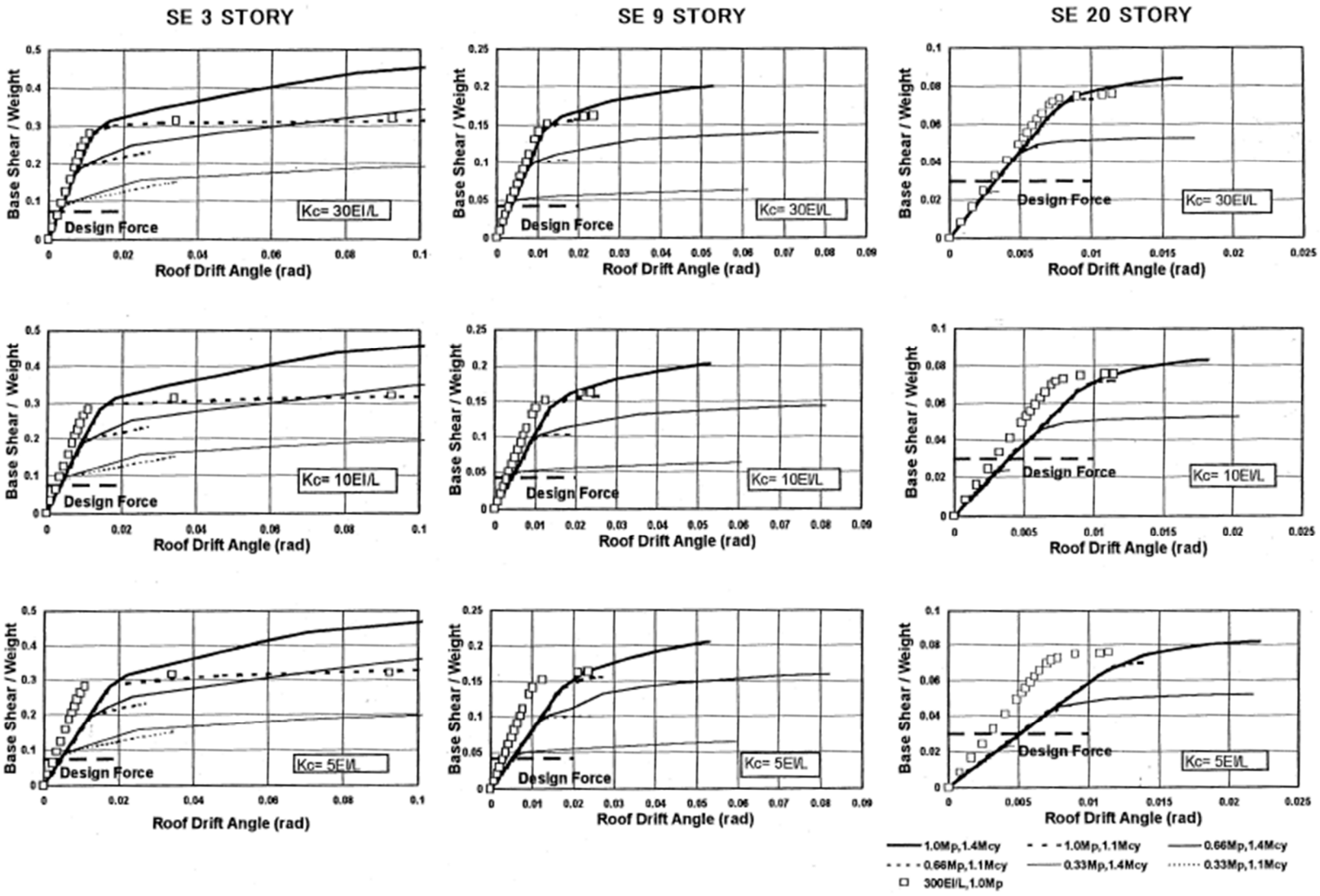


*Figure 2-4: Global Pushover Curves for Los Angeles Buildings with PR and FR Connections (Kasai et al., 2000)*

maximum story drift angles, roof displacements, and roof drift angles were calculated for each of the frames. Smaller $M_{cy}$ resulted in large connection rotations and concentrations of drift at particular story levels. The results also showed that building height significantly impacted the performance of the frames. Frame drifts and frequency of collapse were heavily influenced by the magnitudes of $M_{cy}$, $M_{ch}$, and building height. Figure 2-5 shows the variation of median story drift demands for the LA 3 and 9-story buildings with respect to the different connection parameters for both the 10/50 and 2/50 ground motion intensities (Kasai et al., 2000).

As can be seen from Figure 2-5, the median story drifts of the structures were also significantly affected by the flexibility of the connections. The PR frames with $K_c = 30EI/L$ experienced drifts highly comparable to the FR frames. Again, this is expected since a connection with a stiffness of $30EI/L$ is now considered to be FR. However, as the connection flexibility increased, the PR frames experienced drifts increasingly exceeding those of the FR frames. As anticipated, the magnitudes of these drifts were greater for the frames modeled with weaker connections (Kasai et al., 2000).

One recommendation developed from this study is to provide PR connections with a rotational stiffness of at least $10EI/L$ and yield strengths that are larger than 50% of the beam bending strength. This will limit the lateral drifts of the frames and provide better performance during severe ground motions. Emphasis is placed on providing an appropriate distribution of connection yield strength throughout the height of a frame to prevent concentration of drift at a particular story. It is also recommended that PR connections be designed to withstand large rotations and exhibit large strain hardening behavior similar to the case of $M_{ch} = 1.4M_{cy}$ in order to provide safety against structural collapse (Kasai et al., 2000).

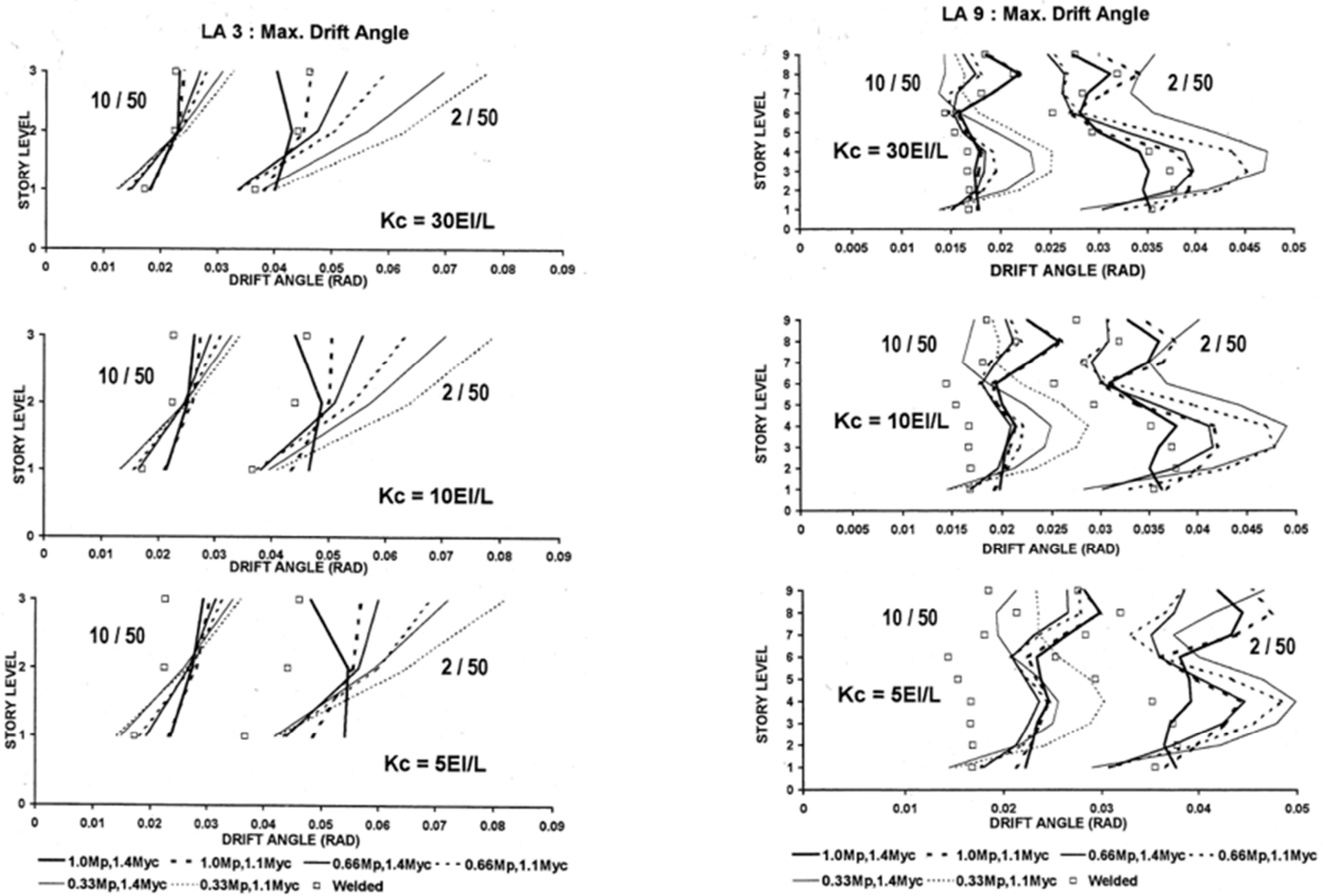


*Figure 2-5: Median Story Drifts for 3 and 9-Story Los Angeles Building (Kasai et al., 2000)*

# Chapter 3: Methodology

This study examined the seismic behavior of both an FR version and numerous PR versions of a building using an Incremental Dynamic Analysis (IDA) procedure. This process involved modeling an FR archetype to serve as a control model to measure and compare the seismic performance of several PR archetypes. Five different classes of PR archetypes were modeled, with each class having a value of connection stiffness that was used for all of the beam-to-column connections in the building. The five connection stiffness values were selected to effectively cover the gamut of PR stiffness values, ranging from almost simple to almost FR. Each class of PR connection stiffness consisted of three connection yield strength values and two strain hardening moment values, resulting in a total of thirty PR building archetypes.

The first step of this process involved selecting a building layout and frame configuration to use for archetypes. Finite element models of the 31 archetypes were constructed in OpenSees, which was then used to simulate their response when subjected to earthquakes. A suite of earthquake records was used to perform an Incremental Dynamic Analysis (IDA) on each archetype. The responses of each PR archetype were recorded and measured against the responses of the FR archetype serving as the control model.

## 3.1 Building Description

The building configuration utilized in this study adopts the 9-Story Los Angeles building design employed by the SAC Joint Venture. The building layout includes five 30-foot bays between six parallel moment frames in both principal directions. The building consists of nine stories, with a first story height of 18 feet, a single level basement height of 12 feet, and a story height of 13 feet for the remaining levels (FEMA, 2000). The column bases were considered pinned. The plan and elevation views of the building are shown in Figure 3-1. The building uses

conventional FR perimeter moment frames to serve as its SFRS, depicted by the bold lines in the plan view displayed in Figure 3-1. The columns in these perimeter moment frames are oriented to bend about their strong axis. The beam-to-column connections at the ends of the fifth bay beams are pinned connections. These pins were incorporated into the design to prevent biaxial bending of the corner columns. The remaining interior beams and columns of the building constitute the gravity framing, which was not designed to carry lateral loads. The penthouse in the original SAC Joint Venture design was excluded from the designs in this study.

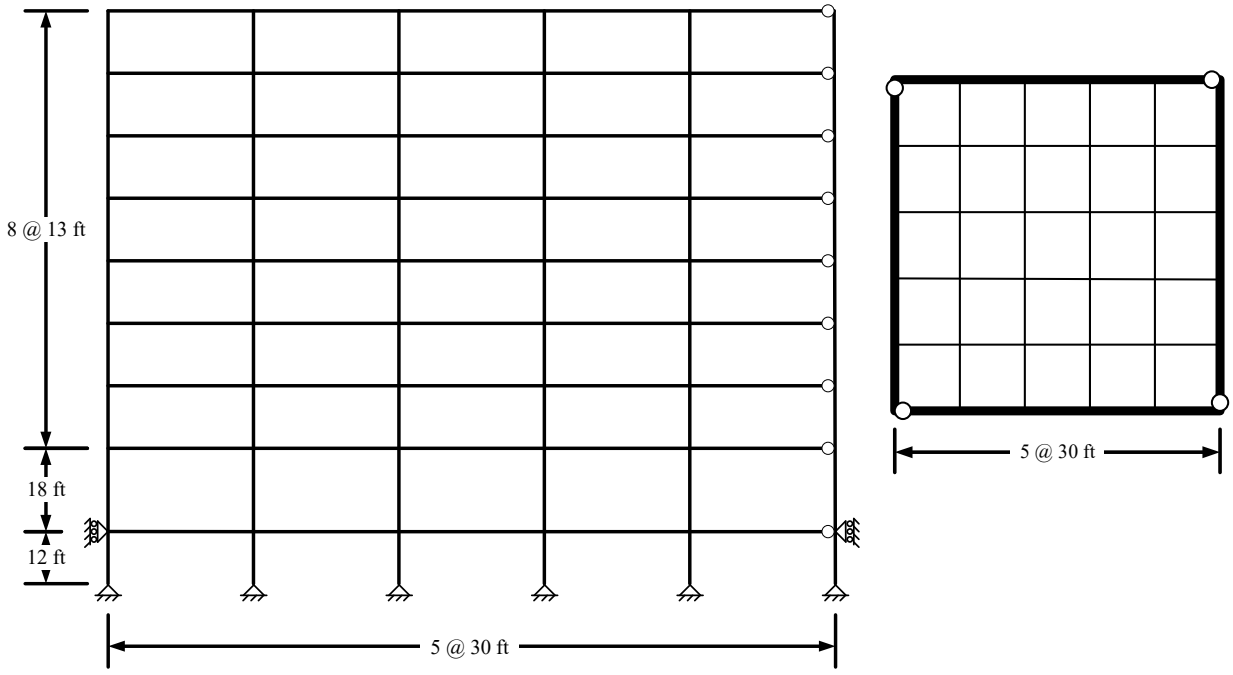


*Figure 3-1: Los Angeles Building Elevation View (left) and Plan View (right) (FEMA, 2000)*

The design loads for the archetypes were based on the original loads used in the SAC Steel Project. The dead loads and live loads are listed in Table 3-1. The floors and roof are constructed from 3-inch metal decking with 2.5 inches of normal weight concrete fill and fireproofing. The weight of the slab was calculated based on a slab thickness of 5.5 inches using 150 lb/ft$^3$ normal weight concrete. The outside surface of the exterior wall is assumed to be two feet from the

perimeter column lines. A 42-inch parapet extends above the surface of the roof. The self-weights of the beams and columns were taken from the values listed in the 2010 AISC Steel Construction Manual.

*Table 3-1: Design Loads*

| Dead Loads | | | |
|---|---|---|---|
| Description | psf | Description | psf |
| Slab | 68.75 | Partitions | 10 |
| Roofing | 7 | Exterior Wall | 25 |
| Ceilings/Flooring | 3 | Floor Total | 88.75 |
| Mech./Electrical | 7 | Roof Total | 85.75 |
| Live Loads | | | |
| Description | psf | Description | psf |
| Office Floor | 50 | Office Roof | 20 |

### 3.2 FR and PR Building Archetypes

The control archetype was modeled to represent the original building design using the perimeter FR moment-resisting frames as the building's SFRS. The two pairs of moment-resisting frames laterally support the building mass in the two principle directions of the building. Each frame was assumed to support half of the building mass in the respective principle direction. Therefore, half of the building was modeled in the analysis, which is shown in Figure 3-2. The model of the building was constructed as a two dimensional replica of one of the perimeter moment-resisting frames. It includes leaning columns to account for the effects of the loads carried by half of the gravity framing. FR connections were used at every beam-to-column joint in the frame except at the external ends of the fifth bay beams, where pins were used per the original SAC design. The frame was modeled using the original member sizes for the beams and columns, which are presented in Figures 3-3 and 3-4.

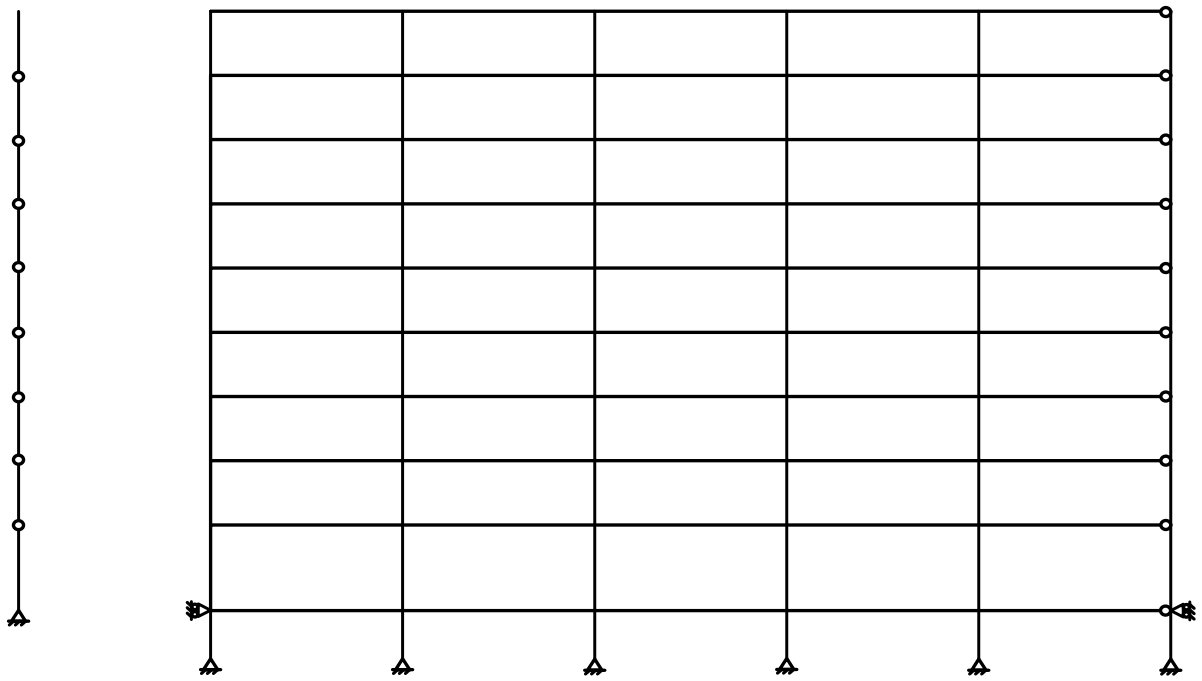

*Figure 3-2: FR Archetype Model (Control)*

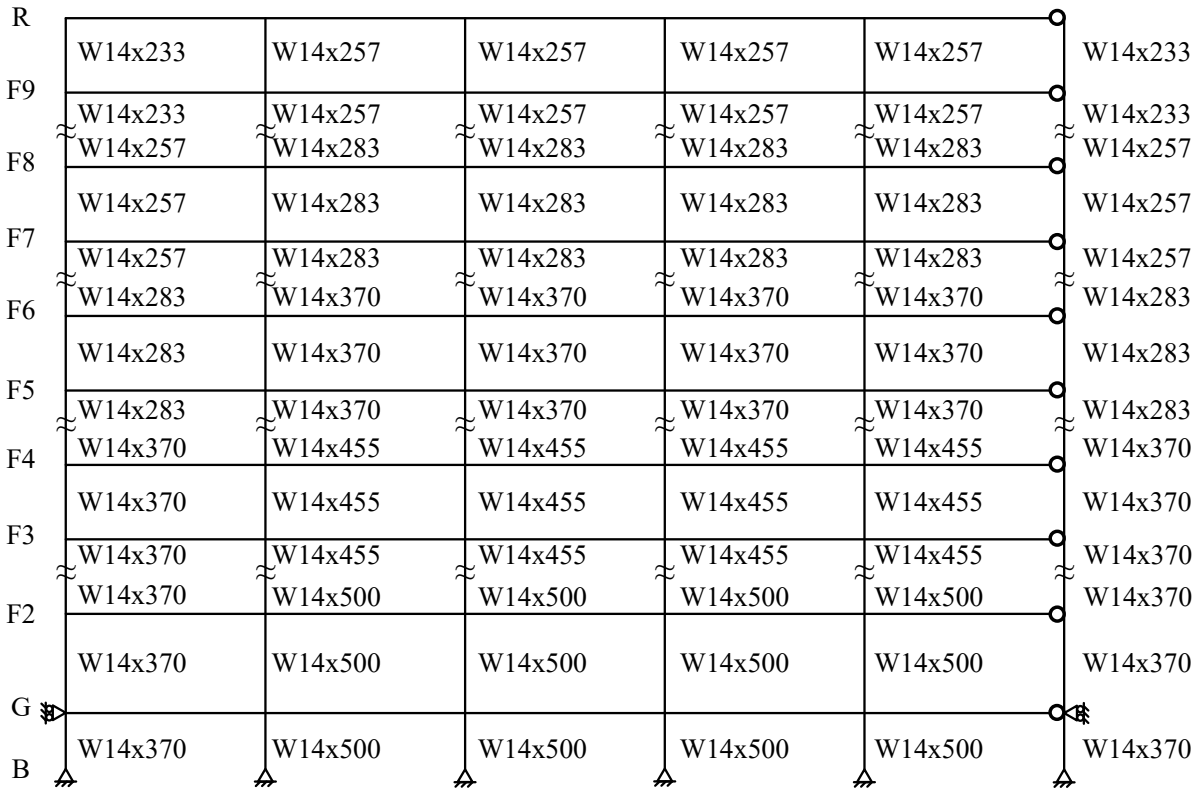


*Figure 3-3: Column Sizes for Control Frame*

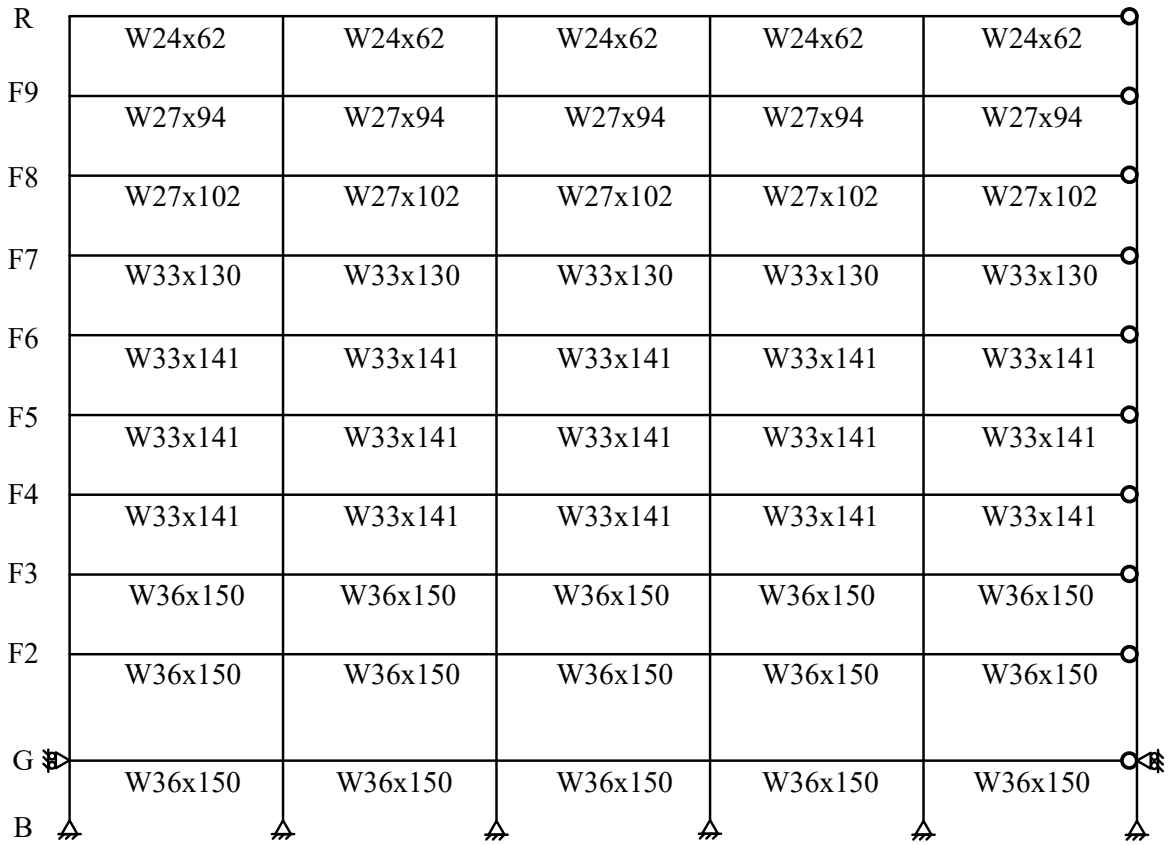


*Figure 3-4: Beam Sizes for Control Frame*

The series of PR archetypes were constructed from a modified version of the original building design. Every beam-to-column connection acted in resisting lateral loads, adopting the concept originally presented by Maison and Kasai in (Maison and Kasai, 2000). These PR buildings employed all six parallel frames in each principle direction and used PR moment connections at every beam-to-column joint to resist lateral loads. The building configuration and member orientations remained unchanged, which resulted in beams connecting to the weak axes of columns with PR connections. This study was conducted under the assumption that such connections are viable.

The beam and column sizes for the PR archetypes were chosen based on a single frame's proportional contribution to the overall stiffness of the building. The member sizes were chosen

so that the PR archetypes would have an equivalent building stiffness to the FR archetype. For each principle direction, moment-resisting frames were applied as the SFRS for the two building archetypes, two in the FR model and six in the PR models. The stiffness of one PR moment-resisting frame corresponds to 1/3 of the stiffness of a FR moment-resisting frame. This concept, combined with the understanding that PR connections have less stiffness than FR connections, lead to the selection of members with about half of the bending resistance for the PR archetypes. The columns have about half of the moment of inertia as the columns in the FR archetype, and the beams have about half of the plastic section modulus as the beams in the FR archetype. The member sizes used for the beams and columns in the PR archetypes are listed in Tables 3-2, 3-3, and 3-4, which show the appropriate property comparisons to the FR archetype members.

*Table 3-2: PR Frame Exterior Column Sizes*

| Story | Control Frame | | Gravity Columns | | PR Frame | | | |
|---|---|---|---|---|---|---|---|---|
| | Size | Ix ($in^4$) | Size | Ag ($in^2$) | Size | Ix ($in^4$) | Ix ratio | Ag ($in^2$) |
| R | W14x233 | 3010 | W14x48 | 14.1 | W14x120 | 1380 | 0.458 | 35.3 |
| F9 | W14x233 | 3010 | W14x48 | 14.1 | W14x120 | 1380 | 0.458 | 35.3 |
| F8 | W14x257 | 3400 | W14x82 | 24.0 | W14x132 | 1530 | 0.450 | 38.8 |
| F7 | W14x257 | 3400 | W14x82 | 24.0 | W14x132 | 1530 | 0.450 | 38.8 |
| F6 | W14x283 | 3840 | W14x109 | 32.0 | W14x159 | 1900 | 0.495 | 46.7 |
| F5 | W14x283 | 3840 | W14x109 | 32.0 | W14x159 | 1900 | 0.495 | 46.7 |
| F4 | W14x370 | 5440 | W14x145 | 42.7 | W14x211 | 2660 | 0.489 | 62.0 |
| F3 | W14x370 | 5440 | W14x145 | 42.7 | W14x211 | 2660 | 0.489 | 62.0 |
| F2 | W14x370 | 5440 | W14x193 | 56.8 | W14x211 | 2660 | 0.489 | 62.0 |
| G | W14x370 | 5440 | W14x193 | 56.8 | W14x211 | 2660 | 0.489 | 62.0 |
| B | W14x370 | 5440 | W14x193 | 56.8 | W14x211 | 2660 | 0.489 | 62.0 |

In the original design, all of the interior columns are oriented in the N-S direction. This means that for the interior frames running in the N-S direction, the interior columns will bend about their strong axis while the exterior columns will bend about their weak axis. However, in

the E-W direction, all of the columns in the interior frames will be bending about their weak axis. This approach resulted in the production of parallel and perpendicular frames with different stiffnesses. The complexity of this approach was recognized; therefore, for simplicity, the PR archetypes were modeled with the columns in each parallel frame oriented in the same direction as those in the exterior frames. This approach was used so that the orientation of the columns in the PR archetypes were the same as those in the FR archetype.

*Table 3-3: PR Frame Interior Column Sizes*

| Story | Control Frame | | Gravity Columns | | PR Frame | | | |
|---|---|---|---|---|---|---|---|---|
| | Size | Ix ($in^4$) | Size | Ag ($in^2$) | Size | Ix ($in^4$) | Ix ratio | Ag ($in^2$) |
| R | W14x257 | 3400 | W14x48 | 14.1 | W14x132 | 1530 | 0.450 | 38.8 |
| F9 | W14x257 | 3400 | W14x48 | 14.1 | W14x132 | 1530 | 0.450 | 38.8 |
| F8 | W14x283 | 3840 | W14x82 | 24.0 | W14x159 | 1900 | 0.495 | 46.7 |
| F7 | W14x283 | 3840 | W14x82 | 24.0 | W14x159 | 1900 | 0.495 | 46.7 |
| F6 | W14x370 | 5440 | W14x109 | 32.0 | W14x211 | 2660 | 0.489 | 62.0 |
| F5 | W14x370 | 5440 | W14x109 | 32.0 | W14x211 | 2660 | 0.489 | 62.0 |
| F4 | W14x455 | 7190 | W14x145 | 42.7 | W14x257 | 3400 | 0.473 | 75.6 |
| F3 | W14x455 | 7190 | W14x145 | 42.7 | W14x257 | 3400 | 0.473 | 75.6 |
| F2 | W14x500 | 8210 | W14x193 | 56.8 | W14x283 | 3840 | 0.468 | 83.3 |
| G | W14x500 | 8210 | W14x193 | 56.8 | W14x283 | 3840 | 0.468 | 83.3 |
| B | W14x500 | 8210 | W14x193 | 56.8 | W14x283 | 3840 | 0.468 | 83.3 |

Each of the PR archetypes was modeled as a two-dimensional replica of one of the interior moment-resisting frames. This is depicted in Figure 3-5 with the modeled frame highlighted by the bold line in the plan view. The interior frame model represents a portion of the entire building, with 1/5 of the applied gravity loads accounting for the proportional tributary area. With the assumption of a rigid diaphragm, the lateral forces acting on the building will be evenly distributed among the six parallel frames. Therefore, 1/6 of the building mass is assumed to be laterally carried by each frame in each principle direction. There are no leaning columns in the PR models, since

*Table 3-4: PR Frame Beam Sizes*

| Story | Control Frame | | Gravity Beams | | PR Frame | | Zx ratio (FR) | Zx ratio (Gravity) |
|---|---|---|---|---|---|---|---|---|
| | Size | Zx ($in^3$) | Size | Zx ($in^3$) | Size | Zx ($in^3$) | | |
| R | W24x62 | 153 | W14x22 | 33.2 | W12x53 | 78 | 0.509 | 2.346 |
| F9 | W27x94 | 278 | W16x26 | 44.2 | W14x82 | 139 | 0.500 | 3.145 |
| F8 | W27x102 | 305 | W16x26 | 44.2 | W16x77 | 150 | 0.492 | 3.394 |
| F7 | W33x130 | 467 | W16x26 | 44.2 | W18x106 | 230 | 0.493 | 5.204 |
| F6 | W33x141 | 514 | W16x26 | 44.2 | W24x94 | 254 | 0.494 | 5.747 |
| F5 | W33x141 | 514 | W16x26 | 44.2 | W24x94 | 254 | 0.494 | 5.747 |
| F4 | W33x141 | 514 | W16x26 | 44.2 | W24x94 | 254 | 0.494 | 5.747 |
| F3 | W36x150 | 581 | W16x26 | 44.2 | W24x104 | 289 | 0.497 | 6.538 |
| F2 | W36x150 | 581 | W16x26 | 44.2 | W24x104 | 289 | 0.497 | 6.538 |
| G | W36x150 | 581 | W16x26 | 44.2 | W24x104 | 289 | 0.497 | 6.538 |

all of the building loads are appropriately accounted for in this design scheme. The pins that were used at the ends of the fifth bay beams in the original SAC design were replaced with PR connections to make every beam-to-column joint a PR connection.

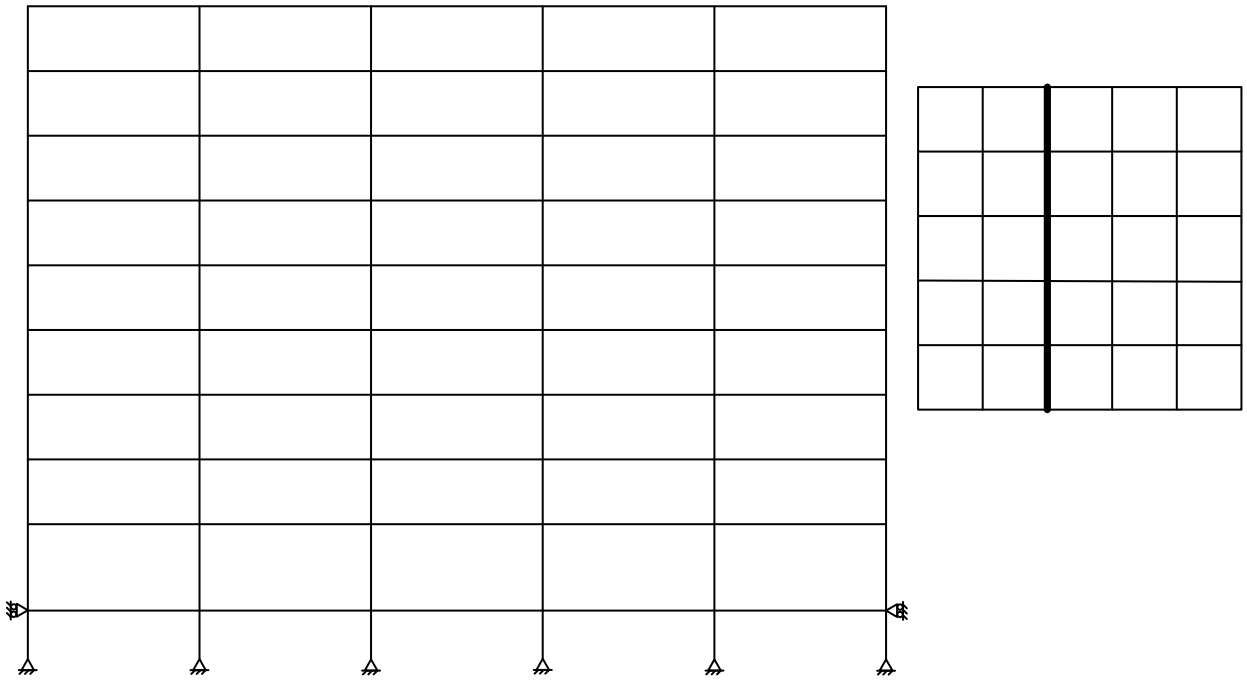

*Figure 3-5: PR Archetype Model Elevation View (left) and Plan View (right)*

### 3.3 PR Connection Characteristics

The PR connection characteristics used by Kasai et el. (2000) were integrated into this study using five different connection stiffnesses ($K_c$), three different connection strengths ($M_{cy}$), and 2 different strain-hardening moments ($M_{ch}$). The five levels of connection stiffness ranged from almost simple to almost FR, with values of 5*EI/L*, 8*EI/L*, 11*EI/L*, 14*EI/L*, and 17*EI/L*, where *E*, *I*, and *L* are the modulus of elasticity, moment of inertia, and length of the beam framing into the connection. The three levels of connection strength considered at each level of stiffness included values of $1.0M_p$, $0.66M_p$, and $0.33M_p$, where $M_p$ is the plastic moment strength of the connected beam. The two values of strain-hardening moments that were considered at each level of strength were $1.4M_{cy}$ and $1.1M_{cy}$ at a connection rotation of 0.03 radians.

The beam-to-column PR connections were modeled with trilinear moment-rotation characteristics. The elastic stiffness of each connection was established using the value of the connection stiffness and the abovementioned beam properties to determine the amount of rotation required at each level of connection strength. The post yield stiffness was established with a linear slope that extends from the yield point to a point that correlates to the two strain-hardening moments at a connection rotation of 0.03 radians. At this level of rotation, the slope of the post yield stiffness becomes zero and is defined by a point equal to the same value of strain-hardening moment at a connection rotation of 0.04 radians. This slope for the post yield stiffness is maintained for rotations that are greater than 0.04 radians. The trilinear moment-rotation characteristics for a PR connection with a W24x104 beam for a stiffness level of 14*EI/L* is depicted in Figure 3-6. The moment-rotation curve designated by 1.0-1.1 represents the PR connection with a connection yield strength equal to $1.0M_p$ and a strain hardening moment equal to $1.1M_{cy}$. The

trilinear moment-rotation characteristics for all of the beam sizes for each level of stiffness are provided in Appendix A.

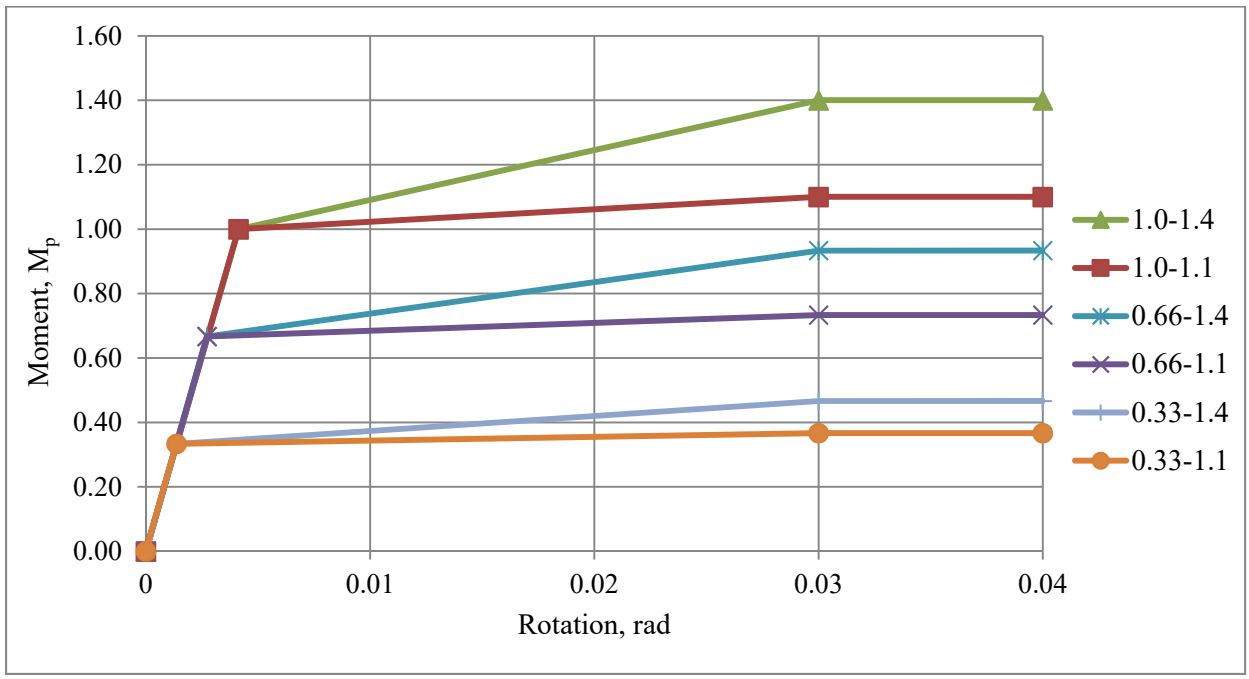


*Figure 3-6: Trilinear Moment-Rotation Behavior of PR Connection with W24x104 Beam for 14EI/L Stiffness*

The PR archetypes were modeled so that every connection in the frame had the same level of stiffness, strength, and post yield stiffness. The values of connection moment and rotation that were calculated based on the beam size and connection stiffness are summarized in the tables in Appendix B.

Each PR model is designated by the levels of connection stiffness, strength, and strain hardening moment and conformed to the following format: PR##M##H##. The number following PR designates the connection stiffness level, the number following M designates the connection strength level, and the number following H designates the connection strain hardening moment. A matrix of the 30 PR frames is displayed in Table 3-5.

*Table 3-5: Matrix of PR Frame Designations*

| Connection Stiffness, $K_c$ | Connection Yield Strength, $M_{cy}$ | | | Strain Hardening Moment, $M_{ch}$ |
|---|---|---|---|---|
| | $1.0M_p$ | $0.66M_p$ | $0.33M_p$ | |
| 5EI/L | PR5M1.0H1.4 | PR5M0.66H1.4 | PR5M0.33H1.4 | $1.4M_{cy}$ |
| 8EI/L | PR8M1.0H1.4 | PR8M0.66H1.4 | PR8M0.33H1.4 | |
| 11EI/L | PR11M1.0H1.4 | PR11M0.66H1.4 | PR11M0.33H1.4 | |
| 14EI/L | PR14M1.0H1.4 | PR14M0.66H1.4 | PR14M0.33H1.4 | |
| 17EI/L | PR17M1.0H1.4 | PR17M0.66H1.4 | PR17M0.33H1.4 | |
| 5EI/L | PR5M1.0H1.1 | PR5M0.66H1.1 | PR5M0.33H1.1 | $1.1M_{cy}$ |
| 8EI/L | PR8M1.0H1.1 | PR8M0.66H1.1 | PR8M0.33H1.1 | |
| 11EI/L | PR11M1.0H1.1 | PR11M0.66H1.1 | PR11M0.33H1.1 | |
| 14EI/L | PR14M1.0H1.1 | PR14M0.66H1.1 | PR14M0.33H1.1 | |
| 17EI/L | PR17M1.0H1.1 | PR17M0.66H1.1 | PR17M0.33H1.1 | |

### 3.4 Incremental Dynamic Analysis Procedure

Incremental dynamic analyses were performed on each of the frames to analyze and compare their seismic behaviors. An incremental dynamic analysis (IDA) is a recently developed parametric analysis method that is used to more adequately assess the behavior of a structure under seismic loads (Vamvatsikos and Cornell, 2002). A structural model is subjected to a series of multiple nonlinear dynamic analyses using acceleration time-histories from recorded ground motions. Each subsequent run of a nonlinear dynamic analysis increases the seismic intensity of the ground motion by incrementally increasing the scale factor applied to the ground accelerations. The main components of an IDA are the intensity measure (IM) and the damage measure (DM). The IM is used to characterize the intensity of a ground motion record, and the DM is a measurable quantity that characterizes the response of a structural model at each level of IM (Vamvatsikos and Cornell, 2002).

Since an IDA is highly dependent on the chosen record, a suite of ground motion records was used to perform a multi-record IDA on each building in order to cover the full range of responses (Vamvatsikos and Cornell, 2002). Table 3-6 lists the twenty-eight horizontal ground motion components from the FEMA P695 Near-Field Record Set that were used to conduct multi-record IDAs on each building. These ground motions were recorded at sites less than 10 km from fault rupture and provided sufficient variability between records to effectively capture the full range of responses for each of the archetypes. This suite of ground motion records contains two subsets: ground motions with strong pulses, referred to as the "NF-Pulse" record subset, and ground motions without such pulses, referred to as the "NF-No Pulse" record subset (FEMA, 2009).

The horizontal components of each record, which are identified in Table 3-6, were obtained from the PEER Next Generation Attenuation database. The records were then scaled to the peak ground acceleration (PGA), determined from the U.S. Geological Survey (USGS), for the building's location in Los Angeles. The USGS Interactive Deaggregation Application was used with a return period of 2475 years to compute a PGA of 0.9247g (USGS, 2008). The resulting twenty-eight time histories are presented in Appendix C.

To characterize the intensity of the ground motions during each IDA, the 2% damped spectral acceleration at each structure's first-mode period was used as the IM. Several DMs, including the maximum roof drift, maximum base shear, and maximum inter-story drift, were used to characterize the responses of the buildings at each level of IM. The 2% damped spectral acceleration at each structure's first-mode period was determined using Newmark's Method presented in (Chopra, 2012). The spectral accelerations computed for each building for each of the twenty-eight time histories are presented in Appendix D.

*Table 3-6: FEMA P695 PEER NGA Near-Field Record Set (FEMA, 2009)*

| ID No. | Record Seq. No. | Earthquake | | | Recording Station | | Comp. Ident. |
|---|---|---|---|---|---|---|---|
| | | M | Year | Name | Name | Owner | |
| Pulse Records Subset | | | | | | | |
| 1 | 181 | 6.5 | 1979 | Imperial Valley-06 | El Centro Array #6 | CDMG | 230 |
| 2 | 182 | 6.5 | 1979 | Imperial Valley-06 | El Centro Array #7 | USGS | 230 |
| 3 | 292 | 6.9 | 1980 | Irpinia, Italy-01 | Sturno | ENEL | 270 |
| 4 | 723 | 6.5 | 1987 | Superstition Hills-02 | Parachute Test Site | USGS | 225 |
| 5 | 802 | 6.9 | 1989 | Loma Prieta | Saratoga - Aloha | CDMG | 90 |
| 6 | 821 | 6.7 | 1992 | Erzican, Turkey | Erzincan | .. | E-W |
| 7 | 828 | 7.0 | 1992 | Cape Mendocino | Petrolia | CDMG | 90 |
| 8 | 879 | 7.3 | 1992 | Landers | Lucerne | SCE | 345 |
| 9 | 1063 | 6.7 | 1994 | Northridge-01 | Rinaldi Receiving Sta | DWP | 318 |
| 10 | 1086 | 6.7 | 1994 | Northridge-01 | Sylmar - Olive View | CDMG | 360 |
| 11 | 1165 | 7.5 | 1999 | Kocaeli, Turkey | Izmit | ERD | 90 |
| 12 | 1503 | 7.6 | 1999 | Chi-Chi, Taiwan | TCU065 | CWB | N |
| 13 | 1529 | 7.6 | 1999 | Chi-Chi, Taiwan | TCU102 | CWB | N |
| 14 | 1605 | 7.1 | 1999 | Duzce, Turkey | Duzce | ERD | 270 |
| No Pulse Records Subset | | | | | | | |
| 15 | 126 | 6.8 | 1976 | Gazli, USSR | Karakyr | .. | 90 |
| 16 | 160 | 6.5 | 1979 | Imperial Valley-06 | Bonds Corner | USGS | 230 |
| 17 | 165 | 6.5 | 1979 | Imperial Valley-06 | Chihuahua | UNAMUCSD | 282 |
| 18 | 495 | 6.8 | 1985 | Nahanni, Canada | Site 1 | .. | 280 |
| 19 | 496 | 6.8 | 1985 | Nahanni, Canada | Site 2 | .. | 330 |
| 20 | 741 | 6.9 | 1989 | Loma Prieta | BRAN | UCSC | 90 |
| 21 | 753 | 6.9 | 1989 | Loma Prieta | Corralitos | CDMG | 90 |
| 22 | 825 | 7.0 | 1992 | Cape Mendocino | Cape Mendocino | CDMG | 90 |
| 23 | 1004 | 6.7 | 1994 | Northridge-01 | LA - Sepulveda VA | USGS/VA | 360 |
| 24 | 1048 | 6.7 | 1994 | Northridge-01 | Northridge - Saticoy | USC | 180 |
| 25 | 1176 | 7.5 | 1999 | Kocaeli, Turkey | Yarimca | KOERI | 330 |
| 26 | 1504 | 7.6 | 1999 | Chi-Chi, Taiwan | TCU067 | CWB | N |
| 27 | 1517 | 7.6 | 1999 | Chi-Chi, Taiwan | TCU084 | CWB | N |
| 28 | 2114 | 7.9 | 2002 | Denali, Alaska | TAPS Pump Sta. #10 | CWB | 317 |

For each IDA performed on a building, the intensity of the ground motions were incrementally increased through the use of a scale factor that is applied to the horizontal ground

accelerations of each record. The chosen IM has the property of being proportional to the scale factor (Vamvatsikos and Cornell, 2002). This same scale factor is then applied to the building's spectral acceleration to provide a measure of the level of IM for each nonlinear dynamic analysis performed during the IDAs. The results of the IDAs are presented as plots of the measured DMs at each level of IM, referred to as IDA curves.

An algorithm was developed to size the scale factor applied to the time histories for each step during the IDAs. The goal of the algorithm was to develop a range of IMs that effectively captured the IDA behavior of each frame to the highest level of intensity possible without sacrificing more time and system resources than appropriate. The size of the step depended upon the amount of change in DM from the previous run. If the change in the amount of total roof drift was less than 0.03%, then the scale factor was increased by 0.01. If the change in total roof drift was greater than 0.03% but less than 0.05%, then the scale factor was increased by 0.006. If the change in total roof drift was greater than 0.05%, then the scale factor was increased by 0.003.

The decrease in the scale factor increment for larger DMs was used in order to capture any possible softening segments in the IDA curves, where the structures would accumulate DMs at accelerated rates and caused the IDA curves to plateau. This increase towards infinity in the amount of DM accumulation for vanishingly smaller increments of IM would signal the onset of dynamic instability in the structures. Such plateaus in the IDA curves can be used to establish the theoretical maximum seismic intensity level that a structure can achieve before collapse (Vamvatsikos and Cornell, 2002).

# Chapter 4: Analytical Modeling Methodology

The Open System for Earthquake Engineering Simulation program, OpenSees, was used to both create finite element models of the archetypes and perform the earthquake simulations (OpenSees, 2006). It is an object-oriented, open-source software framework that was developed at the Pacific Earthquake Engineering Research Center (PEER) in Berkeley, CA. The program uses input files, which are text files written using the Tool Command Language (Tcl) scripting language, in order to perform finite element analyses. The archetypes were modeled and analyzed as two-dimensional frames.

## 4.1 Material and Element Definitions

The material and element definitions followed the same methodology used by Kozma et al. (2014). The models were constructed using material definitions that represent the material properties for ASTM A992 Grade 50 structural steel. The flexural properties of the structural steel were modeled with a yield strength of 50 ksi and a modulus of elasticity of 29,000 ksi using the Giuffre-Menegotto-Pinto steel material object with isotropic hardening (OpenSees, 2006). The strain-hardening ratio was defined as 0.01, and a plot of the general stress-strain relationship is illustrated in Figure 4-1. The shear properties of the structural steel were defined using a poisson's ratio of 0.3 to determine the shear modulus. An elastic uniaxial material object using a linear stress-strain relationship with a tangent defined by the shear modulus was used to model the shear properties. The elastic uniaxial material object's stress-strain relationship is illustrated in Figure 4-2 (OpenSees, 2006).

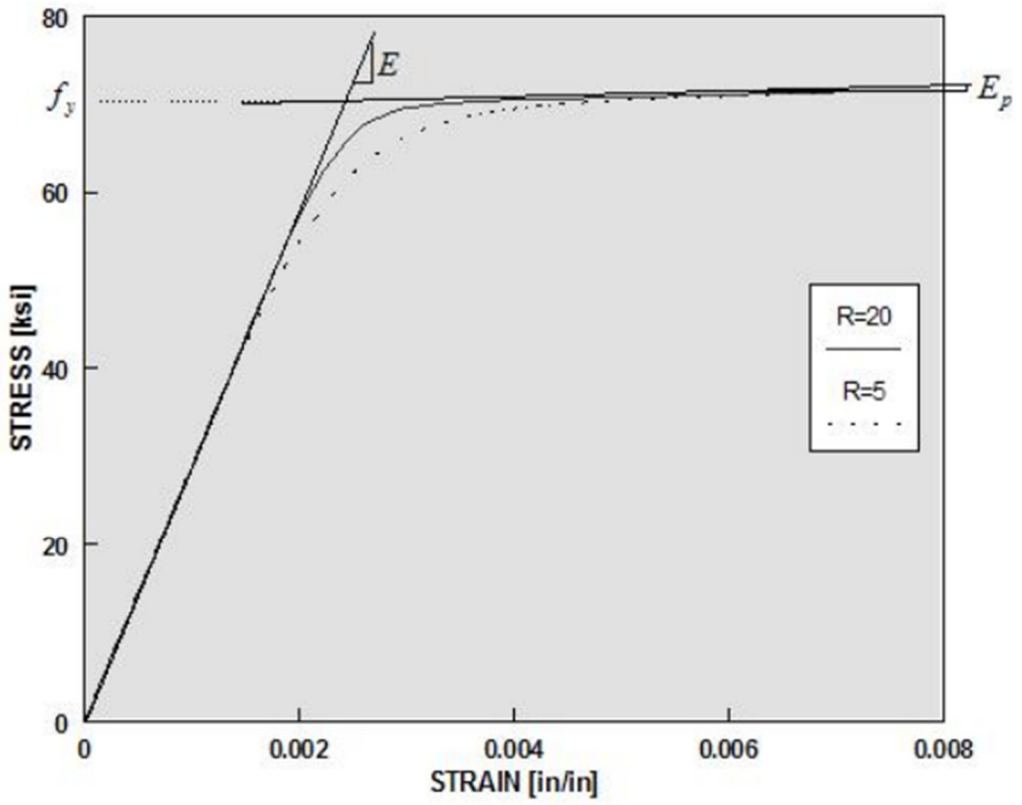


*Figure 4-1: Monotonic Envelope of Giuffre-Menegotto-Pinto Steel Material (OpenSees, 2006)*

The cross-sections of the beam and column elements were modeled as fiber sections using both the cross-sectional areas and dimensions of each shape as defined in the 2010 AISC Steel Construction Manual. These fiber sections were generated using fiber section objects defined with the abovementioned flexural material object. These fiber sections were then combined with the shear material objects into a single section force-deformation model using section aggregator objects (OpenSees, 2006). The column aggregate sections were generated using the presently defined fiber section objects and shear material objects. The beam aggregate sections, however, included an additional uniaxial material object to explicitly define an axial property that was only present in the beam elements. Because a rigid diaphragm is assumed for the analyses of these buildings, the beams were modeled as axially rigid using an elastic uniaxial material object,

defined with a very high tangent value in order to simulate this assumption. Therefore, the beam aggregate sections combined the fiber section objects, the shear material objects, and the rigid axial material objects to generate the beam sections.

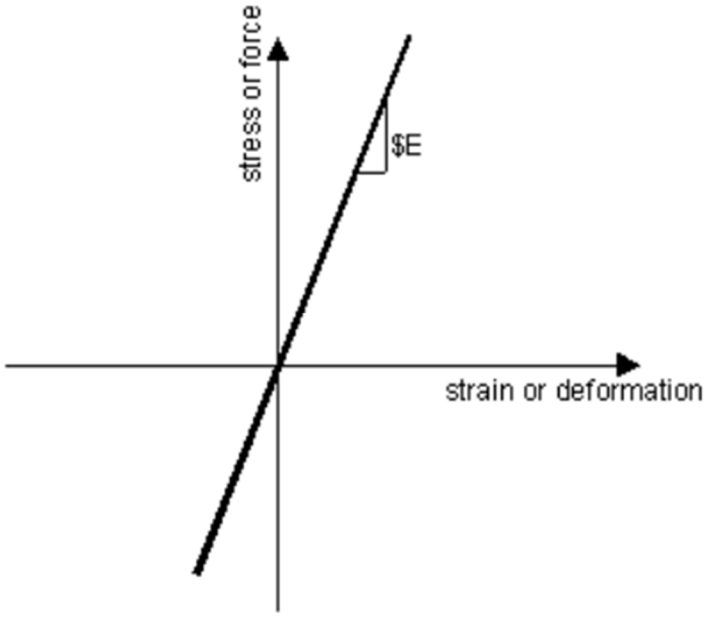


*Figure 4-2: Stress Vs Strain Relationship for Elastic Uniaxial Material (OpenSees, 2006)*

The column and beam aggregate sections were then used to generate nonlinear beam-column element objects. The ends of each beam-column element were defined by the nodes established at the beam-column joints. Each beam-column element was generated using a P-Delta coordinate transformation object, which performs a linear geometric transformation of beam stiffness and resisting force from the element coordinate system to the global coordinate system. This geometric-transformation object also establishes consideration for second order P-Delta effects in the finite element models (OpenSees, 2006).

### 4.2 Beam-to-Column Connections

The beam-to-column connections in the control frame model were generated through the process of framing the ends of the beam elements straight into the nodes that delineate the beam-to-column joints. This was accomplished by using the one node at each beam-to-column joint to define the end of both beams framing into the joint. The resulting assemblage constituted an FR beam-to-column connection. The pins at the exterior ends of the fifth-bay beams were modeled using rotational springs, which were constructed from zero-length elements. Zero-length elements are defined by two nodes at the same location (OpenSees, 2006). These pins connected the nodes at the ends of the fifth-bay beams to the nodes defining the beam-to-column joints along the exterior column line. These elements were generated from an elastic uniaxial material object with a stiffness value of zero to replicate the rotational resistance of a true pin (i.e. zero resistance to rotation).

The beam-to-column connections of the PR frames were modeled with rotational springs that characterize the appropriate moment-rotation behavior based on the designated PR connection parameters and the beam size framing into the connection. These rotational springs were also constructed from zero-length elements that connect the nodes at the ends of the beams to the nodes defining the beam-to-column joints. These zero-length elements were generated from uniaxial trilinear hysteretic material objects that replicate the trilinear moment-rotation behaviors of the PR connections defined in Section 3.4 (OpenSees, 2006). The general force-deformation relationship for this material is detailed in Figure 4-3.

The primary framework for defining the material behavior used to characterize the PR connections includes the moment and rotation values at both the positive and negative yield points defining the elastic stiffness, and at both the positive and negative points defining the

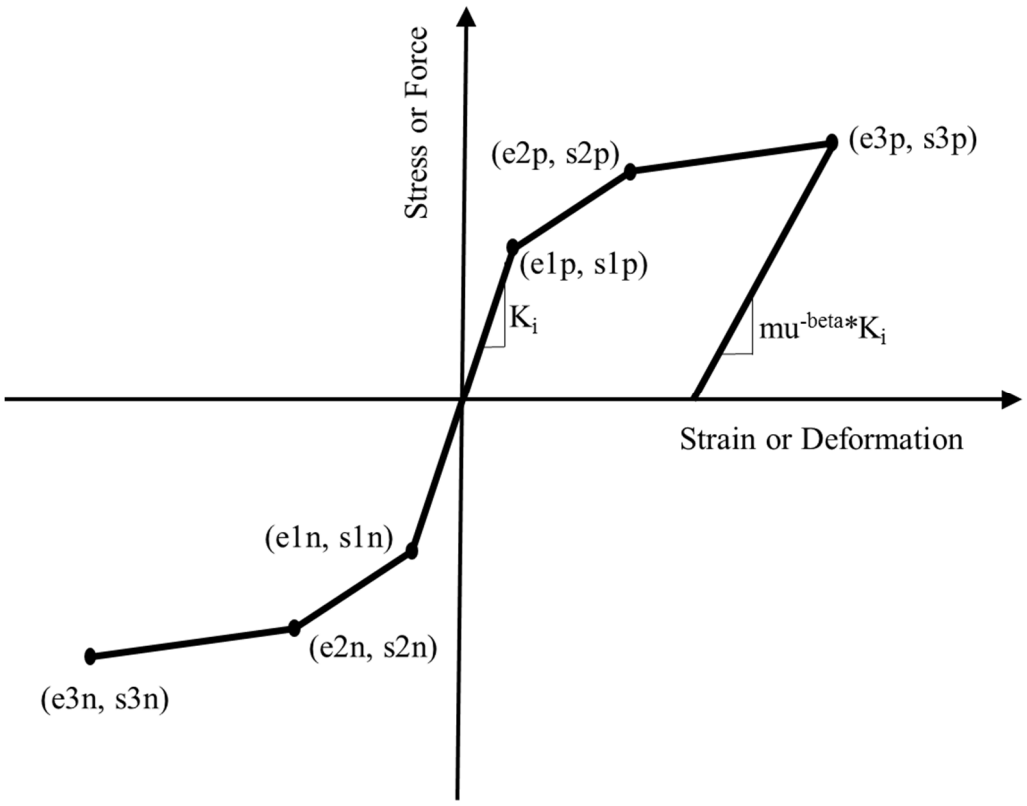


*Figure 4-3: Force Vs Deformation Relationship for Hysteretic Material (OpenSees, 2006)*

post-yield region at ±0.03 and ±0.04 radians. The values of these points for each connection at each level of stiffness, strength, and strain-hardening moment are presented in the tables in Appendix B. Other applicable parameters for this material include criteria for pinching, damage, and degraded unloading stiffness (OpenSees, 2006). A rigorous calibration process was performed to determine these parameter values, included in Table 4-1, which resulted in a suitable moment-rotation response for a PR connection under cyclic loading. The hysteretic response for a PR connection with a W24x104 beam that has a stiffness of 17$EI/L$, a strength of 1.0$M_p$, and a strain-hardening moment of 1.4$M_{cy}$ is shown in Figure 4-4 for the parameter values selected.

*Table 4-1: Hysteretic Material Parameter Values*

| Parameter | Value | Description |
|---|---|---|
| PinchX | 0.40 | Pinching factor for strain during reloading |
| PinchY | 0.50 | Pinching factor for stress during reloading |
| Damage1 | 0.02 | Damage due to ductility |
| Damage2 | 0.05 | Damage due to energy |
| Beta | 0.00 | Power to determine degraded unloading stiffness based on ductility |

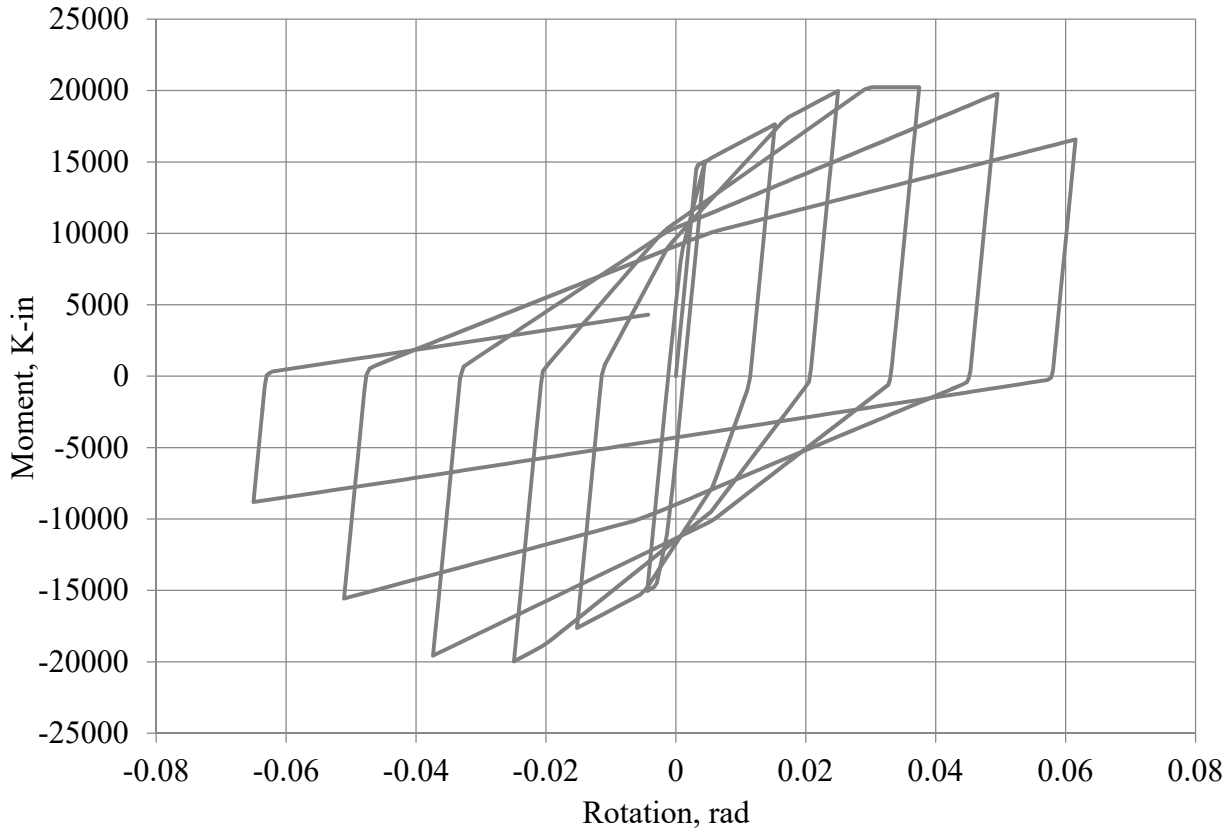


*Figure 4-4: Hysteretic Response of PR Connection for W24x104 Beam with $K_c$ = 17EI/L, $M_{cy}$ = 1.0$M_p$, and $M_{ch}$ = 1.4$M_{cy}$*

### 4.3 Design Loads and Mass

The design loads were applied to the models using nodal and element load objects generated with a linear plain load pattern (OpenSees, 2006). The self-weights of the members were

added to the dead load values applied to the models. The IDAs performed in this study were conducted with the application of the full dead load and thirty percent of the live load in accordance with Section 16.2.3 of ASCE 7-10. Nodal loads were applied at every beam-to-column joint in the frame models to represent the tributary loads carried by the perpendicular beams framing into the joints. Element loads were applied to each beam and column element, representing the tributary loads carried by each member including their self-weight.

In addition to the design loads described above, which account for the tributary area supported by the frames, the control frame model also included the gravity loads carried by half of the gravity framing. These gravity frame loads were applied to the leaning columns as nodal load objects at each floor level and are illustrated in Figure 4-5. The PR frame models included only the nodal and element loads corresponding to their tributary area extending halfway to the adjacent frames on either side.

The mass for each floor, which was computed from the design loads applied, was assigned to the model using the mass command (OpenSees, 2006). For the control frame, the design loads carried directly by the modeled perimeter frame were used to determine the mass assigned to it. The nodes at every beam-to-column joint were assigned a mass value accounting for half of the members and loads extending from that joint. The mass, from the loads and members associated with the gravity framing, was applied to the leaning columns at each floor. The total mass applied to the control frame accounts for half of the total mass for the building. The mass for the PR frame models was applied using the same procedure, minus the application of any gravity framing mass. However, the mass values were adjusted so that $1/6^{th}$ of the building mass was applied to the frame in accordance with the methodology established in Section 3.3.

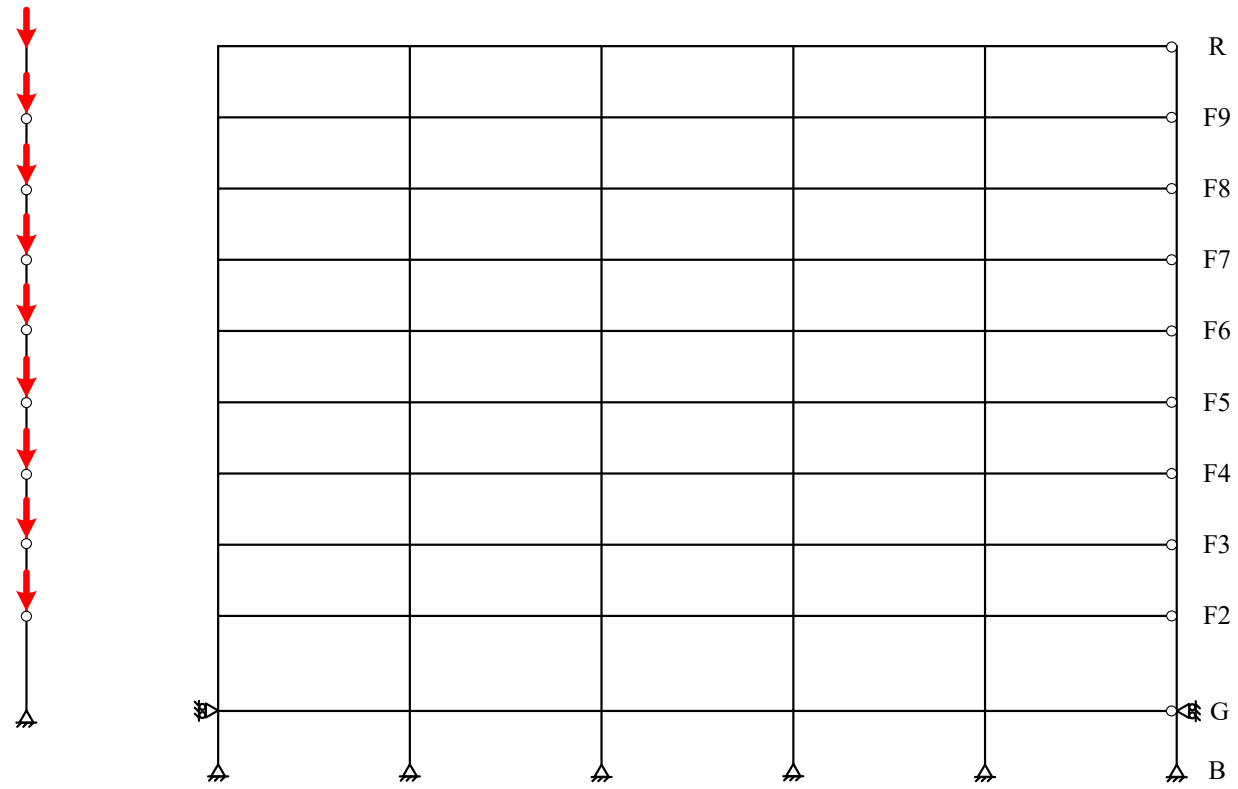


*Figure 4-5: Leaning Column Loads on Control Frame*

### 4.4 Leaning Columns and Damping

In addition to the beam and column elements used to compose the moment-resisting frames, the control frame model utilized leaning column elements to account for P-delta effects. The base of these leaning columns was modeled at a distance equal to the width of one bay, 30 feet, from the base of the left exterior column of the moment-resisting frame. These leaning columns were constructed from elastic beam-column element objects (OpenSees, 2006). The area, modulus of elasticity, and moment of inertia of these column elements were defined as 900 $in^2$, $29.0 \times 10^6$ ksi, and 67,500 $in^4$ respectively. This high modulus of elasticity was used in order to model the columns as rigid elements.

The base of these leaning columns were modeled as pinned, and the ends of each column were pin-connected using rotational springs that were constructed with the same methods used for the pins at the external ends of the fifth bay beams. These elements connected the nodes at the ends of the leaning column elements in order to provide free rotation between the columns. This modeling scheme permitted the leaning columns to induce the effects of the weight and mass from the gravity framing without interfering with the modeshapes of the building.

A classical damping matrix was used to apply 2% damping to each of the frames. In OpenSees, damping is applied to all previously defined elements and nodes using the Rayleigh damping command. The damping matrix is specified as a combination of stiffness and mass-proportional damping matrices (OpenSees, 2006). Coefficients are applied to these matrices with the coefficient $a_0$ applied to the damping matrix and the coefficient $a_1$ applied to the stiffness matrix. These coefficients are displayed in Equations 4-1 and 4-2 (Chopra, 2012).

$$a_0 = \zeta \frac{2\omega_i \omega_j}{\omega_i + \omega_j} \qquad \text{(Eq. 4-1)}$$

$$a_1 = \zeta \frac{2}{\omega_i + \omega_j} \qquad \text{(Eq. 4-2)}$$

where:

$\zeta$ = damping ratio

$\omega_i$ = natural circular frequency for the structure's *i*th mode

$\omega_j$ = natural circular frequency for the structure's *j*th mode

The natural circular frequency for the first mode was used for $\omega_i$ and the natural circular frequency for the second mode was used for $\omega_j$. These natural circular frequencies were calculated for each

frame using the Eigen command (OpenSees, 2006). In executing the Rayleigh damping command, the $a_0$ and $a_1$ coefficients were used for the alphaM and betaK factors respectively, while the betaKinit and betaKcomm factors were set to zero.

# Chapter 5: Analytical Results and Evaluation

## 5.1 Equivalent Lateral Force Procedure

As part of the effort to compare the seismic performance of the 31 frames analyzed, an Equivalent Lateral Force (ELF) analysis was performed on each of the frames. In order to develop a proper comparison, the base shear that was calculated from the ELF procedure summarized in Table 5-1 for the control archetype was used to determine the vertical distribution of forces for all building archetypes. The vertical distribution of seismic forces for both the FR and PR archetypes are outlined in Table 5-2. These forces include the effects of accidental torsion per Section 12.8.4.2 of ASCE 7-10, which are summarized in Table 5-3.

*Table 5-1: Equivalent Lateral Force Procedure (ASCE/SEI 7-10, 2010)*

| Pg. # | Location | Variable | Value | Pg. # | Location | Variable | Value |
|---|---|---|---|---|---|---|---|
| 65 | Sect. 11.4.2 | Site Class | D | | | T = | 1.830 s |
| 2 | Tab. 1.5-1 | Risk Cat | II | 224 | Fig. 22-12 | $T_L$ = | 8.000 s |
| | USGS | $S_S$ = | 2.447 g | 2 | Tab. 1.5-2 | $I_e$ = | 1 |
| | USGS | $S_1$ = | 0.858 g | 67 | Tab. 11.6-1 | SDC | D |
| 66 | Tab. 11.4-1 | $F_a$ = | 1 | 67 | Tab. 11.6-2 | SDC | D |
| 66 | Tab. 11.4-2 | $F_v$ = | 1.5 | 75 | Tab. 12.2-1 | R = | 8 |
| 65 | Eq. 11.4-1 | $S_{MS}$ = | 2.447 g | 88 | Sect. 12.7.2 | W = | 24610 K |
| 65 | Eq. 11.4-2 | $S_{M1}$ = | 1.287 g | 89 | Eq. 12.8-2 | $C_s$ = | 0.204 g |
| 65 | Eq. 11.4-3 | $S_{DS}$ = | 1.631 g | 89 | Eq. 12.8-3 | $C_s \leq$ | 0.059 g |
| 65 | Eq. 11.4-4 | $S_{D1}$ = | 0.858 g | 89 | Eq. 12.8-4 | $C_s \leq$ | 0.256 g |
| 90 | Tab. 12.8-2 | $C_t$ = | 0.028 | | | $C_{s,\,max}$ = | 0.059 g |
| 90 | Tab. 12.8-2 | x = | 0.8 | 90 | Eq. 12.8-5 | $C_s \geq$ | 0.072 g |
| 90 | Sect. 12.8.2.1 | $h_n$ = | 122.0 ft | 90 | Eq. 12.8-6 | $C_s \geq$ | 0.054 g |
| 90 | Eq. 12.8-7 | $T_a$ = | 1.307 s | | | $C_{s,\,min}$ = | 0.072 g |
| 90 | Tab. 12.8-1 | $C_u$ = | 1.4 | | | $C_s$ = | 0.072 g |
| 90 | Sect. 12.8.2 | $C_uT_a$ = | 1.830 s | 89 | Eq. 12.8-1 | V = | 1766 K |
| 90 | Sect. 12.8.2 | $T_{calc}$ = | 2.884 s | 91 | Sect. 12.8.3 | k = | 1.66 |

*Table 5-2: ELF Procedure Distribution of Vertical Forces*

| Level | $w_i$ (Kips) | $h_i$ (ft) | $w_i h_i^k$ | $C_{vx}$ | $F_{Bldg}$ (Kips) | $F_{FR\text{-}frame}$ (Kips) | $F_{PR\text{-}frames}$ (Kips) |
|---|---|---|---|---|---|---|---|
| Roof | 2,235 | 122 | 6,647,208 | 0.2314 | 408.8 | 214.7 | 69.6 |
| 9th | 2,411 | 109 | 5,945,983 | 0.2070 | 365.6 | 192.1 | 62.3 |
| 8th | 2,430 | 96 | 4,849,796 | 0.1688 | 298.2 | 156.7 | 50.8 |
| 7th | 2,447 | 83 | 3,832,743 | 0.1334 | 235.7 | 123.8 | 40.1 |
| 6th | 2,478 | 70 | 2,923,678 | 0.1018 | 179.8 | 94.4 | 30.6 |
| 5th | 2,478 | 57 | 2,076,766 | 0.0723 | 127.7 | 67.1 | 21.7 |
| 4th | 2,508 | 44 | 1,365,826 | 0.0475 | 84.0 | 44.1 | 14.3 |
| 3rd | 2,513 | 31 | 764,051 | 0.0266 | 47.0 | 24.7 | 8.0 |
| 2nd | 2,602 | 18 | 319,997 | 0.0111 | 19.7 | 10.3 | 3.4 |
| Totals | | | 28,726,048 | | 1,766 | 928.0 | 300.8 |

*Table 5-3: ELF Procedure Horizontal Distribution of Base Shear*

| Equations and Variables | Archetype FR | Archetype PR | Units | Description |
|---|---|---|---|---|
| $d_i$ | 75 | 15 | ft | Perpendicular distance from frame to center of resistance |
| $k_{NS}/k_{EW}$ | 1 | 1 | | Ratio of building NS stiffness to EW stiffness |
| $k_{i,x} / \sum k_{i,x}$ | 1/2 | 1/6 | | Ratio of single frame stiffness to sum of frame stiffnesses in "x" direction |
| $\sum k_i d_i^2$ | 22,500 | 31,500 | K·ft | |
| $V_d = V_B * k_{i,x} / \sum k_{i,x}$ | 0.5 | 0.17 | $V_B$ | Direct shear in terms of building base shear |
| $M_{ta} = (0.05) * B * V_B$ | 7.6 | 7.6 | $V_B$·ft | Accidental torsional moment (B is width of building) |
| $V_{ta} = M_{ta} * k_i d_i / \sum k_i d_i^2$ | 0.0253 | 0.0036 | $V_B$ | Shear resulting from accidental torsion |
| $V_{Frame} = V_d + V_{ta}$ | 0.5253 | 0.1703 | $V_B$ | Total base shear that frame is loaded with in “x” direction |

The results of the ELF analysis are presented in Table 5-4. Presented are the fundamental periods of the structures, total roof drift and displacement, and the load factor that was reached in the analysis before convergence failure. The table also provides information indicating if the total roof drift of the structures pass the allowable drift limit mandated by (ASCE/SEI 7-10, 2010). As is demonstrated in Table 5-4, some of the PR frames had fundamental periods that were less than the fundamental period for the control frame.

All of the PR frames with connection strengths of $0.66M_p$ and $1.0M_p$ passed the ASCE 7-10 allowable drift limit. However, the PR frames with a connection strength of $0.33M_p$ all failed the allowable drift limit. Also, the fundamental periods of the PR frames with the $0.33M_p$ connection strength were all greater than the fundamental period of the control frame. These results coincide with the findings from the previous studies examined in the literature on the negative effects of decreased connection strength. The previously developed rationale for using PR connections with strengths greater than 50% of the beam bending strength is reinforced by the results of this study.

*Table 5-4: ELF Analysis Results*

| Strain Hardening ($M_{cy}$) | Strength, $M_{cy}$ ($M_p$) | Stiffness, $K_c$ (K-in/rad) | Fund. Period, $T_n$, (sec) | Ratio to Control $T_n$ | ELF Analysis | | Load Factor Before Failure | ASCE 7 Drift Limit |
|---|---|---|---|---|---|---|---|---|
| | | | | | Roof Disp (in) | Roof Drift | | |
| 1.1 | 0.33 | 5 | 3.21 | 1.113 | 22.49 | 0.0154 | 0.8 | Fail |
| | | 8 | 3.05 | 1.056 | 20.86 | 0.0143 | 0.8 | Fail |
| | | 11 | 3.03 | 1.050 | 20.17 | 0.0138 | 0.8 | Fail |
| | | 14 | 3.50 | 1.215 | 19.77 | 0.0135 | 0.8 | Fail |
| | | 17 | 3.46 | 1.200 | 19.52 | 0.0133 | 0.8 | Fail |
| | 0.66 | 5 | 3.17 | 1.101 | 15.95 | 0.0109 | | Pass |
| | | 8 | 2.91 | 1.009 | 13.92 | 0.0095 | | Pass |
| | | 11 | 2.78 | 0.964 | 13.09 | 0.0089 | | Pass |
| | | 14 | 2.70 | 0.938 | 12.65 | 0.0086 | | Pass |
| | | 17 | 2.65 | 0.920 | 12.37 | 0.0084 | | Pass |
| | 1.0 | 5 | 3.17 | 1.101 | 15.68 | 0.0107 | | Pass |
| | | 8 | 2.91 | 1.009 | 13.06 | 0.0089 | | Pass |
| | | 11 | 2.78 | 0.964 | 11.89 | 0.0081 | | Pass |
| | | 14 | 2.70 | 0.938 | 11.23 | 0.0077 | | Pass |
| | | 17 | 2.65 | 0.920 | 10.81 | 0.0074 | | Pass |
| 1.4 | 0.33 | 5 | 3.20 | 1.109 | 42.42 | 0.0290 | | Fail |
| | | 8 | 3.00 | 1.041 | 41.15 | 0.0281 | | Fail |
| | | 11 | 2.95 | 1.022 | 40.50 | 0.0277 | | Fail |
| | | 14 | 3.18 | 1.102 | 40.12 | 0.0274 | | Fail |
| | | 17 | 3.14 | 1.088 | 39.86 | 0.0272 | | Fail |
| | 0.66 | 5 | 3.17 | 1.101 | 15.80 | 0.0108 | | Pass |
| | | 8 | 2.91 | 1.009 | 13.52 | 0.0092 | | Pass |
| | | 11 | 2.78 | 0.964 | 12.59 | 0.0086 | | Pass |
| | | 14 | 2.70 | 0.938 | 12.09 | 0.0083 | | Pass |
| | | 17 | 2.65 | 0.920 | 11.78 | 0.0080 | | Pass |
| | 1.0 | 5 | 3.17 | 1.101 | 15.68 | 0.0107 | | Pass |
| | | 8 | 2.91 | 1.009 | 13.06 | 0.0089 | | Pass |
| | | 11 | 2.78 | 0.964 | 11.89 | 0.0081 | | Pass |
| | | 14 | 2.70 | 0.938 | 11.23 | 0.0077 | | Pass |
| | | 17 | 2.65 | 0.920 | 10.81 | 0.0074 | | Pass |
| Control | | | 2.88 | 1.000 | 11.94 | 0.0082 | | Pass |

## 5.2 IDA Results

All 31 frames were subjected to IDAs using the 28 ground motion records from the FEMA P695 Near-Field Record Set. The responses of each frame were recorded and plots of the IDA curves were generated. For each frame, the IDA curves for the 28 time histories were plotted on the same graphs. Figure 5-1 shows the IDA curve set for frame PR14M0.66H1.4 for the Maximum Interstory Drifts recorded. In order to effectively compare the IDA results from all of the frames, an average IDA curve was developed for each DM from the set of 28 IDA curves produced for each frame. The average IDA curve is depicted by a thick black line, illustrated in Figure 5-1.

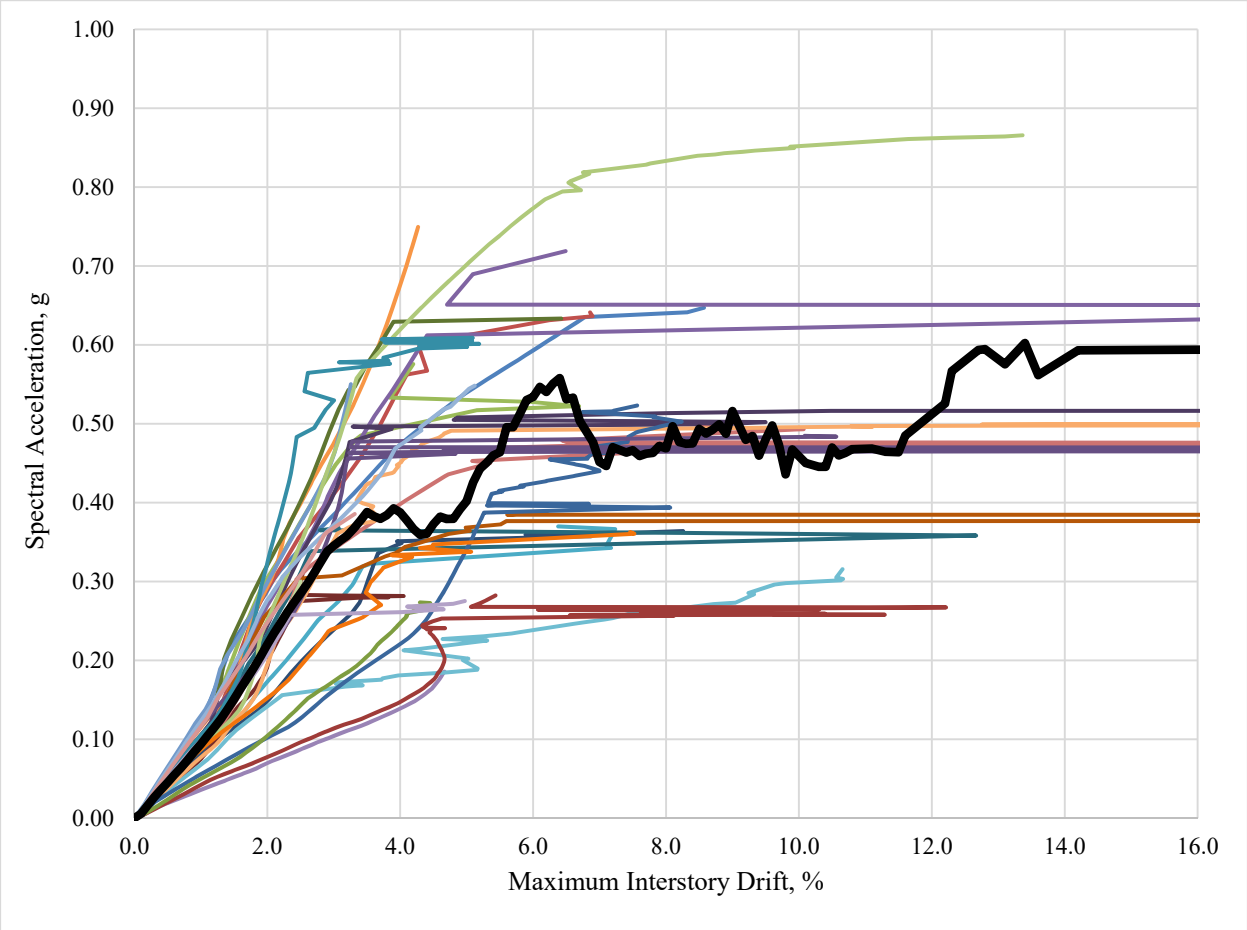


*Figure 5-1: Multi-Record IDA Curve Set for Frame PR14M0.66H1.4*

For each DM, the average IDA curves from all of the frames were combined onto a single graph to produce curve sets displaying the 31 average IDA curves. The average IDA curve sets for total roof drift, maximum interstory drift, and base shear are displayed in Figures 5-2, 5-3 and 5-4 respectively. The frames are designated in the legends by their PR connection characteristics as: stiffness – strength – strain hardening moment. The label 11-0.33-1.1 refers to the PR frame with a connection stiffness of $11EI/L$, a connection strength of $0.33M_p$, and a connection strain hardening moment of $1.1M_{cy}$.

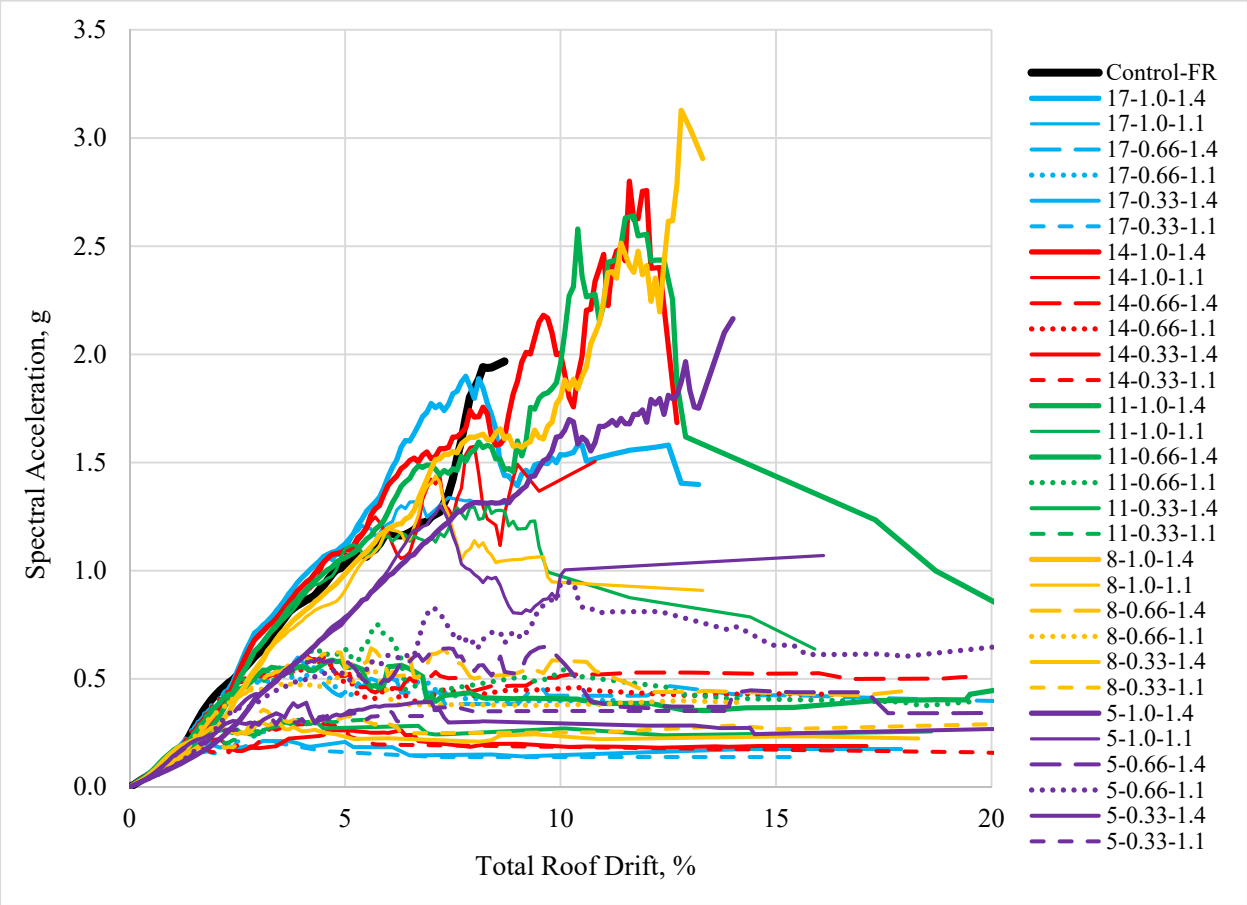


*Figure 5-2: Average Total Roof Drift IDA Curves for All Frames*

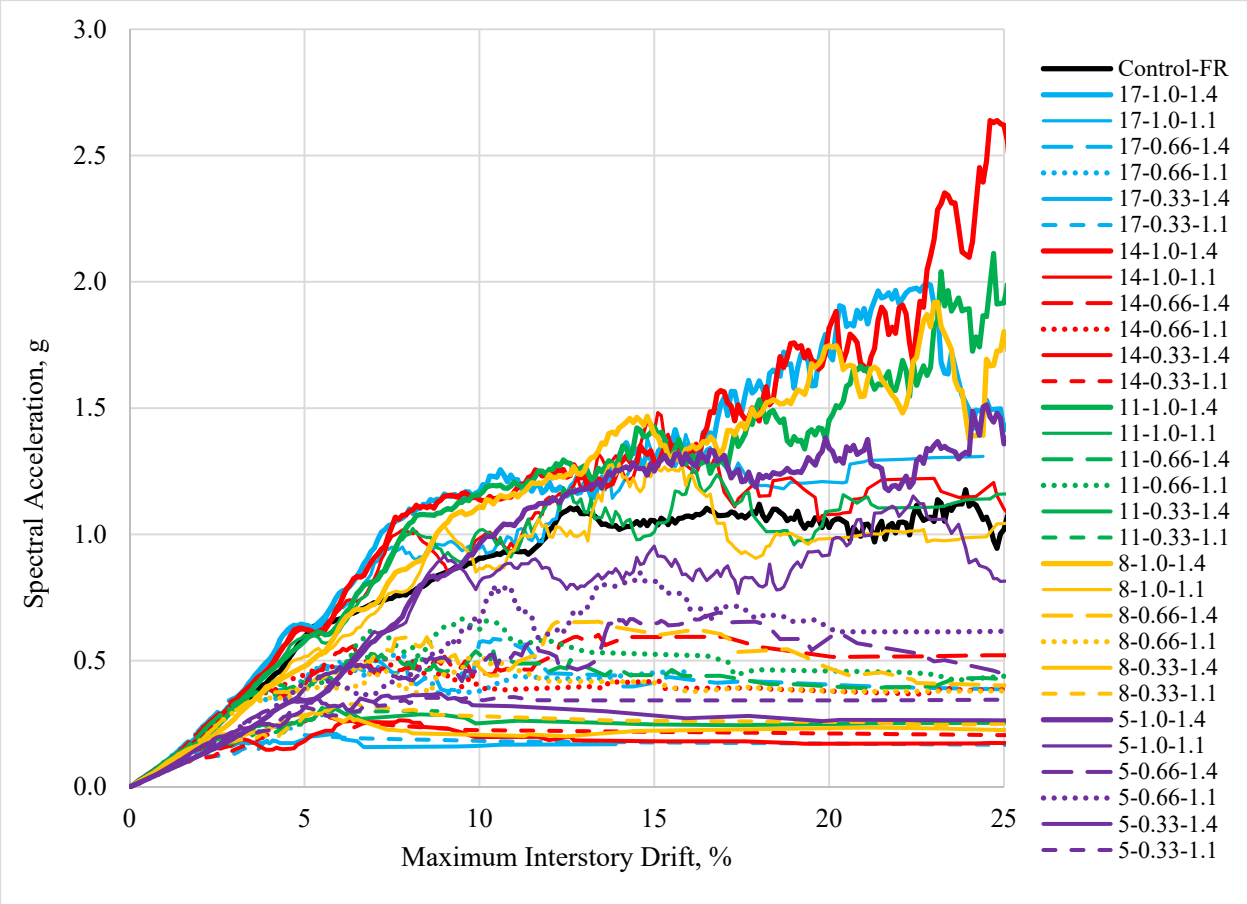


*Figure 5-3: Average Maximum Interstory Drift IDA Curves for All Frames*

Some general observations can be made from Figures 5-2, 5-3 and 5-4. First, the PR frames with connection strengths equal to $1.0M_p$ achieved levels of seismic intensity significantly greater than the PR frames with the two lower connection strengths. Moreover, the levels of seismic intensity reached by the PR frames with connection strengths equal to $0.66M_p$ are only slightly greater than the levels attained by those with connection strengths equal to $0.33M_p$. Earlier yielding of the connections, which can introduce earlier dissipation of the input energy imparted to the structures by an earthquake, does not appear to mitigate the adverse effects that increase the demands on the structures. Therefore, the average IDA curves for the PR frames with the two

lower connection yield strengths are less comparable to the control frame when measured against the PR frames with the higher connection yield strength.

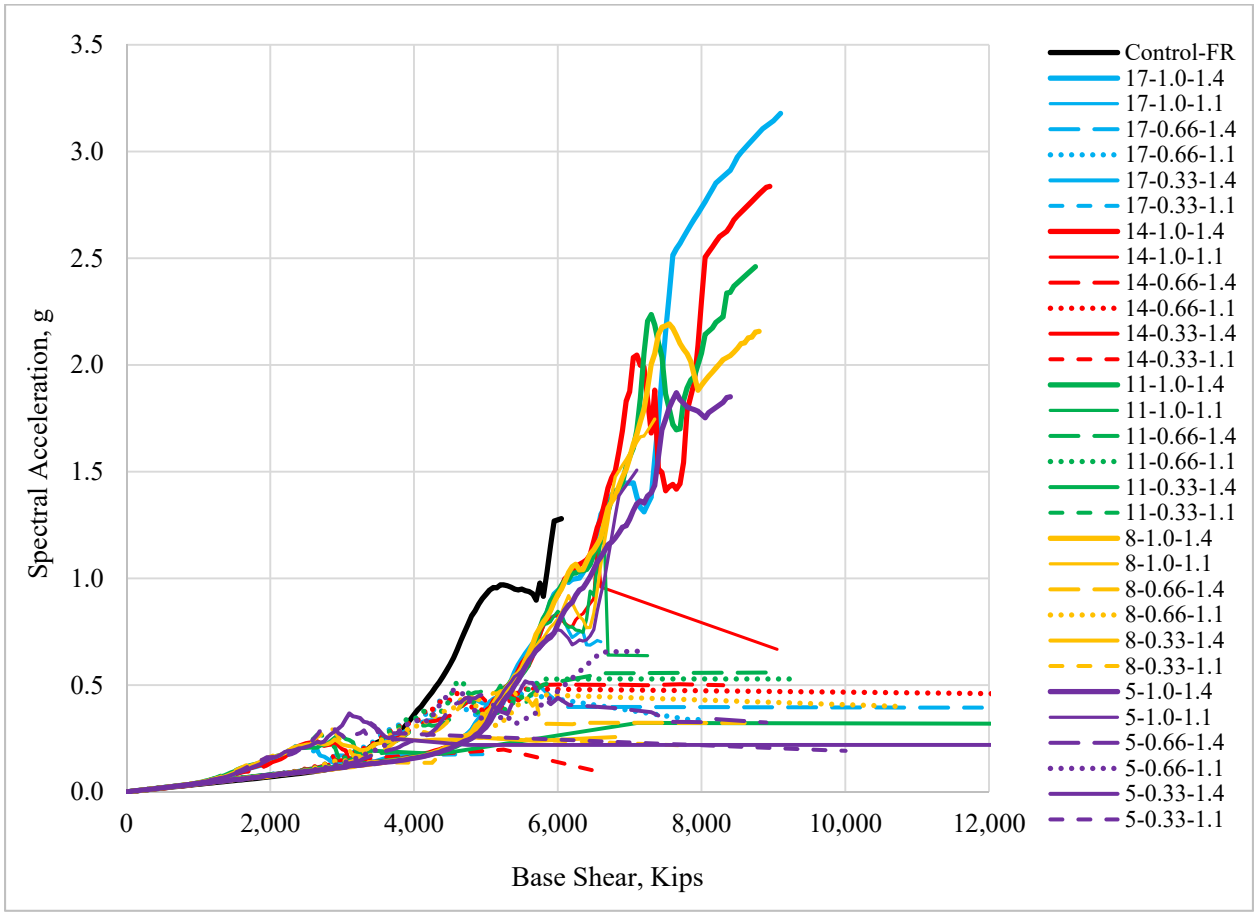


*Figure 5-4: Average Base Shear IDA Curves for All Frames*

After breaking down the plots of the IDA curve sets, the results can be further examined. Figure 5-5 shows the average total roof drift IDA curves for the frames with $1.0M_p$ connection strengths. This figure reveals that the PR frame with $17EI/L$ connection stiffness and $1.4M_{cy}$ connection strain hardening moment achieved lower levels of spectral acceleration at greater levels of roof drift than the equivalent PR frames with lower connection stiffness. Additionally, the PR frames with a strain hardening moment of $1.4M_{cy}$ achieved total levels of spectral acceleration equivalent to or greater than the control frame.

Furthermore, the PR frames with the lower strain hardening moment achieved levels of spectral acceleration that were only slightly less than the those achieved by their $1.4M_{cy}$ counterparts. This result reveals the global effects that the levels of connection strain hardening can have on a building. Also of interest is the fact that the PR frame that achieved the highest level of spectral acceleration incorporated a connection stiffness of $8EI/L$, less than half of the connection stiffness of the PR frame with $17EI/L$ connection stiffness. This result reveals the fact that a moment-resisting frame with stiffer connections is not guaranteed to be able to endure stronger seismic events.

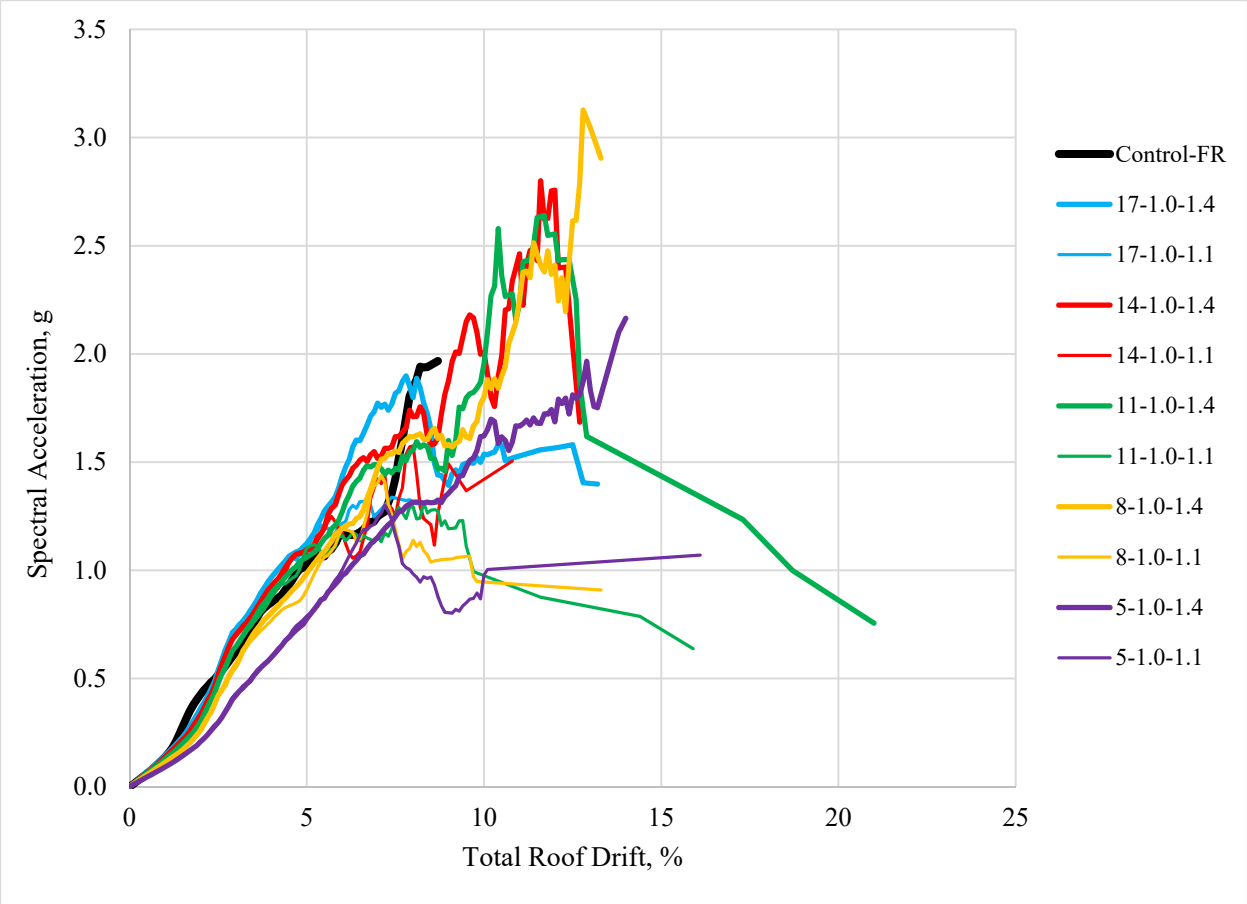


*Figure 5-5: Average Total Roof Drift IDA Curves for $1.0M_p$ Connection Strength*

Figure 5-6 further supports the findings from the average roof drift IDA curve sets. The average maximum interstory drifts of the PR frames with a connection strength of $1.0M_p$ and connection stiffnesses of $17EI/L$, $14EI/L$, and $11EI/L$ were less than those of the control frame for nearly all common levels of spectral acceleration. Additionally, all of the PR frames with a connection yield strength of $1.0M_p$ and a connection strain hardening moment of $1.4M_{cy}$ reached higher levels of spectral acceleration than the control frame. Also, the average IDA curves for the equivalent PR frames with a connection strain hardening moment of $1.1M_{cy}$ were very similar to the control frame.

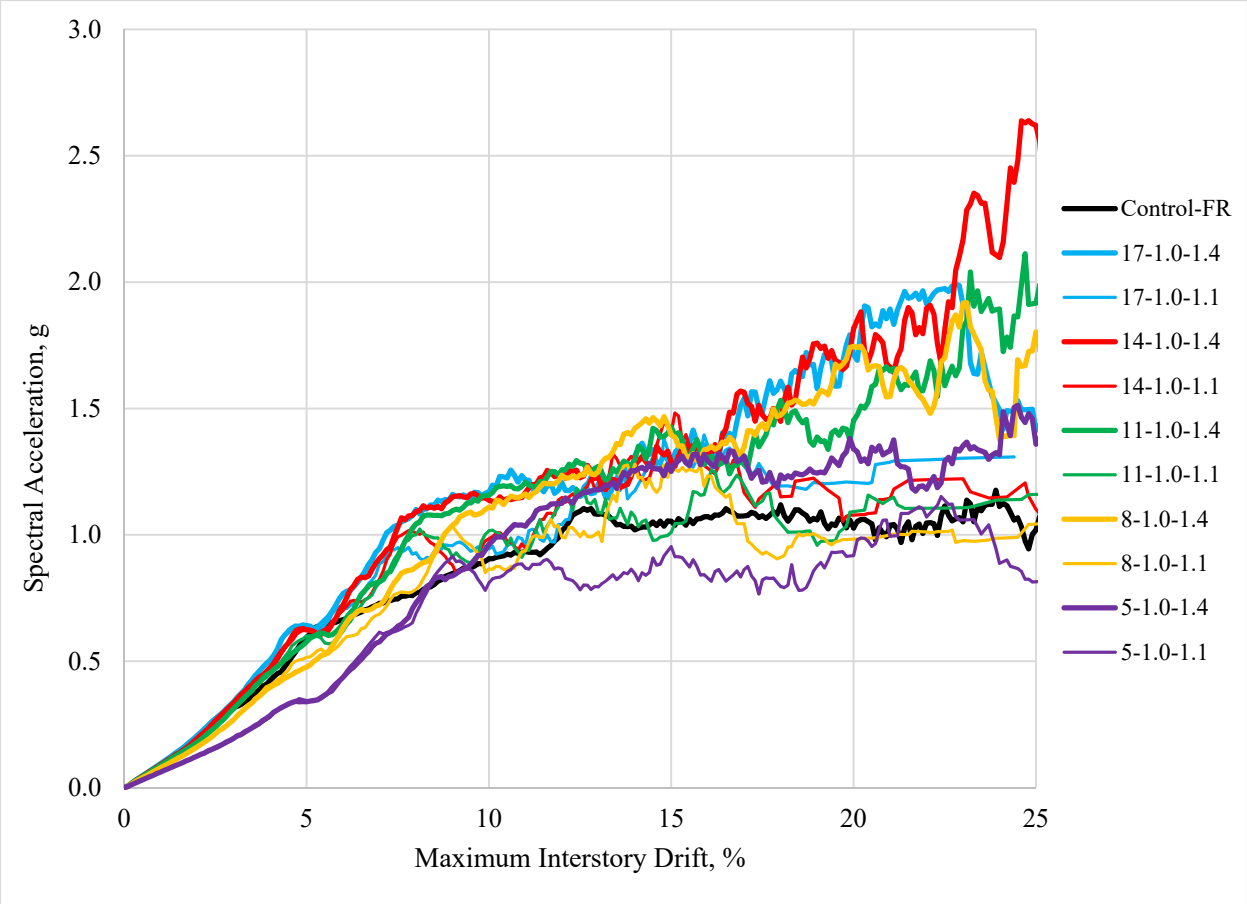


*Figure 5-6: Average Maximum Interstory Drift IDA Curves for $1.0M_p$ Connection Strength*

Figure 5-7 highlights the average base shear IDA curves for the PR frames with a connection yield strength of 1.0$M_p$ and the control frame. As is illustrated in the figure, the control frame accumulated less base shear than the PR frames at all common levels of spectral acceleration. Generally, the control frame base shear was about 80% of the base shears for the PR frames. However, all of the PR frames with a connection strength of 1.0$M_p$ and a strain hardening moment of 1.4$M_{cy}$, achieved significantly higher total levels of spectral acceleration than the control frame. The respective PR frames with a connection stiffness of 17$EI/L$ and 14$EI/L$ reached spectral acceleration levels that were at least double that of the control frame.

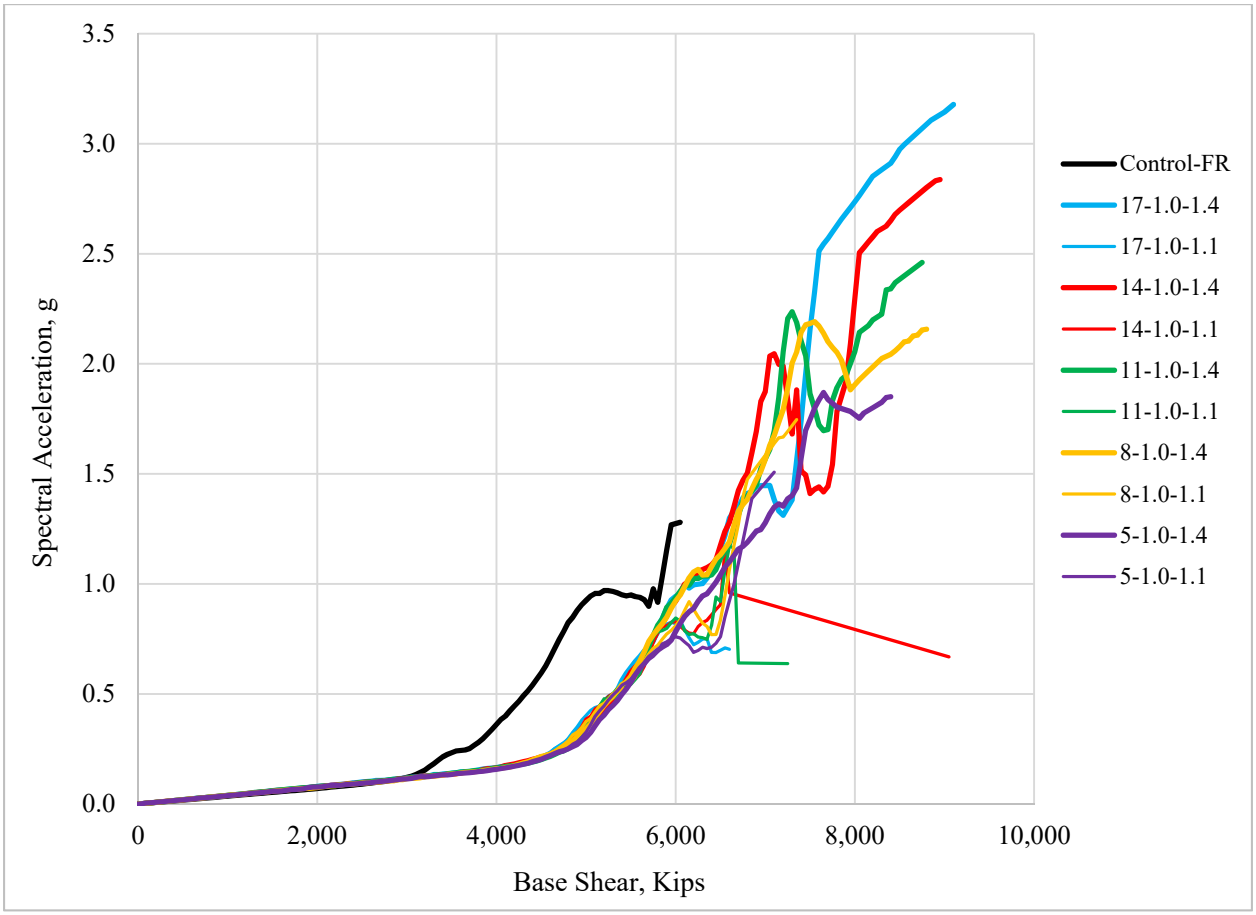


*Figure 5-7: Average Base Shear IDA Curves for 1.0$M_p$ Connection Strength*

Furthermore, the magnitudes of base shear associated with each degree of connection stiffness for these PR frames are highly similar for low to medium levels of spectral acceleration. The PR frames had to acquire higher levels of spectral acceleration before deviations in their levels of base shear became substantial. Also, the final levels of spectral acceleration achieved by the PR frames match the levels of stiffness in the connections. Figure 5-7 illustrates that as the connection stiffness increases, the total level of spectral acceleration attained by the frames also increases.

The lower levels of stiffness in the connections had a disproportionate effect on the seismic behavior of the frames. The increase in fundamental period, resulting from lower connection stiffness, seems to mitigate the increase in the severity of the global seismic demands on the structures. Also, the difference in strain hardening moment of the PR connections had noticeable impact on the seismic behavior of the frames. In general, the higher strain hardening moment consistently attributed to the achievement of higher levels of seismic intensity or demand.

Overall, the levels of connection stiffness and yield strength strongly influence the seismic behaviors of PR moment frames, with the connection yield strength having the greatest impact. As the stiffness levels decrease, the general slopes (IM/DM) of the IDA curves also decrease. Even though some of the PR frames experienced greater DMs than the control frame with increasing levels of IM, the PR frames with the higher connection strength were able to achieve greater levels of IM than the control frame. Consequently, using the right combination of connection stiffness, yield strength, and strain hardening moment can enable a PR moment-resisting frame to yield acceptable seismic behavior compared to a conventional moment-resisting frame constructed with FR connections.

For each of the DMs recorded, some of the PR frames experienced less demand than the control frame. The average IDA curves illustrated in Figures 5-5 and 5-6 demonstrate that some

of the PR frames experienced less total roof drifts and maximum interstory drifts than the control frame for corresponding levels of IM. The PR frames with a connection stiffness of at least 11*EI/L* or greater experienced demands that were either similar or less than the control frame. In general, the seismic demands of the control frame were only less than the seismic demands for the PR frames in regards to base shear. However, the maximum seismic intensity level achieved by the control frame was never greater than the maximum intensity levels achieved by the all of the PR frames.

# Chapter 6: Summary and Conclusions

The goal of this research was to investigate the performance of PR frames in SMFs. The work presented herein aimed to develop an adequate comparison of the seismic performance between structural steel buildings using conventional FR moment-resisting frames and those using PR moment-resisting frames. The results of this work illustrate the variation in the seismic behavior of PR frames constructed with beam-to-column connections ranging from almost simple to almost FR with differing levels of strength and strain hardening. Based on the IDAs performed on the 31 frame models generated, the following conclusions were made.

First, buildings using an SFRS with PR connections can be constructed to have fundamental periods that are comparable to those using an SFRS with conventional FR connections. The sizes and configurations of the beams and columns need to be considered in the design of PR frames. The appropriate selection of beam and column sizes and their configurations can effectively be used to achieve fundamental periods that are either the same or slightly lower than designs using FR connections.

Second, the seismic demands of the PR frames were not only comparable to those for the control frame, but in some cases were less than those for the control frame. The appropriate combination of connection stiffness and strength can limit the global demands on a structure during an earthquake. It is recommended that buildings utilizing PR moment connections as part of the SFRS employ them in every beam to column joint. This increases the redundancy of the system and provides greater stability. Also, based on the levels of base shear measured in the PR frames in this study, it is recommended that PR buildings be designed for 120% of the base shear used to design conventional FR frame buildings.

Lastly, based on the results of this study, minimal levels of connection stiffness and strength should be mandated for PR connections in order to ensure a moment-resisting frame utilizing such connections can provide sufficient seismic performance. It is recommended that PR connections with levels of stiffness of at least 14*EI/L* or higher be used for seismic design in order to limit the amount of excessive drifts in a building during an earthquake. It is also recommended that PR connections with yield strengths equal to the full plastic moment capacity of the beams be used to ensure that buildings can achieve more severe levels of seismic intensity. These minimal levels of connection strength and stiffness will also mitigate any potential developments of strength and stiffness deterioration.

Today, PR connections can be designed and constructed to meet the connection performance requirements designated by AISC for SMFs. The results of this study demonstrate that buildings with PR moment frames will have similar, and sometimes improved, seismic performance compared to buildings with FR moment frames. Therefore, it is recommended that PR connections be accepted for prequalification in SMFs by AISC.

# Chapter 7: Future Research

This study investigated the impacts on the seismic performance of steel buildings using PR connections compared to those using conventional FR connections. However, further research is required to gain a complete understanding of the implications of incorporating PR connections in steel moment-resisting frames for seismic applications. This chapter will discuss recommendations for future investigation.

First, the impact on the cost of building a structure with PR connections as opposed to FR connections needs to be examined. The costs of using PR connections need to be comparable to the costs of using traditional FR connections in order for them to be a practical alternative in the building industry.

Second, the impact of arranging different patterns of PR connection stiffness and strength along the height and width of a building should be examined. Investigating stiffness and strength arrangements similar to those examined in Kozma et al. (2014) will produce a more thorough understanding of the efficiency and versatility of PR connections in steel buildings.

Third, a more comprehensive understanding of the different PR connection types and their properties needs to be acquired. The development of a database with this information, including connection stiffnesses, strengths, and ductility, would stimulate the effectiveness of designing buildings with PR connections.

Lastly, experimental testing should be conducted in order to verify the results of this study and to better understand the behavior and limitations of steel buildings using PR connections. It is suggested to utilize a prototype corresponding to the 9-story SAC building design employed in this study.

## Chapter 8: References


ANSI/AISC 341-10 (2010), *Seismic Provisions for Structural Steel Buildings*, American Institute of Steel Construction, Chicago, IL.

ANSI/AISC 358-10 (2011), *Prequalified Connections for Special and Intermediate Steel Moment Frames for Seismic Applications*, American Institute of Steel Construction, Chicago, IL.

ANSI/AISC 360-10 (2010), *Specification for Structural Steel Buildings*, American Institute of Steel Construction, Chicago, IL.

ASCE/SEI 7-10 (2010), *Minimum Design Loads for Buildings and Other Structures*, American Society of Civil Engineers, Reston, VA.

Chopra A.K. (2012), *Dynamics of Structures: Theory and Applications to Earthquake Engineering*, Prentice Hall, Upper Saddle River, NJ, pp. 165-194.

FEMA (2000), *State of the Art Report on Systems Performance of Steel Moment Frames Subject to Earthquake Ground Shaking*, FEMA-355C, prepared by the SAC Joint Venture on behalf of the Federal Emergency Management Agency, Washington D.C.

FEMA (2009), *Quantification of Building Seismic Performance Factors*, FEMA P695, prepared by the SAC Joint Venture on behalf of the Federal Emergency Management Agency, Washington D.C.

Kasai, K., Maison, B.F., and Mayangarum, A. (2000), *Effects of Partially Restrained Connection Stiffness and Strength on Frame Seismic Performance*, SAC/BD-99/17, SAC Joint Venture.

Kozma-Thomas, M.A. (2014), "Analytical Investigation of the Effect of Partially-Restrained Connections on Hybrid Moment-Resisting Steel Frames," MS Thesis. University of Cincinnati, Cincinnati, OH.

Kozma-Thomas M.A., Rassati G.A., Swanson J.A., Manning S.O., "Application of Partially and Fully Restrained Connections to Hybrid Moment-Resisting Frames for Seismic Loads", *EuroSteel 2014*, Naples, Italy, 2014.

Maison B.F., Kasai K. (2000), *Seismic Performance of 3 and 9 Story Partially Restrained Moment Frame Buildings*, SAC/BD-99/16, SAC Joint Venture.

OpenSees (2006), *Open System for Earthquake Engineering Simulation*, Computer Program, Pacific Earthquake Engineering Research Center, University of California, Berkeley, CA.

USGS (2008), *Interactive Deaggregations*, National Seismic Hazard Mapping Program (NSHMP) Hazard Maps, U.S. Geological Survey (USGS), Reston, VA.

Vamvatsikos D., Cornell C.A. (2002), "Incremental Dynamic Analysis", *Earthquake Engineering and Structural Dynamics*, Vol. 31, Issue 3, pp. 491-514.

## Appendix A: PR Connection Trilinear Moment-Rotation Curves

This Appendix contains the PR trilinear moment-rotation (M-Θ) characteristics for all of the beam sizes for each level of PR connection stiffness. Each PR connection moment-rotation curve is designated as ##-##, where the first number represents the connection yield strength ($1.0M_p$, $0.66M_p$, or $0.33M_p$) and the second number represents the level of connection strain-hardening moment ($1.4M_{cy}$ or $1.1M_{cy}$).

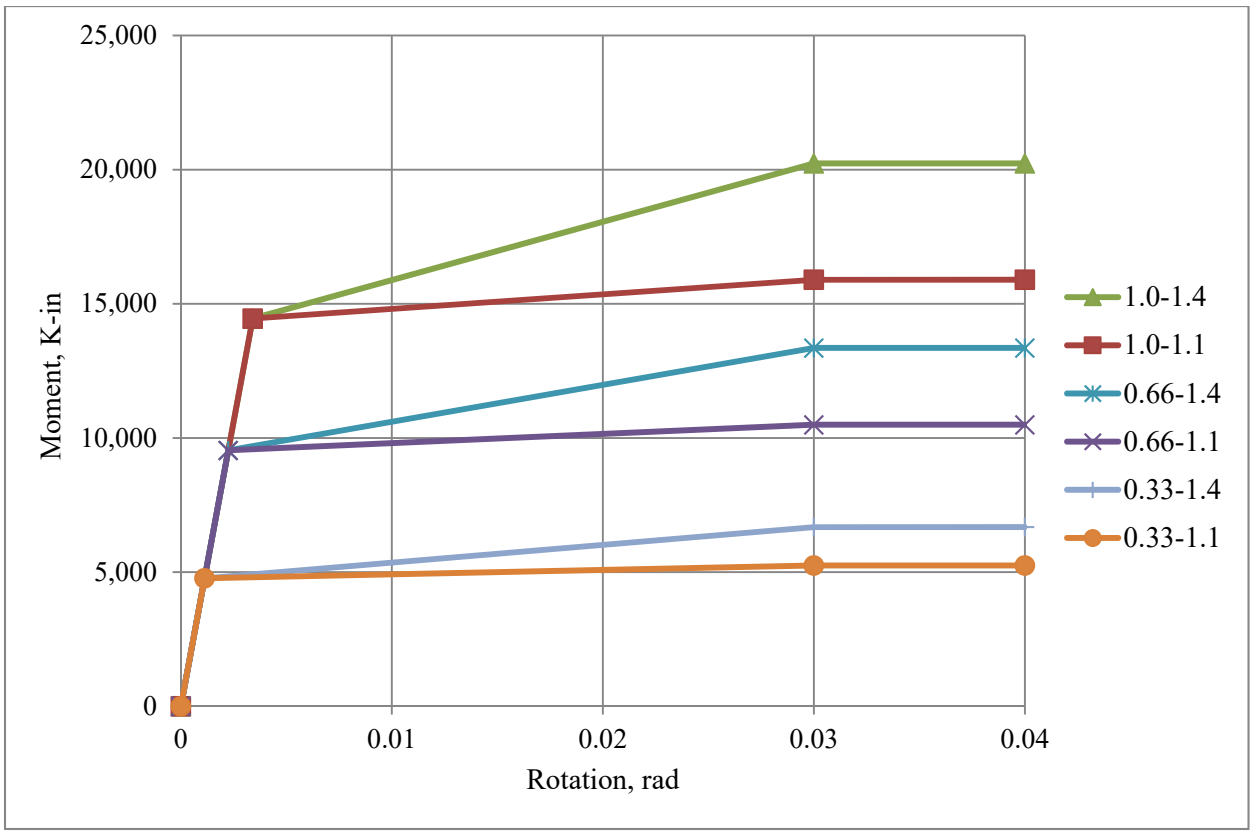


*Figure A-1: W24x104 Trilinear M-Θ Characteristics with 17EI/L Connection Stiffness*

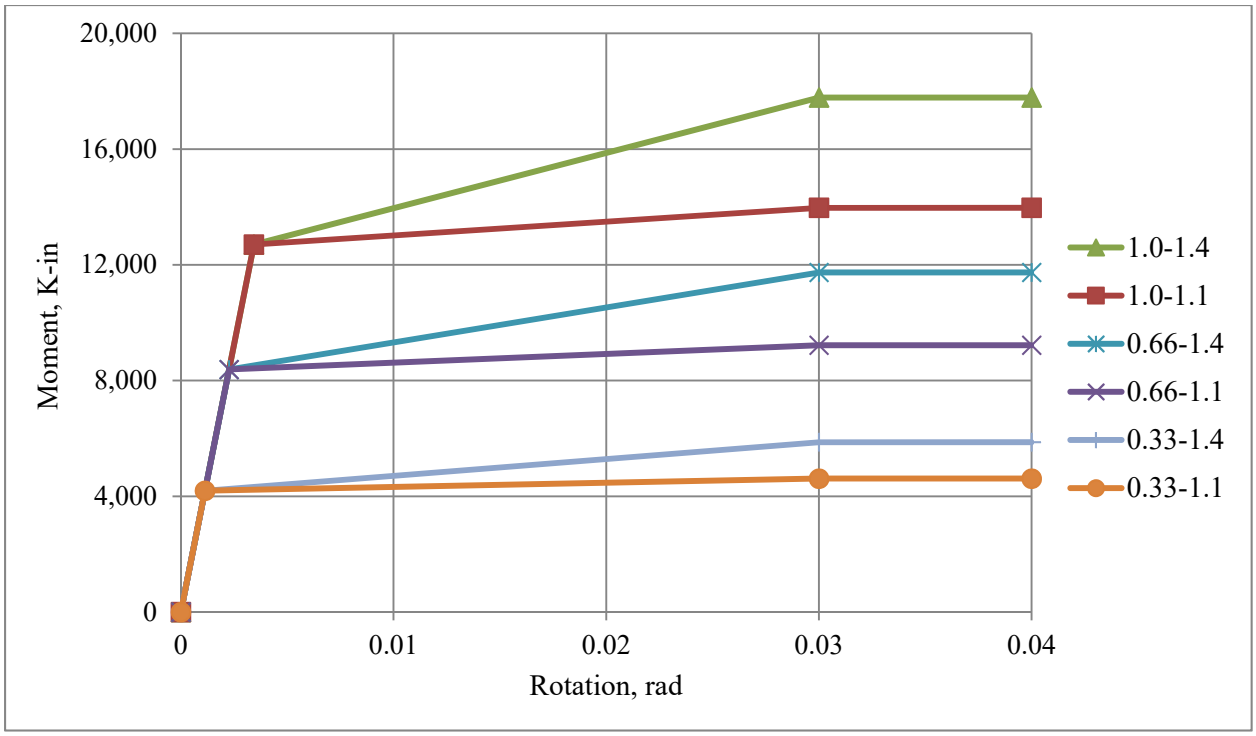


*Figure A-2: W24x94 Trilinear M-Θ Characteristics with 17EI/L Connection Stiffness*

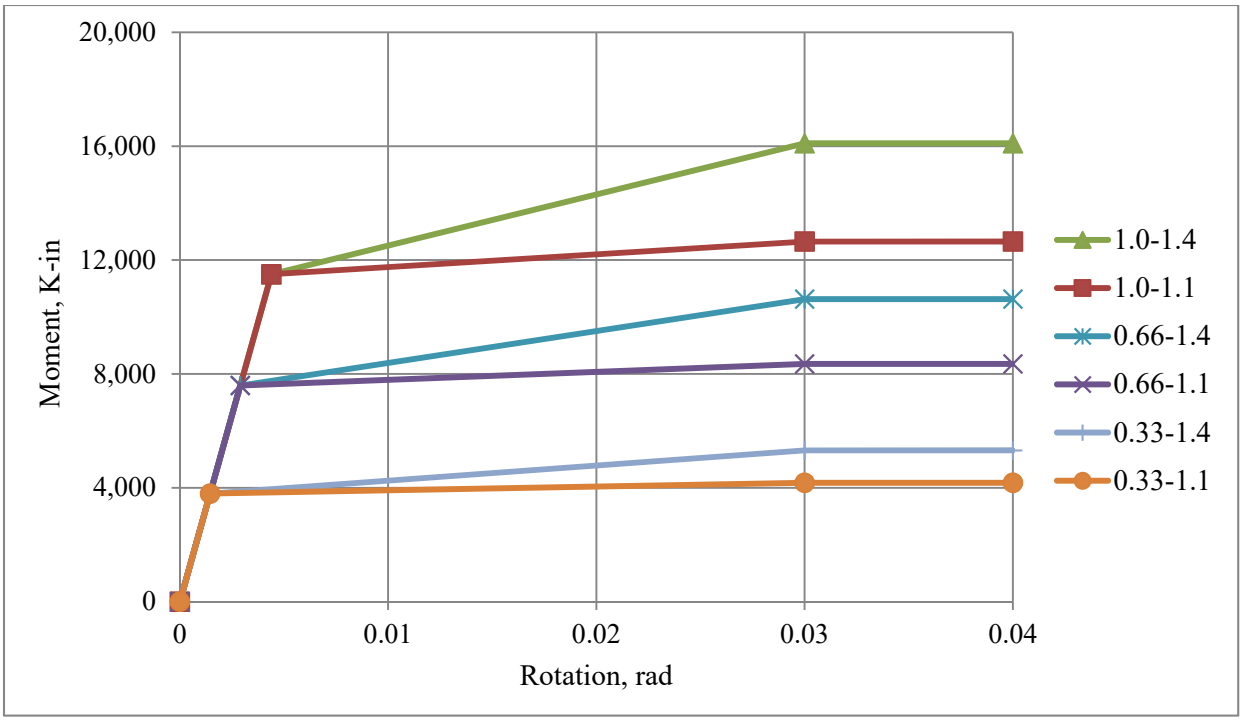


*Figure A-3: W18x106 Trilinear M-Θ Characteristics with 17EI/L Connection Stiffness*

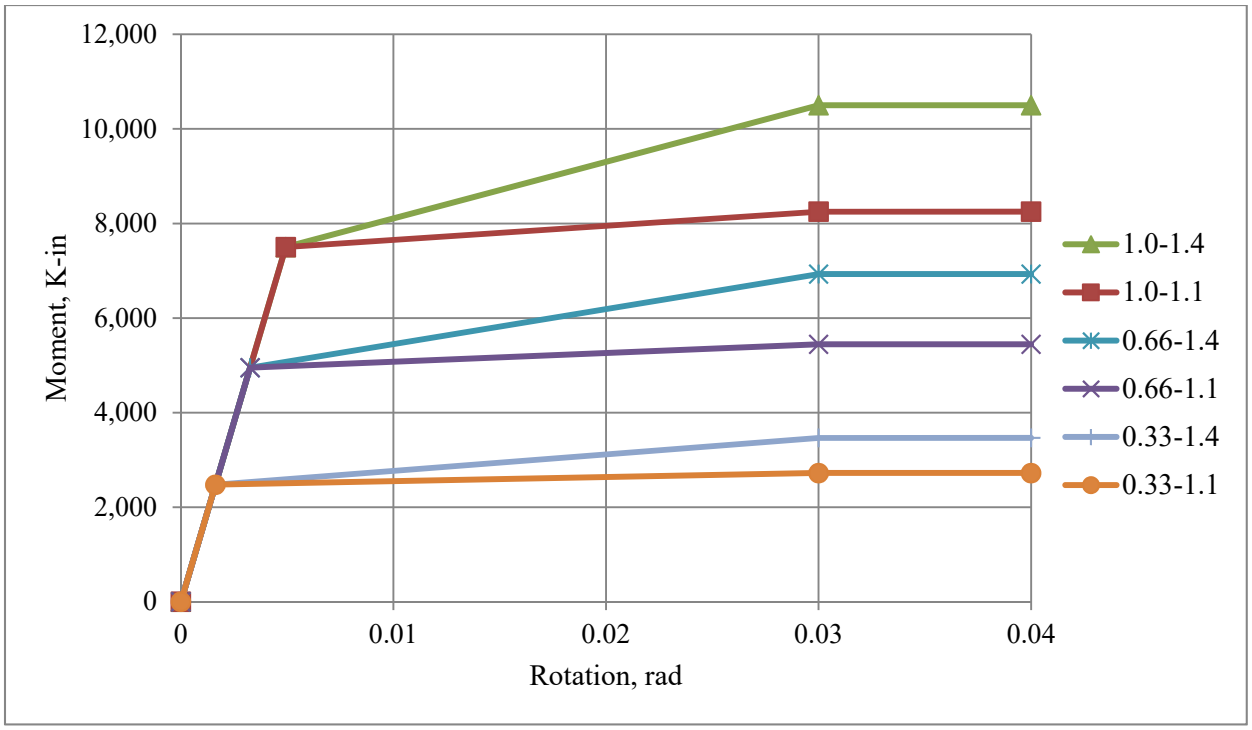


*Figure A-4: W16x77 Trilinear M-Θ Characteristics with 17EI/L Connection Stiffness*

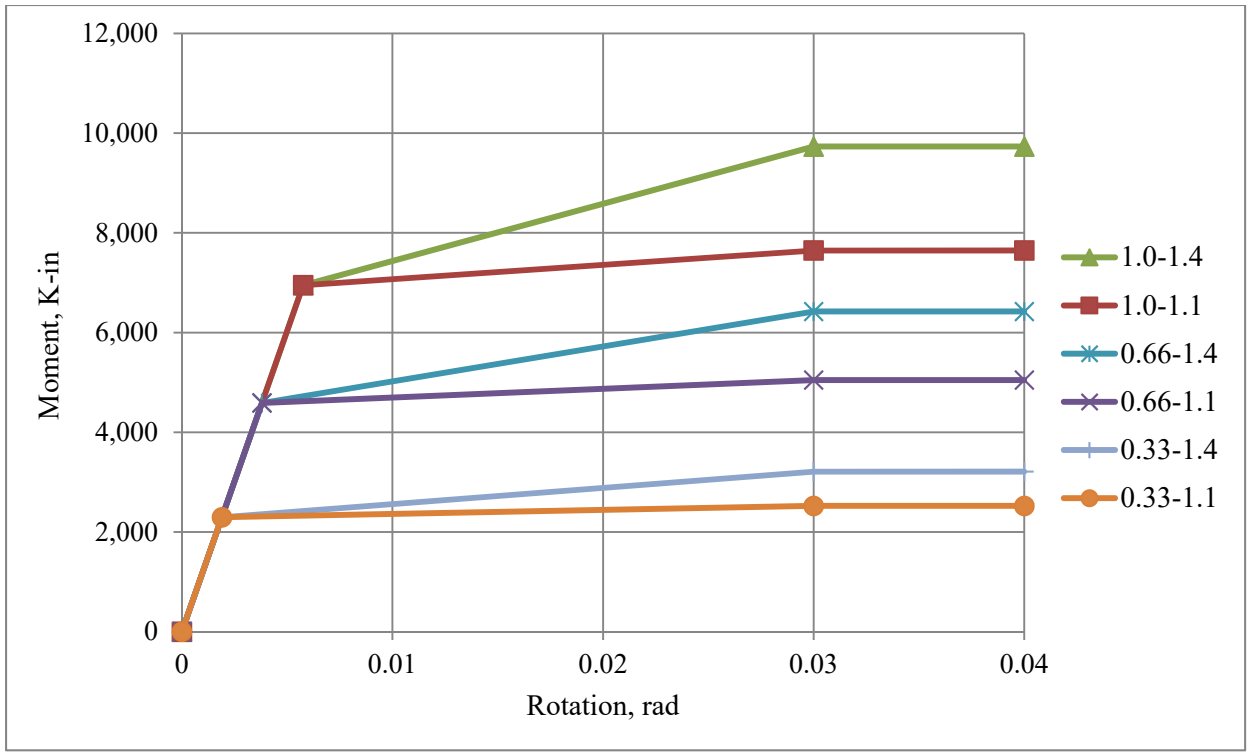


*Figure A-5: W14x82 Trilinear M-Θ Characteristics with 17EI/L Connection Stiffness*

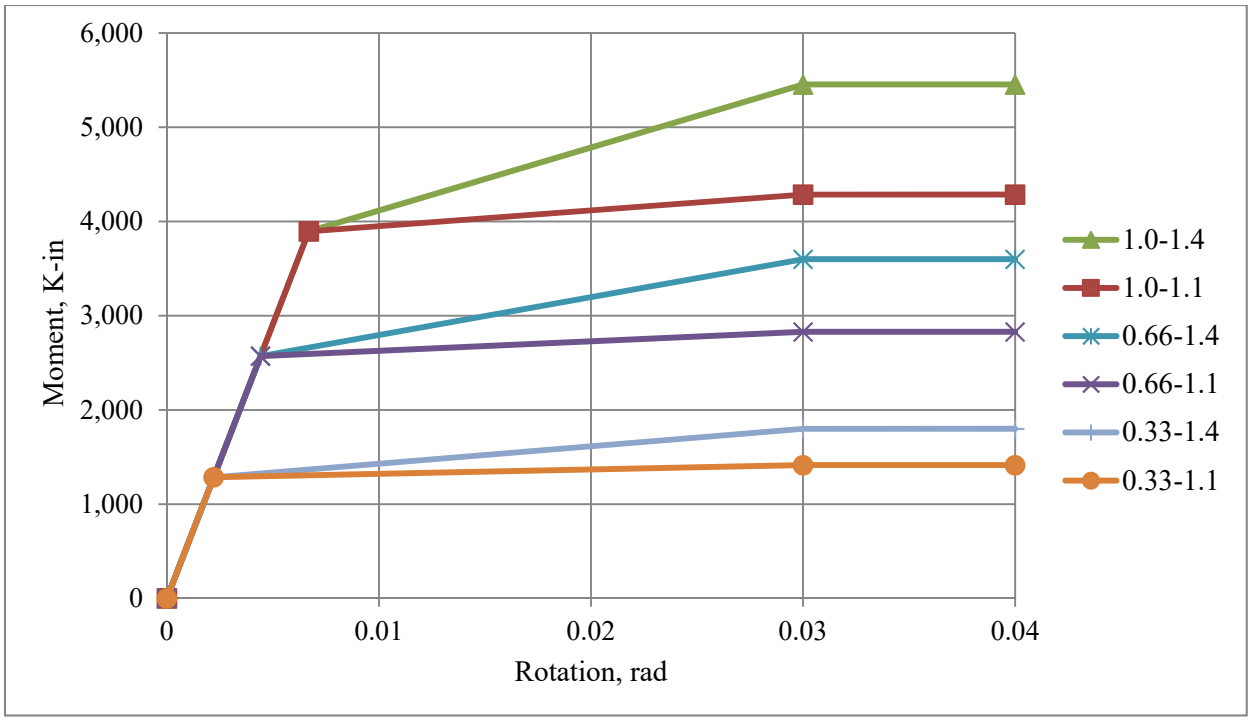


*Figure A-6: W12x53 Trilinear M-Θ Characteristics with 17EI/L Connection Stiffness*

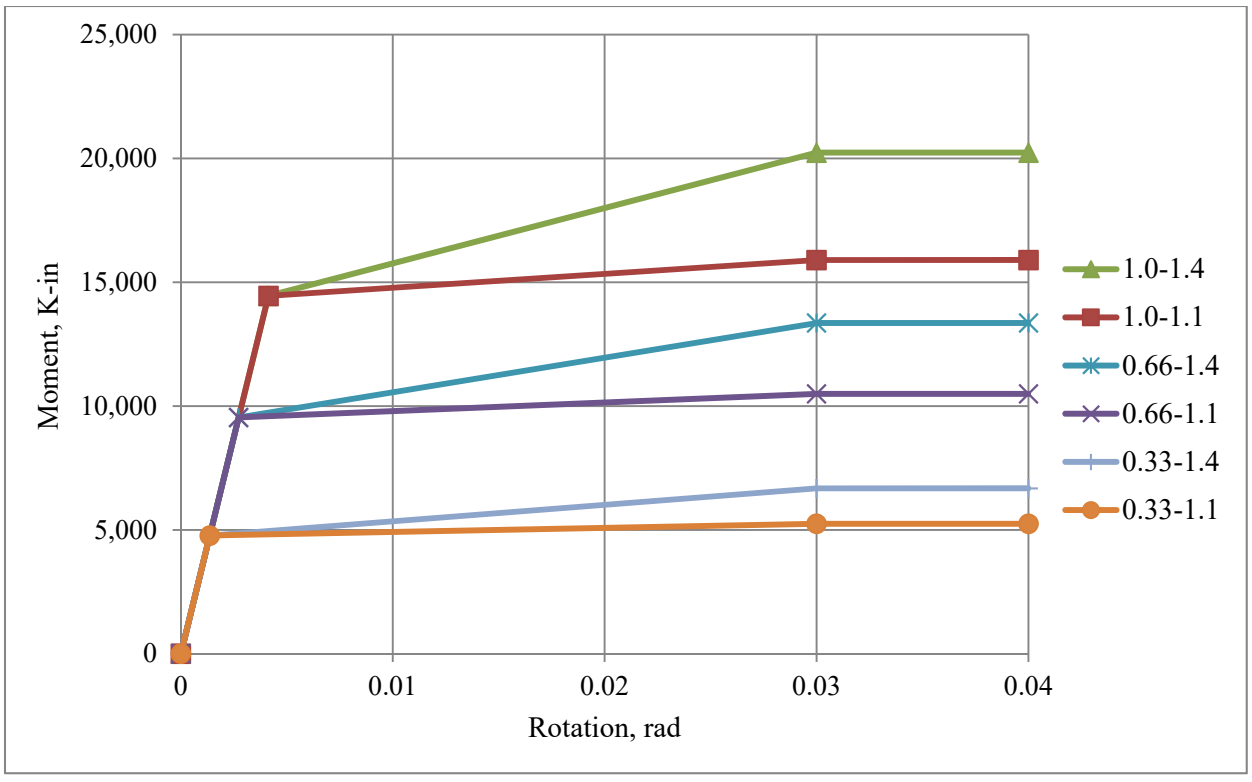


*Figure A-7: W24x104 Trilinear M-Θ Characteristics with 14EI/L Connection Stiffness*

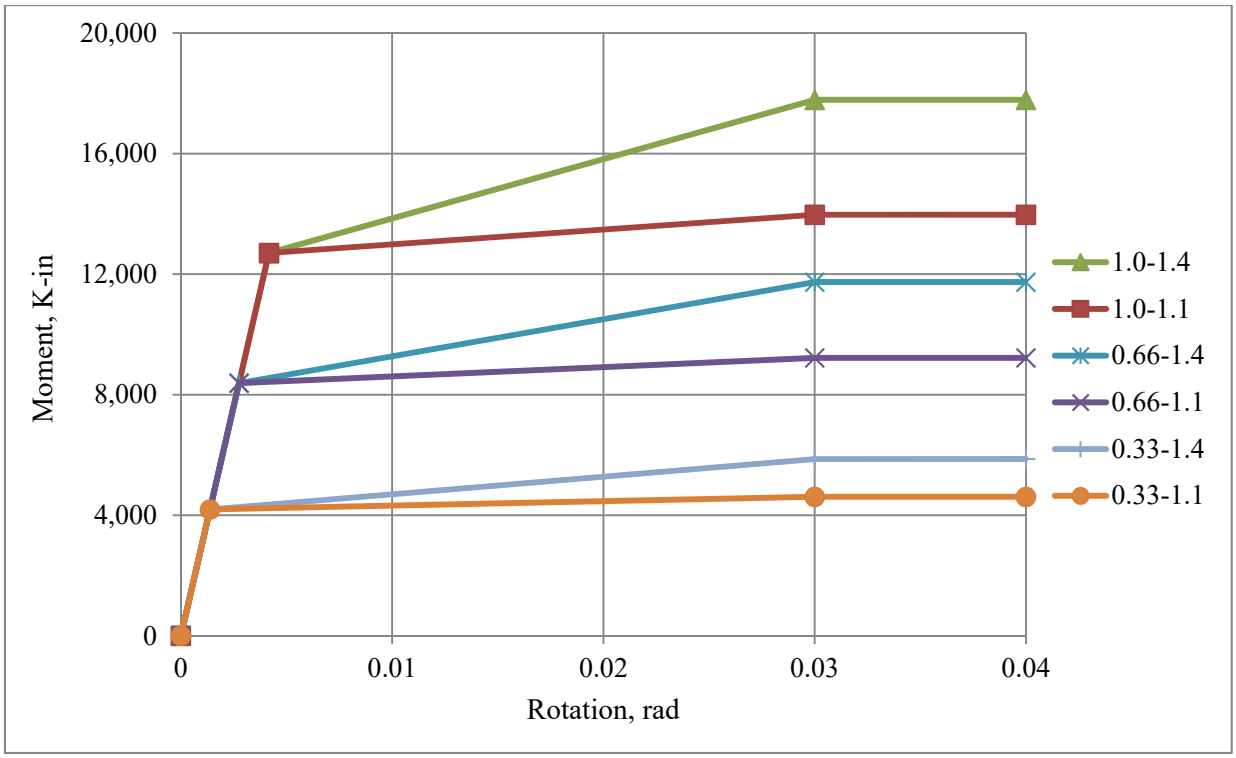


*Figure A-8: W24x94 Trilinear M-Θ Characteristics with 14EI/L Connection Stiffness*

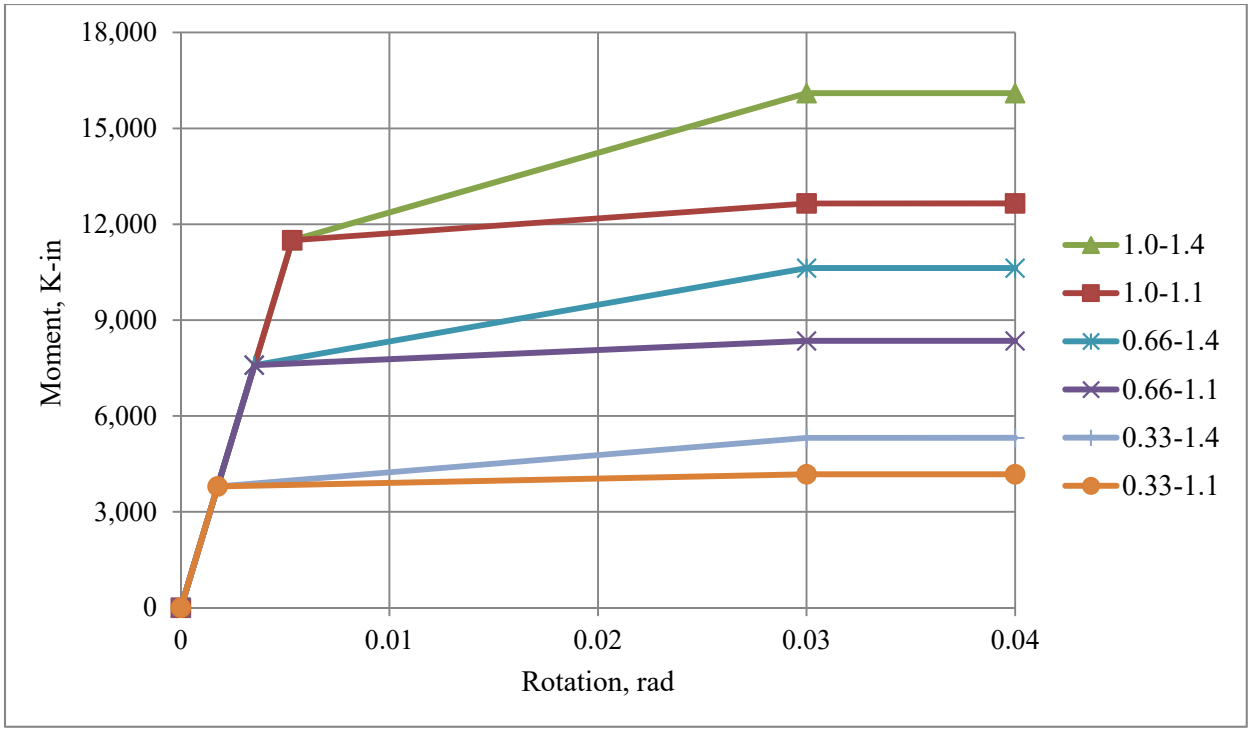


*Figure A-9: W18x106 Trilinear M-Θ Characteristics with 14EI/L Connection Stiffness*

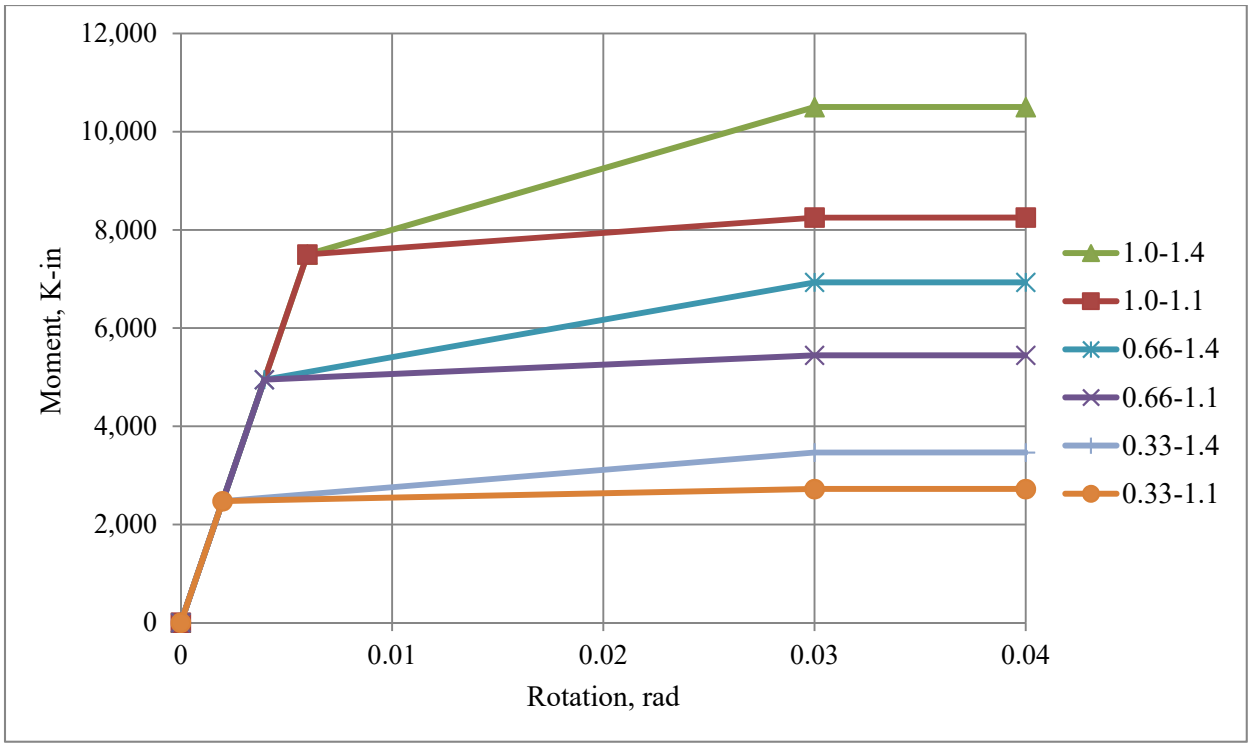


*Figure A-10: W16x77 Trilinear M-Θ Characteristics with 14EI/L Connection Stiffness*

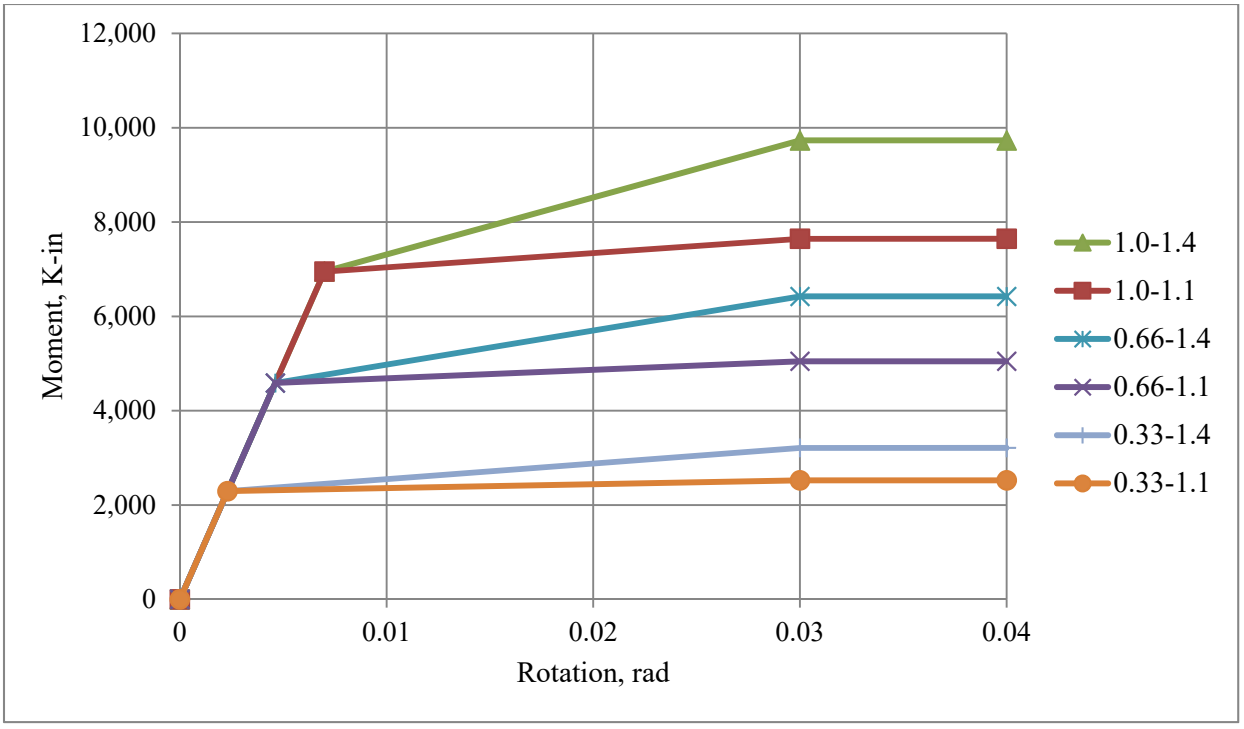


*Figure A-11: W14x82 Trilinear M-Θ Characteristics with 14EI/L Connection Stiffness*

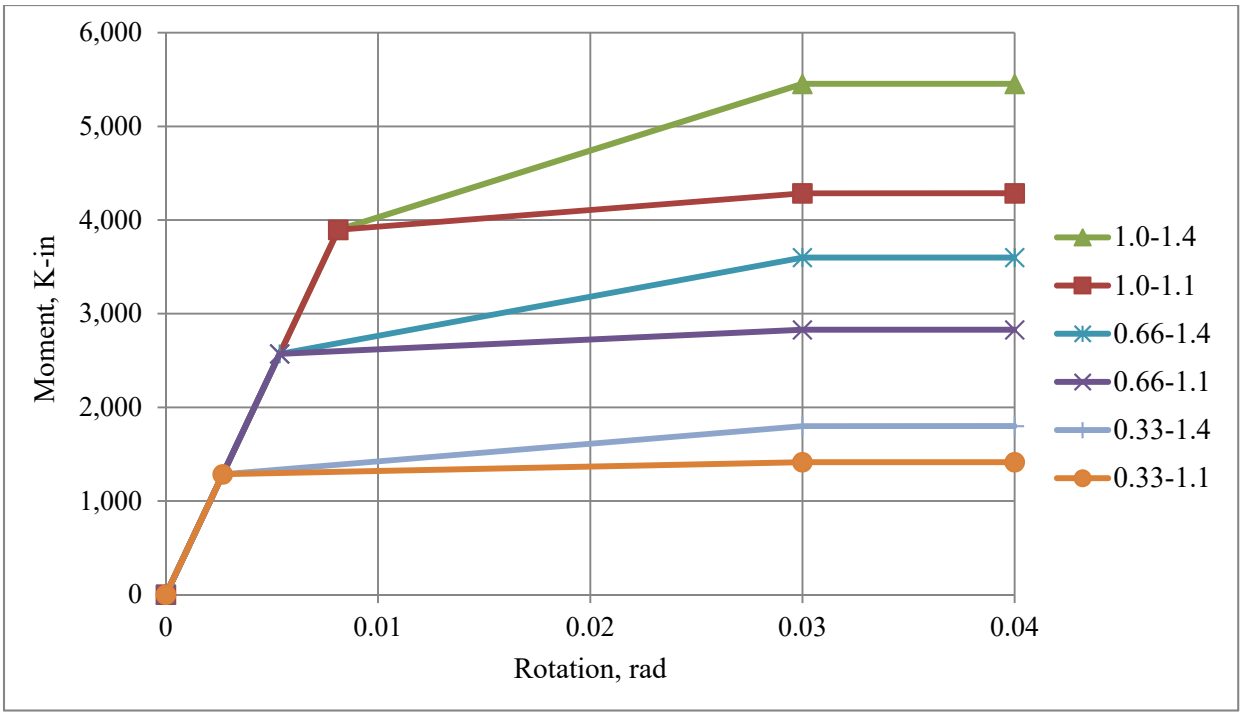


*Figure A-12: W12x53 Trilinear M-Θ Characteristics with 14EI/L Connection Stiffness*

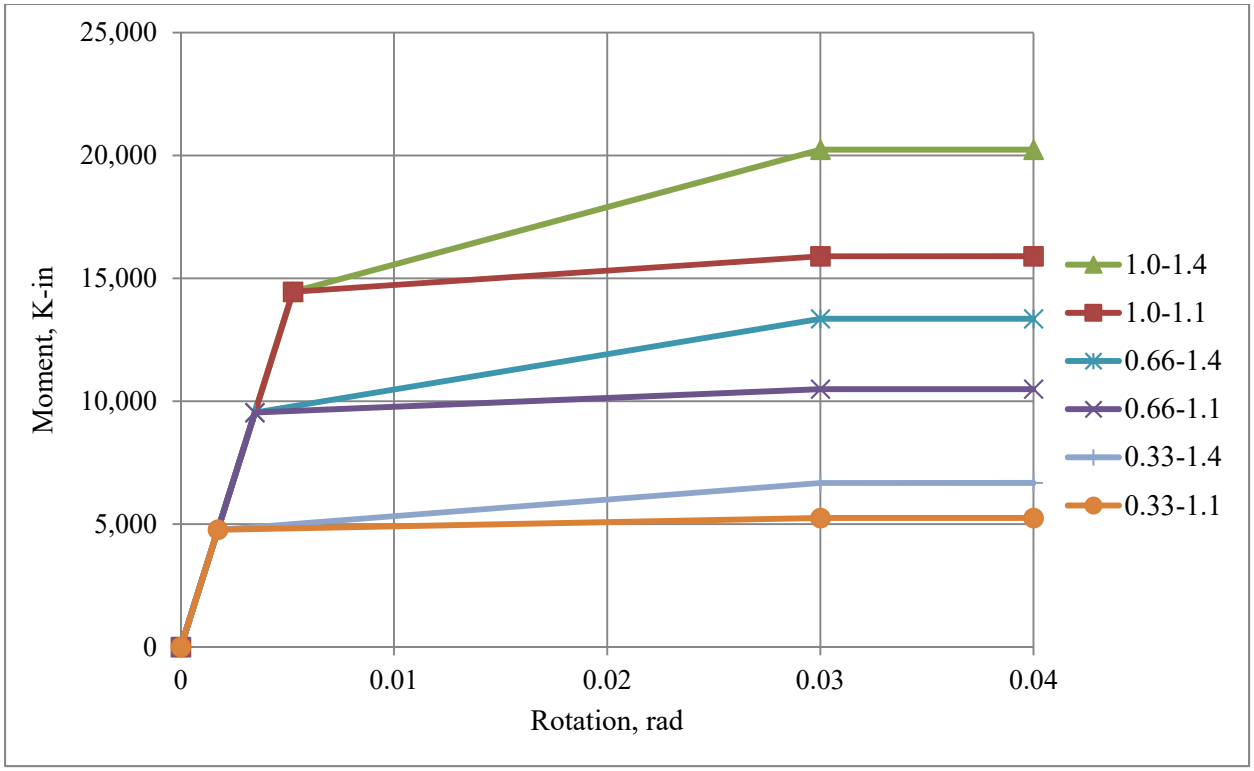


*Figure A-13: W24x104 Trilinear M-Θ Characteristics with 11EI/L Connection Stiffness*

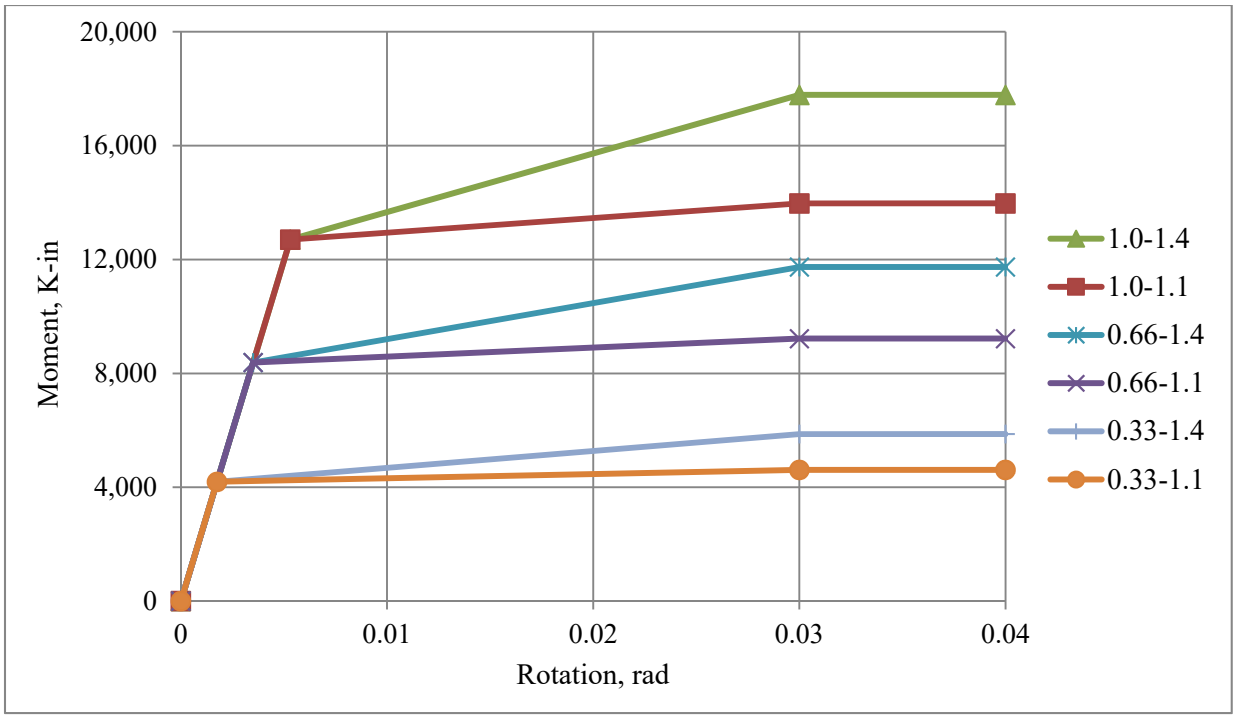


*Figure A-14: W24x94 Trilinear M-Θ Characteristics with 11EI/L Connection Stiffness*

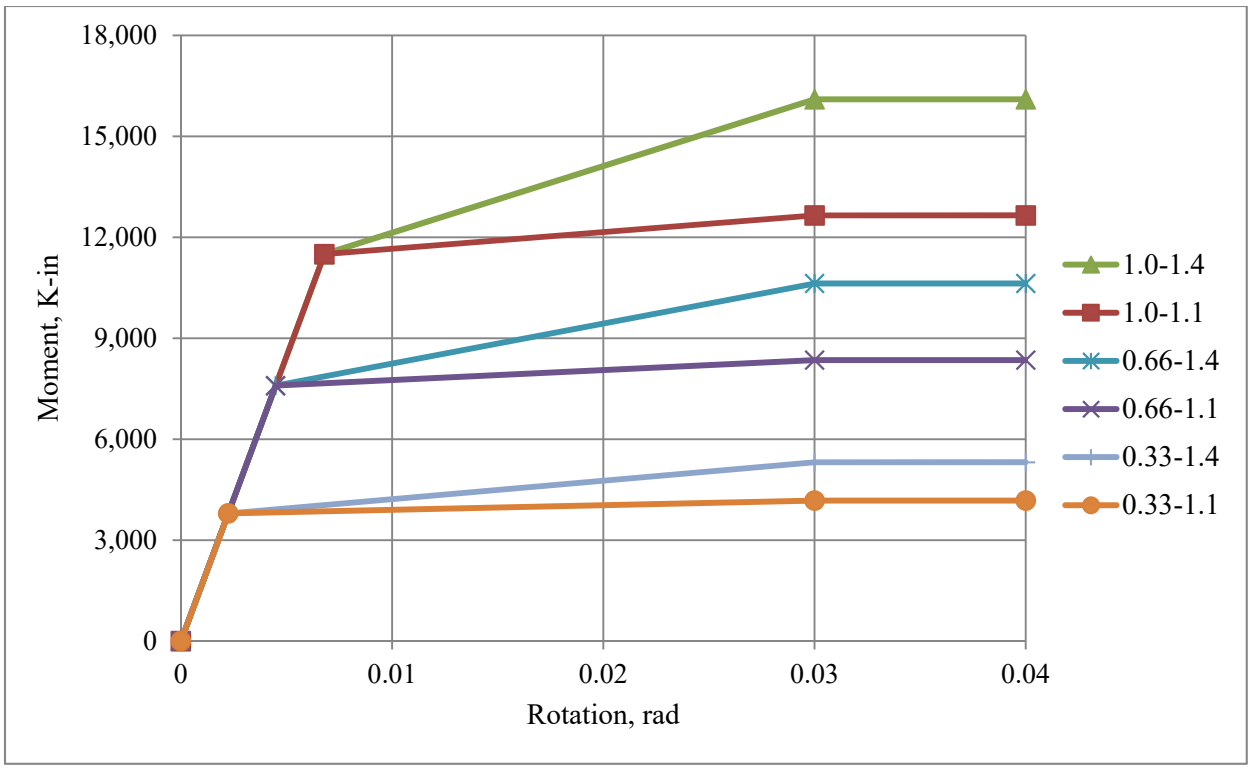


*Figure A-15: W18x106 Trilinear M-Θ Characteristics with 11EI/L Connection Stiffness*

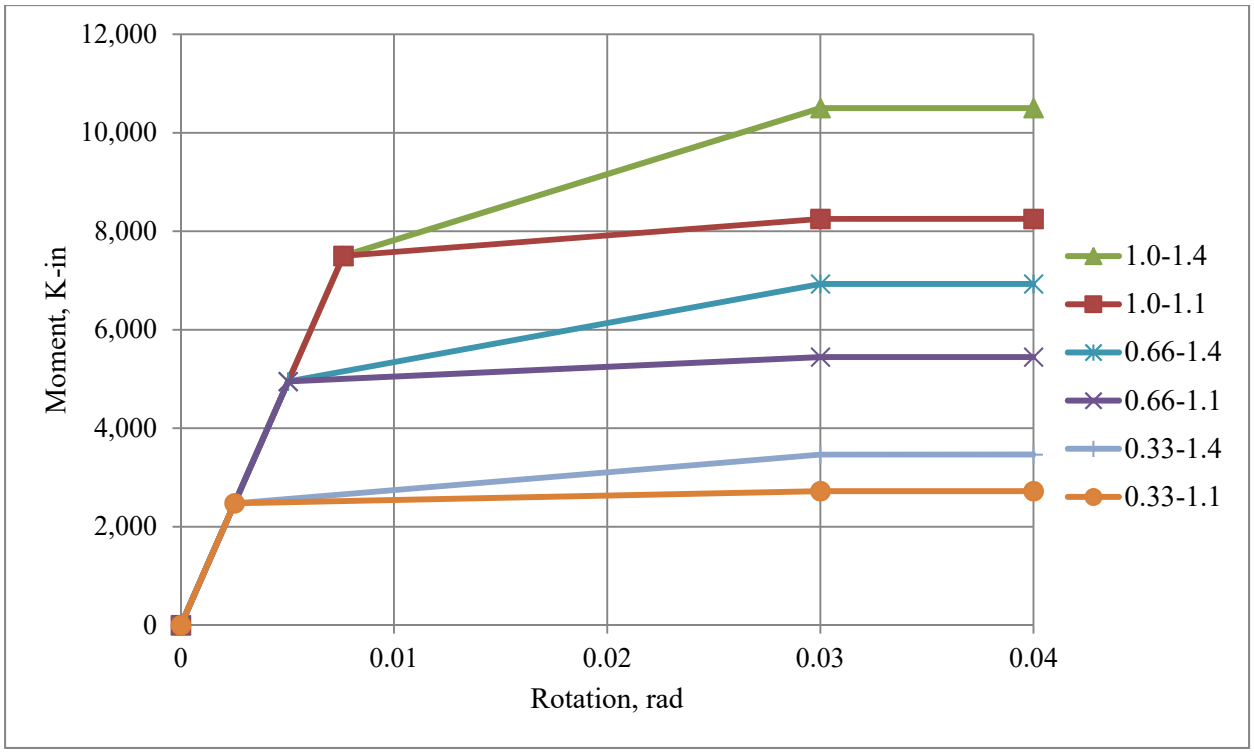


*Figure A-16: W16x77 Trilinear M-Θ Characteristics with 11EI/L Connection Stiffness*

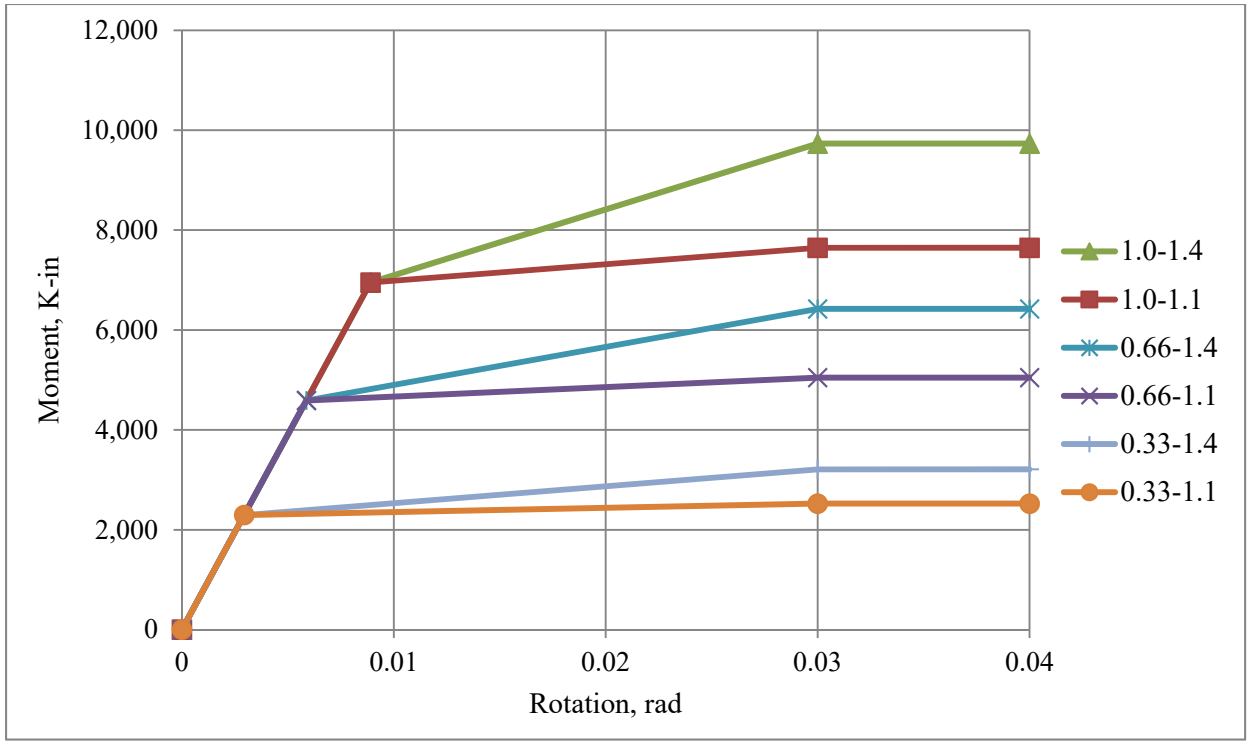


*Figure A-17: W14x82 Trilinear M-Θ Characteristics with 11EI/L Connection Stiffness*

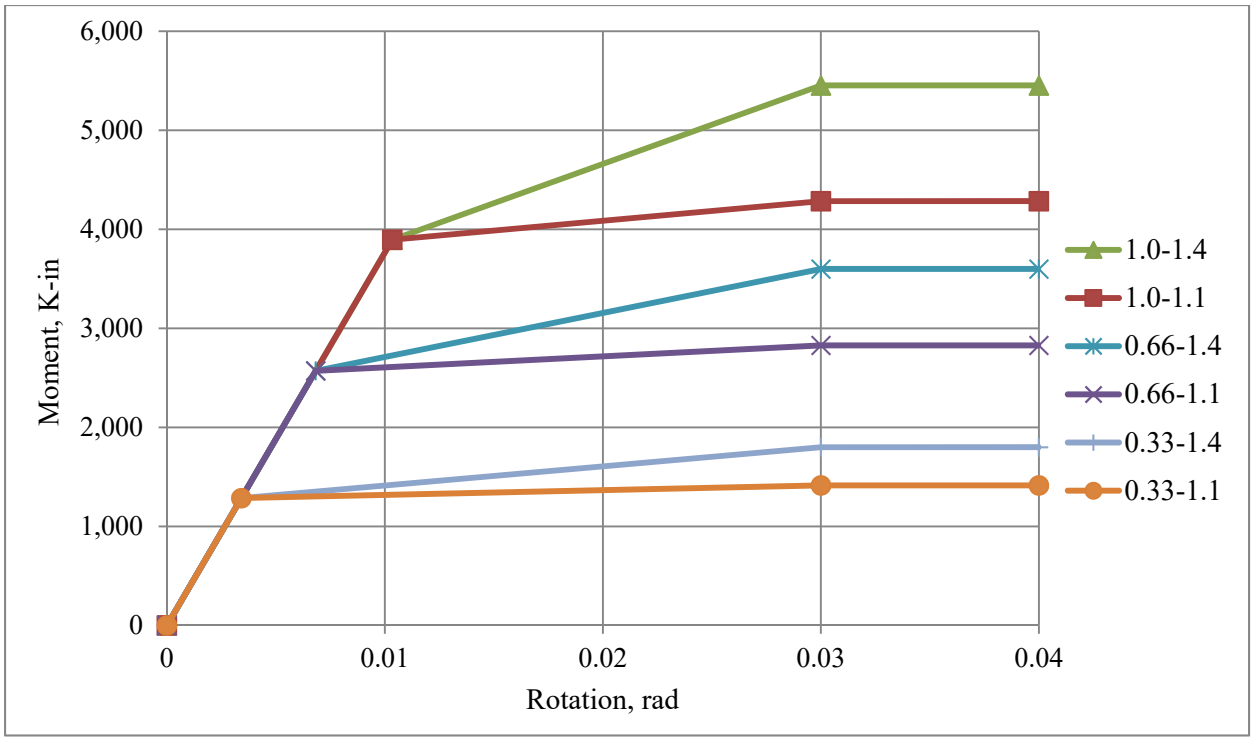


*Figure A-18: W12x53 Trilinear M-Θ Characteristics with 11EI/L Connection Stiffness*

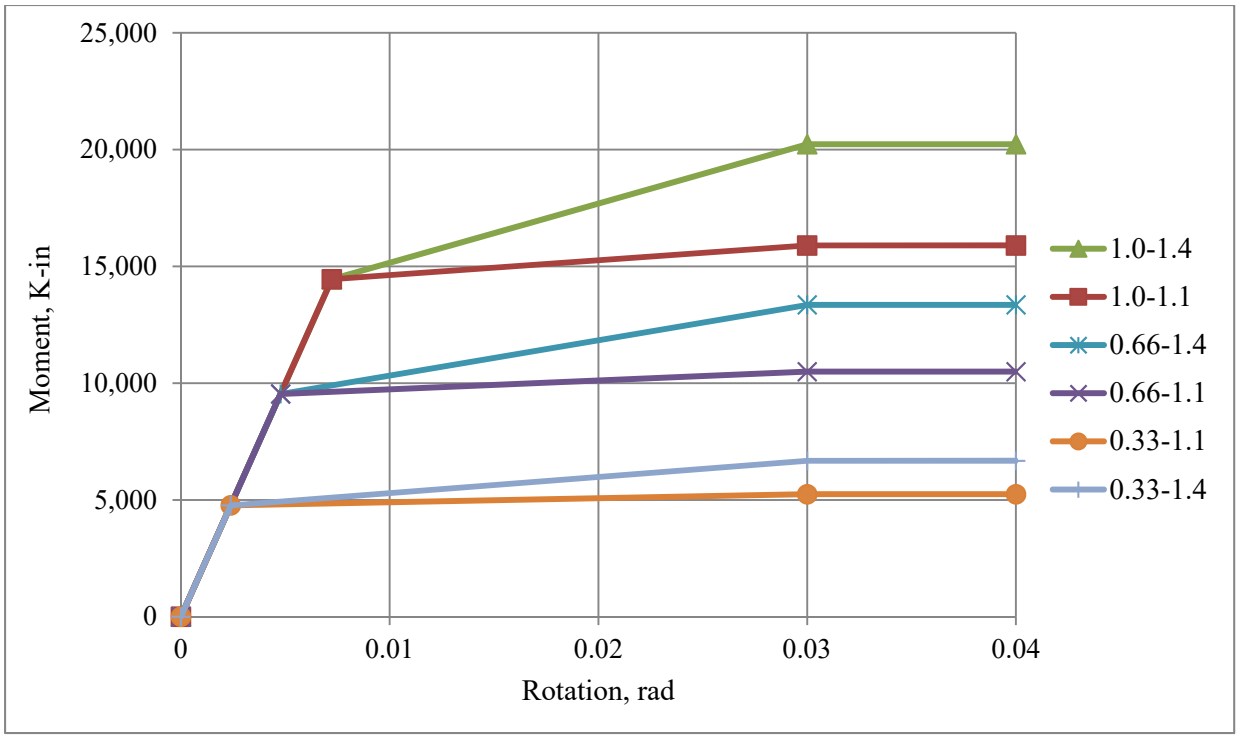


*Figure A-19: W24x104 Trilinear M-Θ Characteristics with 8EI/L Connection Stiffness*

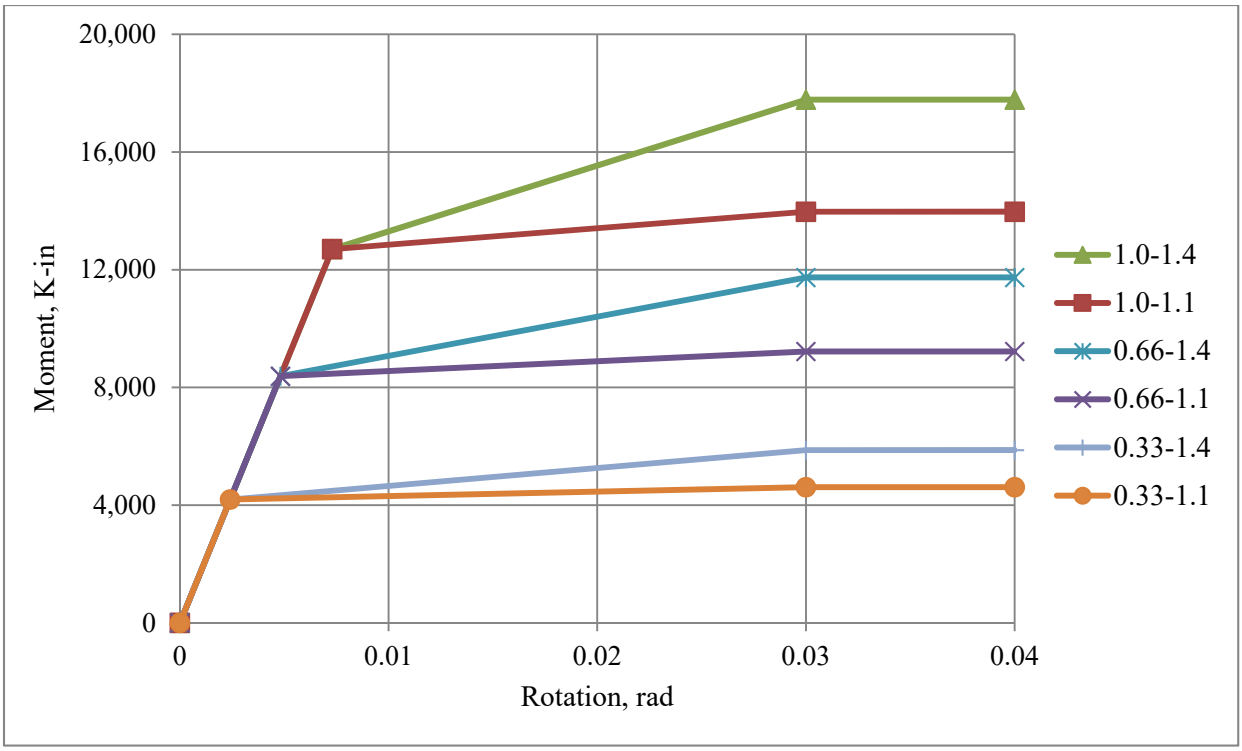


*Figure A-20: W24x94 Trilinear M-Θ Characteristics with 8EI/L Connection Stiffness*

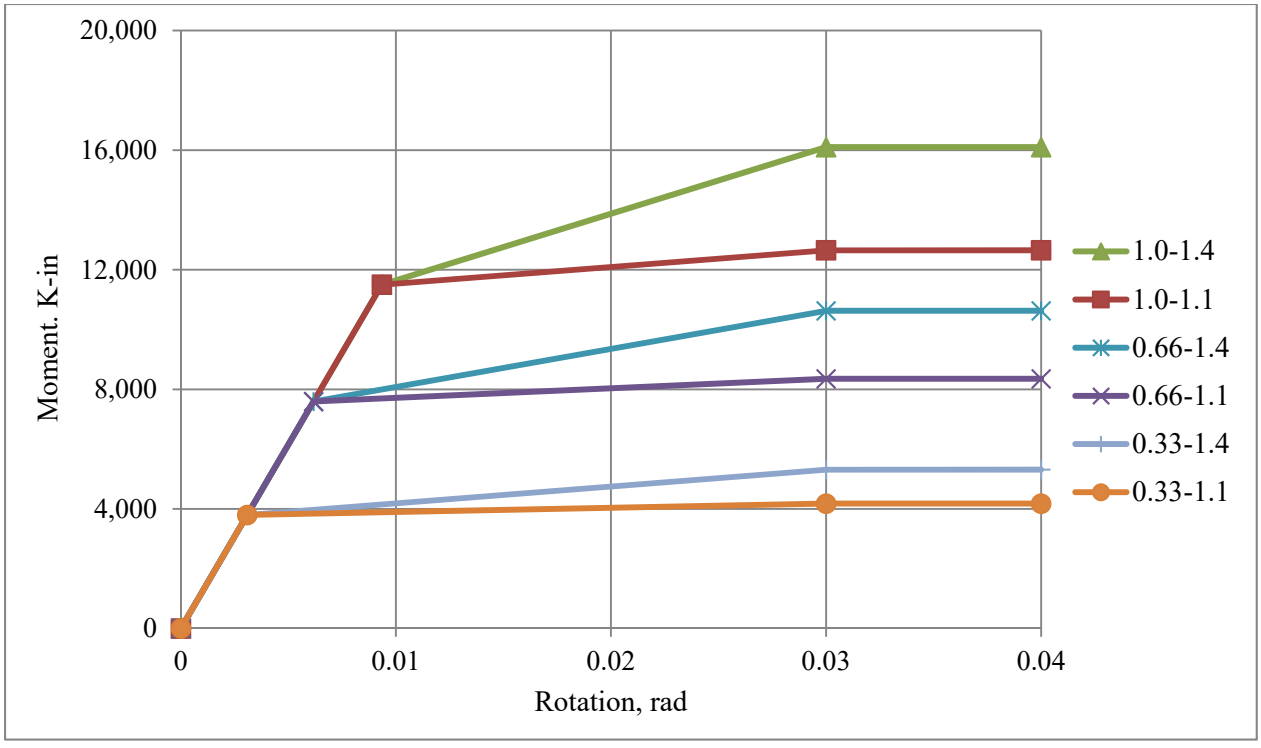


*Figure A-21: W18x106 Trilinear M-Θ Characteristics with 8EI/L Connection Stiffness*

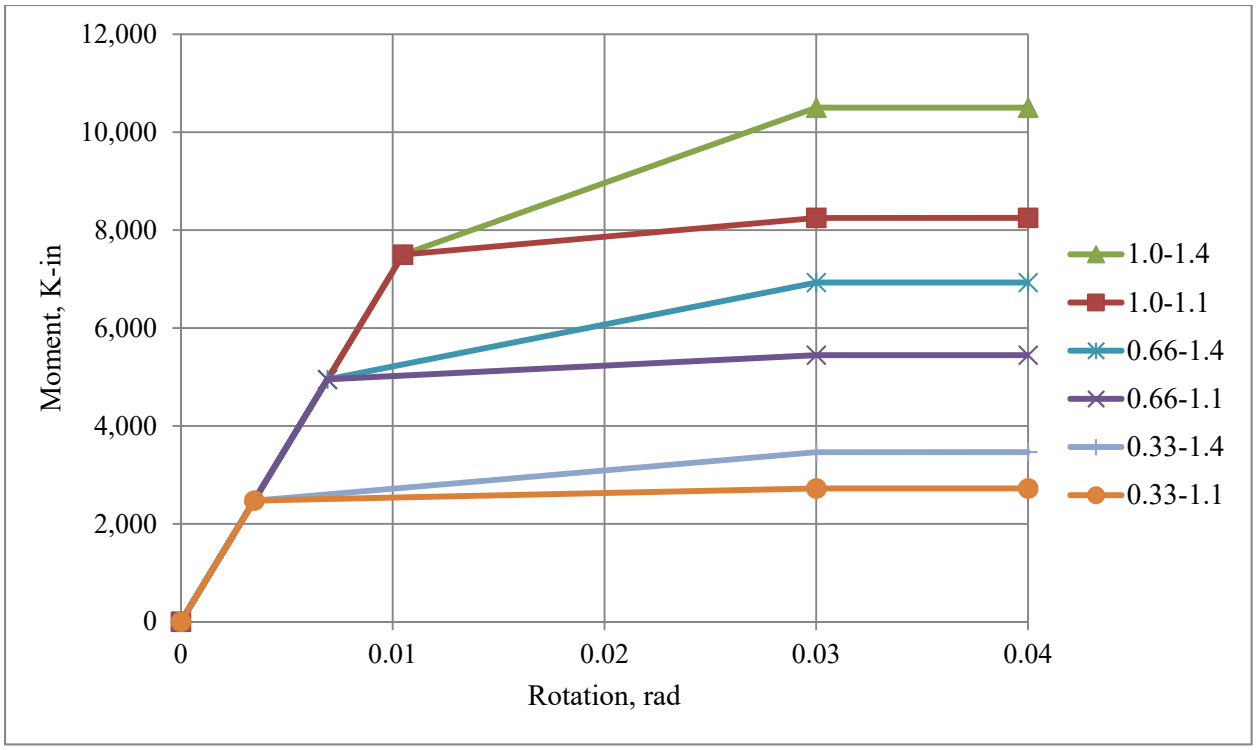


*Figure A-22: W16x77 Trilinear M-Θ Characteristics with 8EI/L Connection Stiffness*

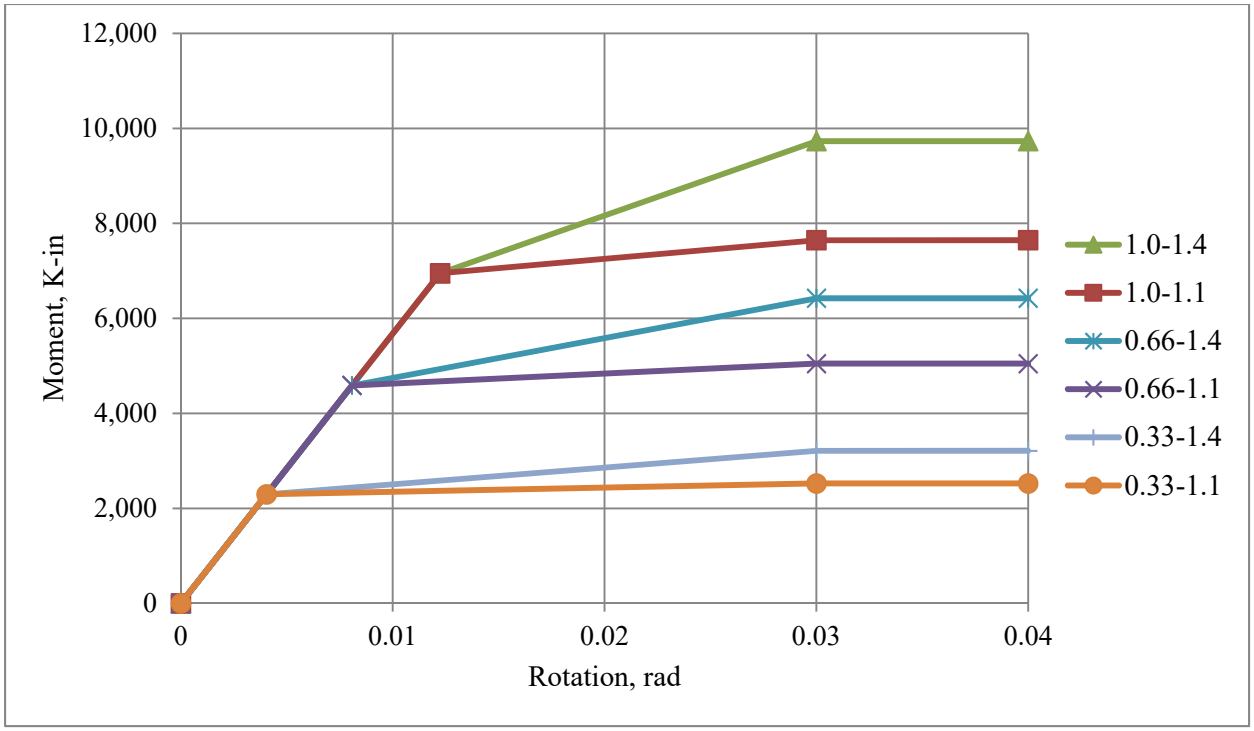


*Figure A-23: W14x82 Trilinear M-Θ Characteristics with 8EI/L Connection Stiffness*

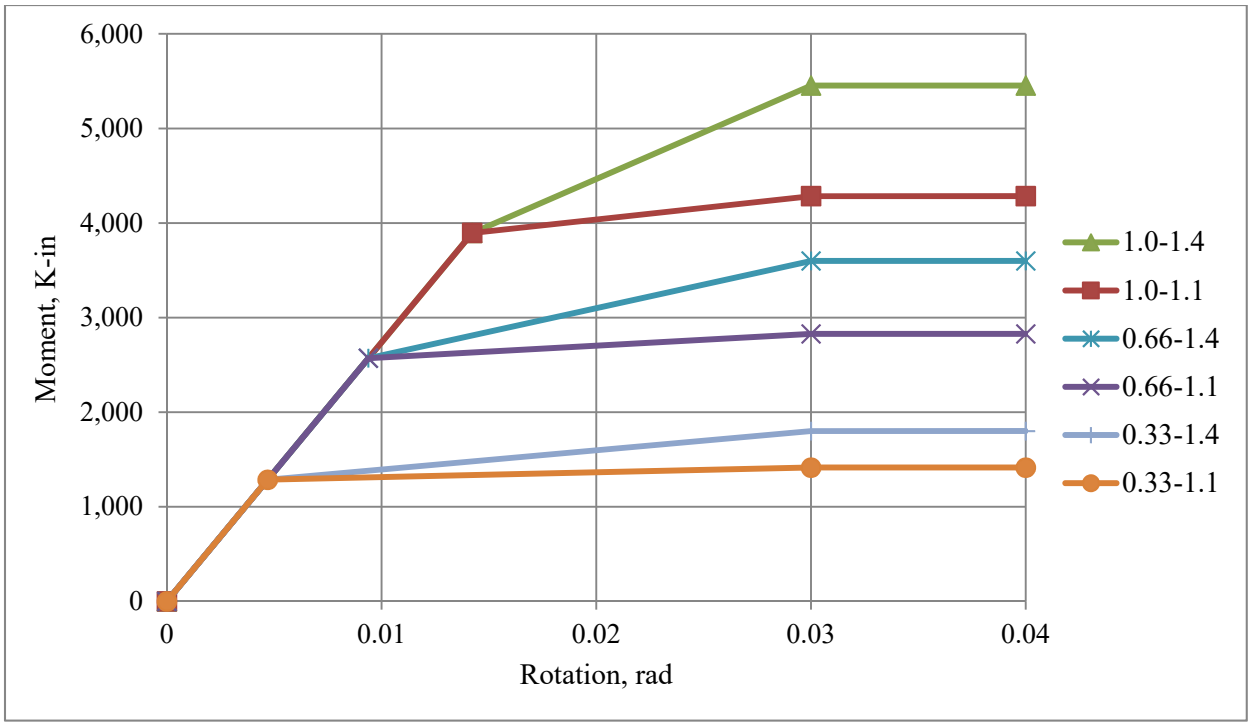


*Figure A-24: W12x53 Trilinear M-Θ Characteristics with 8EI/L Connection Stiffness*

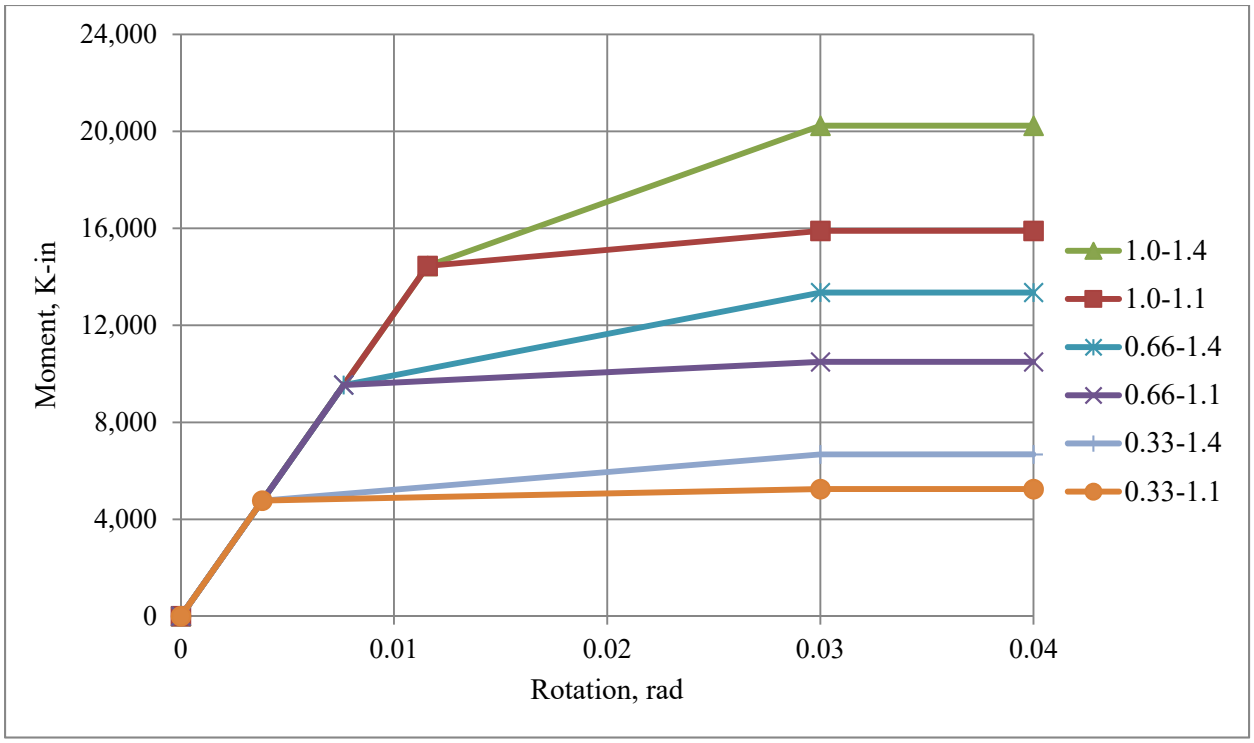


*Figure A-25: W24x104 Trilinear M-Θ Characteristics with 5EI/L Connection Stiffness*

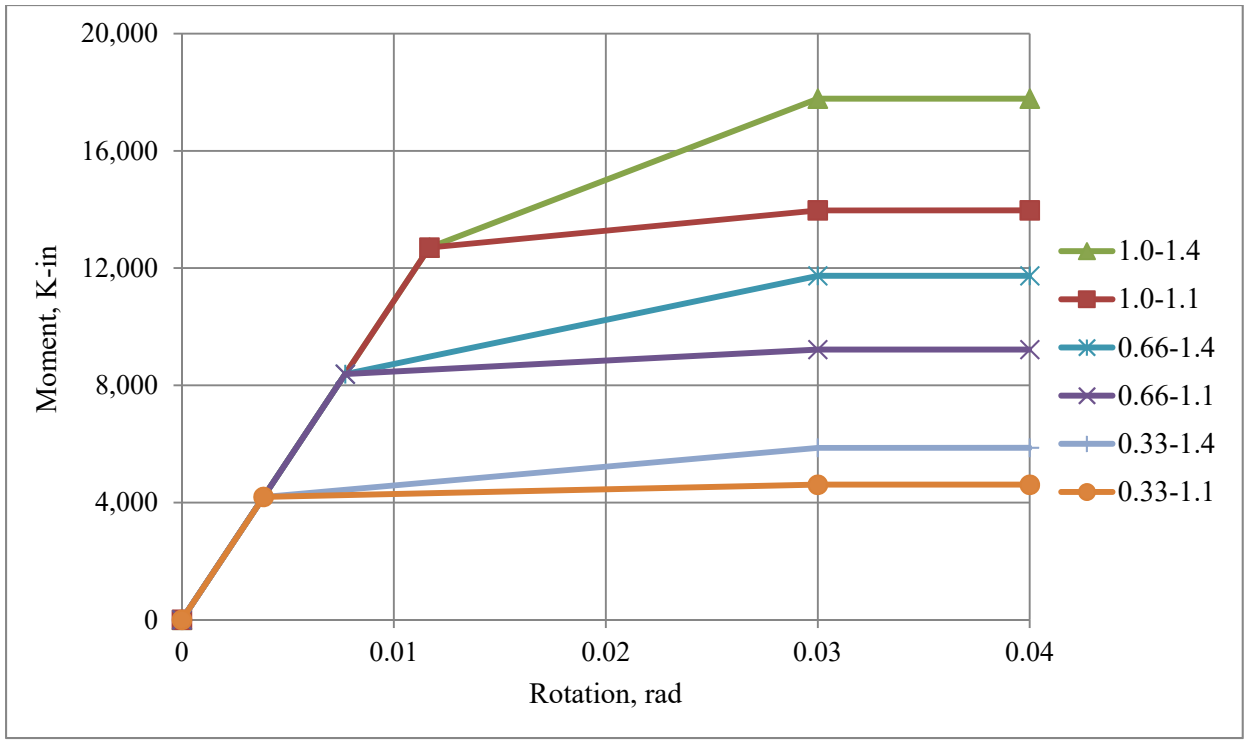


*Figure A-26: W24x94 Trilinear M-Θ Characteristics with 5EI/L Connection Stiffness*

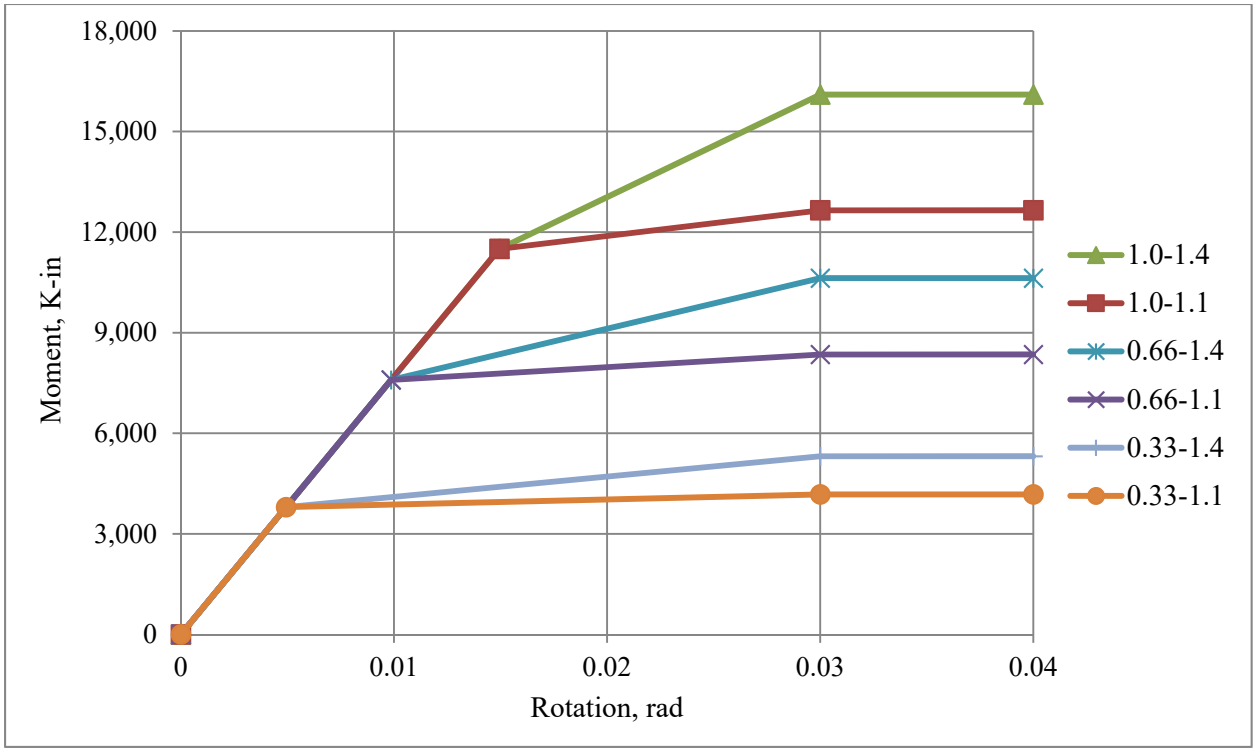


*Figure A-27: W18x106 Trilinear M-Θ Characteristics with 5EI/L Connection Stiffness*

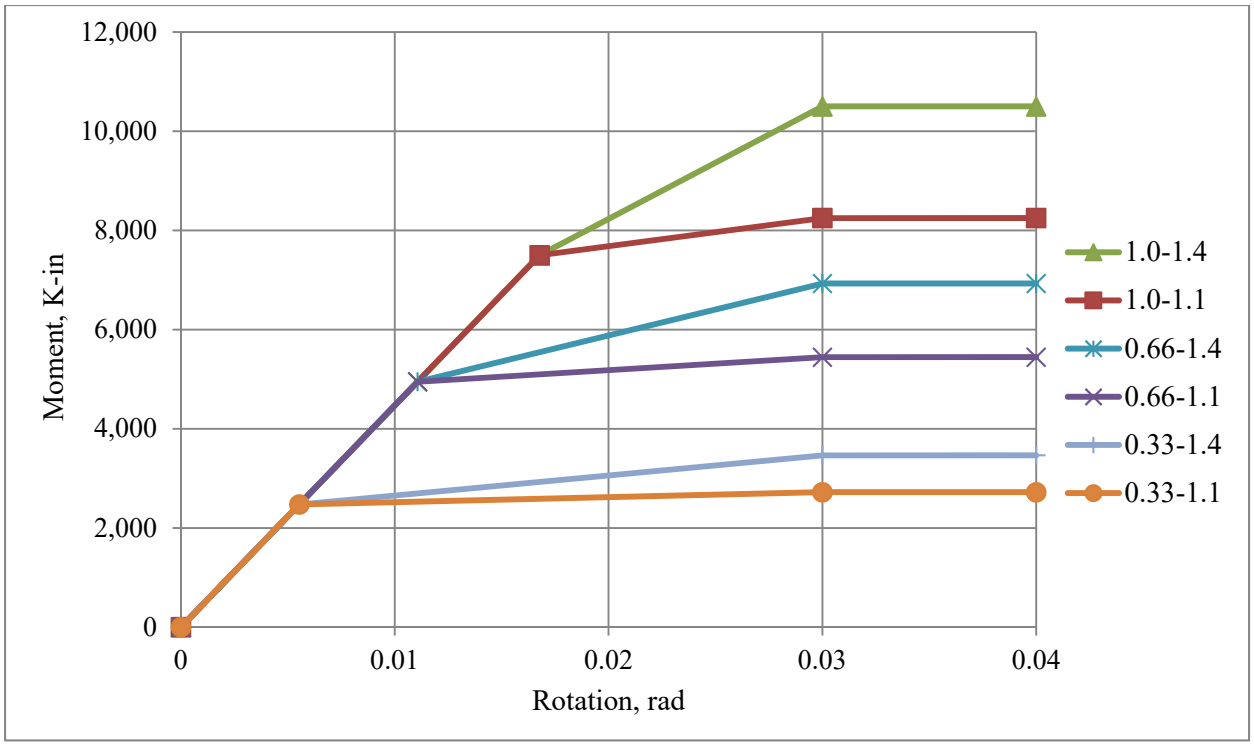


*Figure A-28: W16x77 Trilinear M-Θ Characteristics with 5EI/L Connection Stiffness*

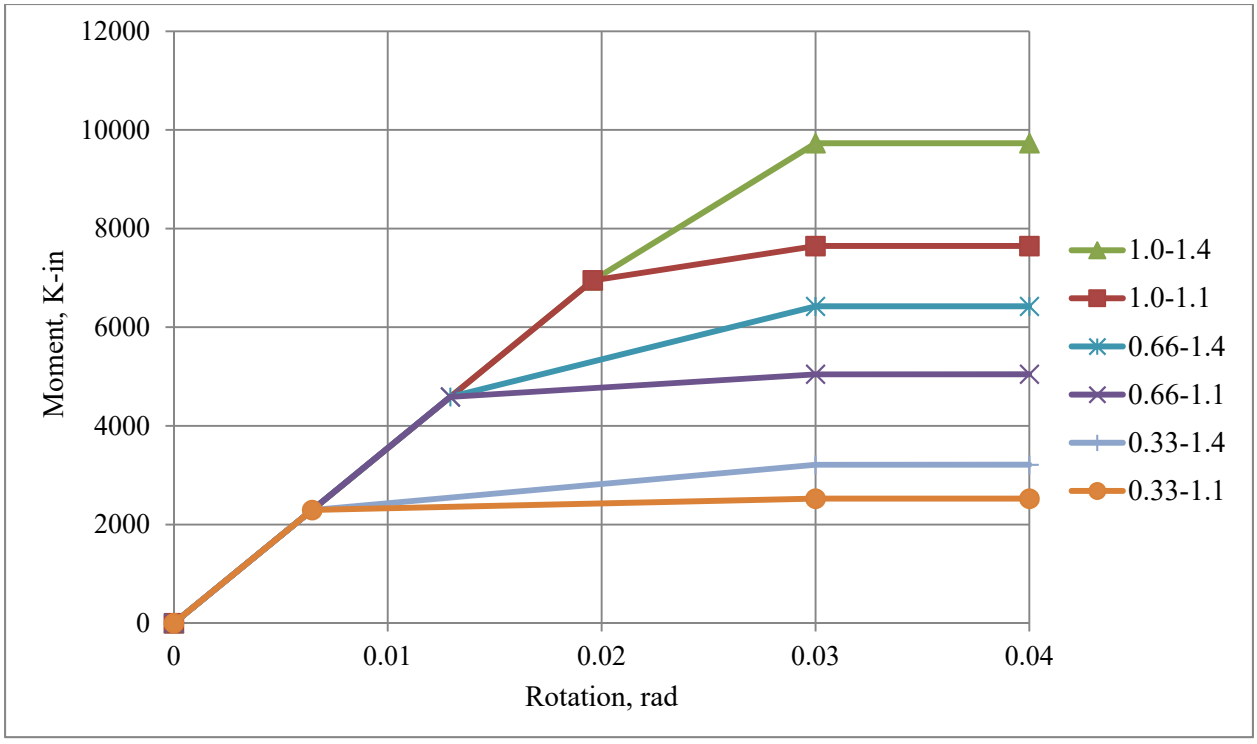


*Figure A-29: W14x82 Trilinear M-Θ Characteristics with 5EI/L Connection Stiffness*

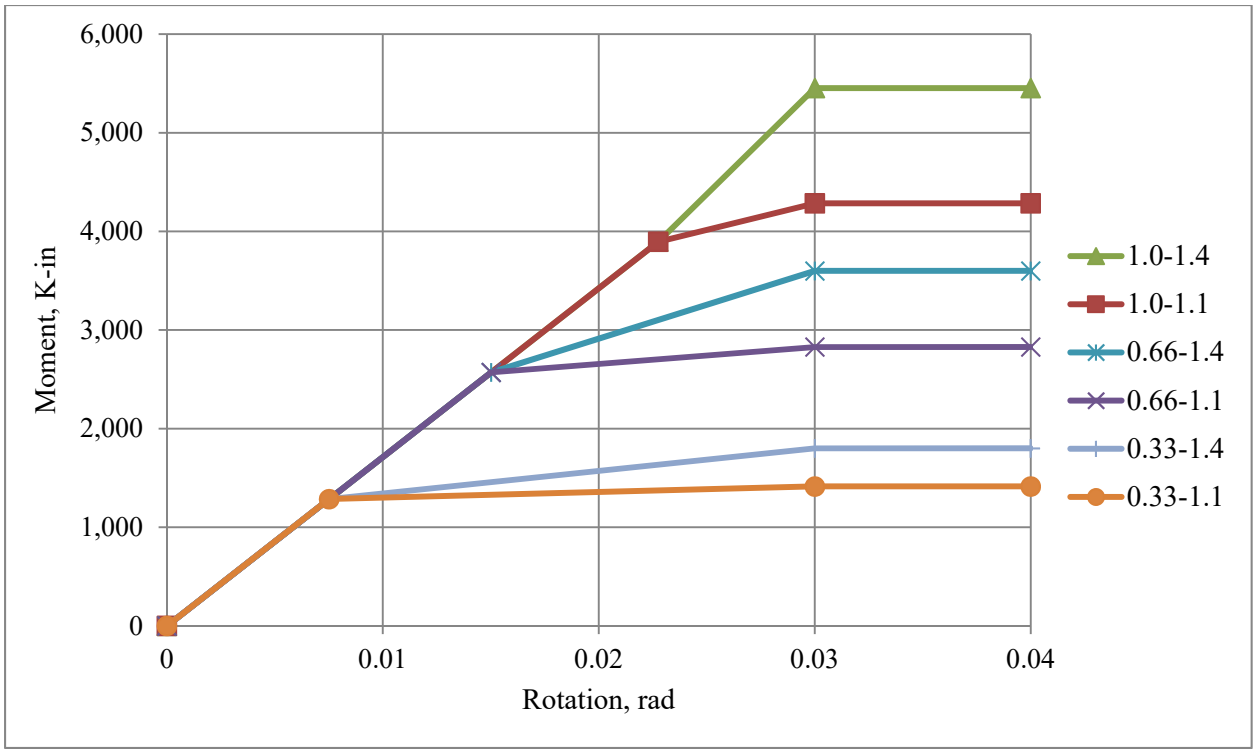


*Figure A-30: W12x53 Trilinear M-Θ Characteristics with 5EI/L Connection Stiffness*

## Appendix B: PR Connection Trilinear Moment-Rotation Values

This Appendix contains the values of connection moment and rotation for each PR connection that were calculated based on the beam sizes and connection stiffnesses. These values were used to establish the positive and negative yield points defining the elastic stiffnesses and the positive and negative points defining the post-yield stiffnesses for the trilinear hysteretic materials. The columns in these tables list the values used for the connection yield strength, the connection rotation at the yield strength, and both of the connection strain hardening moments for $1.4M_{cy}$ and $1.1M_{cy}$ that occur at 0.03 and 0.04 radians.

*Table B-1: PR Connection M-Θ Values for $M_{cy} = 1.0M_p$ and $K_c = 17EI/L$*

| Story | Beam Size | $M_{cy}$ (K-in) | Rotation (rad) | $1.4M_{cy}$ (K-in) | $1.1M_{cy}$ (K-in) |
|---|---|---|---|---|---|
| R | 12x53 | 3,895 | 0.00669 | 5,453 | 4,285 |
| F9 | 14x82 | 6,950 | 0.00576 | 9,730 | 7,645 |
| F8 | 16x77 | 7,500 | 0.00493 | 10,500 | 8,250 |
| F7 | 18x106 | 11,500 | 0.00440 | 16,100 | 12,650 |
| F6 | 24x94 | 12,700 | 0.00343 | 17,780 | 13,970 |
| F5 | | | | | |
| F4 | | | | | |
| F3 | 24x104 | 14,450 | 0.00340 | 20,230 | 15,895 |
| F2 | | | | | |
| G | | | | | |

*Table B-2: PR Connection M-Θ Values for $M_{cy} = 0.66M_p$ and $K_c = 17EI/L$*

| Story | Beam Size | $M_{cy}$ (K-in) | Rotation (rad) | $1.4M_{cy}$ (K-in) | $1.1M_{cy}$ (K-in) |
|---|---|---|---|---|---|
| R | 12x53 | 2,571 | 0.00442 | 3,599 | 2,828 |
| F9 | 14x82 | 4,587 | 0.00380 | 6,422 | 5,046 |
| F8 | 16x77 | 4,950 | 0.00326 | 6,930 | 5,445 |
| F7 | 18x106 | 7,590 | 0.00290 | 10,626 | 8,349 |
| F6 | 24x94 | 8,382 | 0.00227 | 11,735 | 9,220 |
| F5 | | | | | |
| F4 | | | | | |
| F3 | 24x104 | 9,537 | 0.00225 | 13,352 | 10,491 |
| F2 | | | | | |
| G | | | | | |

*Table B-3: PR Connection M-Θ Values for $M_{cy} = 0.33M_p$ and $K_c = 17EI/L$*

| Story | Beam Size | $M_{cy}$ (K-in) | Rotation (rad) | $1.4M_{cy}$ (K-in) | $1.1M_{cy}$ (K-in) |
|---|---|---|---|---|---|
| R | 12x53 | 1,285 | 0.00221 | 1,799 | 1,414 |
| F9 | 14x82 | 2,294 | 0.00190 | 3,211 | 2,523 |
| F8 | 16x77 | 2,475 | 0.00163 | 3,465 | 2,723 |
| F7 | 18x106 | 3,795 | 0.00145 | 5,313 | 4,175 |
| F6 | 24x94 | 4,191 | 0.00113 | 5,867 | 4,610 |
| F5 | | | | | |
| F4 | | | | | |
| F3 | 24x104 | 4,769 | 0.00112 | 6,676 | 5,245 |
| F2 | | | | | |
| G | | | | | |

*Table B-4: PR Connection M-Θ Values for $M_{cy} = 1.0M_p$ and $K_c = 14EI/L$*

| Story | Beam Size | $M_{cy}$ (K-in) | Rotation (rad) | $1.4M_{cy}$ (K-in) | $1.1M_{cy}$ (K-in) |
|---|---|---|---|---|---|
| R | 12x53 | 3,895 | 0.00813 | 5,453 | 4,285 |
| F9 | 14x82 | 6,950 | 0.00699 | 9,730 | 7,645 |
| F8 | 16x77 | 7,500 | 0.00599 | 10,500 | 8,250 |
| F7 | 18x106 | 11,500 | 0.00534 | 16,100 | 12,650 |
| F6 | 24x94 | 12,700 | 0.00417 | 17,780 | 13,970 |
| F5 | | | | | |
| F4 | | | | | |
| F3 | 24x104 | 14,450 | 0.00413 | 20,230 | 15,895 |
| F2 | | | | | |
| G | | | | | |

*Table B-5: PR Connection M-Θ Values for $M_{cy} = 0.66M_p$ and $K_c = 14EI/L$*

| Story | Beam Size | $M_{cy}$ (K-in) | Rotation (rad) | $1.4M_{cy}$ (K-in) | $1.1M_{cy}$ (K-in) |
|---|---|---|---|---|---|
| R | 12x53 | 2,571 | 0.00536 | 3,599 | 2,828 |
| F9 | 14x82 | 4,587 | 0.00462 | 6,422 | 5,046 |
| F8 | 16x77 | 4,950 | 0.00395 | 6,930 | 5,445 |
| F7 | 18x106 | 7,590 | 0.00352 | 10,626 | 8,349 |
| F6 | 24x94 | 8,382 | 0.00275 | 11,735 | 9,220 |
| F5 | | | | | |
| F4 | | | | | |
| F3 | 24x104 | 9,537 | 0.00273 | 13,352 | 10,491 |
| F2 | | | | | |
| G | | | | | |

*Table B-6: PR Connection M-Θ Values for $M_{cy} = 0.33M_p$ and $K_c = 14EI/L$*

| Story | Beam Size | $M_{cy}$ (K-in) | Rotation (rad) | $1.4M_{cy}$ (K-in) | $1.1M_{cy}$ (K-in) |
|---|---|---|---|---|---|
| R | 12x53 | 1,285 | 0.00268 | 1,799 | 1,414 |
| F9 | 14x82 | 2,294 | 0.00231 | 3,211 | 2,523 |
| F8 | 16x77 | 2,475 | 0.00198 | 3,465 | 2,723 |
| F7 | 18x106 | 3,795 | 0.00176 | 5,313 | 4,175 |
| F6 | 24x94 | 4,191 | 0.00138 | 5,867 | 4,610 |
| F5 | | | | | |
| F4 | | | | | |
| F3 | 24x104 | 4,769 | 0.00136 | 6,676 | 5,245 |
| F2 | | | | | |
| G | | | | | |

*Table B-7: PR Connection M-Θ Values for $M_{cy} = 1.0M_p$ and $K_c = 11EI/L$*

| Story | Beam Size | $M_{cy}$ (K-in) | Rotation (rad) | $1.4M_{cy}$ (K-in) | $1.1M_{cy}$ (K-in) |
|---|---|---|---|---|---|
| R | 12x53 | 3,895 | 0.01034 | 5,453 | 4,285 |
| F9 | 14x82 | 6,950 | 0.00890 | 9,730 | 7,645 |
| F8 | 16x77 | 7,500 | 0.00763 | 10,500 | 8,250 |
| F7 | 18x106 | 11,500 | 0.00679 | 16,100 | 12,650 |
| F6 | 24x94 | 12,700 | 0.00531 | 17,780 | 13,970 |
| F5 | | | | | |
| F4 | | | | | |
| F3 | 24x104 | 14,450 | 0.00526 | 20,230 | 15,895 |
| F2 | | | | | |
| G | | | | | |

*Table B-8: PR Connection M-Θ Values for $M_{cy} = 0.66M_p$ and $K_c = 11EI/L$*

| Story | Beam Size | $M_{cy}$ (K-in) | Rotation (rad) | $1.4M_{cy}$ (K-in) | $1.1M_{cy}$ (K-in) |
|---|---|---|---|---|---|
| R | 12x53 | 2,571 | 0.00683 | 3,599 | 2,828 |
| F9 | 14x82 | 4,587 | 0.00588 | 6,422 | 5,046 |
| F8 | 16x77 | 4,950 | 0.00503 | 6,930 | 5,445 |
| F7 | 18x106 | 7,590 | 0.00448 | 10,626 | 8,349 |
| F6 | 24x94 | 8,382 | 0.00350 | 11,735 | 9,220 |
| F5 | | | | | |
| F4 | | | | | |
| F3 | 24x104 | 9,537 | 0.00347 | 13,352 | 10,491 |
| F2 | | | | | |
| G | | | | | |

*Table B-9: PR Connection M-Θ Values for $M_{cy} = 0.33M_p$ and $K_c = 11EI/L$*

| Story | Beam Size | $M_{cy}$ (K-in) | Rotation (rad) | $1.4M_{cy}$ (K-in) | $1.1M_{cy}$ (K-in) |
|---|---|---|---|---|---|
| R | 12x53 | 1,285 | 0.00341 | 1,799 | 1,414 |
| F9 | 14x82 | 2,294 | 0.00294 | 3,211 | 2,523 |
| F8 | 16x77 | 2,475 | 0.00252 | 3,465 | 2,723 |
| F7 | 18x106 | 3,795 | 0.00224 | 5,313 | 4,175 |
| F6 | 24x94 | 4,191 | 0.00175 | 5,867 | 4,610 |
| F5 | | | | | |
| F4 | | | | | |
| F3 | 24x104 | 4,769 | 0.00174 | 6,676 | 5,245 |
| F2 | | | | | |
| G | | | | | |

*Table B-10: PR Connection M-Θ Values for $M_{cy} = 1.0M_p$ and $K_c = 8EI/L$*

| Story | Beam Size | $M_{cy}$ (K-in) | Rotation (rad) | $1.4M_{cy}$ (K-in) | $1.1M_{cy}$ (K-in) |
|---|---|---|---|---|---|
| R | 12x53 | 3,895 | 0.01422 | 5,453 | 4,285 |
| F9 | 14x82 | 6,950 | 0.01224 | 9,730 | 7,645 |
| F8 | 16x77 | 7,500 | 0.01048 | 10,500 | 8,250 |
| F7 | 18x106 | 11,500 | 0.00934 | 16,100 | 12,650 |
| F6 | 24x94 | 12,700 | 0.00730 | 17,780 | 13,970 |
| F5 | | | | | |
| F4 | | | | | |
| F3 | 24x104 | 14,450 | 0.00723 | 20,230 | 15,895 |
| F2 | | | | | |
| G | | | | | |

*Table B-11: PR Connection M-Θ Values for $M_{cy} = 0.66M_p$ and $K_c = 8EI/L$*

| Story | Beam Size | $M_{cy}$ (K-in) | Rotation (rad) | $1.4M_{cy}$ (K-in) | $1.1M_{cy}$ (K-in) |
|---|---|---|---|---|---|
| R | 12x53 | 2,571 | 0.00939 | 3,599 | 2,828 |
| F9 | 14x82 | 4,587 | 0.00808 | 6,422 | 5,046 |
| F8 | 16x77 | 4,950 | 0.00692 | 6,930 | 5,445 |
| F7 | 18x106 | 7,590 | 0.00617 | 10,626 | 8,349 |
| F6 | 24x94 | 8,382 | 0.00482 | 11,735 | 9,220 |
| F5 | | | | | |
| F4 | | | | | |
| F3 | 24x104 | 9,537 | 0.00477 | 13,352 | 10,491 |
| F2 | | | | | |
| G | | | | | |

*Table B-12: PR Connection M-Θ Values for $M_{cy} = 0.33M_p$ and $K_c = 8EI/L$*

| Story | Beam Size | $M_{cy}$ (K-in) | Rotation (rad) | $1.4M_{cy}$ (K-in) | $1.1M_{cy}$ (K-in) |
|---|---|---|---|---|---|
| R | 12x53 | 1,285 | 0.00469 | 1,799 | 1,414 |
| F9 | 14x82 | 2,294 | 0.00404 | 3,211 | 2,523 |
| F8 | 16x77 | 2,475 | 0.00346 | 3,465 | 2,723 |
| F7 | 18x106 | 3,795 | 0.00308 | 5,313 | 4,175 |
| F6 | 24x94 | 4,191 | 0.00241 | 5,867 | 4,610 |
| F5 | | | | | |
| F4 | | | | | |
| F3 | 24x104 | 4,769 | 0.00239 | 6,676 | 5,245 |
| F2 | | | | | |
| G | | | | | |

*Table B-13: PR Connection M-Θ Values for $M_{cy} = 1.0M_p$ and $K_c = 5EI/L$*

| Story | Beam Size | $M_{cy}$ (K-in) | Rotation (rad) | $1.4M_{cy}$ (K-in) | $1.1M_{cy}$ (K-in) |
|---|---|---|---|---|---|
| R | 12x53 | 3,895 | 0.02275 | 5,453 | 4,285 |
| F9 | 14x82 | 6,950 | 0.01959 | 9,730 | 7,645 |
| F8 | 16x77 | 7,500 | 0.01678 | 10,500 | 8,250 |
| F7 | 18x106 | 11,500 | 0.01495 | 16,100 | 12,650 |
| F6 | 24x94 | 12,700 | 0.01168 | 17,780 | 13,970 |
| F5 | | | | | |
| F4 | | | | | |
| F3 | 24x104 | 14,450 | 0.01157 | 20,230 | 15,895 |
| F2 | | | | | |
| G | | | | | |

*Table B-14: PR Connection M-Θ Values for $M_{cy} = 0.66M_p$ and $K_c = 5EI/L$*

| Story | Beam Size | $M_{cy}$ (K-in) | Rotation (rad) | $1.4M_{cy}$ (K-in) | $1.1M_{cy}$ (K-in) |
|---|---|---|---|---|---|
| R | 12x53 | 2,571 | 0.01502 | 3,599 | 2,828 |
| F9 | 14x82 | 4,587 | 0.01293 | 6,422 | 5,046 |
| F8 | 16x77 | 4,950 | 0.01107 | 6,930 | 5,445 |
| F7 | 18x106 | 7,590 | 0.00987 | 10,626 | 8,349 |
| F6 | 24x94 | 8,382 | 0.00771 | 11,735 | 9,220 |
| F5 | | | | | |
| F4 | | | | | |
| F3 | 24x104 | 9,537 | 0.00764 | 13,352 | 10,491 |
| F2 | | | | | |
| G | | | | | |

*Table B-15: PR Connection M-Θ Values for $M_{cy} = 0.33M_p$ and $K_c = 5EI/L$*

| Story | Beam Size | $M_{cy}$ (K-in) | Rotation (rad) | $1.4M_{cy}$ (K-in) | $1.1M_{cy}$ (K-in) |
|---|---|---|---|---|---|
| R | 12x53 | 1,285 | 0.00751 | 1,799 | 1,414 |
| F9 | 14x82 | 2,294 | 0.00646 | 3,211 | 2,523 |
| F8 | 16x77 | 2,475 | 0.00554 | 3,465 | 2,723 |
| F7 | 18x106 | 3,795 | 0.00493 | 5,313 | 4,175 |
| F6 | 24x94 | 4,191 | 0.00385 | 5,867 | 4,610 |
| F5 | | | | | |
| F4 | | | | | |
| F3 | 24x104 | 4,769 | 0.00382 | 6,676 | 5,245 |
| F2 | | | | | |
| G | | | | | |

## Appendix C: FEMA P695 Near-Field Scaled Ground Motion Accelerograms

This Appendix contains the scaled accelerograms for the 28 ground motion records used to conduct the multi-record IDAs on each frame.

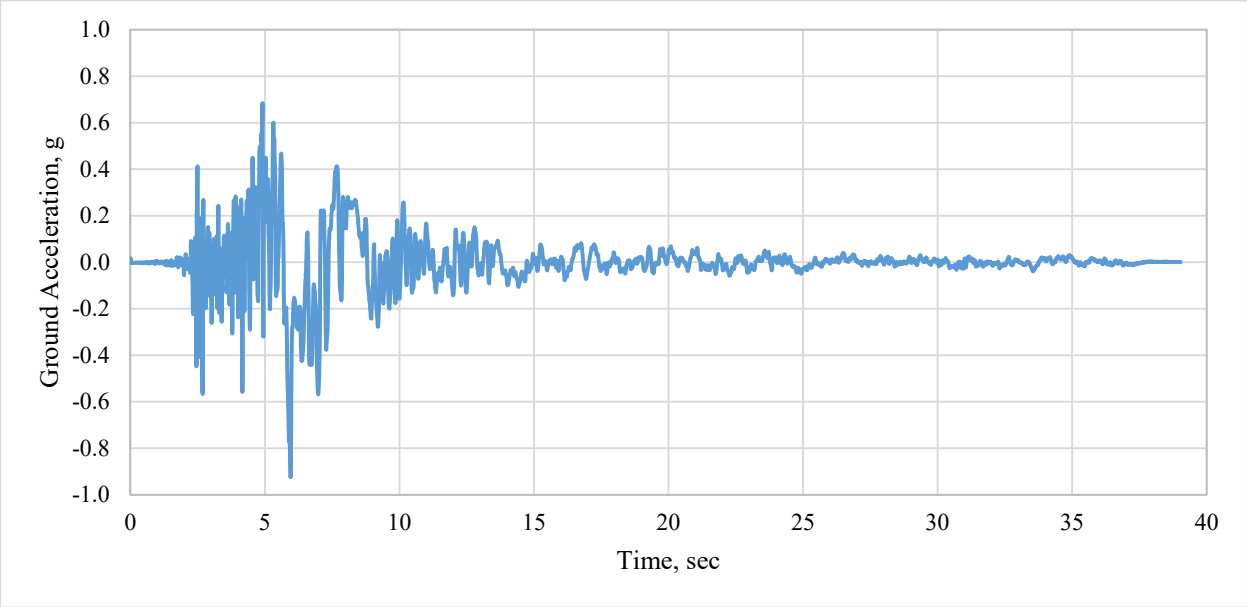


*Figure C-1: PEER181 Scaled Accelerogram*

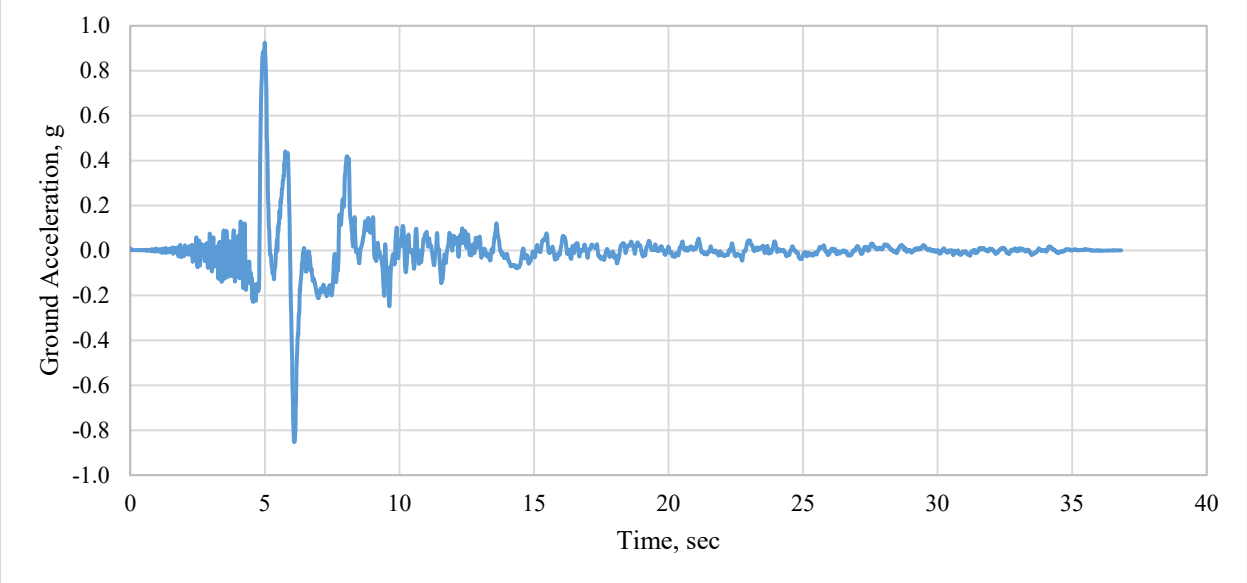


*Figure C-2: PEER182 Scaled Accelerogram*

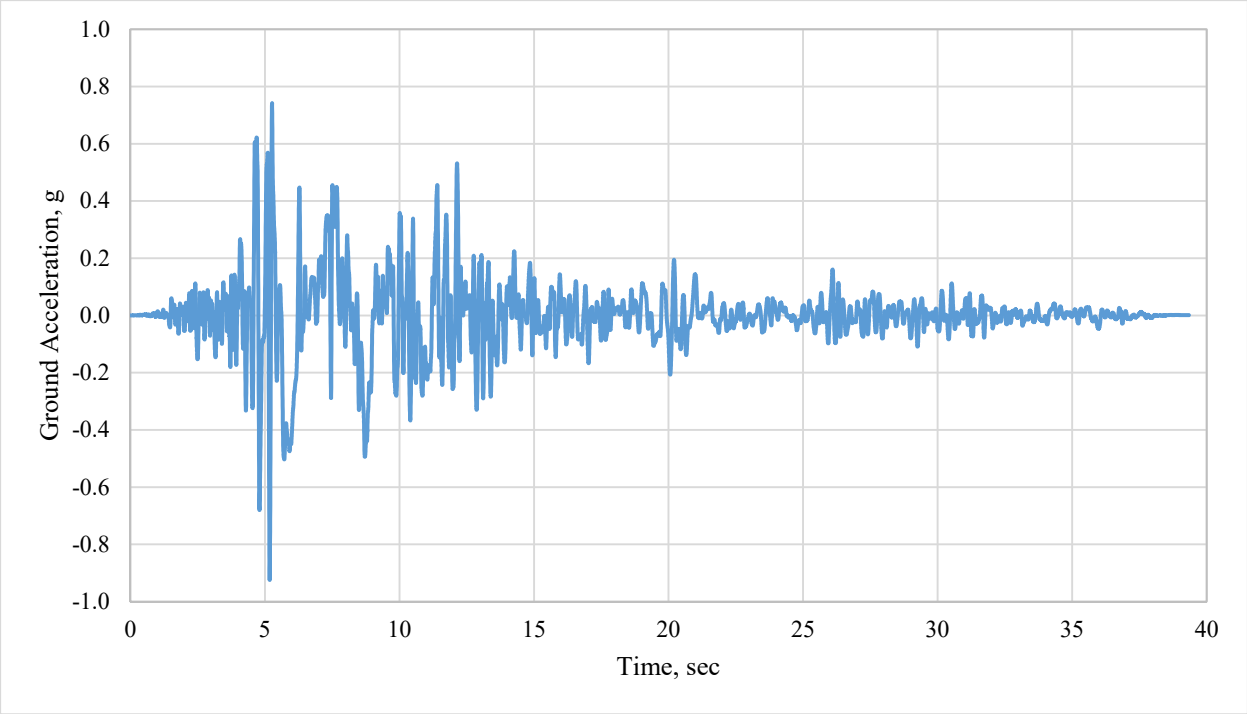


*Figure C-3: PEER292 Scaled Accelerogram*

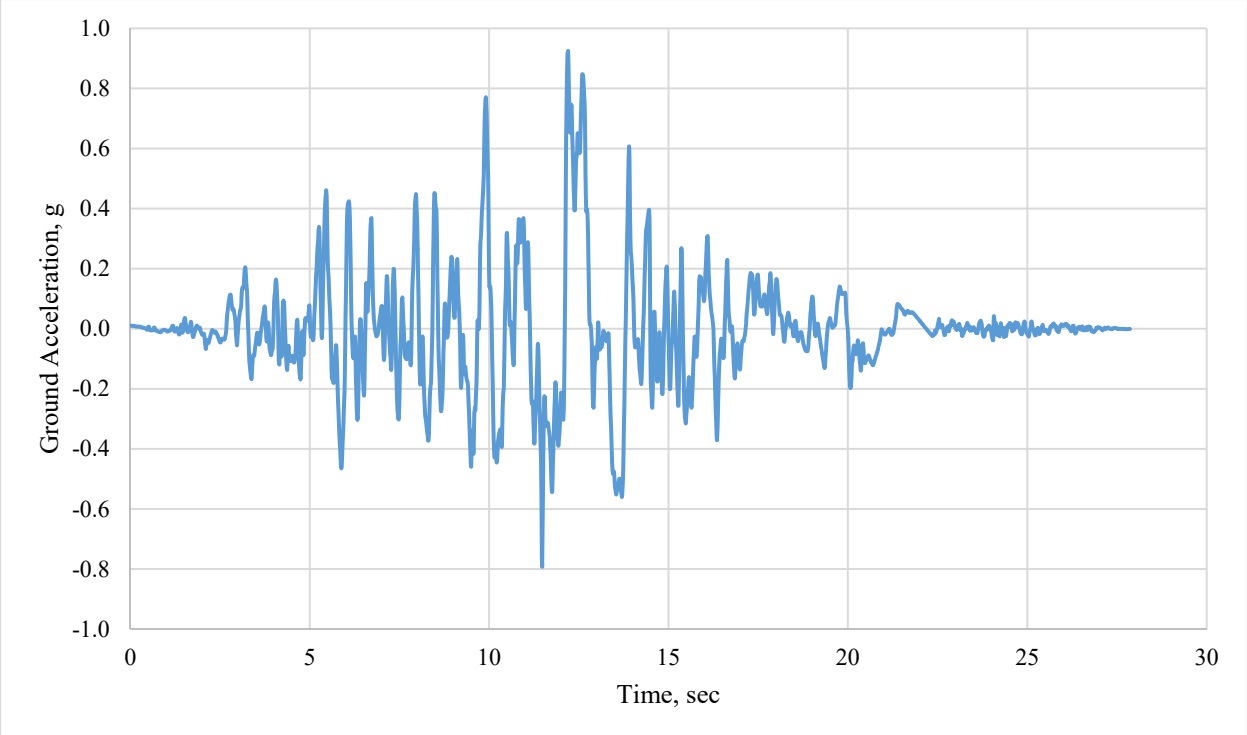


*Figure C-4: PEER723 Scaled Accelerogram*

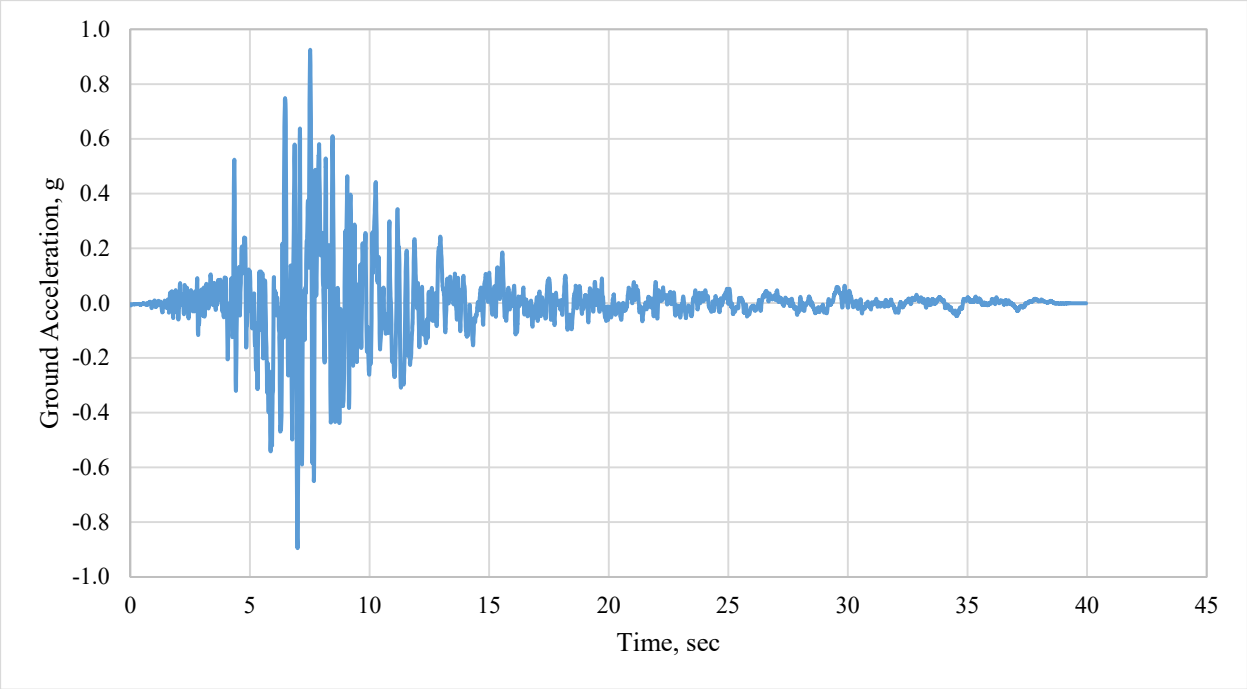


*Figure C-5: PEER802 Scaled Accelerogram*

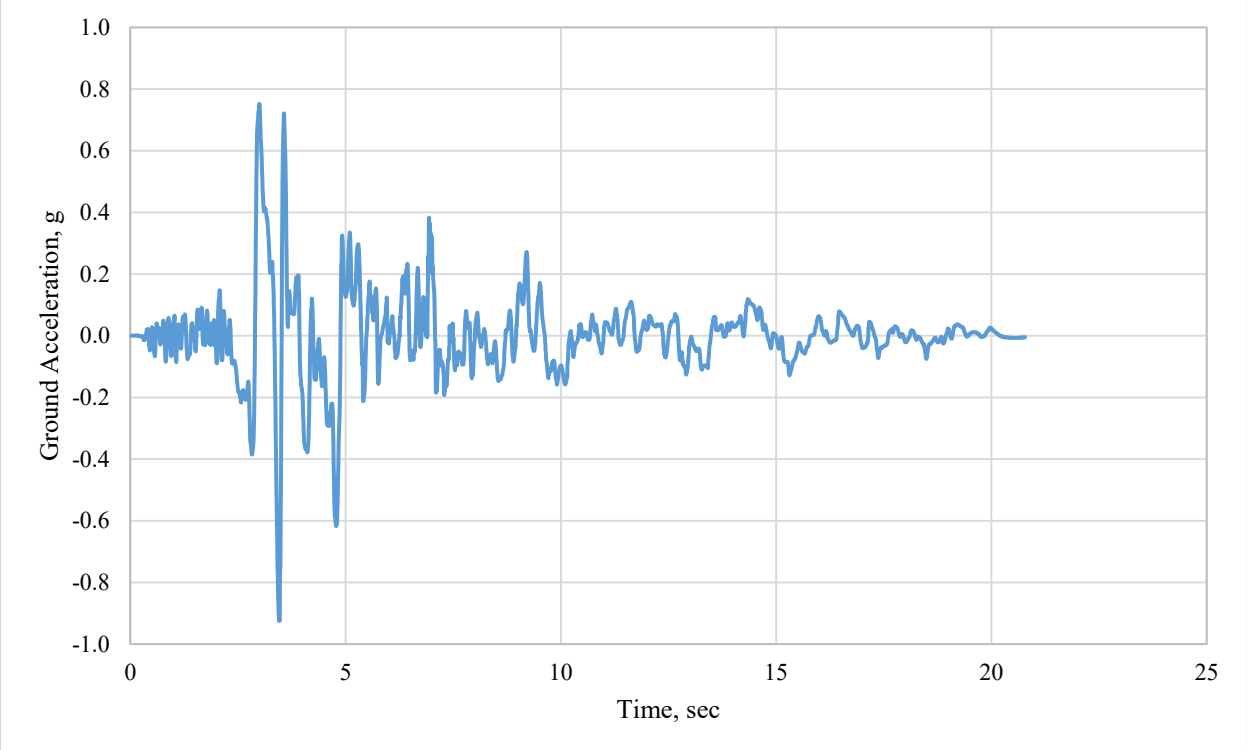


*Figure C-6: PEER821 Scaled Accelerogram*

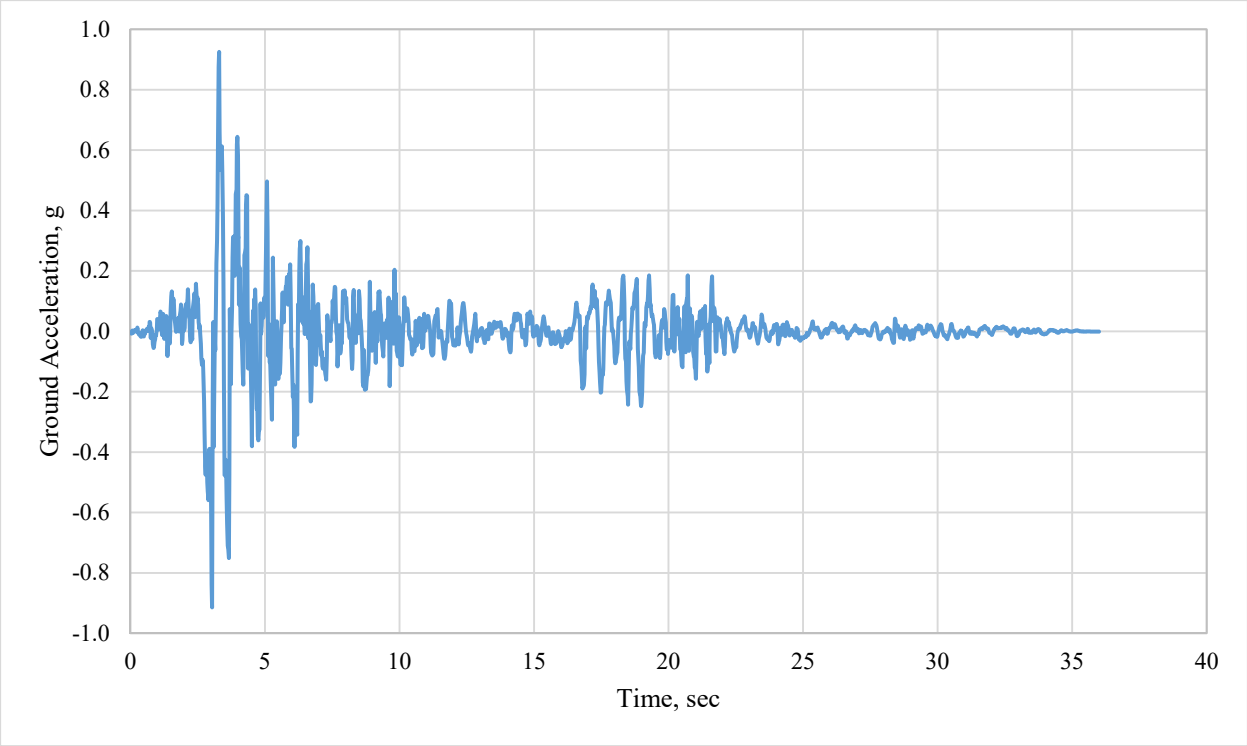


*Figure C-7: PEER828 Scaled Accelerogram*

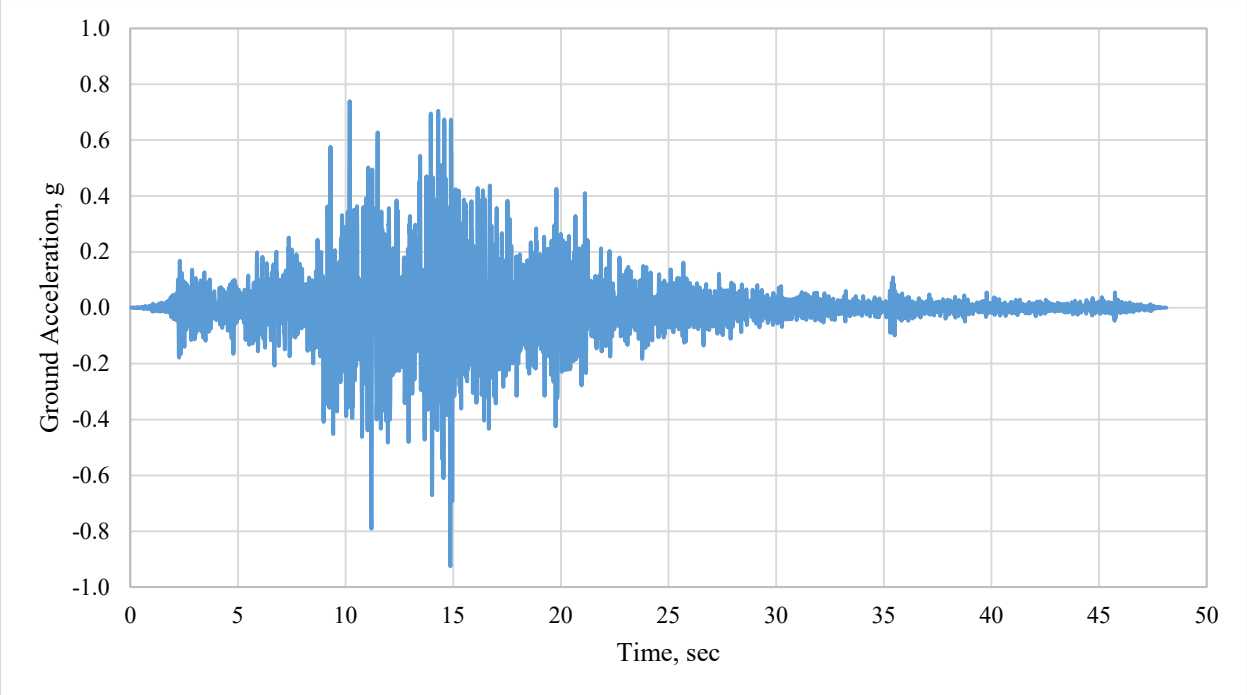


*Figure C-8: PEER879 Scaled Accelerogram*

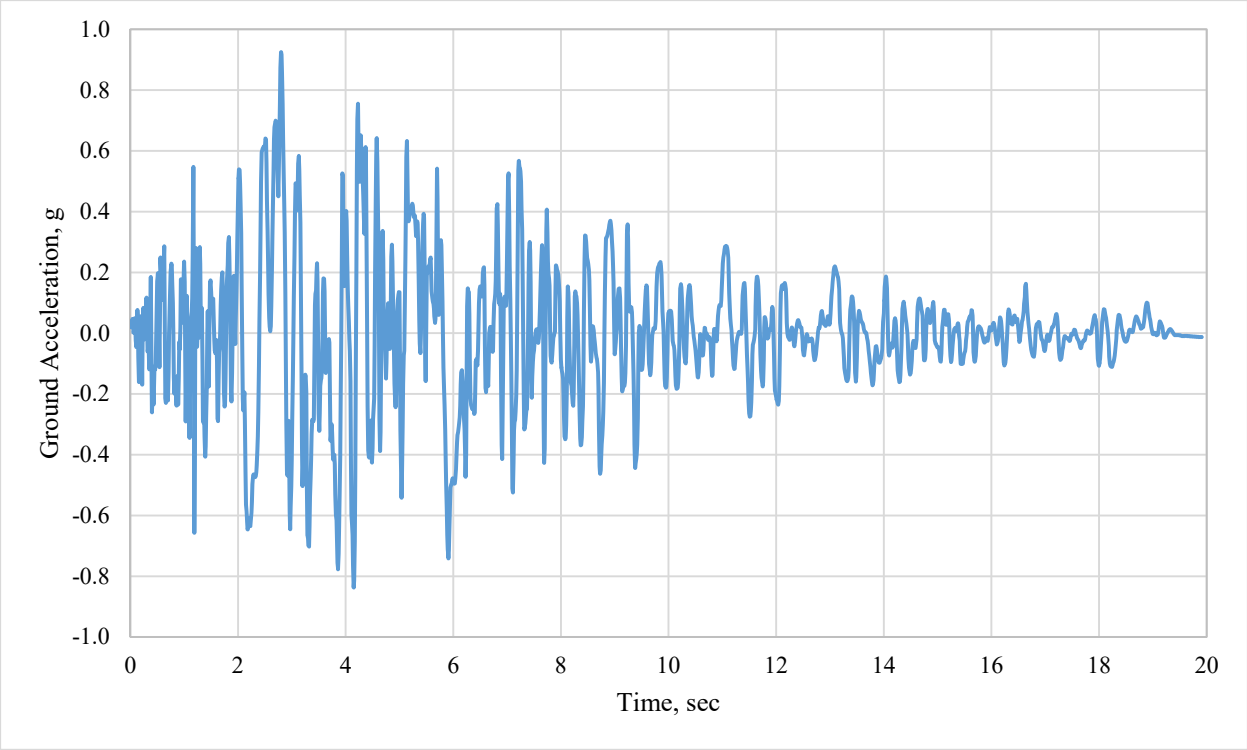


*Figure C-9: PEER1063 Scaled Accelerogram*

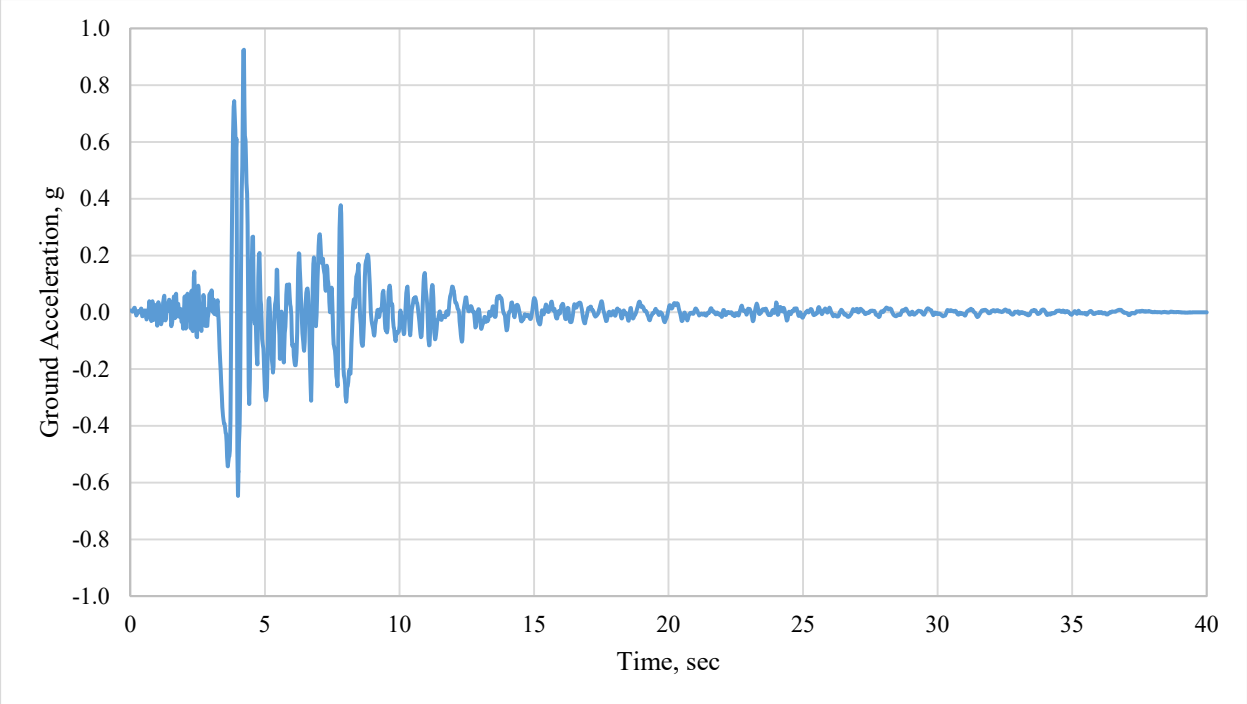


*Figure C-10: PEER1086 Scaled Accelerogram*

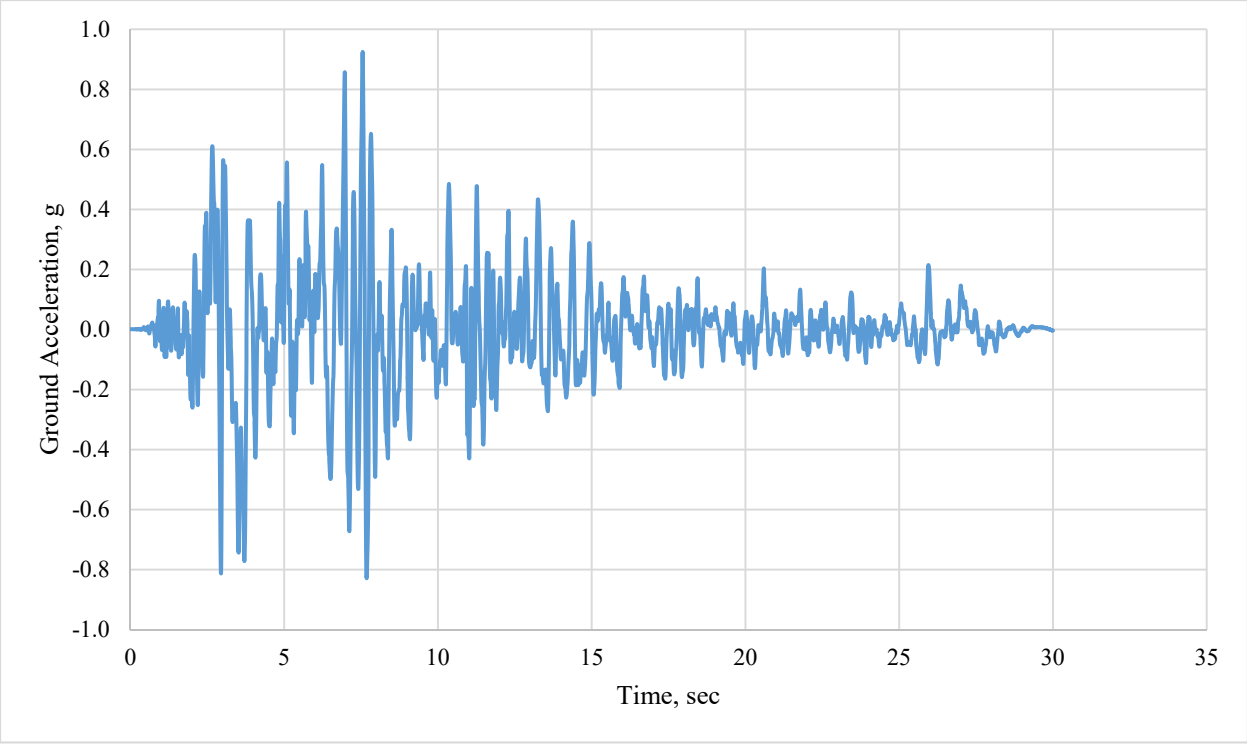


*Figure C-11: PEER1165 Scaled Accelerogram*

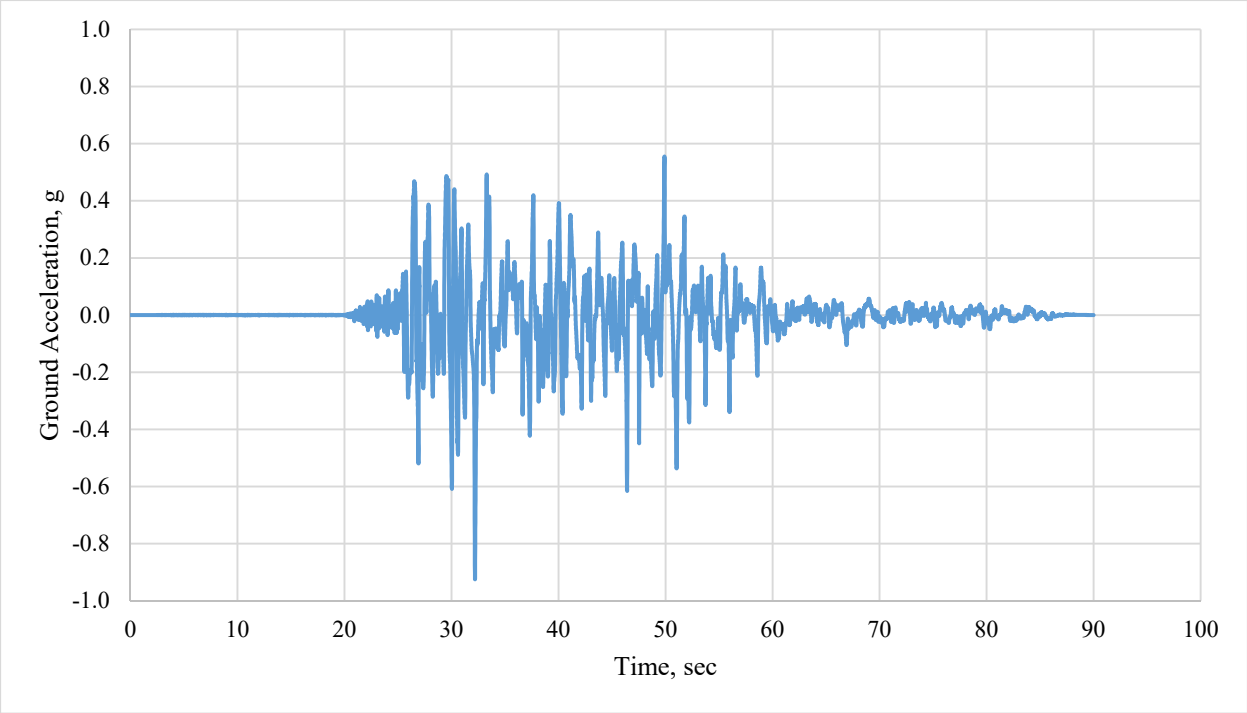


*Figure C-12: PEER1503 Scaled Accelerogram*

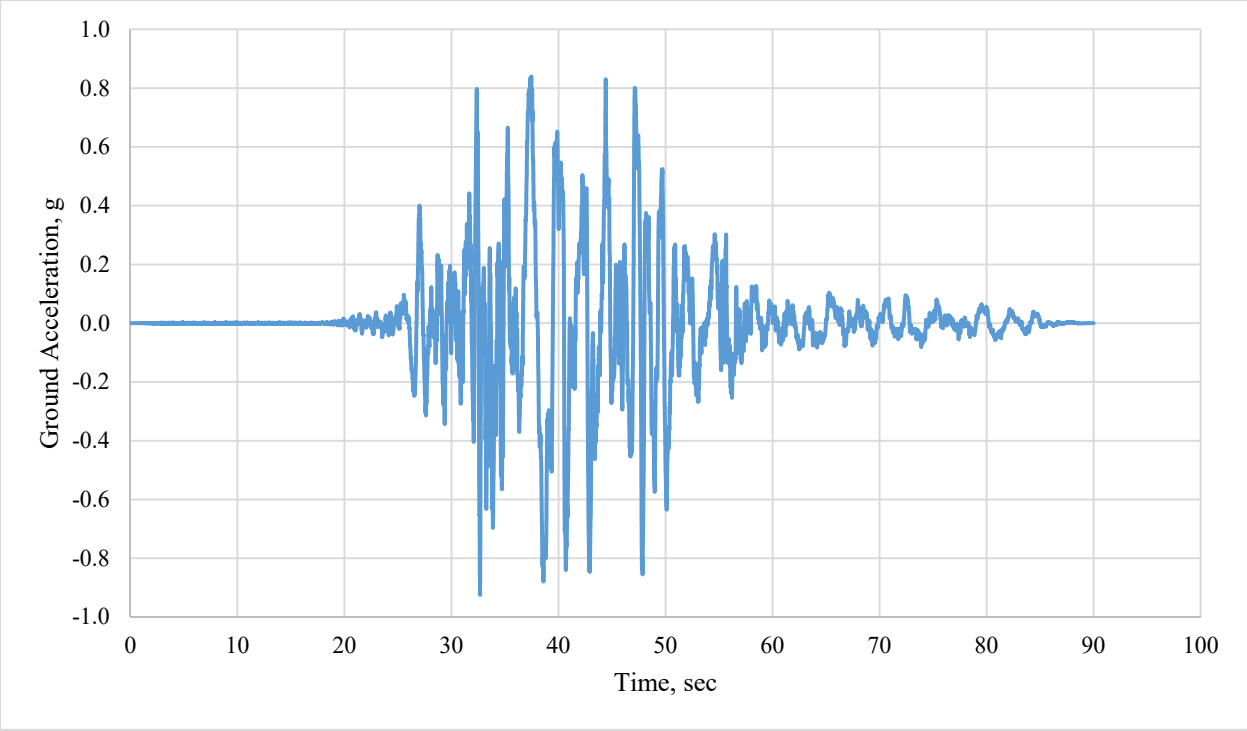


*Figure C-13: PEER1529 Scaled Accelerogram*

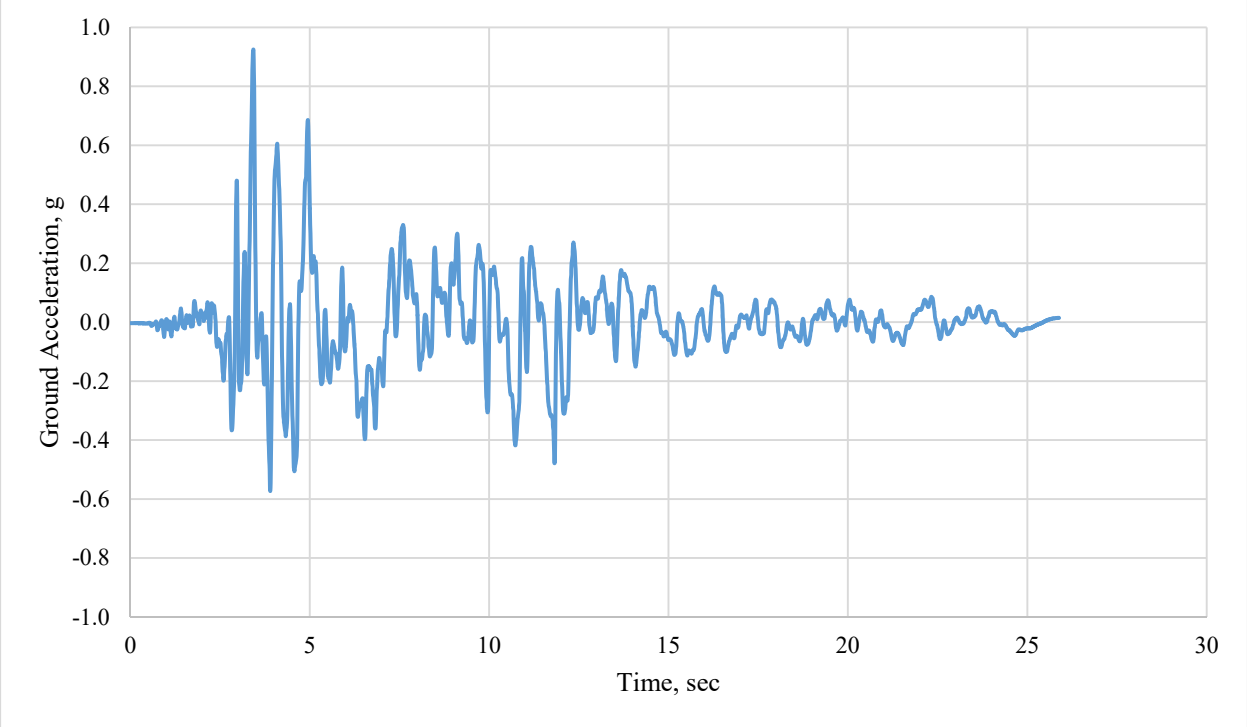


*Figure C-14: PEER1605 Scaled Accelerogram*

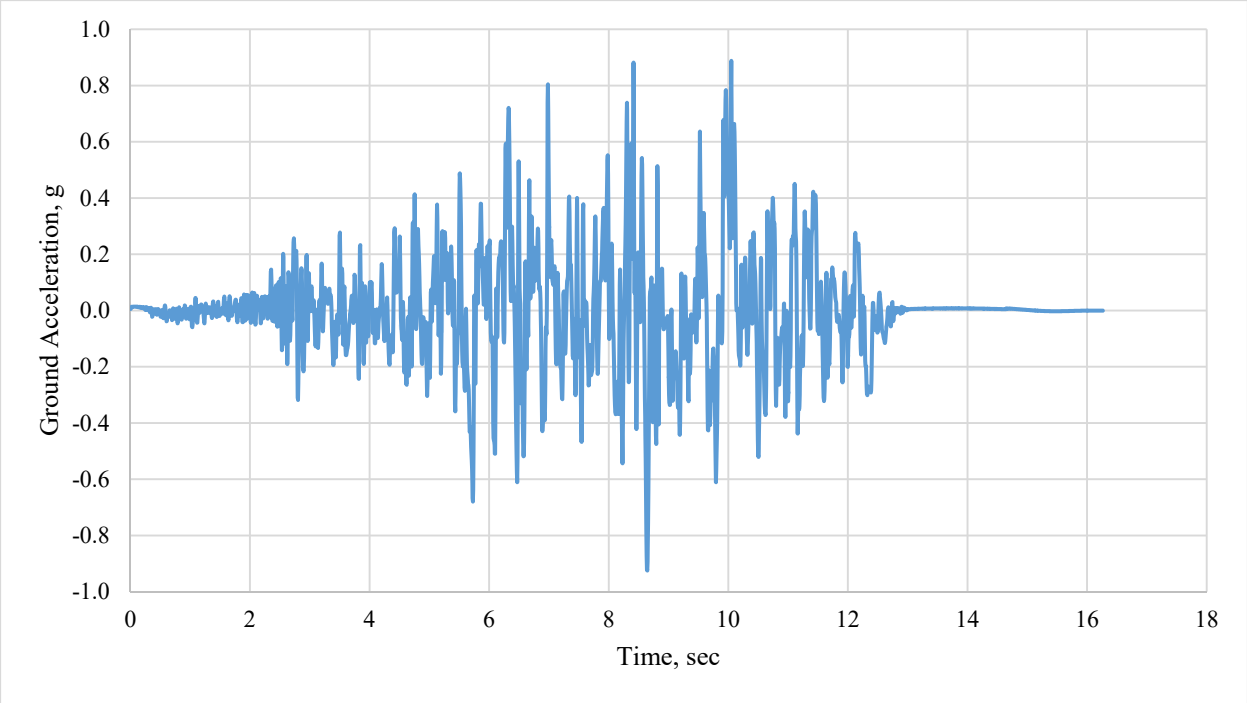


*Figure C-15: PEER126 Scaled Accelerogram*

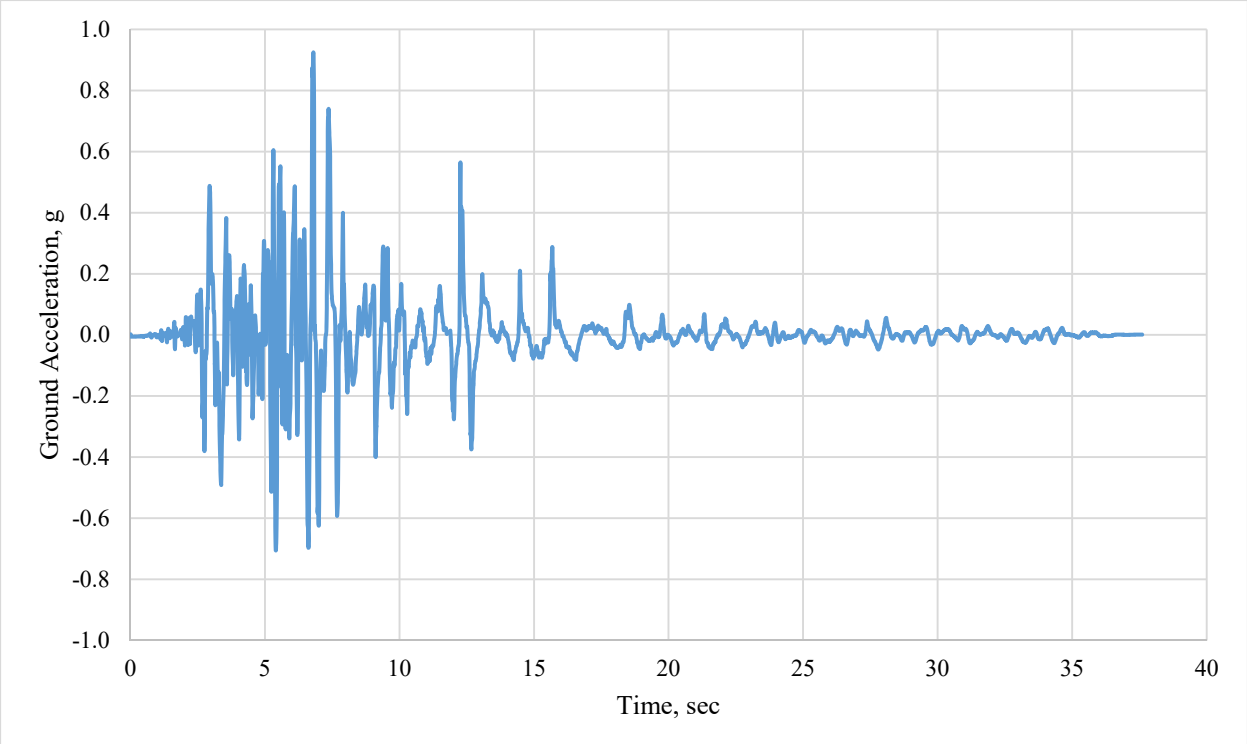


*Figure C-16: PEER160 Scaled Accelerogram*

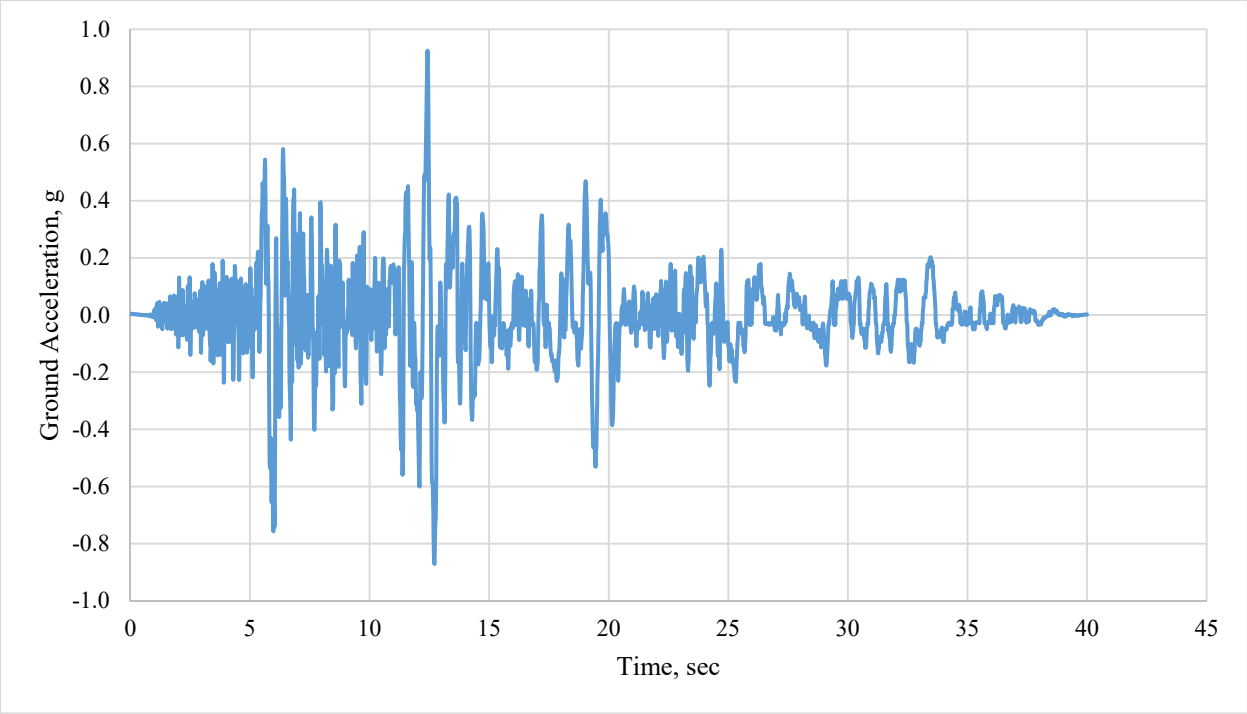


*Figure C-17: PEER165 Scaled Accelerogram*

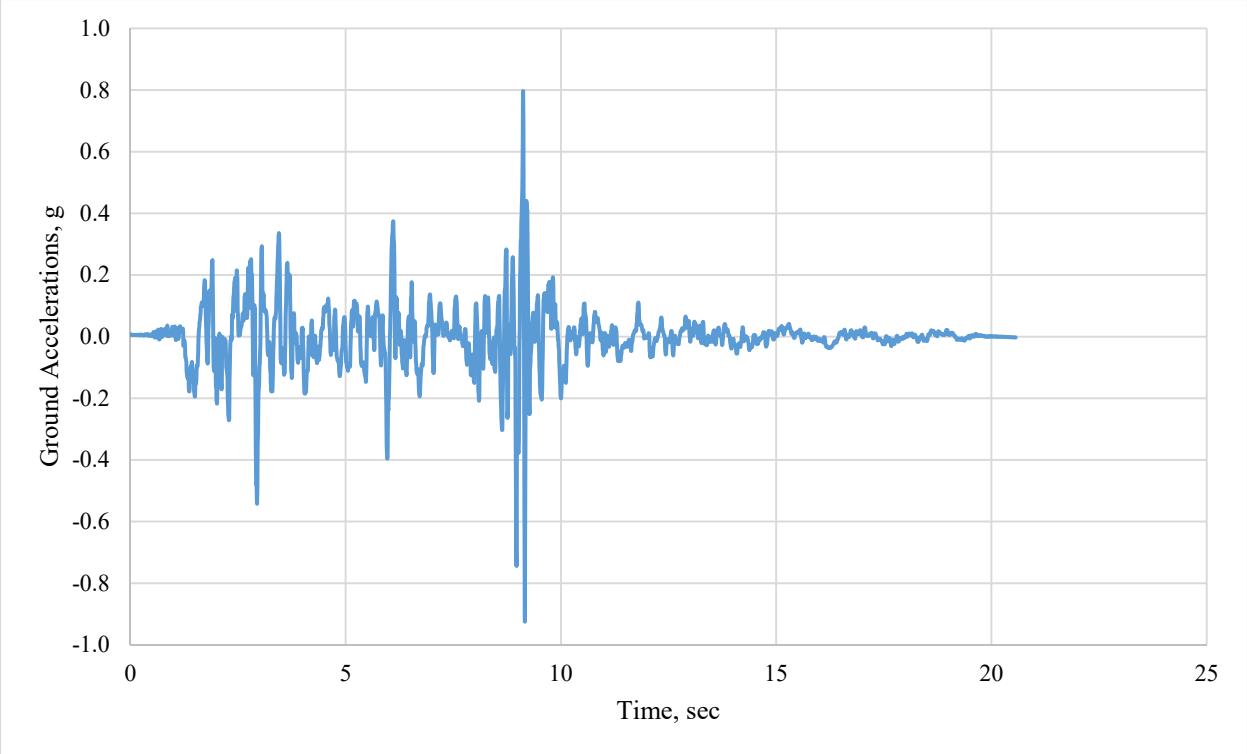


*Figure C-18: PEER495 Scaled Accelerogram*

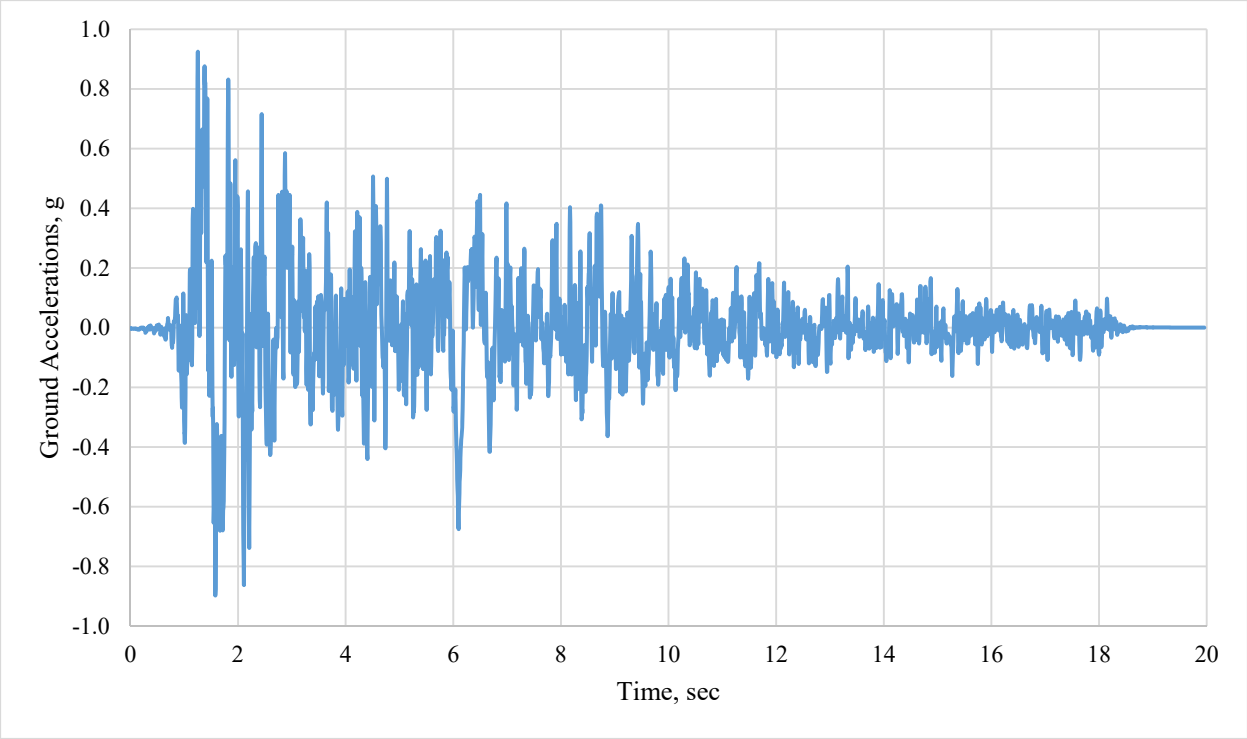


*Figure C-19: PEER496 Scaled Accelerogram*

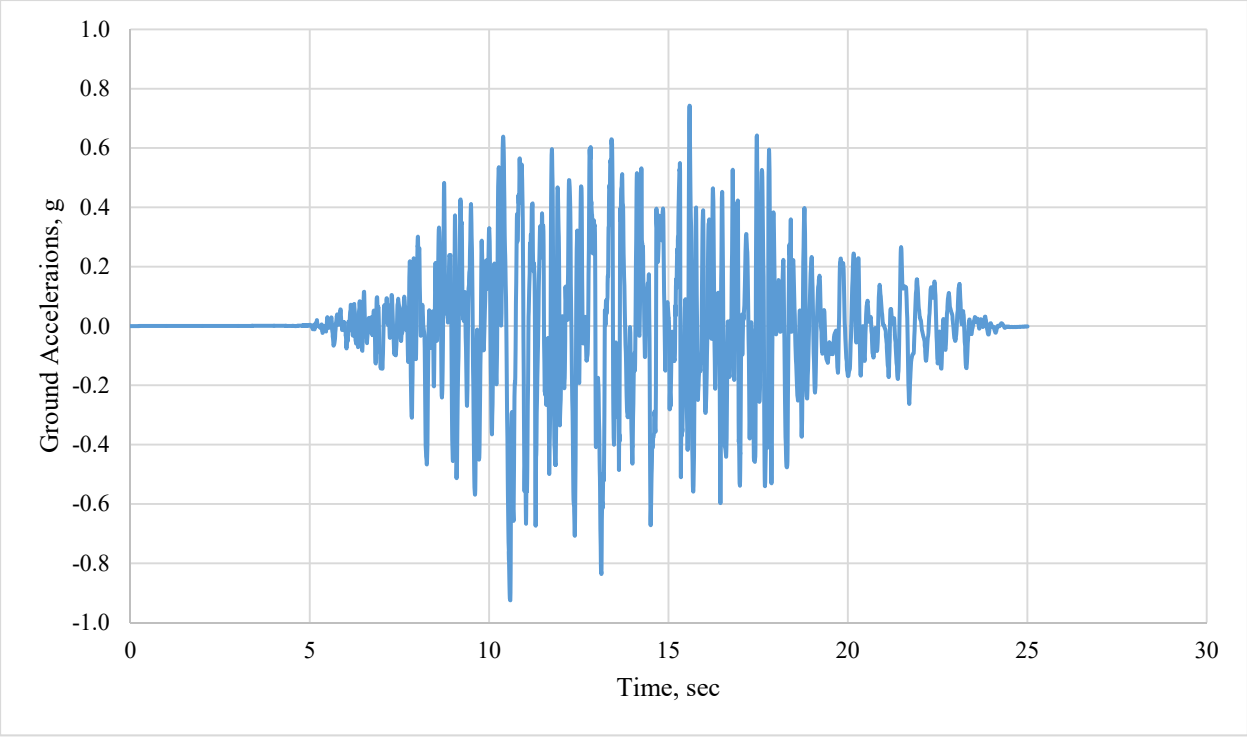


*Figure C-20: PEER741 Scaled Accelerogram*

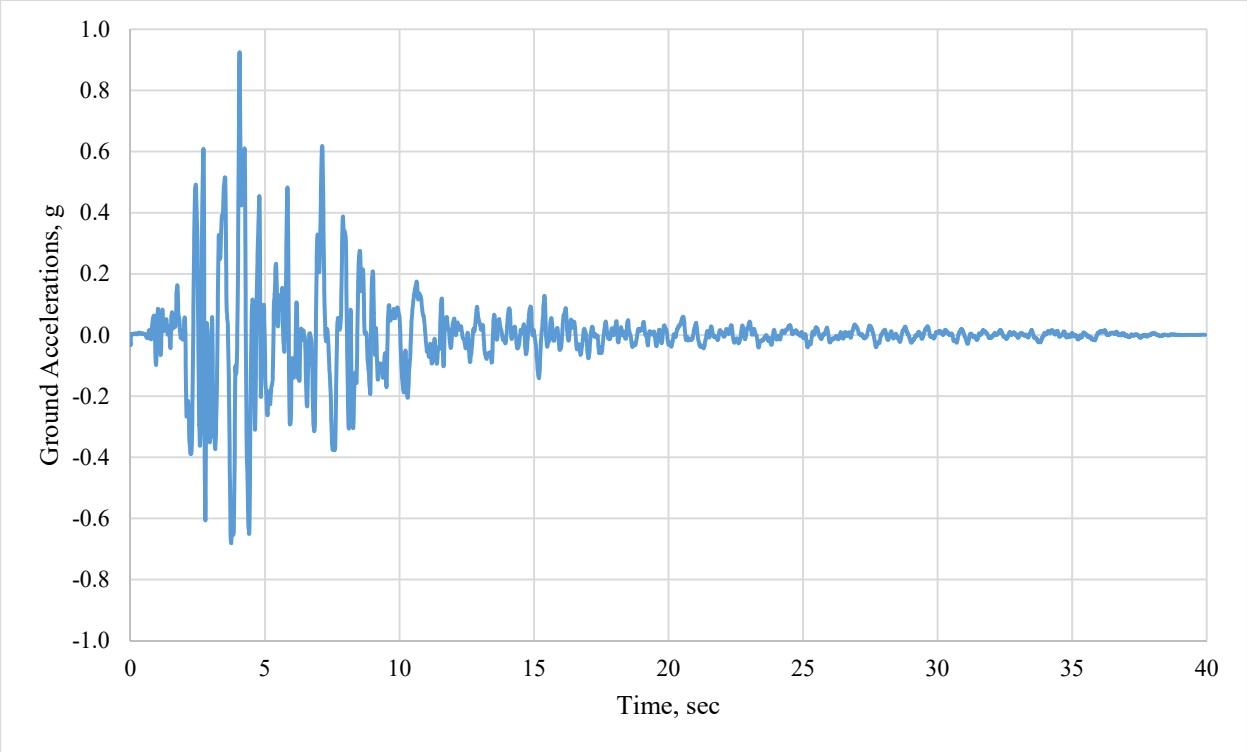


*Figure C-21: PEER753 Scaled Accelerogram*

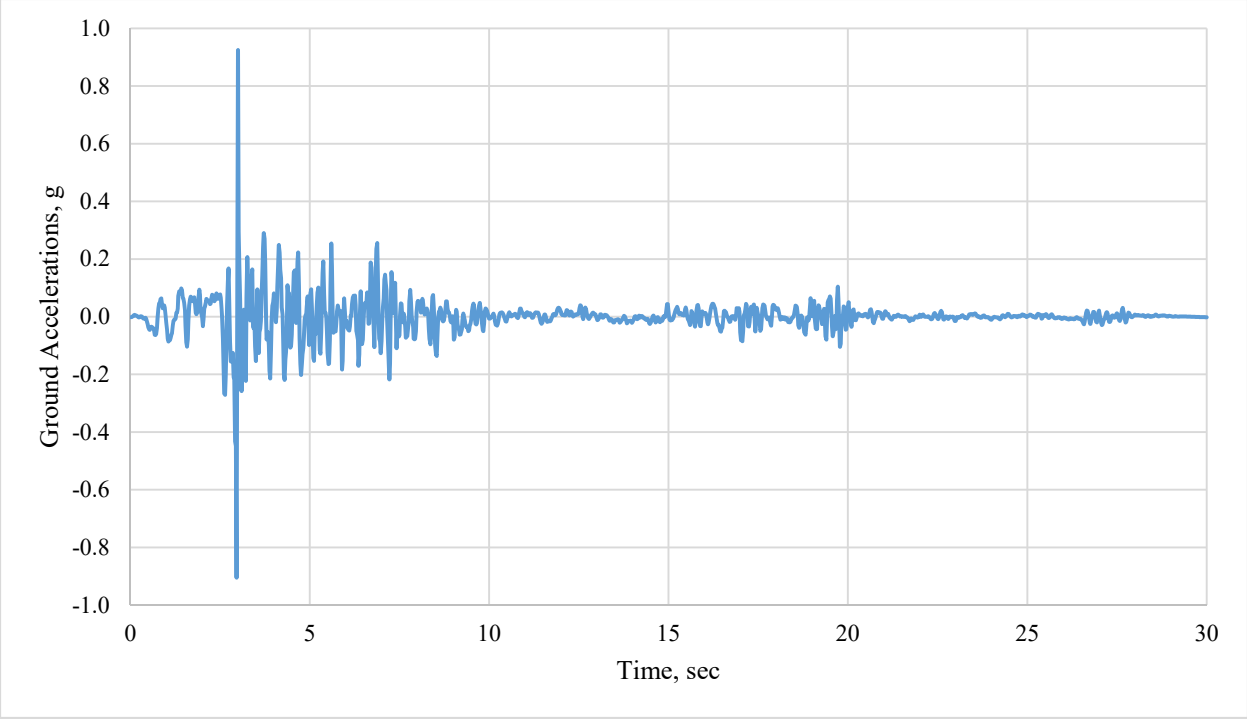


*Figure C-22: PEER825 Scaled Accelerogram*

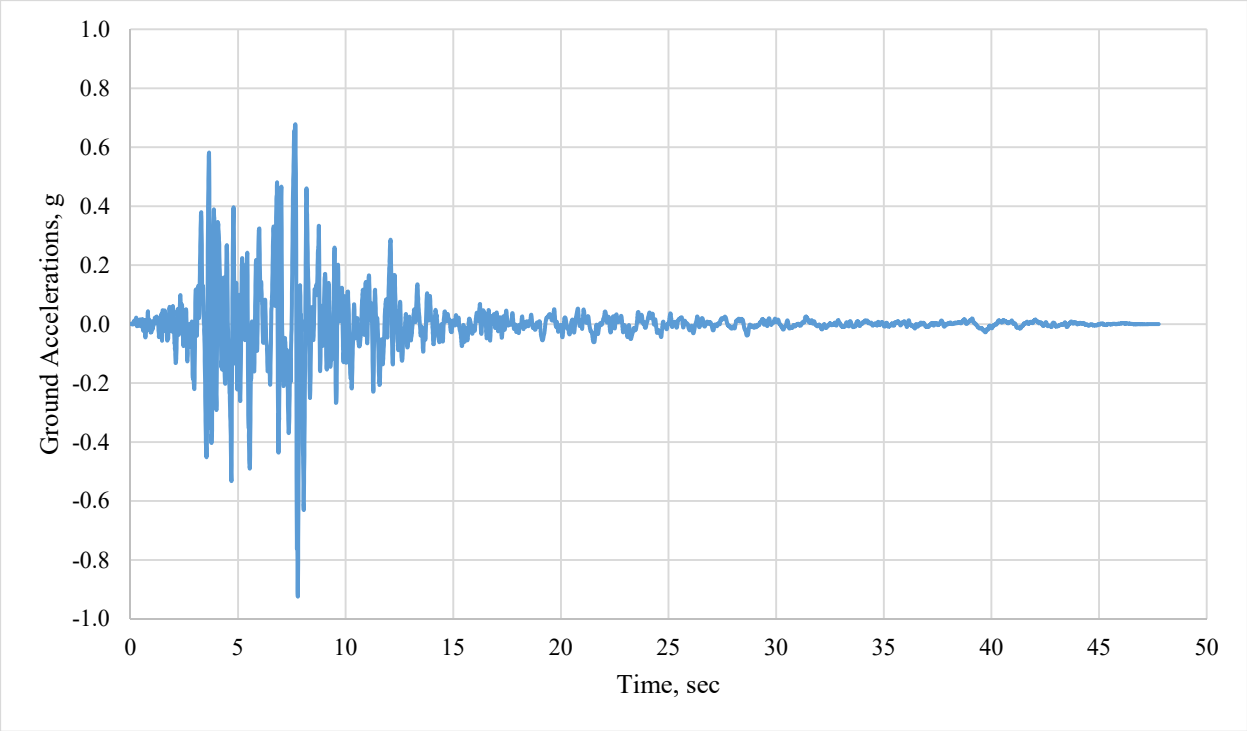


*Figure C-23: PEER1004 Scaled Accelerogram*

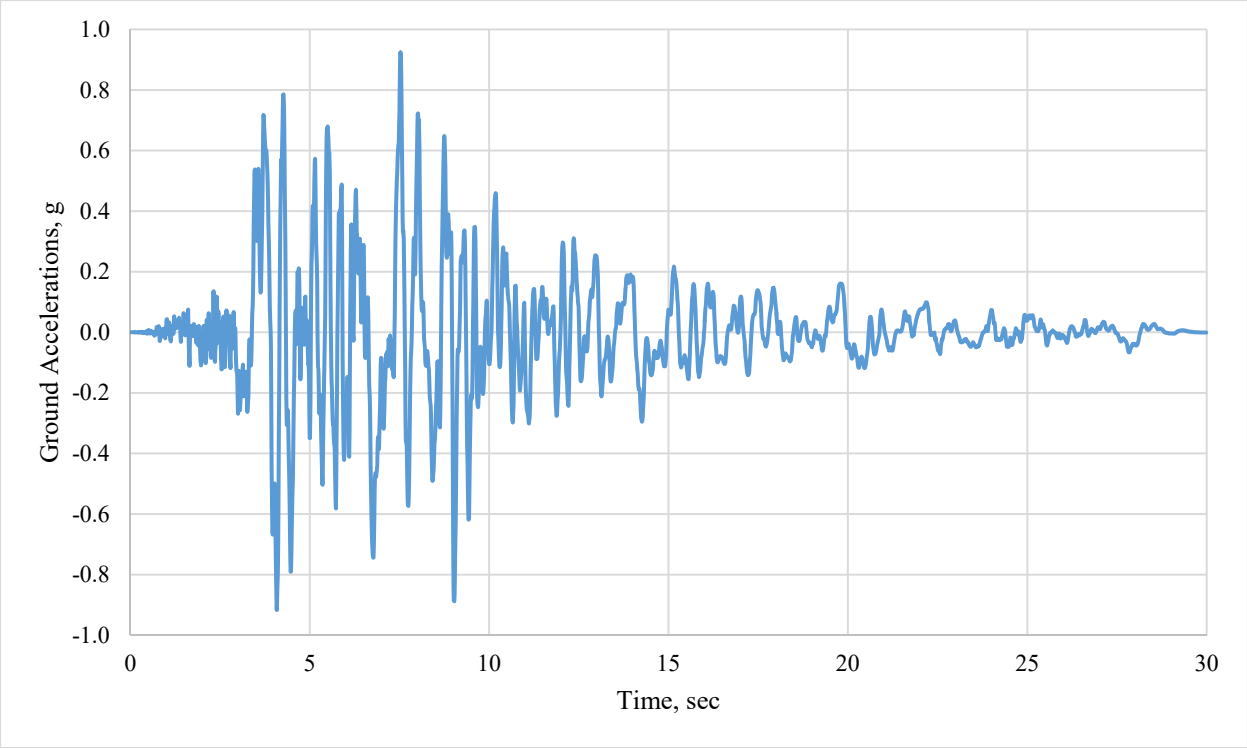


*Figure C-24: PEER1048 Scaled Accelerogram*

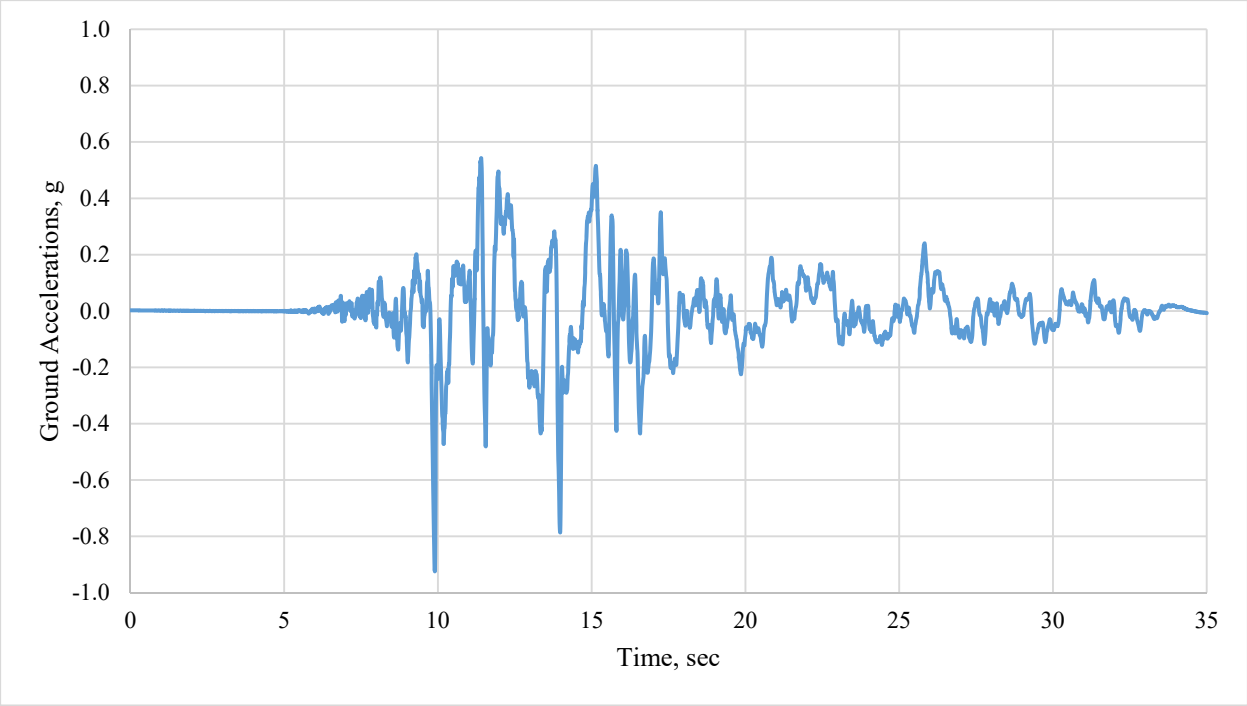


*Figure C-25: PEER1176 Scaled Accelerogram*

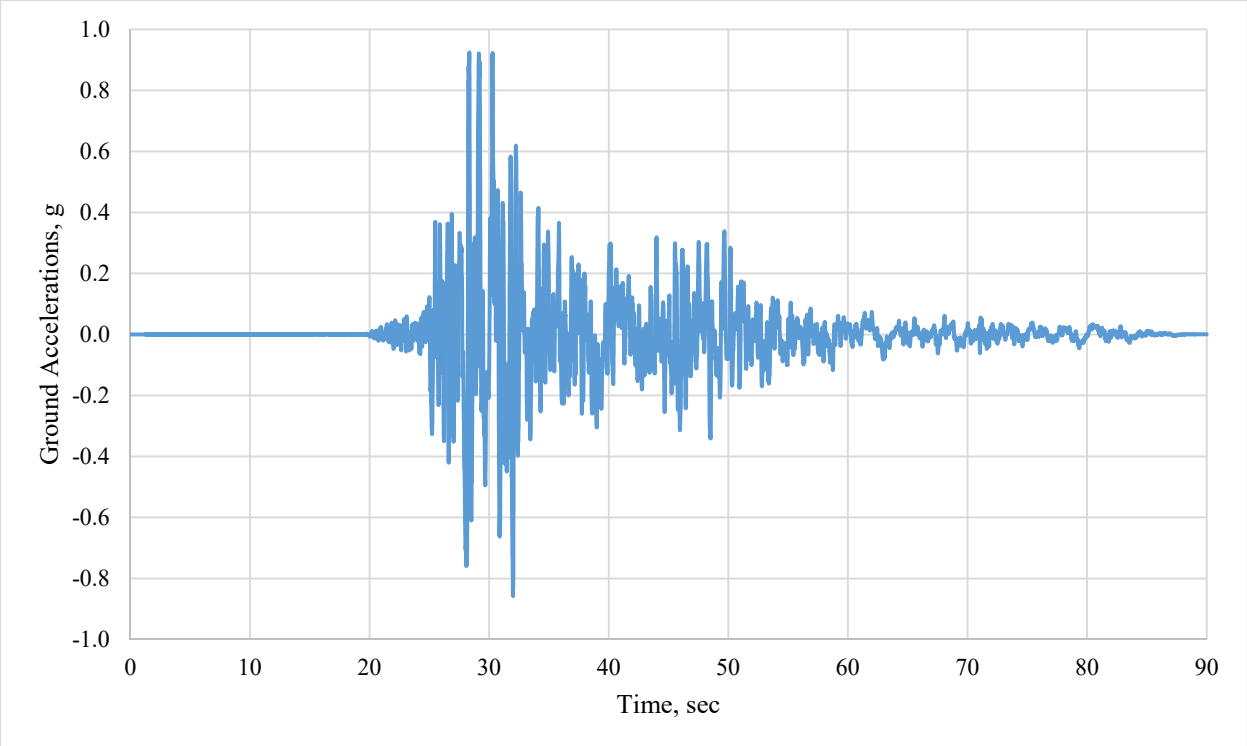


*Figure C-26: PEER1504 Scaled Accelerogram*

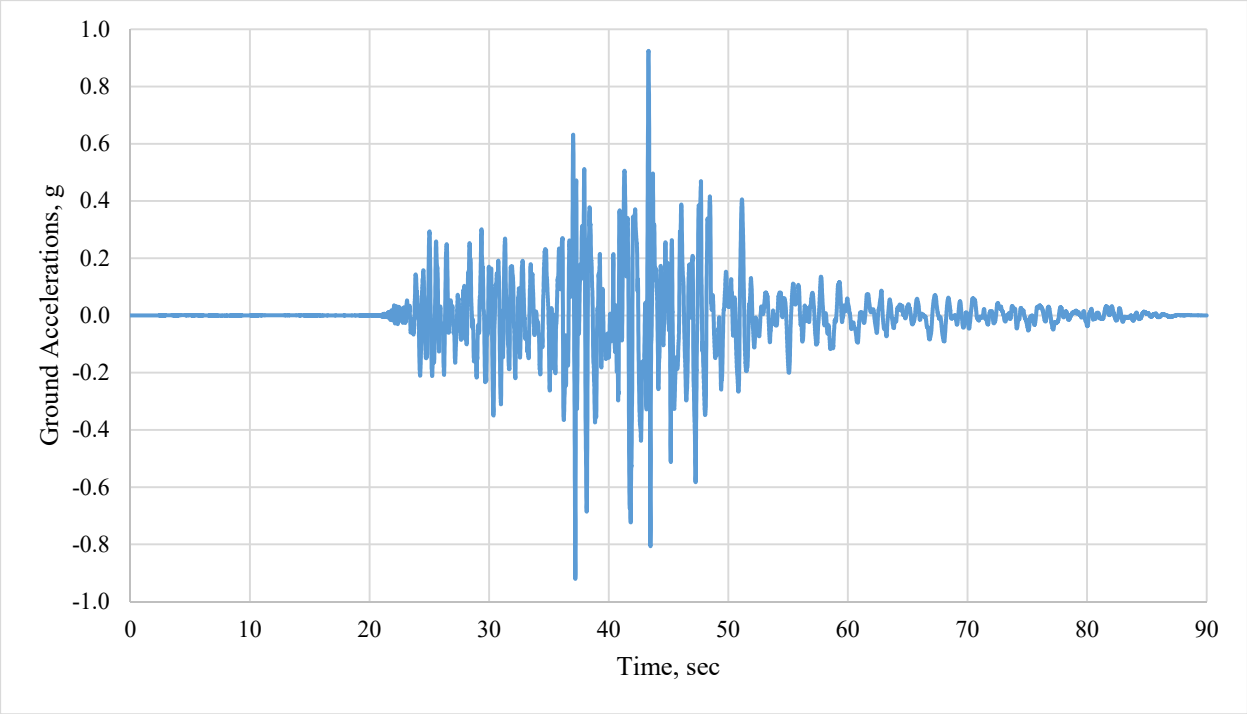


*Figure C-27: PEER1517 Scaled Accelerogram*

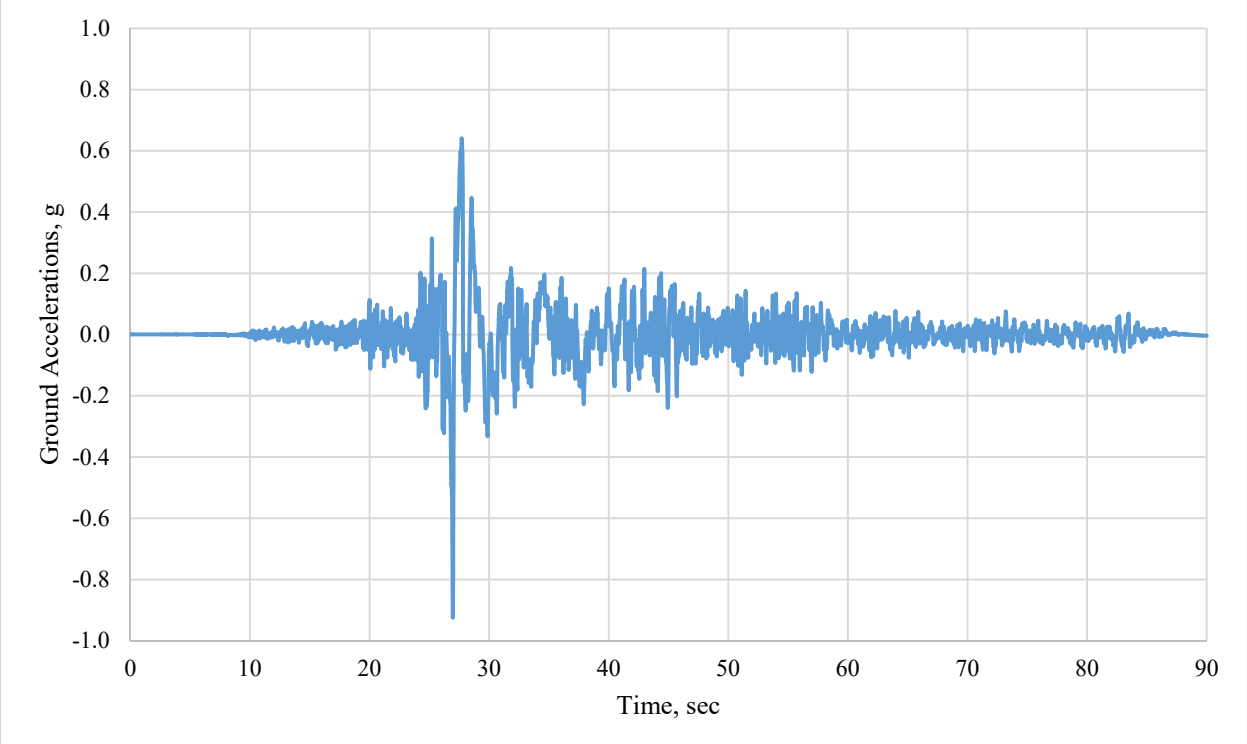


*Figure C-28: PEER2114 Scaled Accelerogram*

## Appendix D: Spectral Accelerations

This Appendix contains the spectral accelerations calculated for each of the frames for all 28 time histories using Newmark's Method presented in (Chopra, 2012).

*Table D-1: Spectral Accelerations Part 1*

| ID No. | PEER Seq. No. | Frame | | | |
|---|---|---|---|---|---|
| | | Control | PR17M1.0H1.4 | PR17M1.0H1.1 | PR17M0.66H1.4 |
| 1 | 181 | 1.26289593 | 1.18400986 | 1.18400986 | 1.18400959 |
| 2 | 182 | 0.99795952 | 0.98118851 | 0.98118851 | 0.98118844 |
| 3 | 292 | 1.00925037 | 1.07447179 | 1.07447179 | 1.07447185 |
| 4 | 723 | 0.78608851 | 1.05760932 | 1.05760932 | 1.05761021 |
| 5 | 802 | 0.62976332 | 0.67583824 | 0.67583824 | 0.67583811 |
| 6 | 821 | 0.63692471 | 0.68325598 | 0.68325598 | 0.68325562 |
| 7 | 828 | 0.36985146 | 0.45059140 | 0.45059140 | 0.45059157 |
| 8 | 879 | 0.15961577 | 0.14507171 | 0.14507171 | 0.14507173 |
| 9 | 1063 | 0.67144081 | 0.86935150 | 0.86935150 | 0.86935192 |
| 10 | 1086 | 0.49752768 | 0.60439972 | 0.60439972 | 0.60440008 |
| 11 | 1165 | 0.62254943 | 0.67309993 | 0.67309993 | 0.67310002 |
| 12 | 1503 | 0.82817036 | 0.74212945 | 0.74212945 | 0.74212961 |
| 13 | 1529 | 2.72495807 | 3.60880234 | 3.60880234 | 3.60880383 |
| 14 | 1605 | 0.44567988 | 0.49193644 | 0.49193644 | 0.49193660 |
| 15 | 126 | 0.27266871 | 0.33366469 | 0.33366469 | 0.33366475 |
| 16 | 160 | 0.08165161 | 0.10754717 | 0.10754717 | 0.10754720 |
| 17 | 165 | 0.32723761 | 0.40833926 | 0.40833926 | 0.40833966 |
| 18 | 495 | 0.12813069 | 0.12533247 | 0.12533247 | 0.12533243 |
| 19 | 496 | 0.16103563 | 0.19175669 | 0.19175669 | 0.19175675 |
| 20 | 741 | 0.12120595 | 0.12070261 | 0.12070261 | 0.12070257 |
| 21 | 753 | 0.18797081 | 0.17525475 | 0.17525475 | 0.17525482 |
| 22 | 825 | 0.16793333 | 0.21482237 | 0.21482237 | 0.21482246 |
| 23 | 1004 | 0.33072497 | 0.40141031 | 0.40141031 | 0.40141042 |
| 24 | 1048 | 0.29768354 | 0.50807321 | 0.50807321 | 0.50807376 |
| 25 | 1176 | 0.95054148 | 0.68635408 | 0.68635408 | 0.68635341 |
| 26 | 1504 | 0.52326209 | 0.80344622 | 0.80344622 | 0.80344642 |
| 27 | 1517 | 0.58483302 | 0.57879322 | 0.57879322 | 0.57879330 |
| 28 | 2114 | 0.88481968 | 0.70207125 | 0.70207125 | 0.70207157 |

*Table D-2: Spectral Accelerations Part 2*

| ID No. | PEER Seq. No. | Frame | | | |
|---|---|---|---|---|---|
| | | PR17M0.66H1.1 | PR17M0.33H1.4 | PR17M0.33H1.1 | PR14M1.0H1.4 |
| 1 | 181 | 1.18400959 | 1.23091123 | 1.12350993 | 1.20969431 |
| 2 | 182 | 0.98118844 | 0.94711744 | 0.85630865 | 0.98652377 |
| 3 | 292 | 1.07447185 | 0.87914691 | 0.69441713 | 1.06625210 |
| 4 | 723 | 1.05761021 | 0.69895517 | 0.56884448 | 0.97155240 |
| 5 | 802 | 0.67583811 | 0.49385839 | 0.45601307 | 0.67859570 |
| 6 | 821 | 0.68325562 | 0.49251808 | 0.41667330 | 0.70706149 |
| 7 | 828 | 0.45059157 | 0.30090005 | 0.24483776 | 0.43322750 |
| 8 | 879 | 0.14507173 | 0.16957532 | 0.16710570 | 0.14740122 |
| 9 | 1063 | 0.86935192 | 0.49482779 | 0.33436309 | 0.82261060 |
| 10 | 1086 | 0.60440008 | 0.38124572 | 0.26013846 | 0.56742710 |
| 11 | 1165 | 0.67310002 | 0.58371073 | 0.52618075 | 0.66346856 |
| 12 | 1503 | 0.74212961 | 0.52198385 | 0.53046696 | 0.80970547 |
| 13 | 1529 | 3.60880383 | 1.79553711 | 1.44239278 | 3.43855317 |
| 14 | 1605 | 0.49193660 | 0.43528116 | 0.43118520 | 0.47653007 |
| 15 | 126 | 0.33366475 | 0.22401794 | 0.24737519 | 0.32423768 |
| 16 | 160 | 0.10754720 | 0.05148170 | 0.04788827 | 0.10412105 |
| 17 | 165 | 0.40833966 | 0.38467372 | 0.24010774 | 0.35470471 |
| 18 | 495 | 0.12533243 | 0.14518794 | 0.13535715 | 0.12775336 |
| 19 | 496 | 0.19175675 | 0.13112683 | 0.10059724 | 0.18484632 |
| 20 | 741 | 0.12070257 | 0.10388113 | 0.07887380 | 0.12281751 |
| 21 | 753 | 0.17525482 | 0.17497598 | 0.15909650 | 0.17934824 |
| 22 | 825 | 0.21482246 | 0.12092380 | 0.08480785 | 0.20488495 |
| 23 | 1004 | 0.40141042 | 0.25475471 | 0.18724957 | 0.38661973 |
| 24 | 1048 | 0.50807376 | 0.24475772 | 0.24382934 | 0.45049185 |
| 25 | 1176 | 0.68635341 | 1.08481626 | 1.14332531 | 0.75622555 |
| 26 | 1504 | 0.80344642 | 0.51118710 | 0.67530067 | 0.77113975 |
| 27 | 1517 | 0.57879330 | 0.54526662 | 0.42888814 | 0.56604215 |
| 28 | 2114 | 0.70207157 | 0.99638127 | 0.81927693 | 0.70574429 |

*Table D-3: Spectral Accelerations Part 3*

| ID No. | PEER Seq. No. | Frame | | | |
|---|---|---|---|---|---|
| | | PR14M1.0H1.1 | PR14M0.66H1.4 | PR14M0.66H1.1 | PR14M0.33H1.4 |
| 1 | 181 | 1.20969431 | 1.20969409 | 1.20969409 | 1.21706500 |
| 2 | 182 | 0.98652377 | 0.98652374 | 0.98652374 | 0.93861235 |
| 3 | 292 | 1.06625210 | 1.06625220 | 1.06625220 | 0.85470338 |
| 4 | 723 | 0.97155240 | 0.97155318 | 0.97155318 | 0.68826570 |
| 5 | 802 | 0.67859570 | 0.67859575 | 0.67859575 | 0.47384750 |
| 6 | 821 | 0.70706149 | 0.70706141 | 0.70706141 | 0.47673240 |
| 7 | 828 | 0.43322750 | 0.43322768 | 0.43322768 | 0.29406903 |
| 8 | 879 | 0.14740122 | 0.14740118 | 0.14740118 | 0.16937421 |
| 9 | 1063 | 0.82261060 | 0.82261108 | 0.82261108 | 0.47340798 |
| 10 | 1086 | 0.56742710 | 0.56742746 | 0.56742746 | 0.36044066 |
| 11 | 1165 | 0.66346856 | 0.66346866 | 0.66346866 | 0.57955823 |
| 12 | 1503 | 0.80970547 | 0.80970374 | 0.80970374 | 0.55832170 |
| 13 | 1529 | 3.43855317 | 3.43855498 | 3.43855498 | 1.67955557 |
| 14 | 1605 | 0.47653007 | 0.47653021 | 0.47653021 | 0.43475846 |
| 15 | 126 | 0.32423768 | 0.32423779 | 0.32423779 | 0.22215929 |
| 16 | 160 | 0.10412105 | 0.10412109 | 0.10412109 | 0.05109657 |
| 17 | 165 | 0.35470471 | 0.35470524 | 0.35470524 | 0.39250716 |
| 18 | 495 | 0.12775336 | 0.12775334 | 0.12775334 | 0.14894438 |
| 19 | 496 | 0.18484632 | 0.18484639 | 0.18484639 | 0.12686506 |
| 20 | 741 | 0.12281751 | 0.12281752 | 0.12281752 | 0.10071275 |
| 21 | 753 | 0.17934824 | 0.17934814 | 0.17934814 | 0.17765272 |
| 22 | 825 | 0.20488495 | 0.20488505 | 0.20488505 | 0.11367488 |
| 23 | 1004 | 0.38661973 | 0.38661991 | 0.38661991 | 0.24156302 |
| 24 | 1048 | 0.45049185 | 0.45049240 | 0.45049240 | 0.24536696 |
| 25 | 1176 | 0.75622555 | 0.75622487 | 0.75622487 | 1.10169066 |
| 26 | 1504 | 0.77113975 | 0.77114017 | 0.77114017 | 0.51074673 |
| 27 | 1517 | 0.56604215 | 0.56604230 | 0.56604230 | 0.51668205 |
| 28 | 2114 | 0.70574429 | 0.70574415 | 0.70574415 | 0.98664250 |

*Table D-4: Spectral Accelerations Part 4*

| ID No. | PEER Seq. No. | Frame | | | |
|---|---|---|---|---|---|
| | | PR14M0.33H1.1 | PR11M1.0H1.4 | PR11M1.0H1.1 | PR11M0.66H1.4 |
| 1 | 181 | 1.10768056 | 1.24130668 | 1.24130668 | 1.24130659 |
| 2 | 182 | 0.84123273 | 0.99778631 | 0.99778631 | 0.99778628 |
| 3 | 292 | 0.67322668 | 1.04697439 | 1.04697439 | 1.04697448 |
| 4 | 723 | 0.54663353 | 0.87173618 | 0.87173618 | 0.87173648 |
| 5 | 802 | 0.45416210 | 0.65749618 | 0.65749618 | 0.65749624 |
| 6 | 821 | 0.40945269 | 0.69492292 | 0.69492292 | 0.69492295 |
| 7 | 828 | 0.23786121 | 0.40603536 | 0.40603536 | 0.40603545 |
| 8 | 879 | 0.16503405 | 0.15244628 | 0.15244628 | 0.15244626 |
| 9 | 1063 | 0.31535323 | 0.75328477 | 0.75328477 | 0.75328499 |
| 10 | 1086 | 0.25126893 | 0.53057074 | 0.53057074 | 0.53057082 |
| 11 | 1165 | 0.51485390 | 0.64615653 | 0.64615653 | 0.64615660 |
| 12 | 1503 | 0.50679736 | 0.94137106 | 0.94137106 | 0.94137105 |
| 13 | 1529 | 1.42775248 | 3.14557155 | 3.14557155 | 3.14557264 |
| 14 | 1605 | 0.43010596 | 0.45916930 | 0.45916930 | 0.45916935 |
| 15 | 126 | 0.25268059 | 0.30405797 | 0.30405797 | 0.30405806 |
| 16 | 160 | 0.04732925 | 0.09599875 | 0.09599875 | 0.09599879 |
| 17 | 165 | 0.23655633 | 0.35860884 | 0.35860884 | 0.35860902 |
| 18 | 495 | 0.12887953 | 0.12814935 | 0.12814935 | 0.12814935 |
| 19 | 496 | 0.09708929 | 0.17456403 | 0.17456403 | 0.17456407 |
| 20 | 741 | 0.07784389 | 0.11893282 | 0.11893282 | 0.11893280 |
| 21 | 753 | 0.15629458 | 0.18927731 | 0.18927731 | 0.18927730 |
| 22 | 825 | 0.08194987 | 0.18665049 | 0.18665049 | 0.18665056 |
| 23 | 1004 | 0.18161611 | 0.35779862 | 0.35779862 | 0.35779868 |
| 24 | 1048 | 0.24095267 | 0.37345317 | 0.37345317 | 0.37345342 |
| 25 | 1176 | 1.13690936 | 0.85111881 | 0.85111881 | 0.85111850 |
| 26 | 1504 | 0.68798543 | 0.68313649 | 0.68313649 | 0.68313690 |
| 27 | 1517 | 0.41650590 | 0.55382003 | 0.55382003 | 0.55382002 |
| 28 | 2114 | 0.80137149 | 0.74132248 | 0.74132248 | 0.74132203 |

*Table D-5: Spectral Accelerations Part 5*

| ID No. | PEER Seq. No. | Frame | | | |
|---|---|---|---|---|---|
| | | PR11M0.66H1.1 | PR11M0.33H1.4 | PR11M0.33H1.1 | PR8M1.0H1.4 |
| 1 | 181 | 1.24130659 | 1.26783737 | 1.26129725 | 1.26563789 |
| 2 | 182 | 0.99778628 | 0.99165196 | 0.97533854 | 0.99617515 |
| 3 | 292 | 1.04697448 | 0.98232279 | 0.94249893 | 0.99879907 |
| 4 | 723 | 0.87173648 | 0.75371458 | 0.72268695 | 0.77196231 |
| 5 | 802 | 0.65749624 | 0.61175865 | 0.57238001 | 0.62323837 |
| 6 | 821 | 0.69492295 | 0.57164976 | 0.52593469 | 0.61036141 |
| 7 | 828 | 0.40603545 | 0.34968872 | 0.32560370 | 0.36168488 |
| 8 | 879 | 0.15244626 | 0.16357456 | 0.16730635 | 0.16136192 |
| 9 | 1063 | 0.75328499 | 0.61939219 | 0.55440137 | 0.65084370 |
| 10 | 1086 | 0.53057082 | 0.47313755 | 0.43681283 | 0.48815947 |
| 11 | 1165 | 0.64615660 | 0.60901661 | 0.59262853 | 0.61715467 |
| 12 | 1503 | 0.94137105 | 0.70787429 | 0.53855838 | 0.78745507 |
| 13 | 1529 | 3.14557264 | 2.47166619 | 2.14616794 | 2.62361902 |
| 14 | 1605 | 0.45916935 | 0.44124084 | 0.43764659 | 0.44369329 |
| 15 | 126 | 0.30405806 | 0.25519117 | 0.23732192 | 0.26540303 |
| 16 | 160 | 0.09599879 | 0.07234844 | 0.06016528 | 0.07797416 |
| 17 | 165 | 0.35860902 | 0.32757934 | 0.31210549 | 0.32900945 |
| 18 | 495 | 0.12814935 | 0.12688385 | 0.13068521 | 0.12790920 |
| 19 | 496 | 0.17456407 | 0.15325896 | 0.14357637 | 0.15789906 |
| 20 | 741 | 0.11893280 | 0.11483650 | 0.11270391 | 0.11963119 |
| 21 | 753 | 0.18927730 | 0.18031374 | 0.16455535 | 0.18545650 |
| 22 | 825 | 0.18665056 | 0.15833426 | 0.14352122 | 0.16404569 |
| 23 | 1004 | 0.35779868 | 0.31615019 | 0.29241061 | 0.32528456 |
| 24 | 1048 | 0.37345342 | 0.27000447 | 0.25087959 | 0.28509504 |
| 25 | 1176 | 0.85111850 | 0.99320807 | 1.02977478 | 0.96906693 |
| 26 | 1504 | 0.68313690 | 0.49067464 | 0.50477446 | 0.50137874 |
| 27 | 1517 | 0.55382002 | 0.60669305 | 0.60556315 | 0.59500458 |
| 28 | 2114 | 0.74132203 | 0.94252698 | 0.98578539 | 0.91067123 |

*Table D-6: Spectral Accelerations Part 6*

| ID No. | PEER Seq. No. | Frame | | | |
|---|---|---|---|---|---|
| | | PR8M1.0H1.1 | PR8M0.66H1.4 | PR8M0.66H1.1 | PR8M0.33H1.4 |
| 1 | 181 | 1.26563789 | 1.26563783 | 1.26563783 | 1.26495765 |
| 2 | 182 | 0.99617515 | 0.99617521 | 0.99617521 | 0.98080431 |
| 3 | 292 | 0.99879907 | 0.99879933 | 0.99879933 | 0.95473930 |
| 4 | 723 | 0.77196231 | 0.77196264 | 0.77196264 | 0.73023066 |
| 5 | 802 | 0.62323837 | 0.62323854 | 0.62323854 | 0.58593223 |
| 6 | 821 | 0.61036141 | 0.61036212 | 0.61036212 | 0.53060666 |
| 7 | 828 | 0.36168488 | 0.36168508 | 0.36168508 | 0.33238607 |
| 8 | 879 | 0.16136192 | 0.16136187 | 0.16136187 | 0.16606704 |
| 9 | 1063 | 0.65084370 | 0.65084422 | 0.65084422 | 0.57046176 |
| 10 | 1086 | 0.48815947 | 0.48815973 | 0.48815973 | 0.44777382 |
| 11 | 1165 | 0.61715467 | 0.61715480 | 0.61715480 | 0.59685714 |
| 12 | 1503 | 0.78745507 | 0.78745626 | 0.78745626 | 0.58006888 |
| 13 | 1529 | 2.62361902 | 2.62362155 | 2.62362155 | 2.23999892 |
| 14 | 1605 | 0.44369329 | 0.44369334 | 0.44369334 | 0.43848324 |
| 15 | 126 | 0.26540303 | 0.26540320 | 0.26540320 | 0.24183210 |
| 16 | 160 | 0.07797416 | 0.07797426 | 0.07797426 | 0.06366706 |
| 17 | 165 | 0.32900945 | 0.32900943 | 0.32900943 | 0.31801213 |
| 18 | 495 | 0.12790920 | 0.12790921 | 0.12790921 | 0.12637204 |
| 19 | 496 | 0.15789906 | 0.15789914 | 0.15789914 | 0.14634089 |
| 20 | 741 | 0.11963119 | 0.11963125 | 0.11963125 | 0.11354512 |
| 21 | 753 | 0.18545650 | 0.18545657 | 0.18545657 | 0.16967986 |
| 22 | 825 | 0.16404569 | 0.16404578 | 0.16404578 | 0.14801481 |
| 23 | 1004 | 0.32528456 | 0.32528470 | 0.32528470 | 0.29984312 |
| 24 | 1048 | 0.28509504 | 0.28509533 | 0.28509533 | 0.25476102 |
| 25 | 1176 | 0.96906693 | 0.96906649 | 0.96906649 | 1.02163009 |
| 26 | 1504 | 0.50137874 | 0.50137940 | 0.50137940 | 0.50160018 |
| 27 | 1517 | 0.59500458 | 0.59500434 | 0.59500434 | 0.61006570 |
| 28 | 2114 | 0.91067123 | 0.91067063 | 0.91067063 | 0.97643182 |

*Table D-7: Spectral Accelerations Part 7*

| ID No. | PEER Seq. No. | Frame | | | |
|---|---|---|---|---|---|
| | | PR8M0.33H1.1 | PR5M1.0H1.4 | PR5M1.0H1.1 | PR5M0.66H1.4 |
| 1 | 181 | 1.25740963 | 1.21840318 | 1.21840318 | 1.21840361 |
| 2 | 182 | 0.97057619 | 0.93943931 | 0.93943931 | 0.93943958 |
| 3 | 292 | 0.93230905 | 0.85693648 | 0.85693648 | 0.85693723 |
| 4 | 723 | 0.71881022 | 0.68928641 | 0.68928641 | 0.68928675 |
| 5 | 802 | 0.56052819 | 0.47574502 | 0.47574502 | 0.47574564 |
| 6 | 821 | 0.52144889 | 0.47824304 | 0.47824304 | 0.47824353 |
| 7 | 828 | 0.32033160 | 0.29467592 | 0.29467592 | 0.29467612 |
| 8 | 879 | 0.16805970 | 0.16928834 | 0.16928834 | 0.16928831 |
| 9 | 1063 | 0.54427659 | 0.47534857 | 0.47534857 | 0.47534921 |
| 10 | 1086 | 0.42761002 | 0.36235565 | 0.36235565 | 0.36235629 |
| 11 | 1165 | 0.59070336 | 0.57997471 | 0.57997471 | 0.57997485 |
| 12 | 1503 | 0.51412043 | 0.55410063 | 0.55410063 | 0.55409923 |
| 13 | 1529 | 2.07146356 | 1.69005329 | 1.69005329 | 1.69005678 |
| 14 | 1605 | 0.43708449 | 0.43479739 | 0.43479739 | 0.43479741 |
| 15 | 126 | 0.23412572 | 0.22227309 | 0.22227309 | 0.22227313 |
| 16 | 160 | 0.05739589 | 0.05113232 | 0.05113232 | 0.05113233 |
| 17 | 165 | 0.31309762 | 0.39277818 | 0.39277818 | 0.39277827 |
| 18 | 495 | 0.13352069 | 0.14873073 | 0.14873073 | 0.14873065 |
| 19 | 496 | 0.14138803 | 0.12724690 | 0.12724690 | 0.12724703 |
| 20 | 741 | 0.11174579 | 0.10103392 | 0.10103392 | 0.10103403 |
| 21 | 753 | 0.16020134 | 0.17752358 | 0.17752358 | 0.17752353 |
| 22 | 825 | 0.13993215 | 0.11435096 | 0.11435096 | 0.11435118 |
| 23 | 1004 | 0.28615478 | 0.24276541 | 0.24276541 | 0.24276581 |
| 24 | 1048 | 0.24857360 | 0.24528764 | 0.24528764 | 0.24528761 |
| 25 | 1176 | 1.03478680 | 1.10051518 | 1.10051518 | 1.10051478 |
| 26 | 1504 | 0.50681545 | 0.51083762 | 0.51083762 | 0.51083765 |
| 27 | 1517 | 0.59950343 | 0.51914417 | 0.51914417 | 0.51914499 |
| 28 | 2114 | 0.99144803 | 0.98781250 | 0.98781250 | 0.98781288 |

*Table D-8: Spectral Accelerations Part 8*

| ID No. | PEER Seq. No. | Frame | | |
|---|---|---|---|---|
| | | PR5M0.66H1.1 | PR5M0.33H1.4 | PR5M0.33H1.1 |
| 1 | 181 | 1.21840361 | 1.20939420 | 1.20557392 |
| 2 | 182 | 0.93943958 | 0.93396054 | 0.93165325 |
| 3 | 292 | 0.85693723 | 0.84237951 | 0.83652841 |
| 4 | 723 | 0.68928675 | 0.68229930 | 0.67926920 |
| 5 | 802 | 0.47574564 | 0.46298413 | 0.45758045 |
| 6 | 821 | 0.47824353 | 0.46819546 | 0.46402150 |
| 7 | 828 | 0.29467612 | 0.29062535 | 0.28899129 |
| 8 | 879 | 0.16928831 | 0.16966264 | 0.16970986 |
| 9 | 1063 | 0.47534921 | 0.46280542 | 0.45781189 |
| 10 | 1086 | 0.36235629 | 0.35014542 | 0.34517102 |
| 11 | 1165 | 0.57997485 | 0.57713636 | 0.57592353 |
| 12 | 1503 | 0.55409923 | 0.58153859 | 0.59221310 |
| 13 | 1529 | 1.69005678 | 1.62206104 | 1.59503046 |
| 14 | 1605 | 0.43479741 | 0.43453828 | 0.43444671 |
| 15 | 126 | 0.22227313 | 0.22170325 | 0.22158094 |
| 16 | 160 | 0.05113233 | 0.05089661 | 0.05080020 |
| 17 | 165 | 0.39277827 | 0.38891922 | 0.38706599 |
| 18 | 495 | 0.14873065 | 0.14969691 | 0.14983654 |
| 19 | 496 | 0.12724703 | 0.12478548 | 0.12381450 |
| 20 | 741 | 0.10103403 | 0.09883624 | 0.09789018 |
| 21 | 753 | 0.17752353 | 0.17798082 | 0.17792415 |
| 22 | 825 | 0.11435118 | 0.10987490 | 0.10807026 |
| 23 | 1004 | 0.24276581 | 0.23495154 | 0.23182427 |
| 24 | 1048 | 0.24528761 | 0.24584249 | 0.24607608 |
| 25 | 1176 | 1.10051478 | 1.10706473 | 1.10896222 |
| 26 | 1504 | 0.51083765 | 0.51014134 | 0.50977651 |
| 27 | 1517 | 0.51914499 | 0.50447188 | 0.50338318 |
| 28 | 2114 | 0.98781288 | 0.97919720 | 0.97510530 |

## Appendix E: Maximum Total Roof Drift Multi-Record IDA Curve Sets

This Appendix contains the multi-record IDA curve sets for the maximum total roof drift DMs for all of the frames.

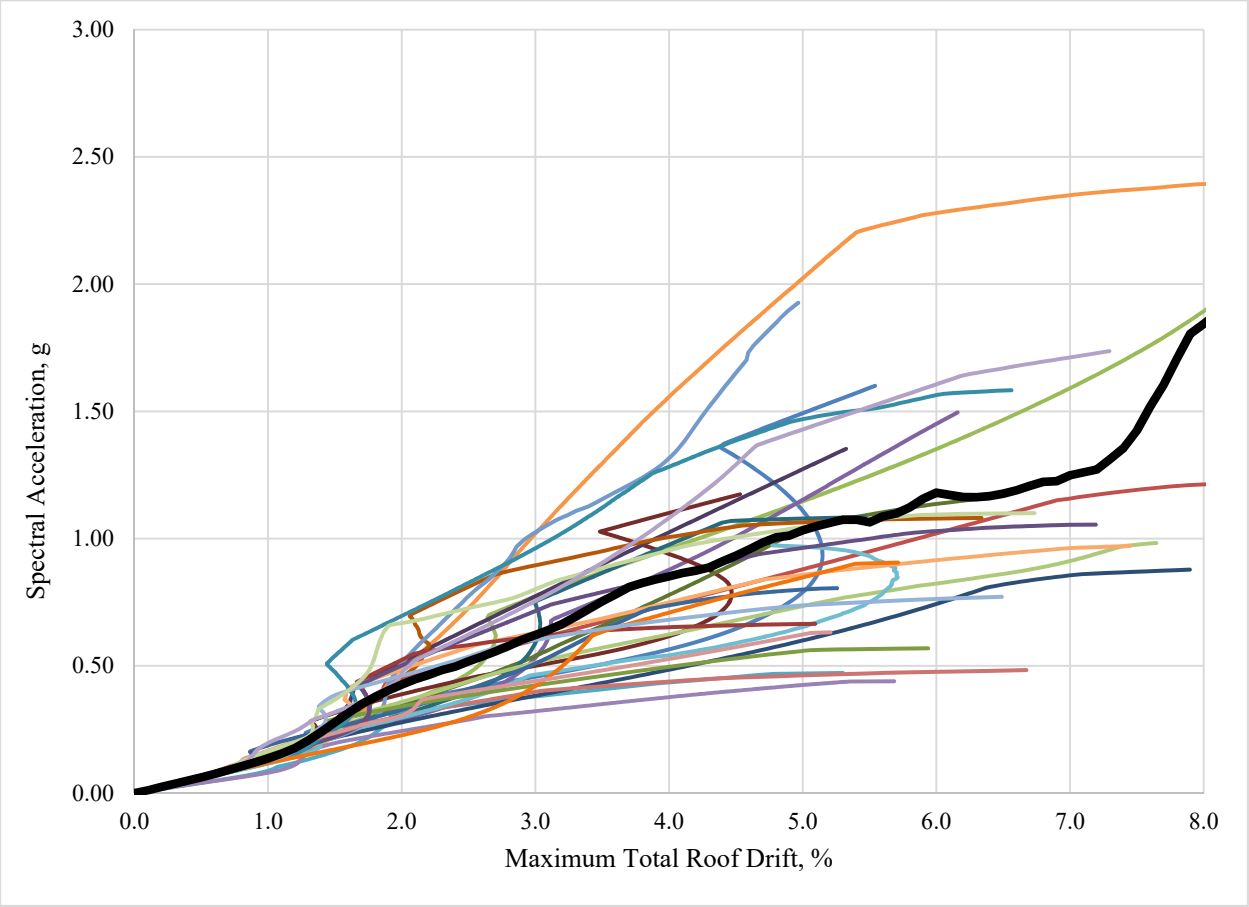


*Figure E-1: Maximum Total Roof Drift for Control Frame Multi-Record IDA Curve Set*

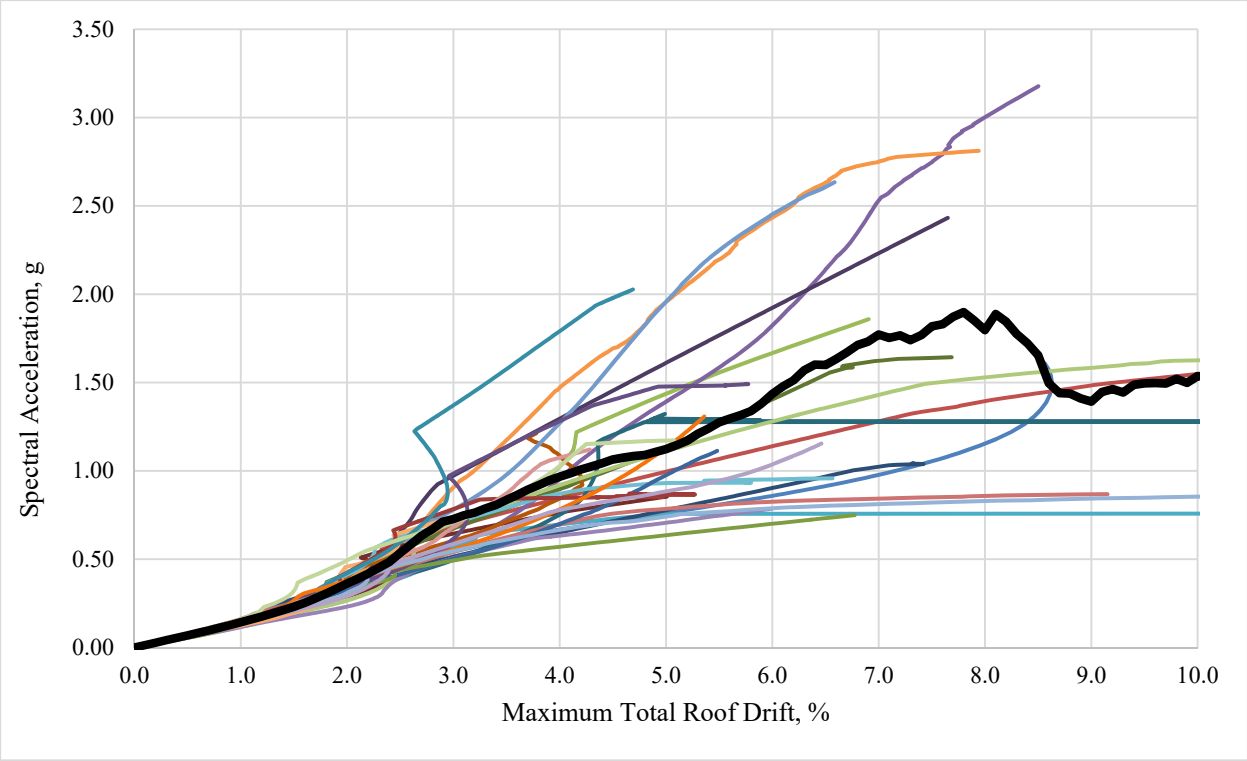


*Figure E-2: Maximum Total Roof Drift for PR17M1.0H1.4 Multi-Record IDA Curve Set*

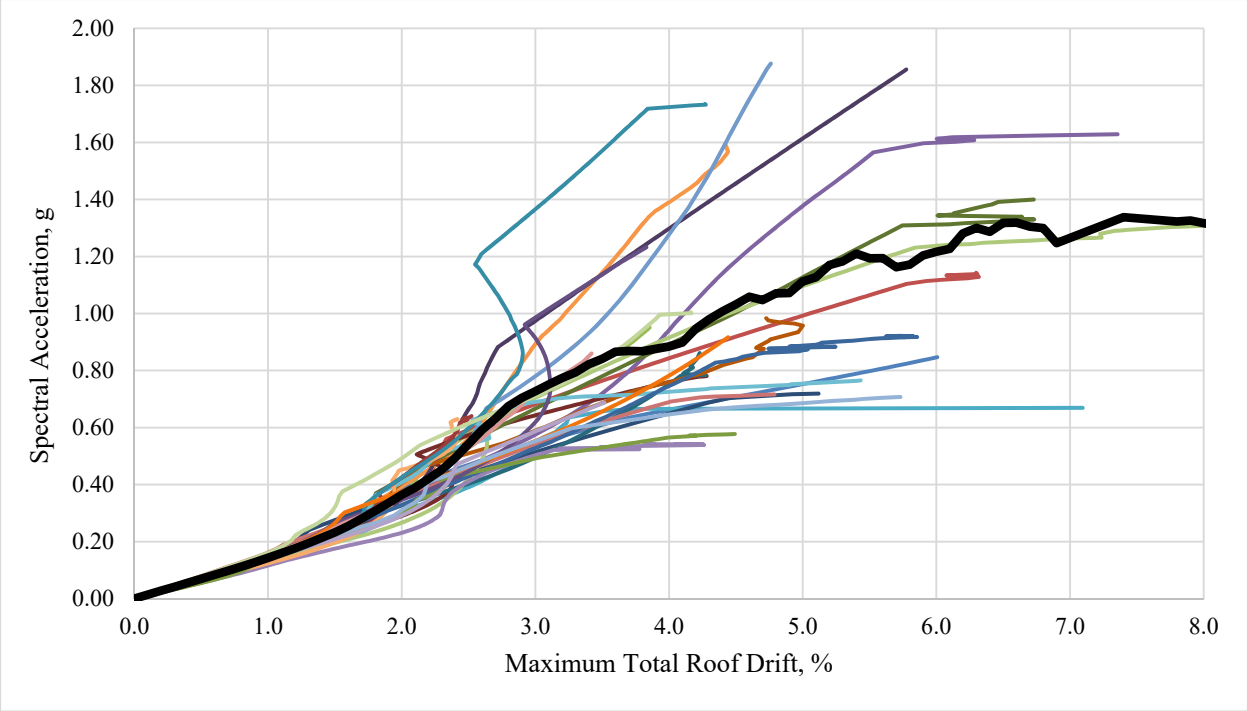


*Figure E-3: Maximum Total Roof Drift for PR17M1.0H1.1 Multi-Record IDA Curve Set*

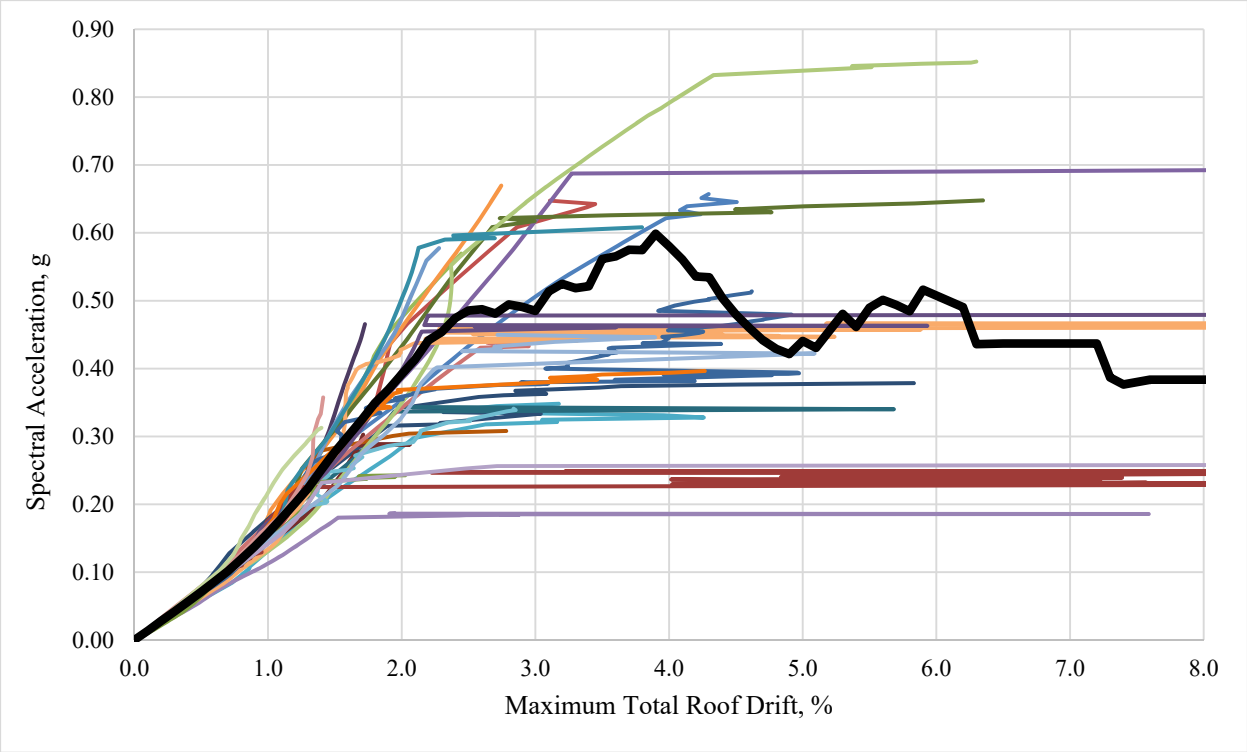


*Figure E-4: Maximum Total Roof Drift for PR17M0.66H1.4 Multi-Record IDA Curve Set*

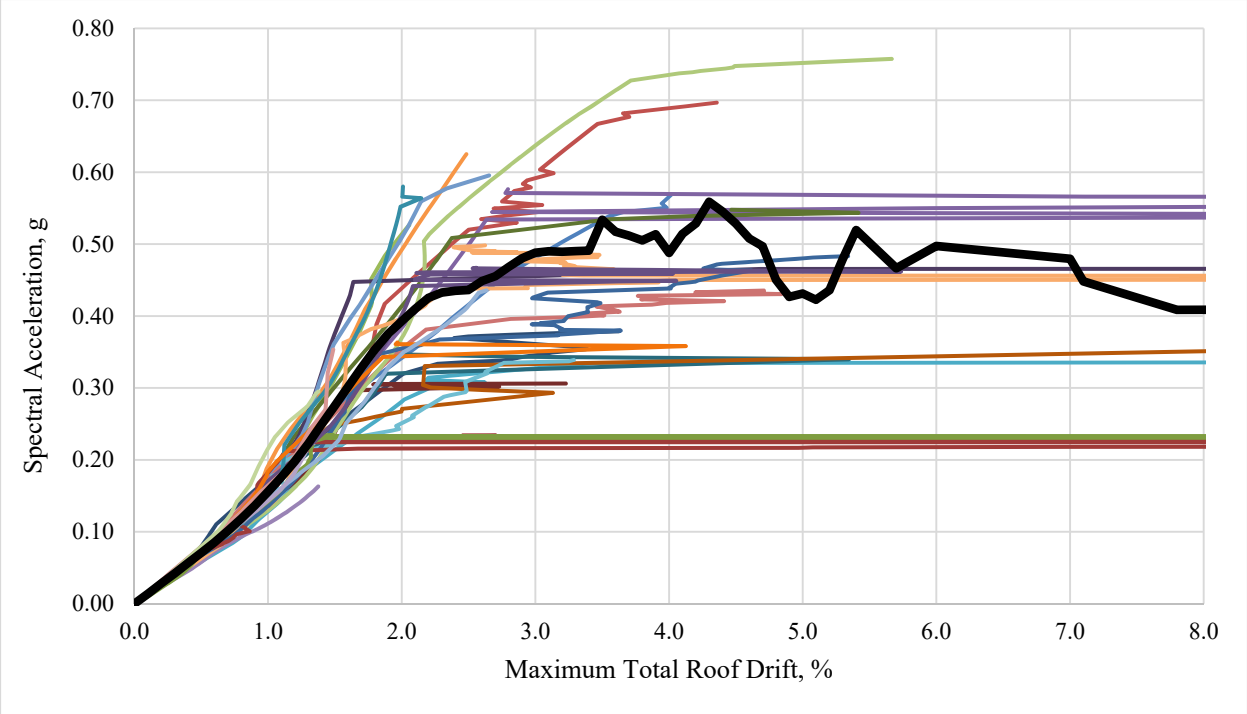


*Figure E-5: Maximum Total Roof Drift for PR17M0.66H1.1 Multi-Record IDA Curve Set*

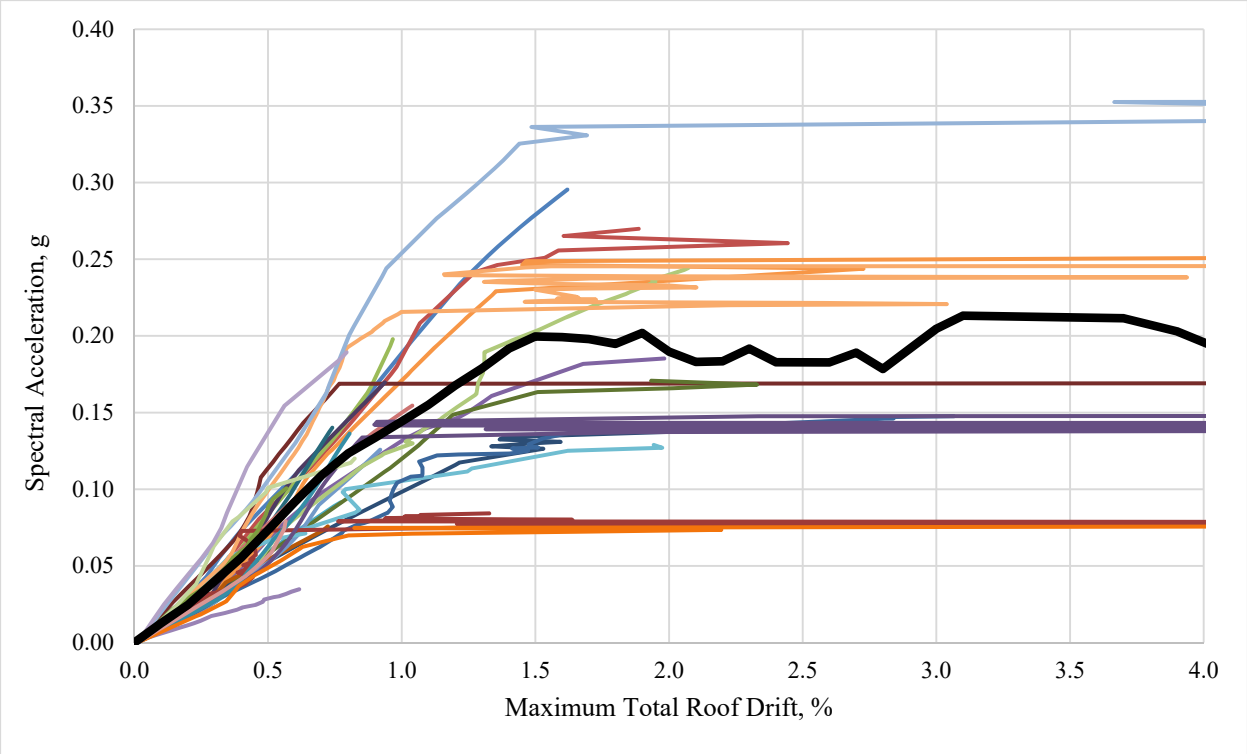


*Figure E-6: Maximum Total Roof Drift for PR17M0.33H1.4 Multi-Record IDA Curve Set*

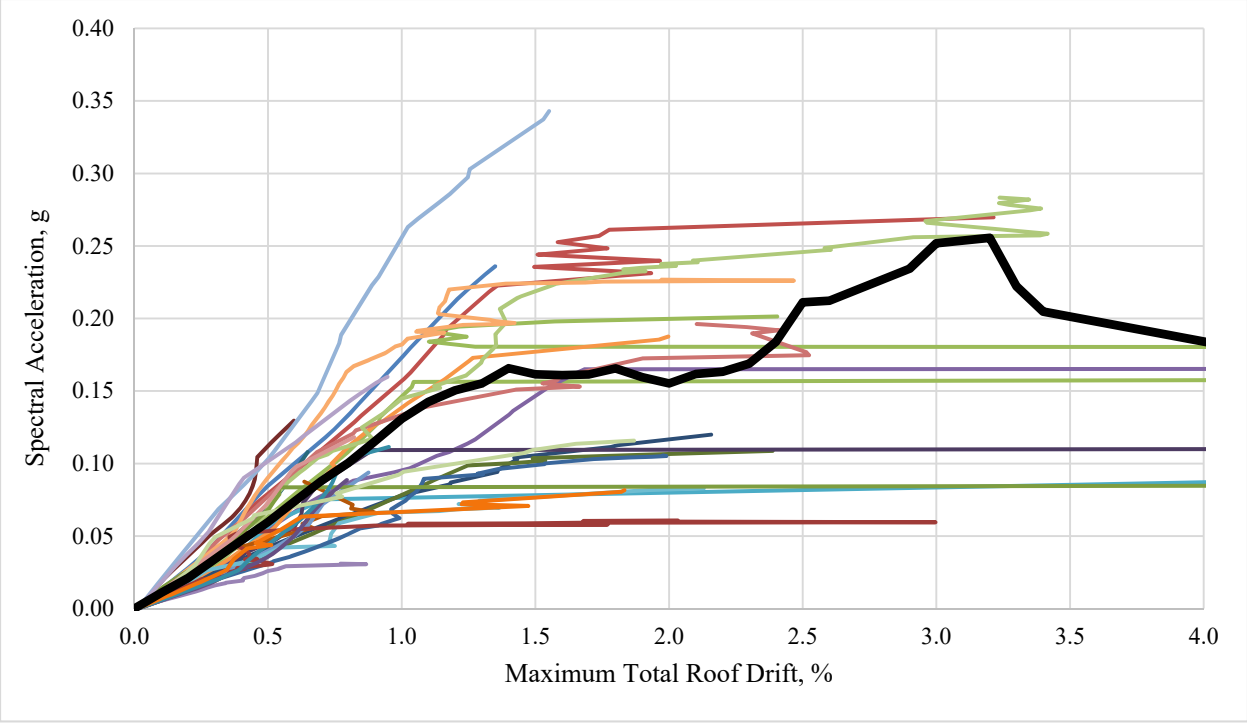


*Figure E-7: Maximum Total Roof Drift for PR17M0.33H1.1 Multi-Record IDA Curve Set*

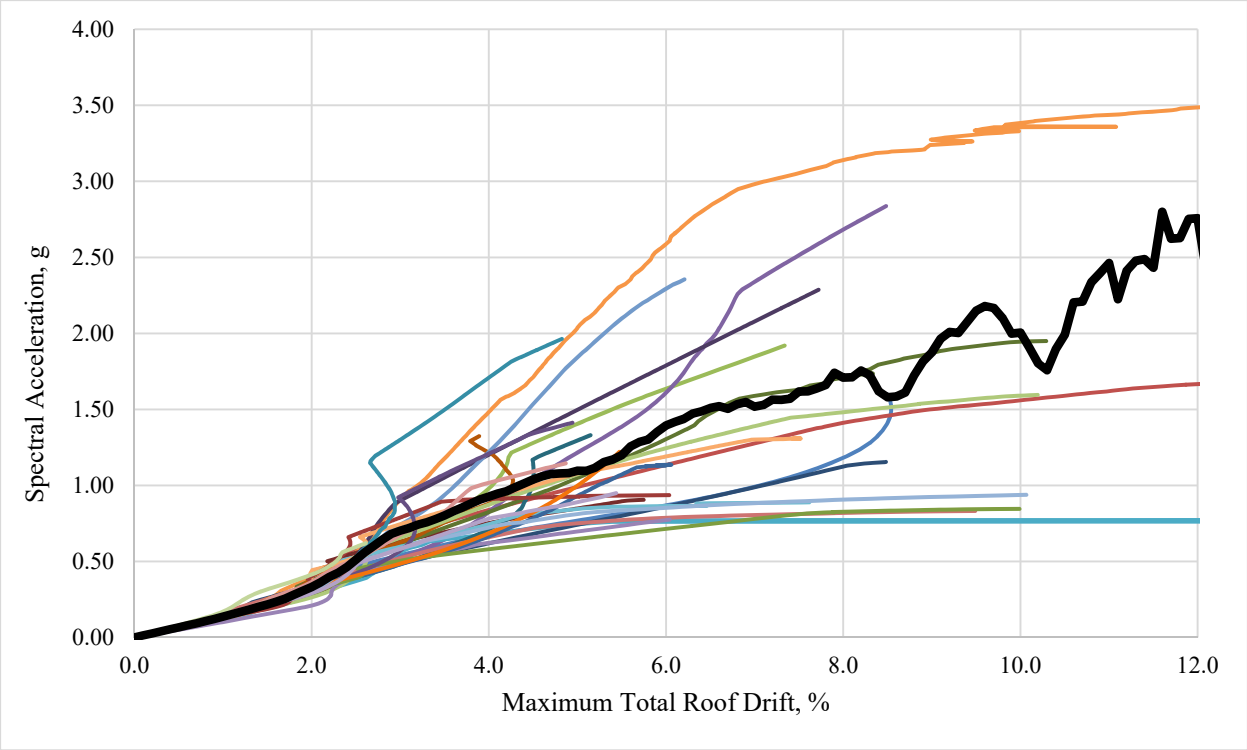


*Figure E-8: Maximum Total Roof Drift for PR14M1.0H1.4 Multi-Record IDA Curve Set*

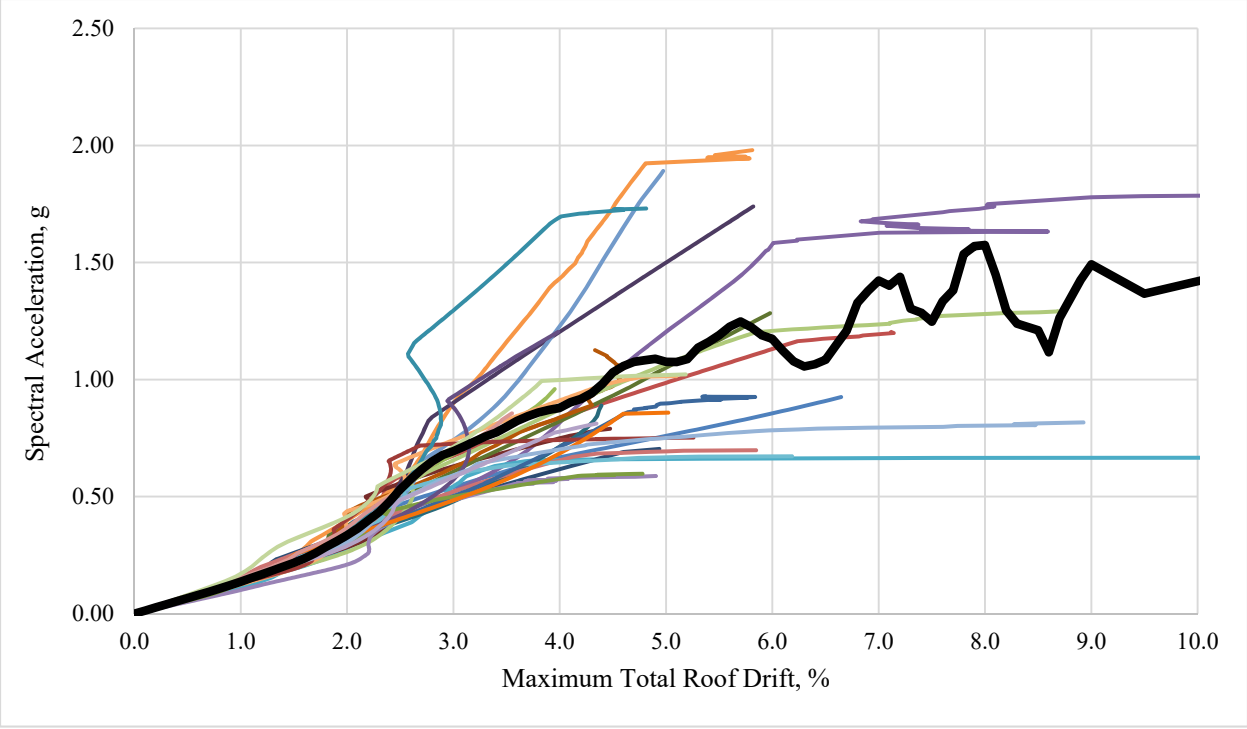


*Figure E-9: Maximum Total Roof Drift for PR14M1.0H1.1 Multi-Record IDA Curve Set*

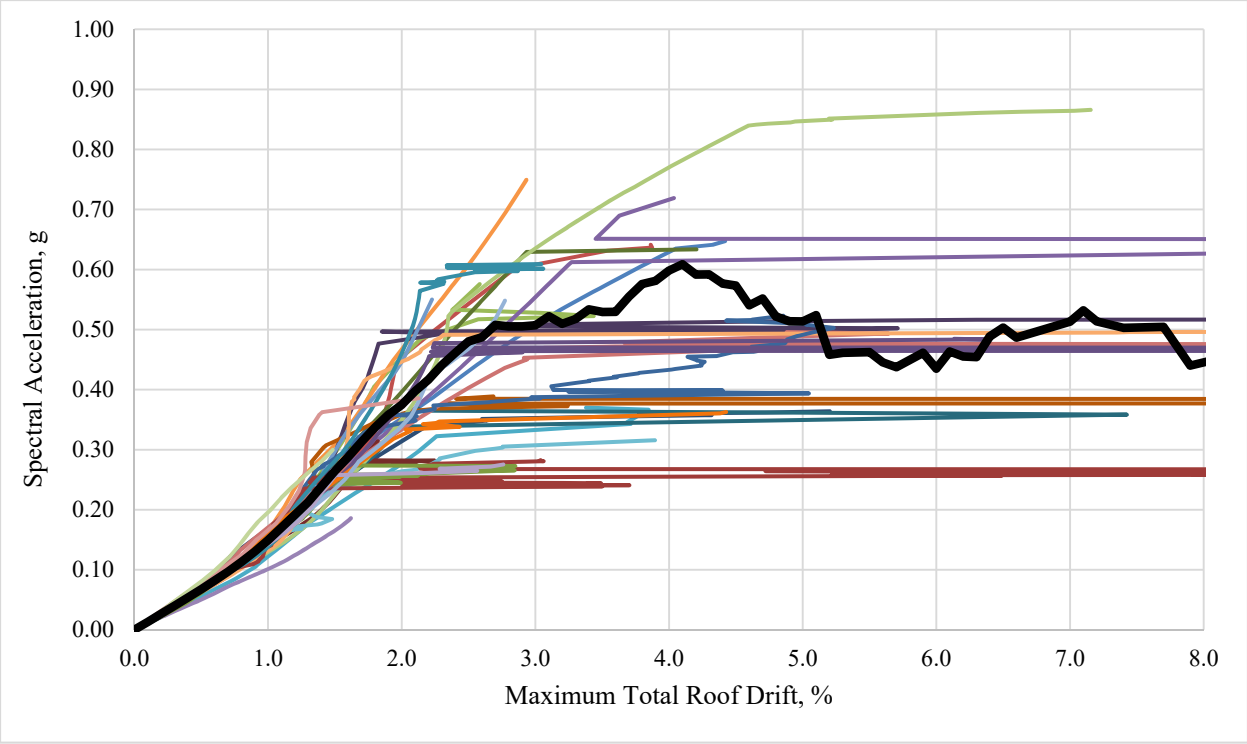


*Figure E-10: Maximum Total Roof Drift for PR14M0.66H1.4 Multi-Record IDA Curve Set*

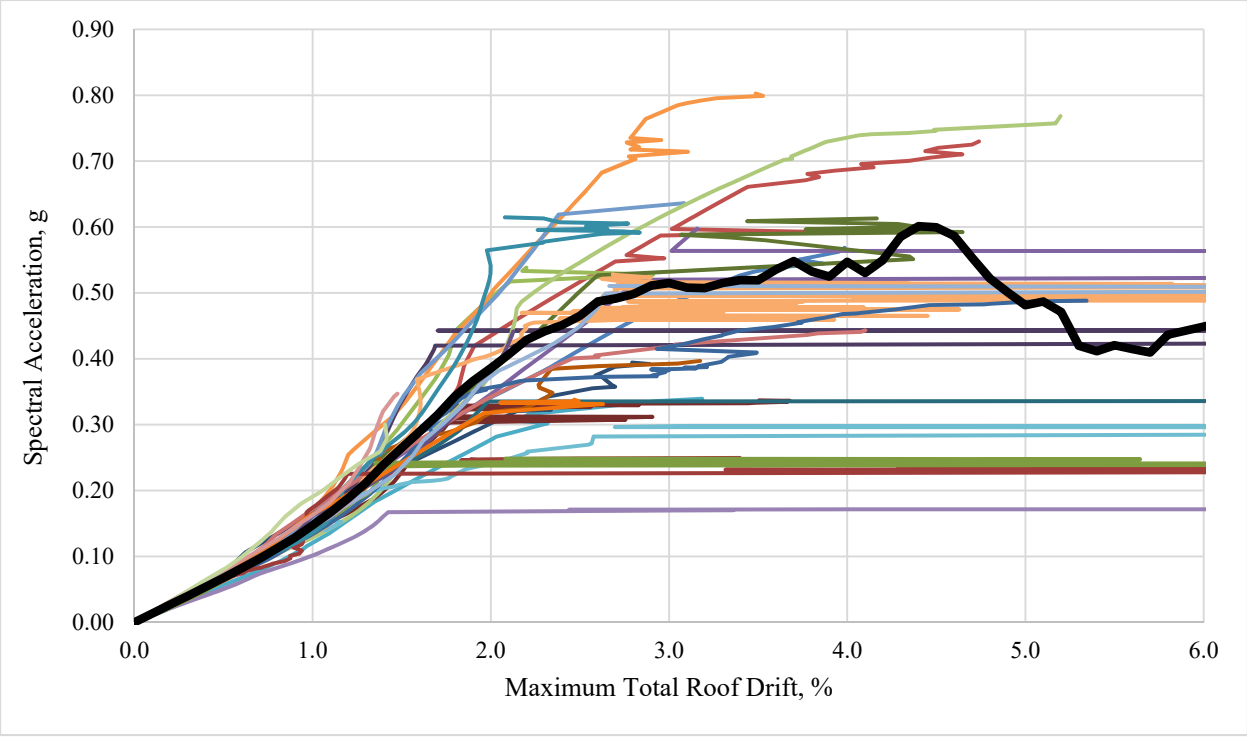


*Figure E-11: Maximum Total Roof Drift for PR14M0.66H1.1 Multi-Record IDA Curve Set*

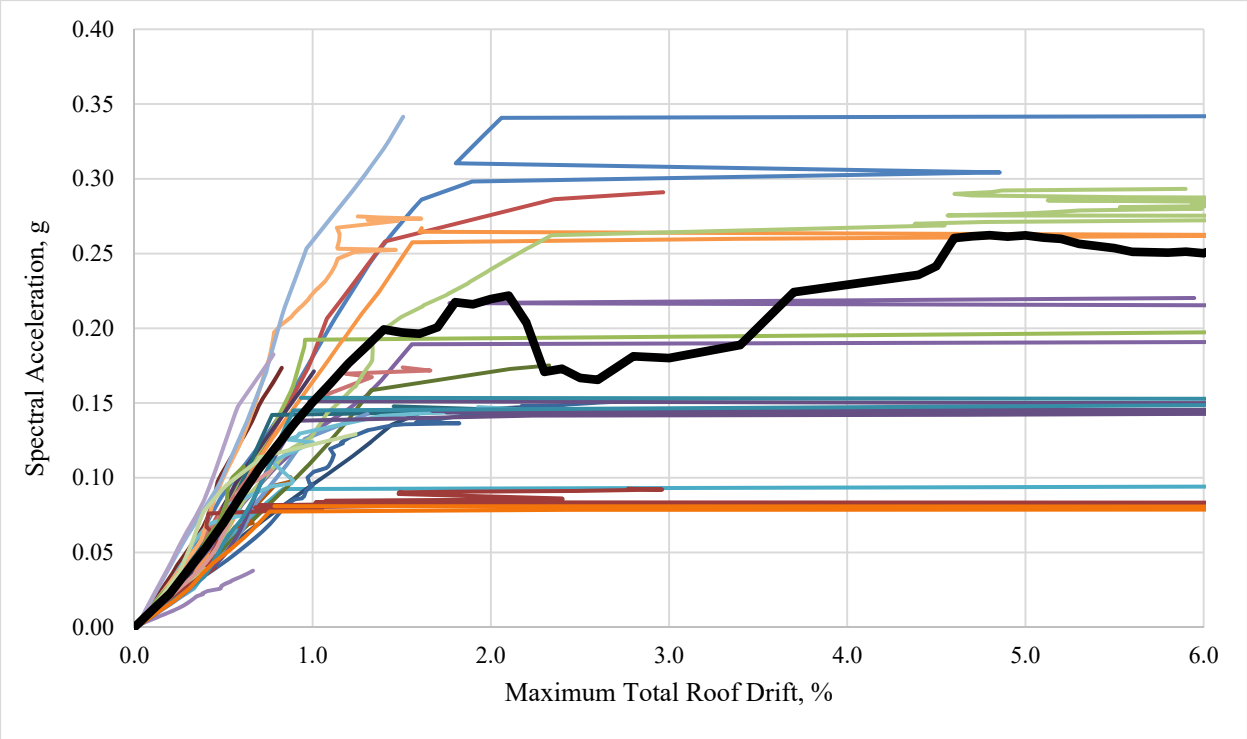


*Figure E-12: Maximum Total Roof Drift for PR14M0.33H1.4 Multi-Record IDA Curve Set*

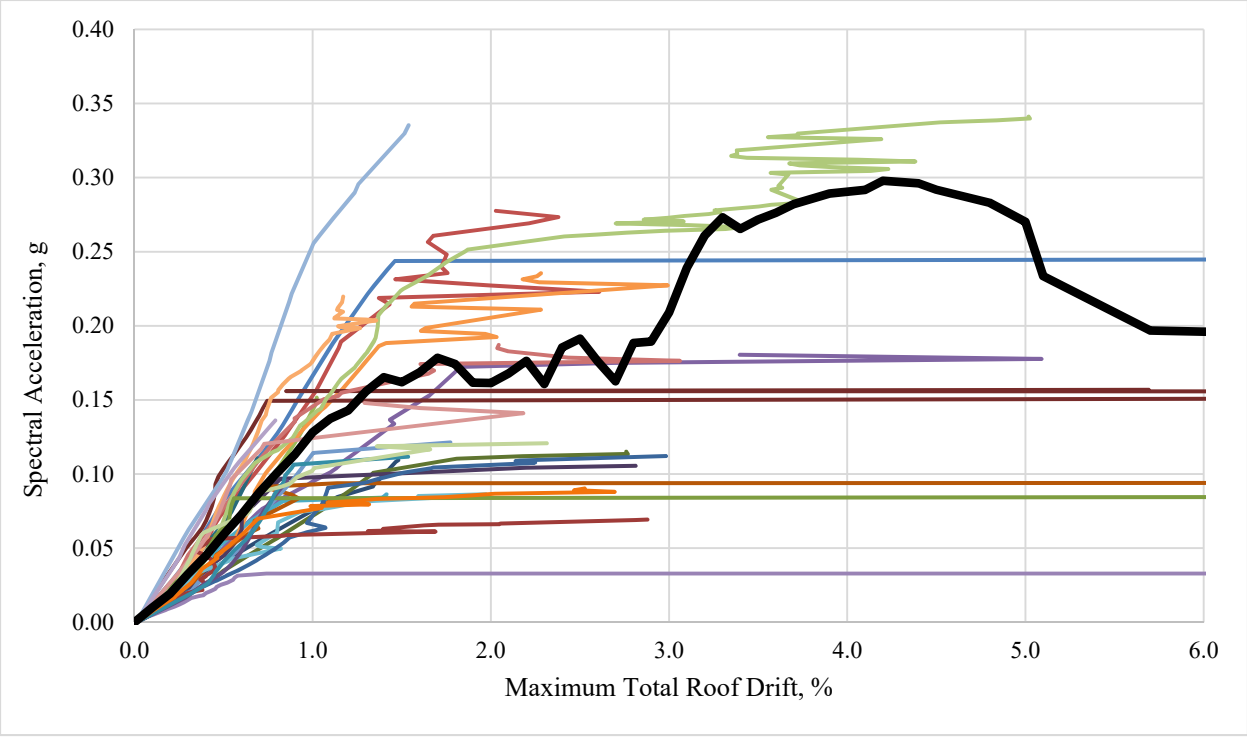


*Figure E-13: Maximum Total Roof Drift for PR14M0.33H1.1 Multi-Record IDA Curve Set*

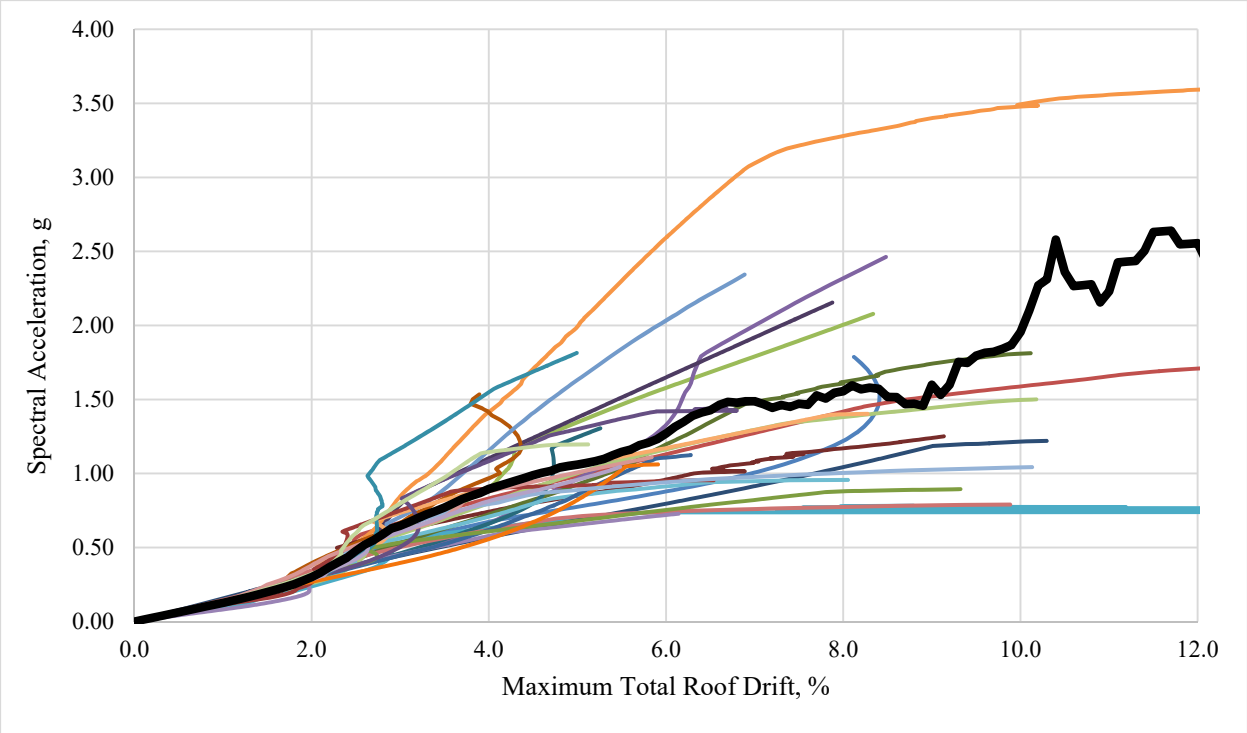


*Figure E-14: Maximum Total Roof Drift for PR11M1.0H1.4 Multi-Record IDA Curve Set*

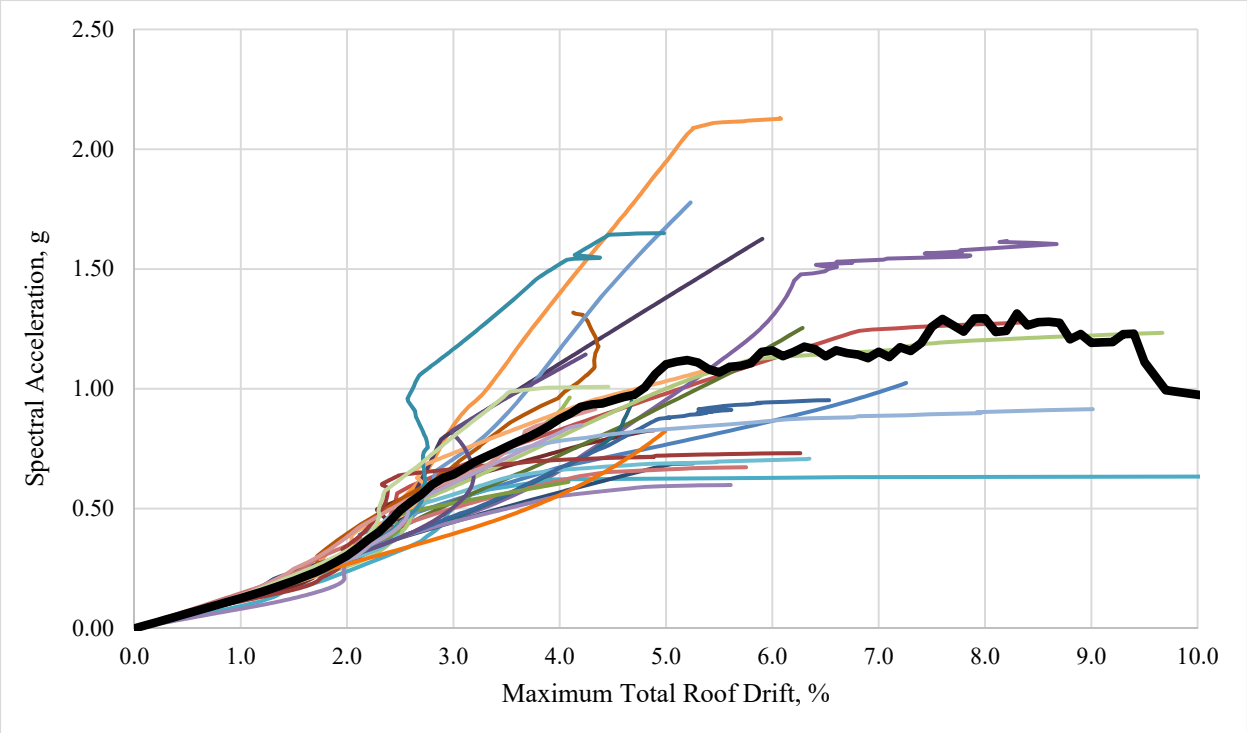


*Figure E-15: Maximum Total Roof Drift for PR11M1.0H1.1 Multi-Record IDA Curve Set*

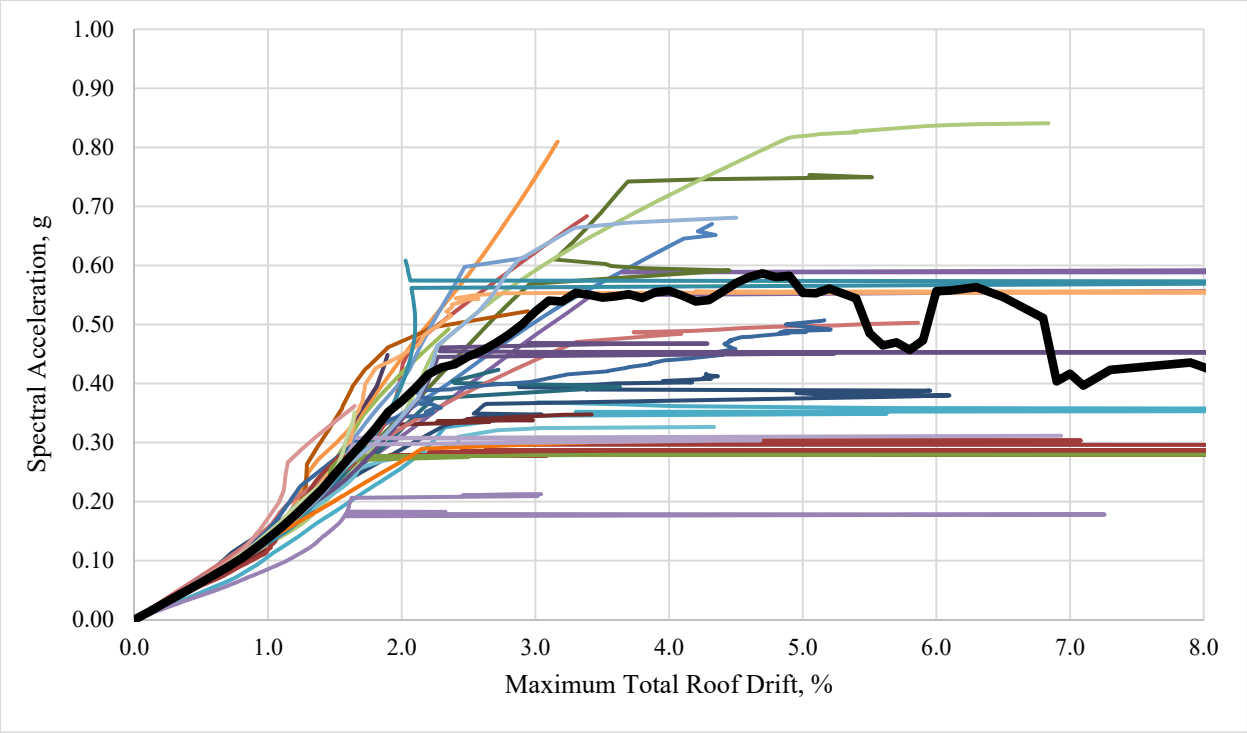


*Figure E-16: Maximum Total Roof Drift for PR11M0.66H1.4 Multi-Record IDA Curve Set*

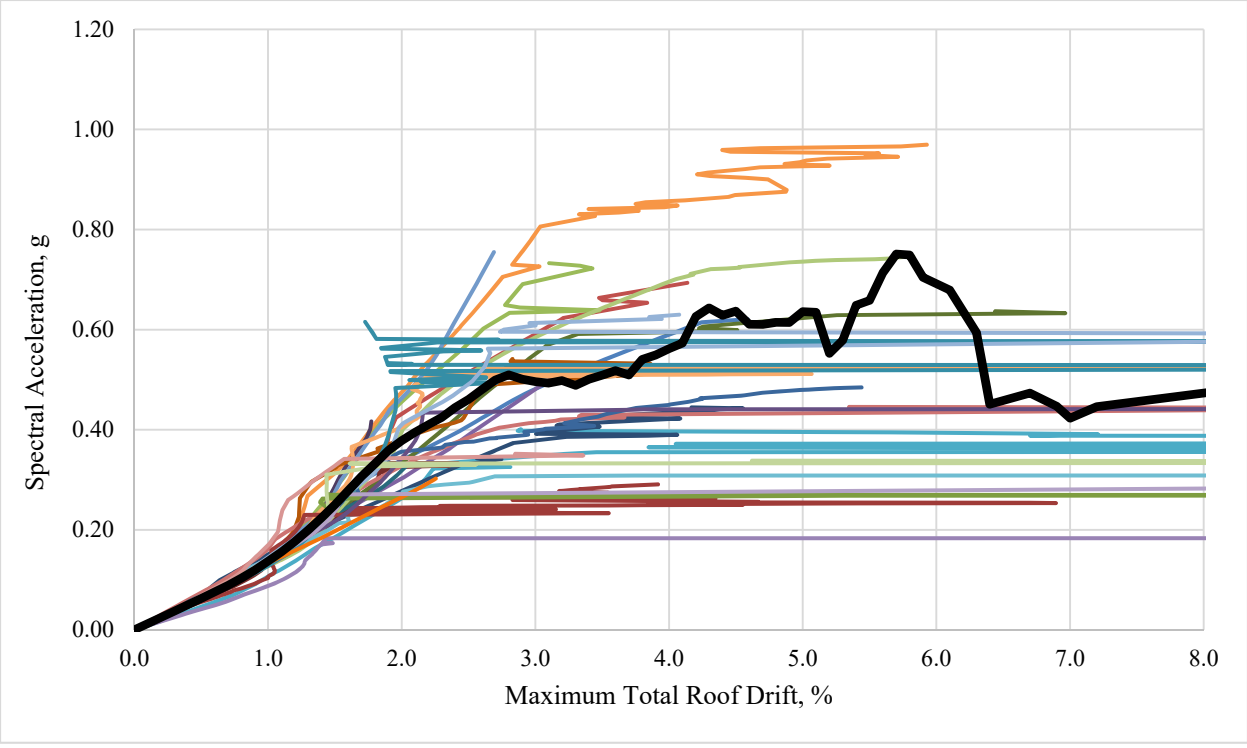


*Figure E-17: Maximum Total Roof Drift for PR11M0.66H1.1 Multi-Record IDA Curve Set*

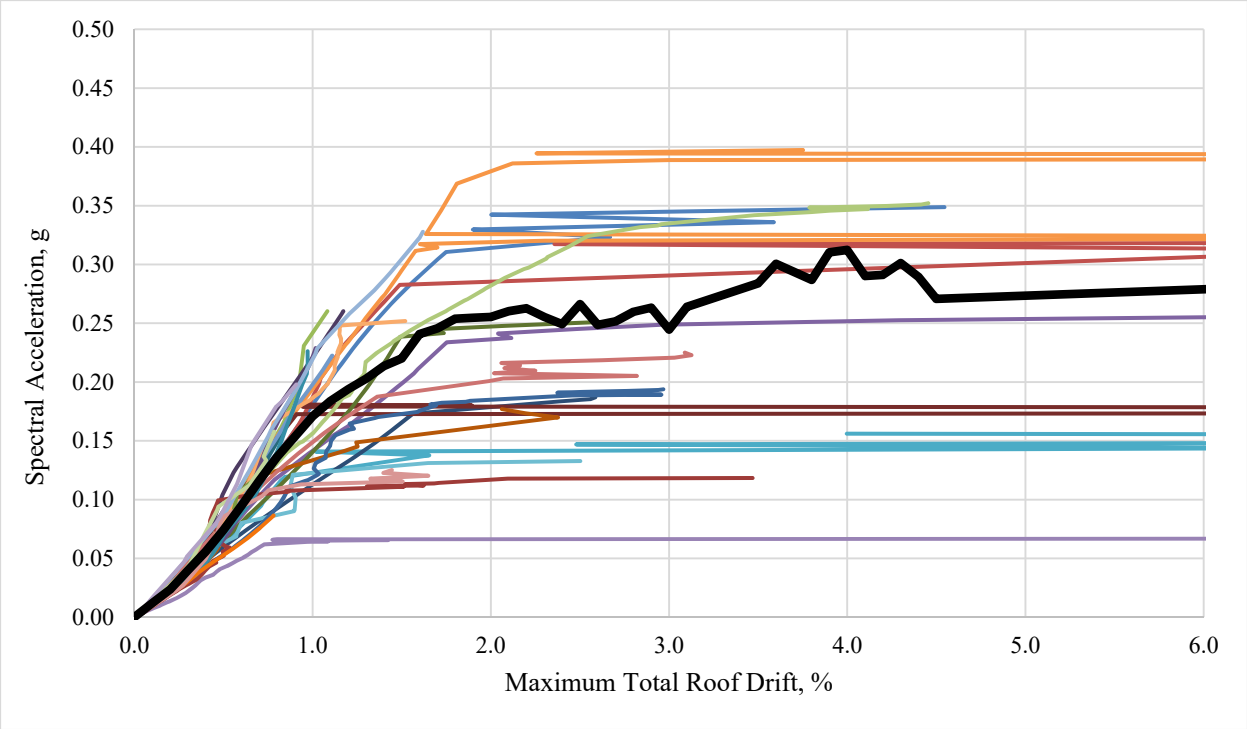


*Figure E-18: Maximum Total Roof Drift for PR11M0.33H1.4 Multi-Record IDA Curve Set*

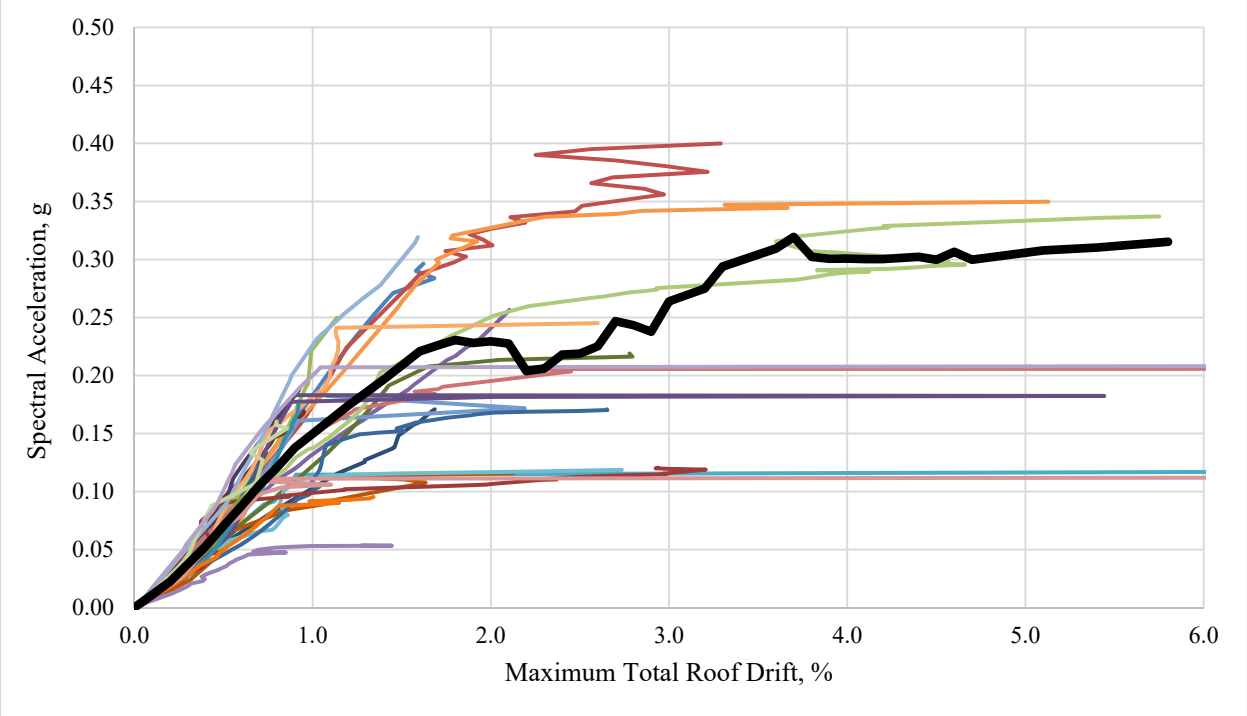


*Figure E-19: Maximum Total Roof Drift for PR11M0.33H1.1 Multi-Record IDA Curve Set*

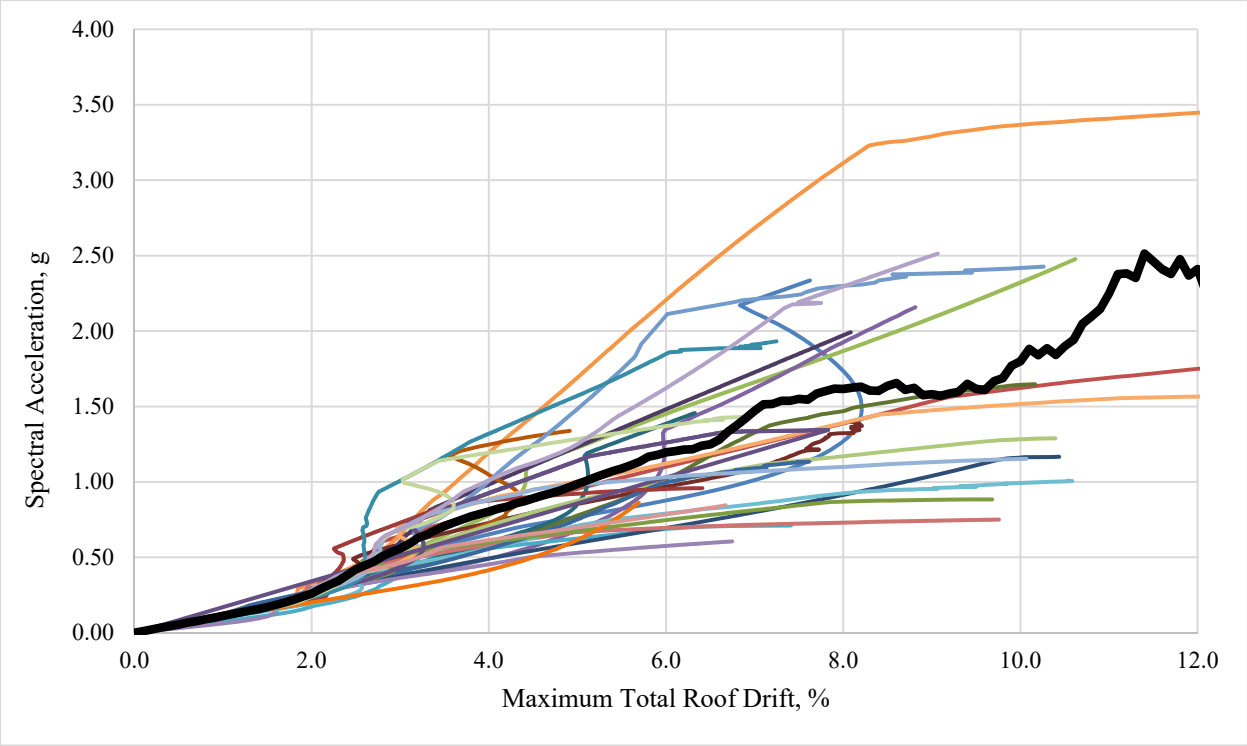


*Figure E-20: Maximum Total Roof Drift for PR8M1.0H1.4 Multi-Record IDA Curve Set*

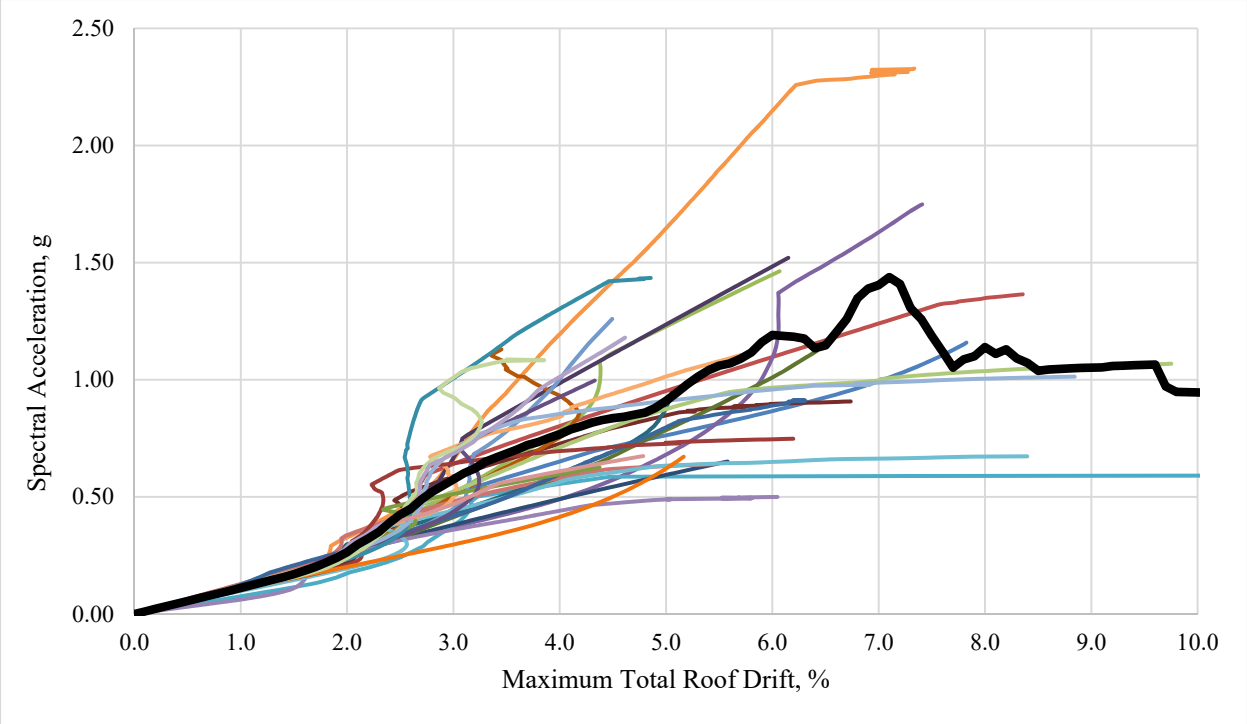


*Figure E-21: Maximum Total Roof Drift for PR8M1.0H1.1 Multi-Record IDA Curve Set*

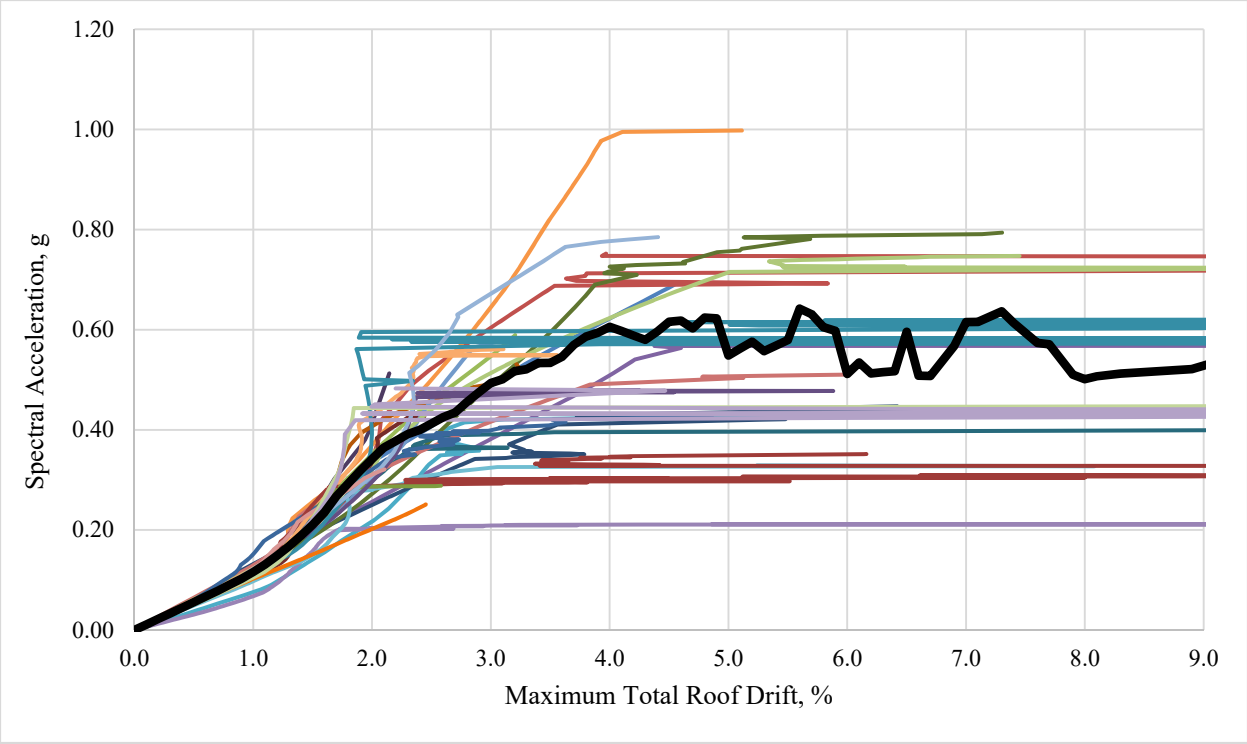


*Figure E-22: Maximum Total Roof Drift for PR8M0.66H1.4 Multi-Record IDA Curve Set*

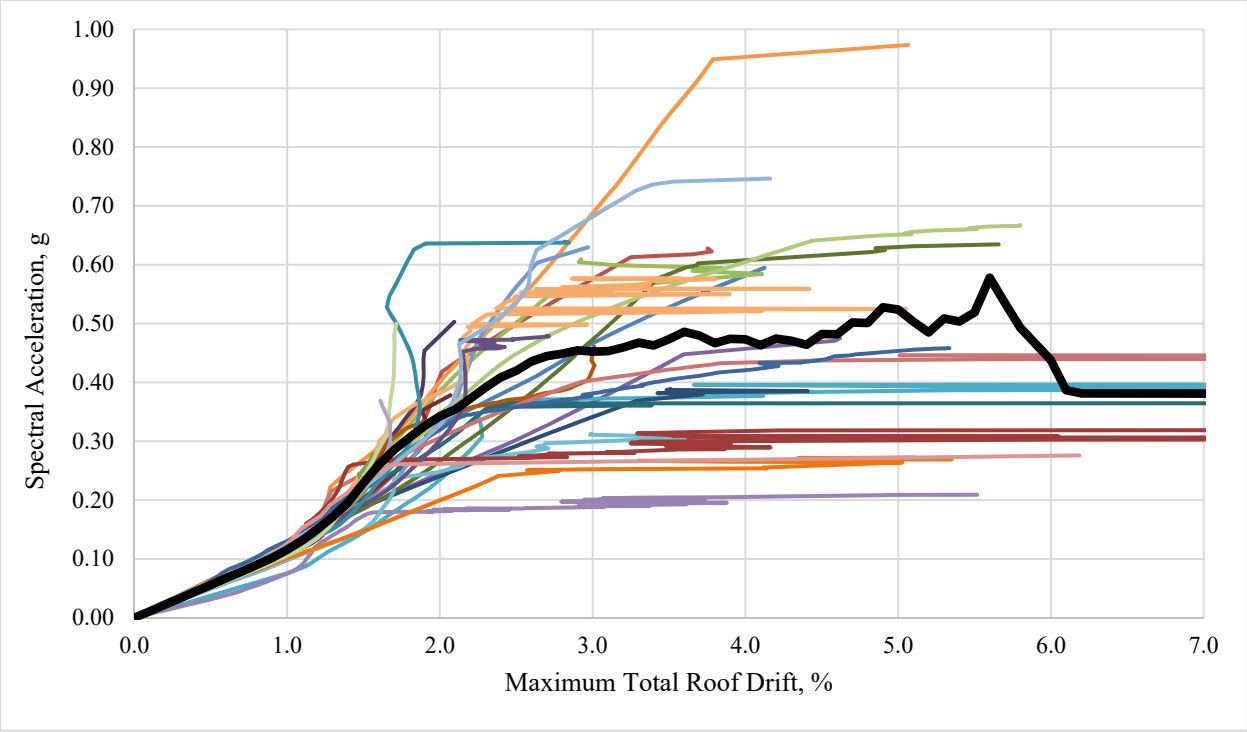


*Figure E-23: Maximum Total Roof Drift for PR8M0.66H1.1 Multi-Record IDA Curve Set*

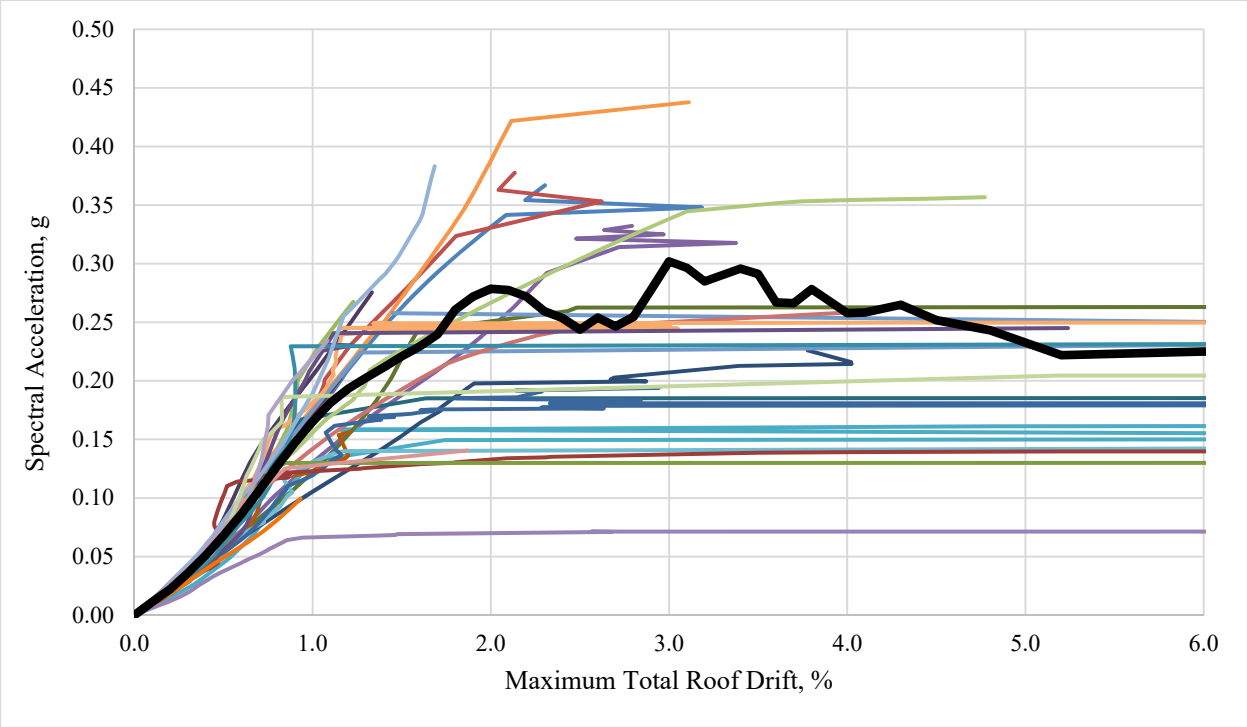


*Figure E-24: Maximum Total Roof Drift for PR8M0.33H1.4 Multi-Record IDA Curve Set*

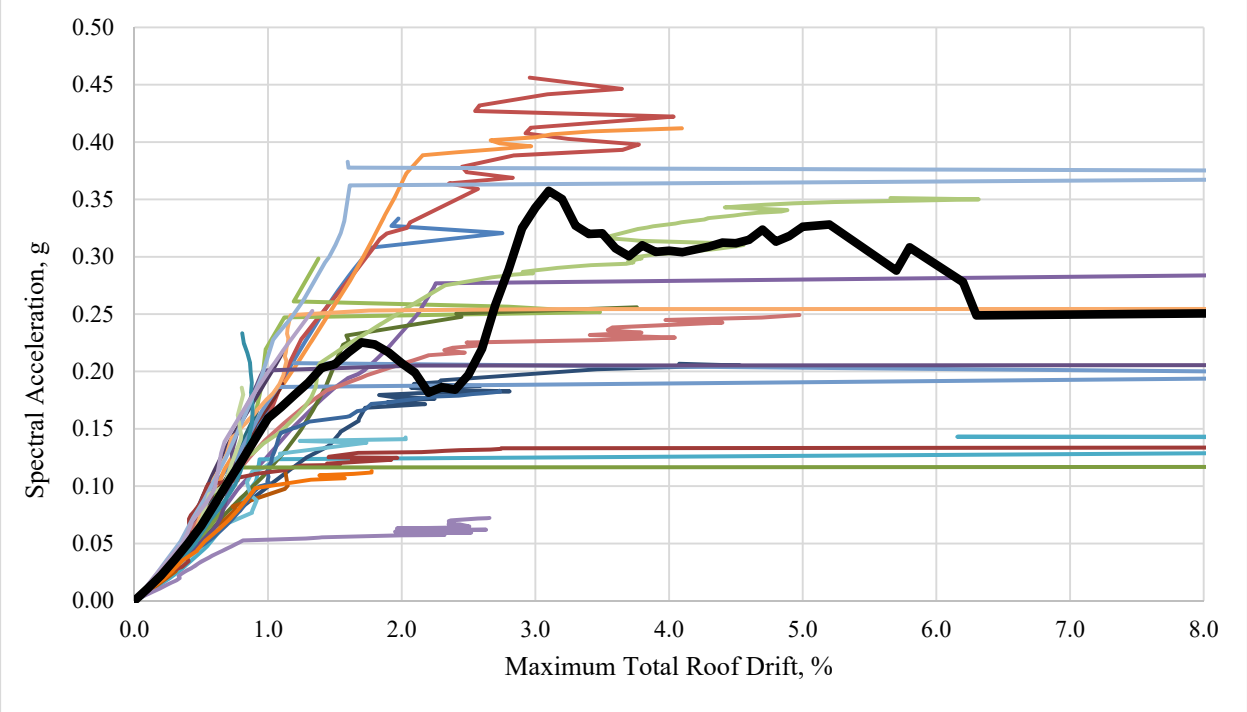


*Figure E-25: Maximum Total Roof Drift for PR8M0.33H1.1 Multi-Record IDA Curve Set*

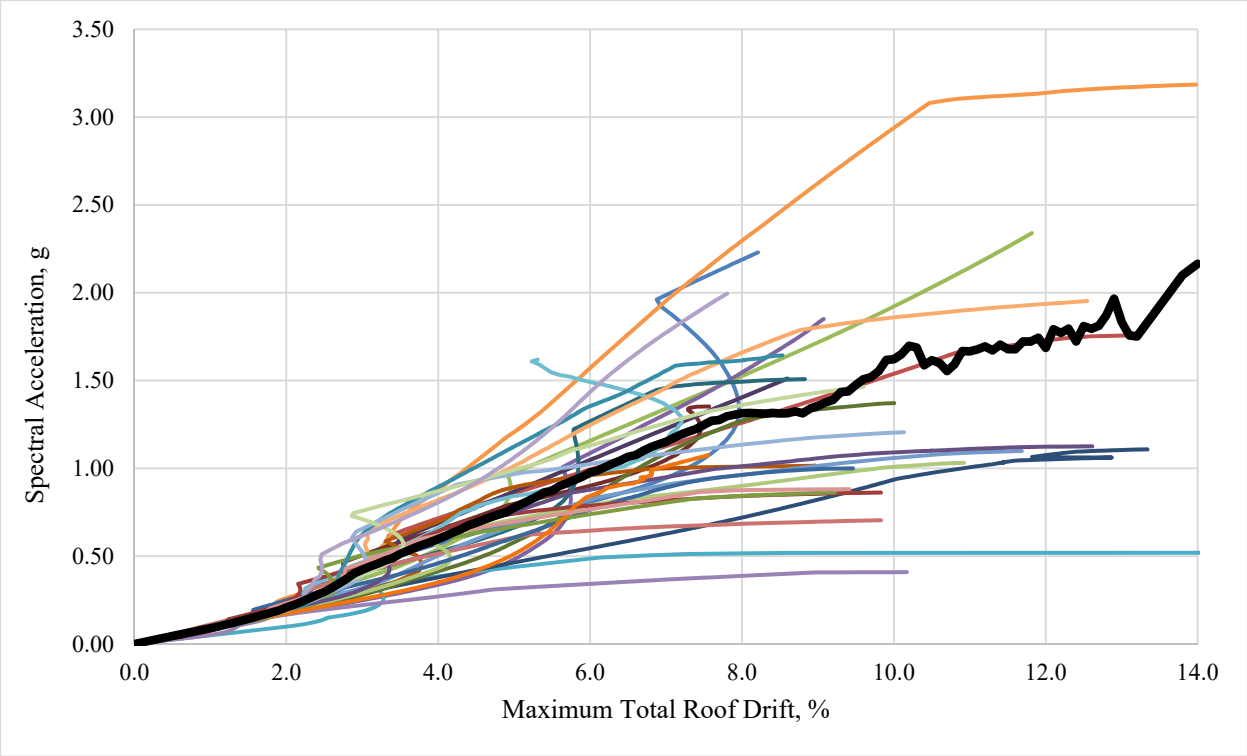


*Figure E-26: Maximum Total Roof Drift for PR5M1.0H1.4 Multi-Record IDA Curve Set*

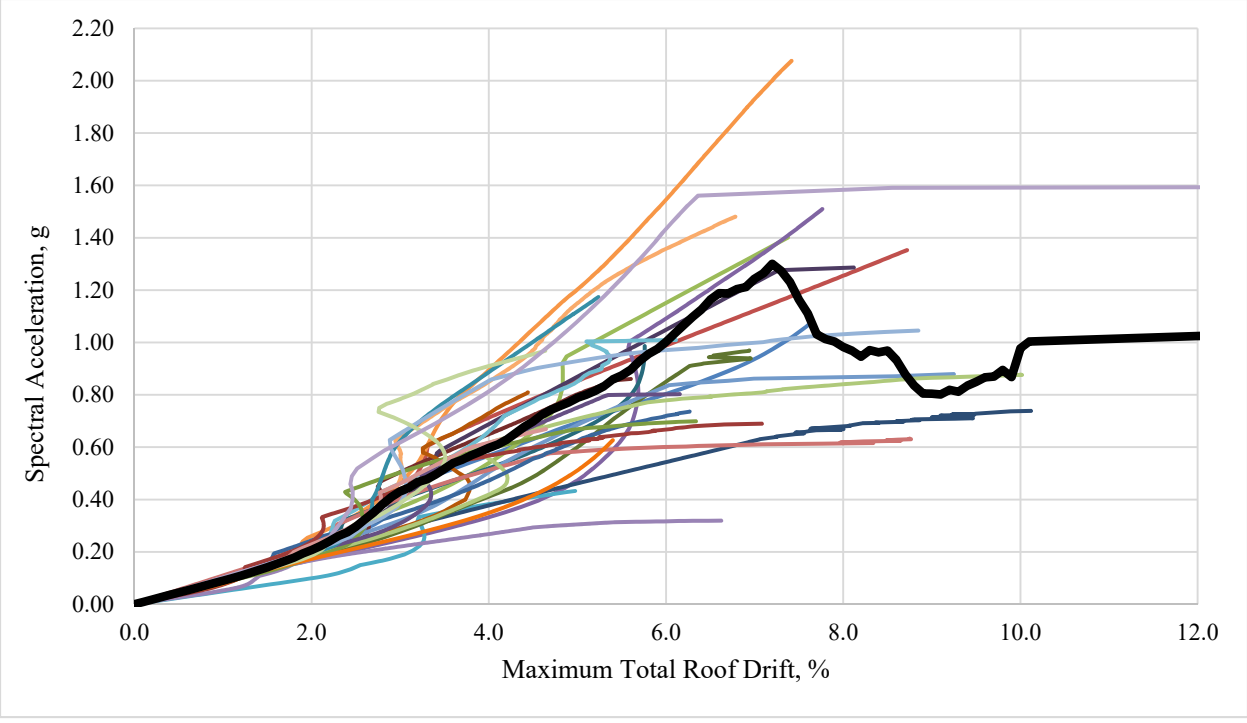


*Figure E-27: Maximum Total Roof Drift for PR5M1.0H1.1 Multi-Record IDA Curve Set*

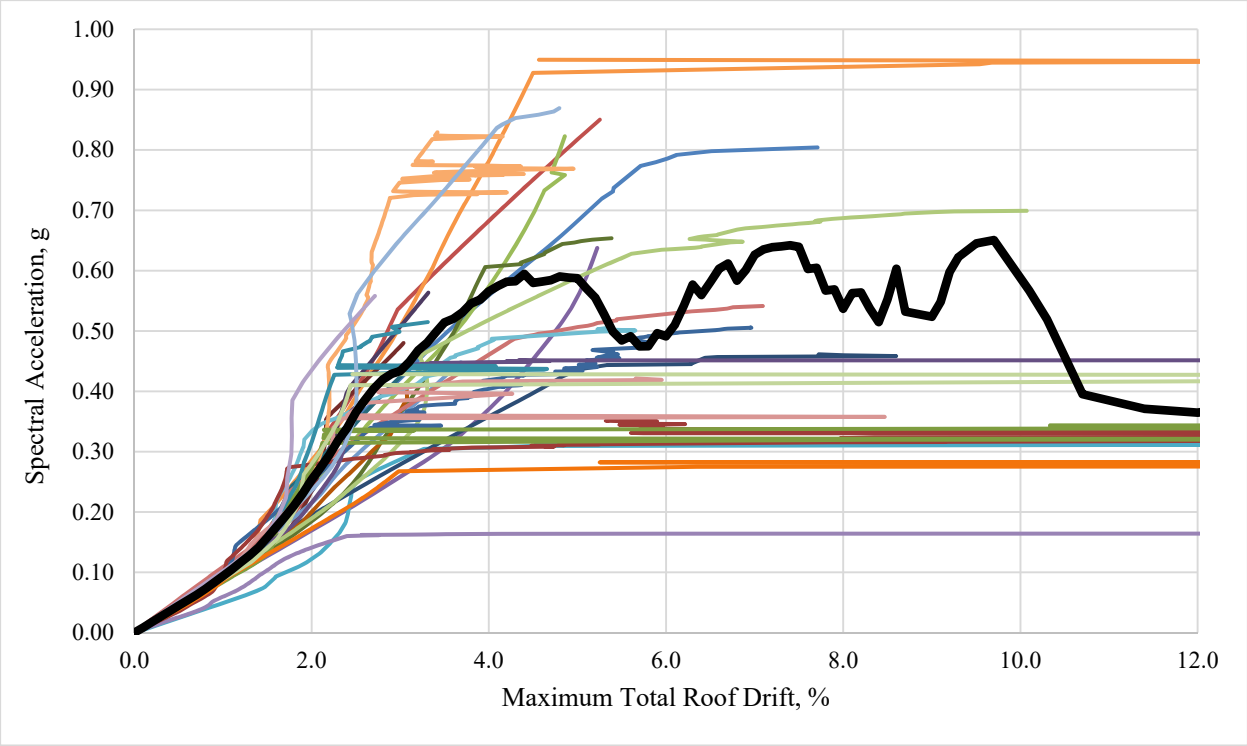


*Figure E-28: Maximum Total Roof Drift for PR5M0.66H1.4 Multi-Record IDA Curve Set*

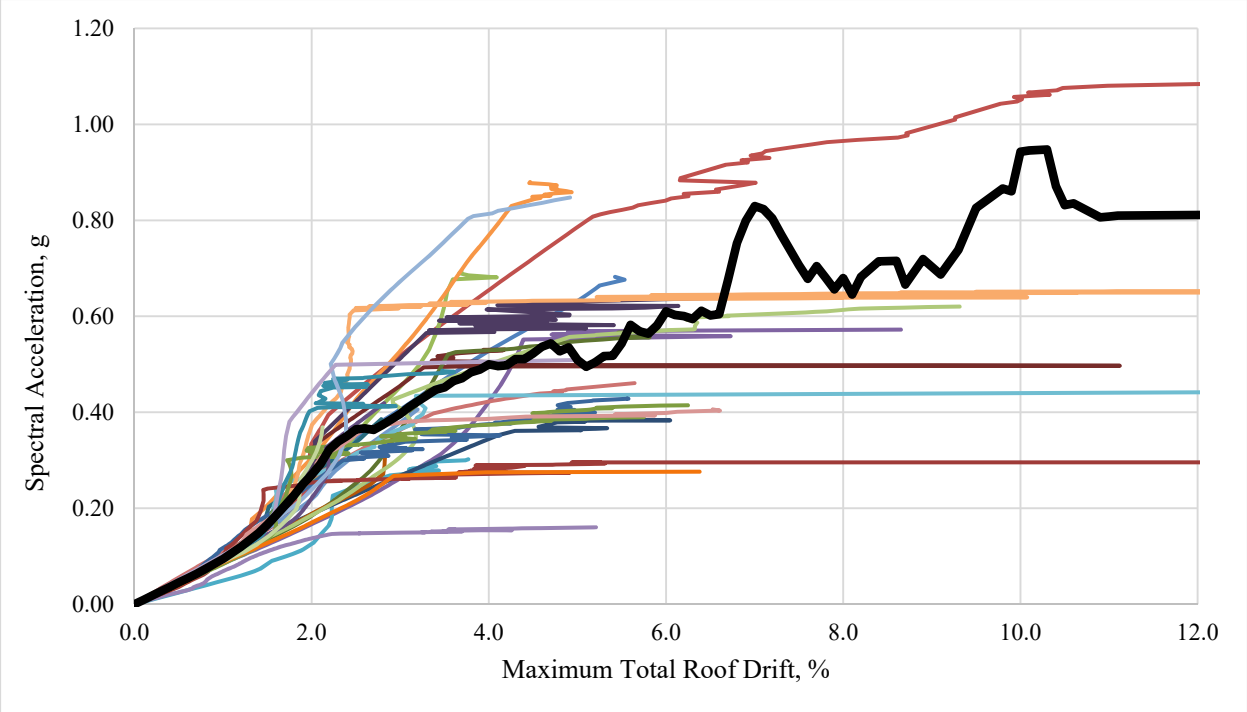


*Figure E-29: Maximum Total Roof Drift for PR5M0.66H1.1 Multi-Record IDA Curve Set*

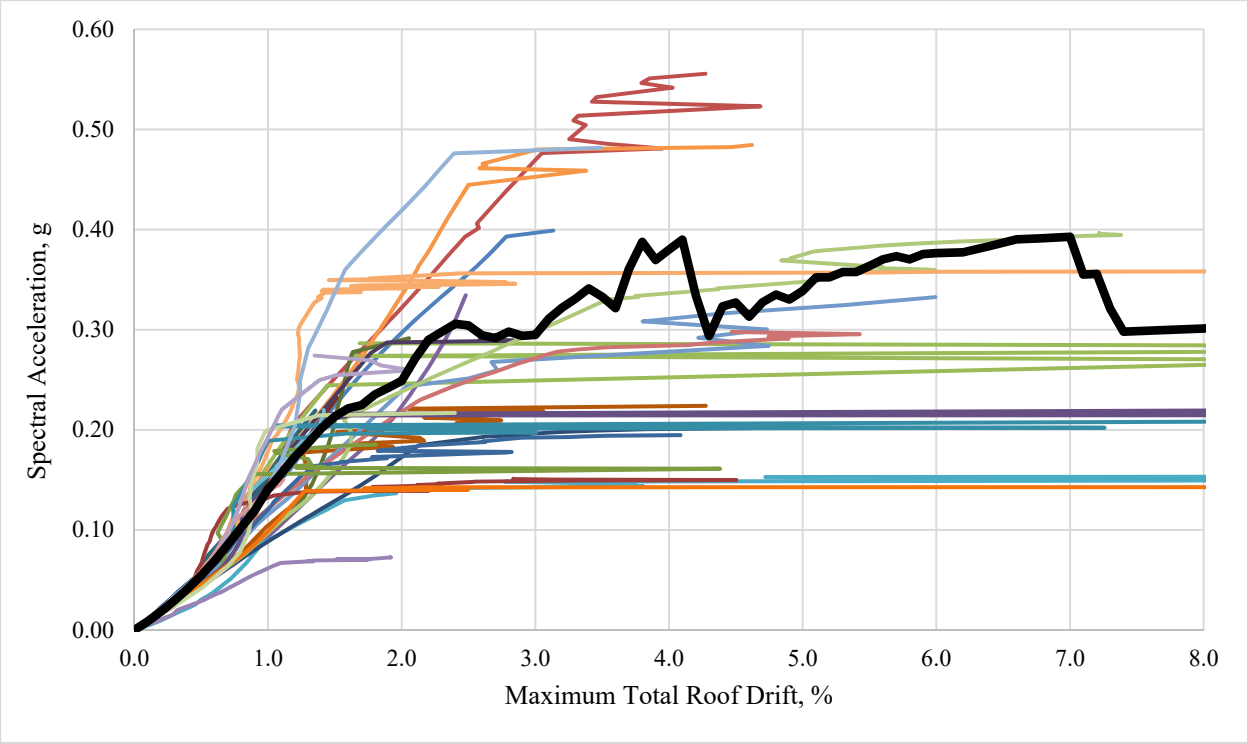


*Figure E-30: Maximum Total Roof Drift for PR5M0.33H1.4 Multi-Record IDA Curve Set*

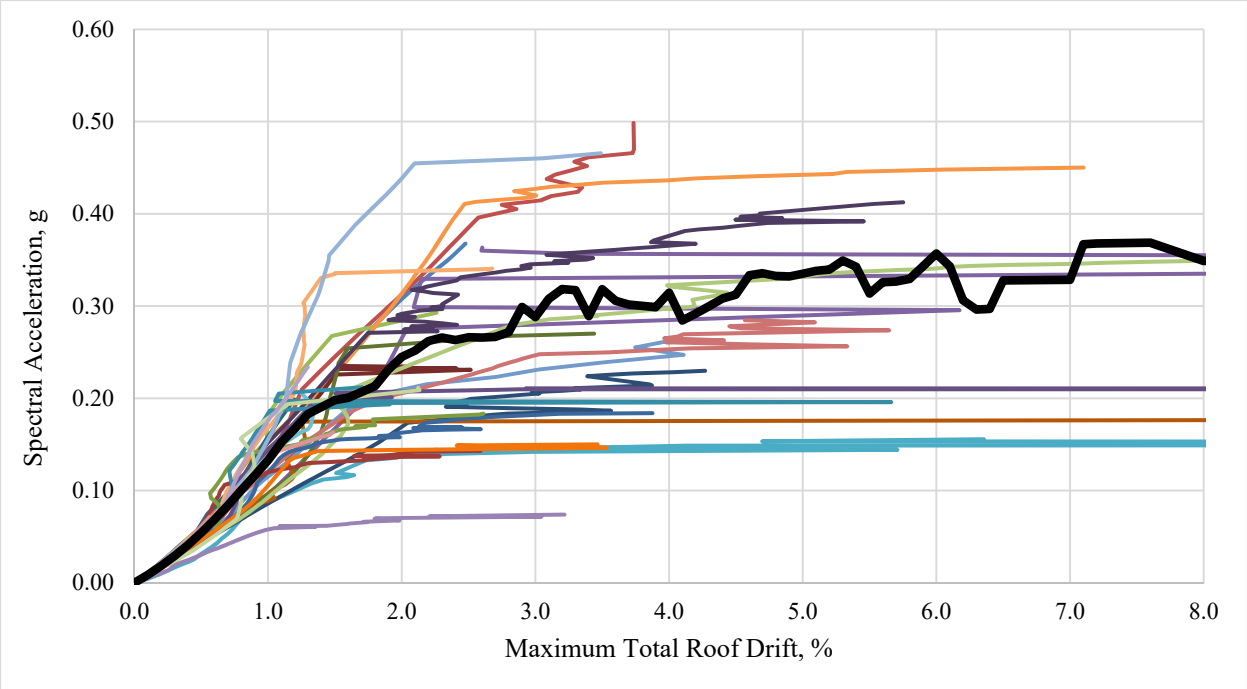


*Figure E-31: Maximum Total Roof Drift for PR5M0.33H1.1 Multi-Record IDA Curve Set*

## Appendix F: Maximum Interstory Drift Multi-Record IDA Curve Sets

This Appendix contains the multi-record IDA curve sets for the maximum interstory drift DMs for all of the frames.

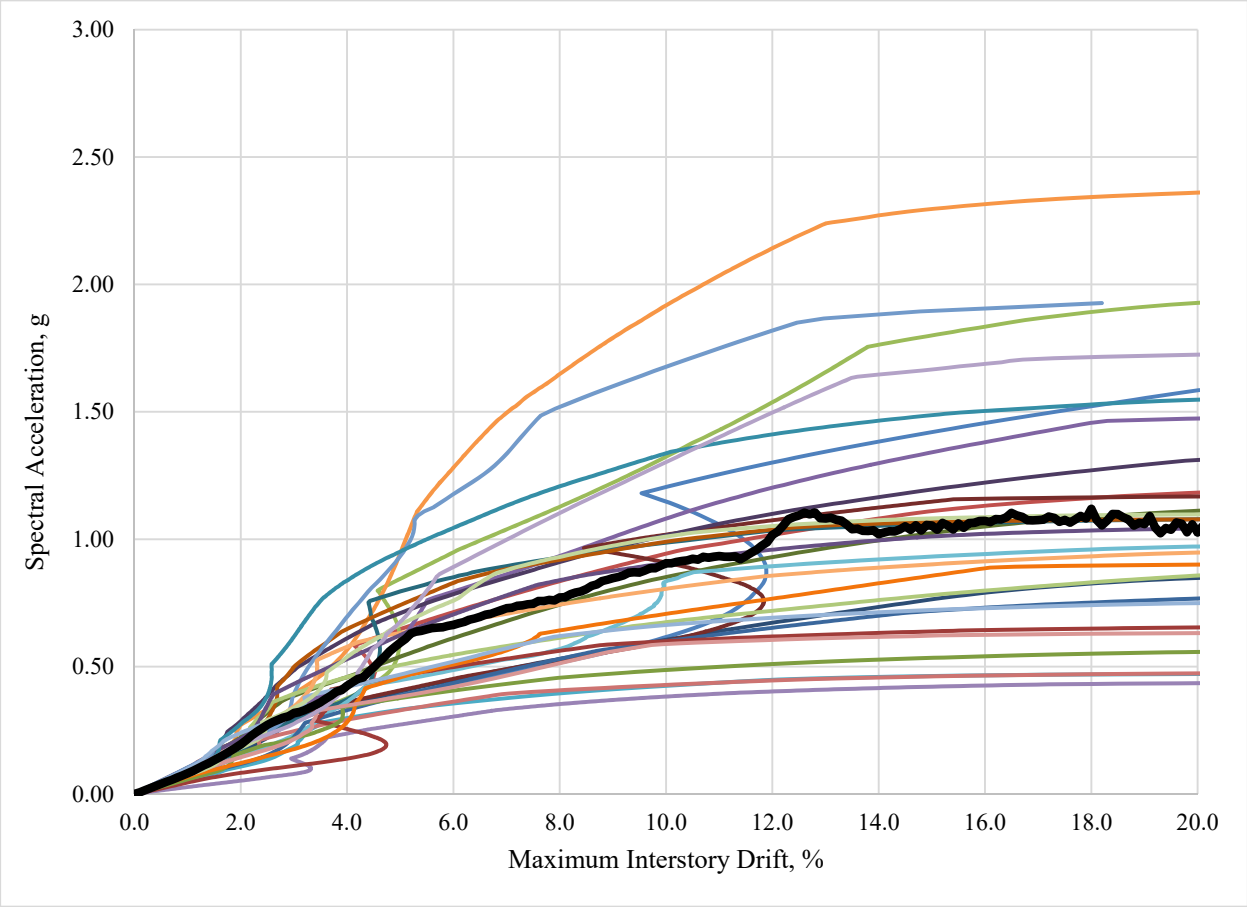


*Figure F-1: Maximum Interstory Drift for Control Frame Multi-Record IDA Curve Set*

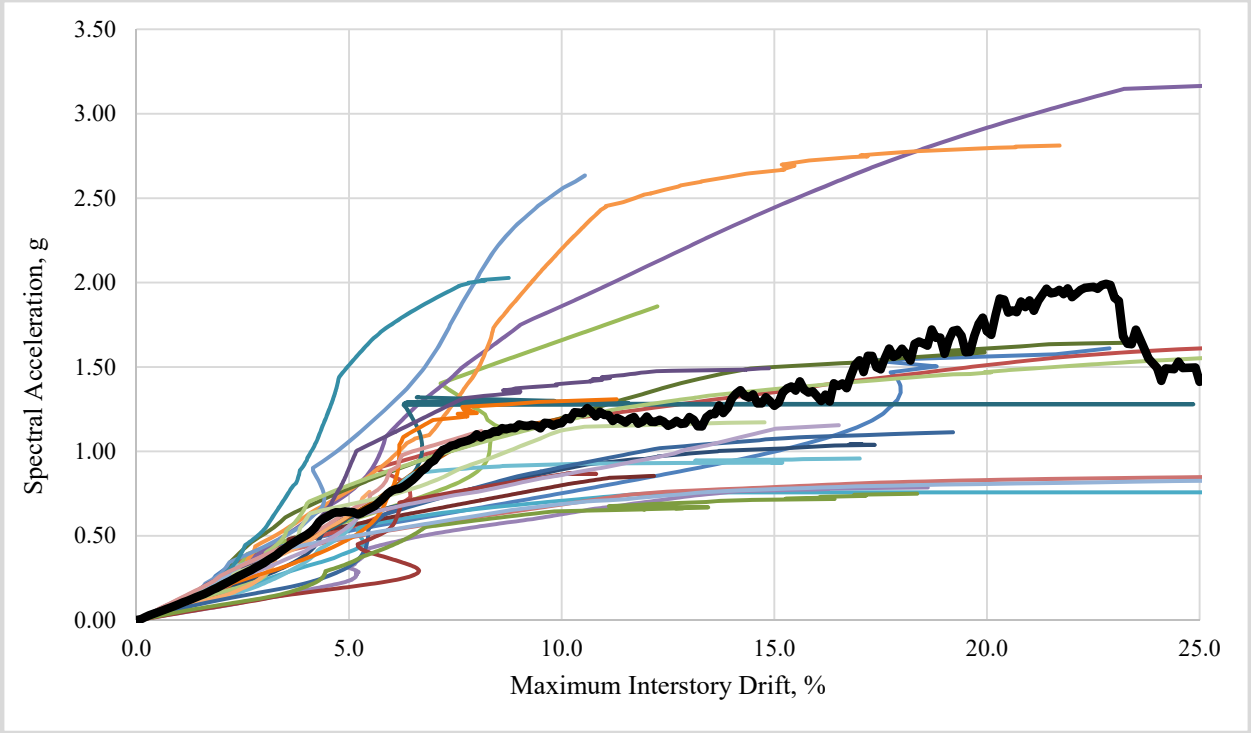


*Figure F-2: Maximum Interstory Drift for PR17M1.0H1.4 Multi-Record IDA Curve Set*

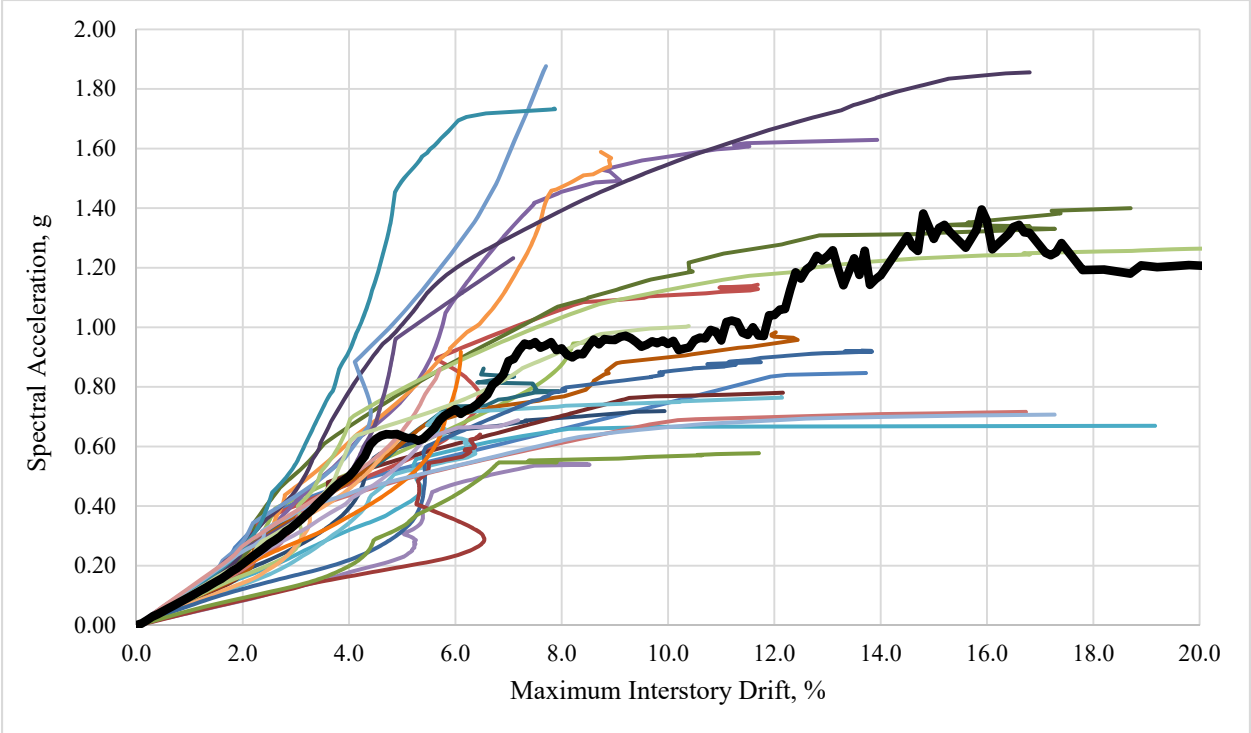


*Figure F-3: Maximum Interstory Drift for PR17M1.0H1.1 Multi-Record IDA Curve Set*

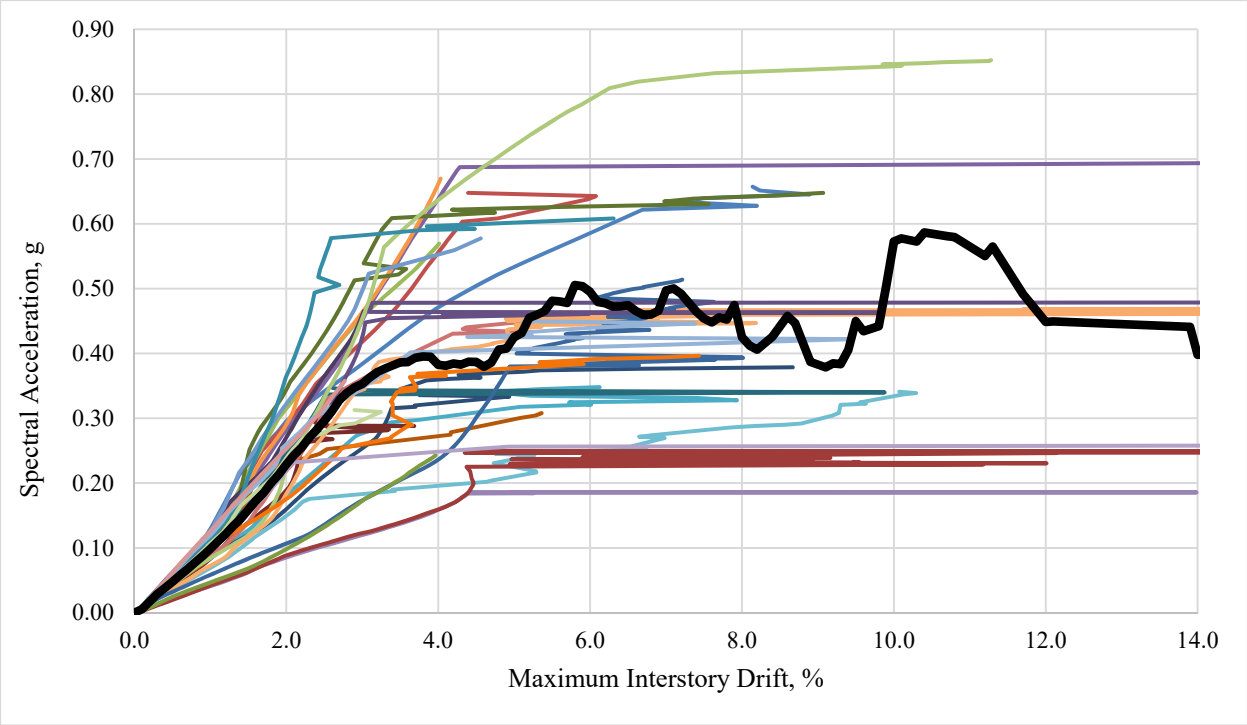


*Figure F-4: Maximum Interstory Drift for PR17M0.66H1.4 Multi-Record IDA Curve Set*

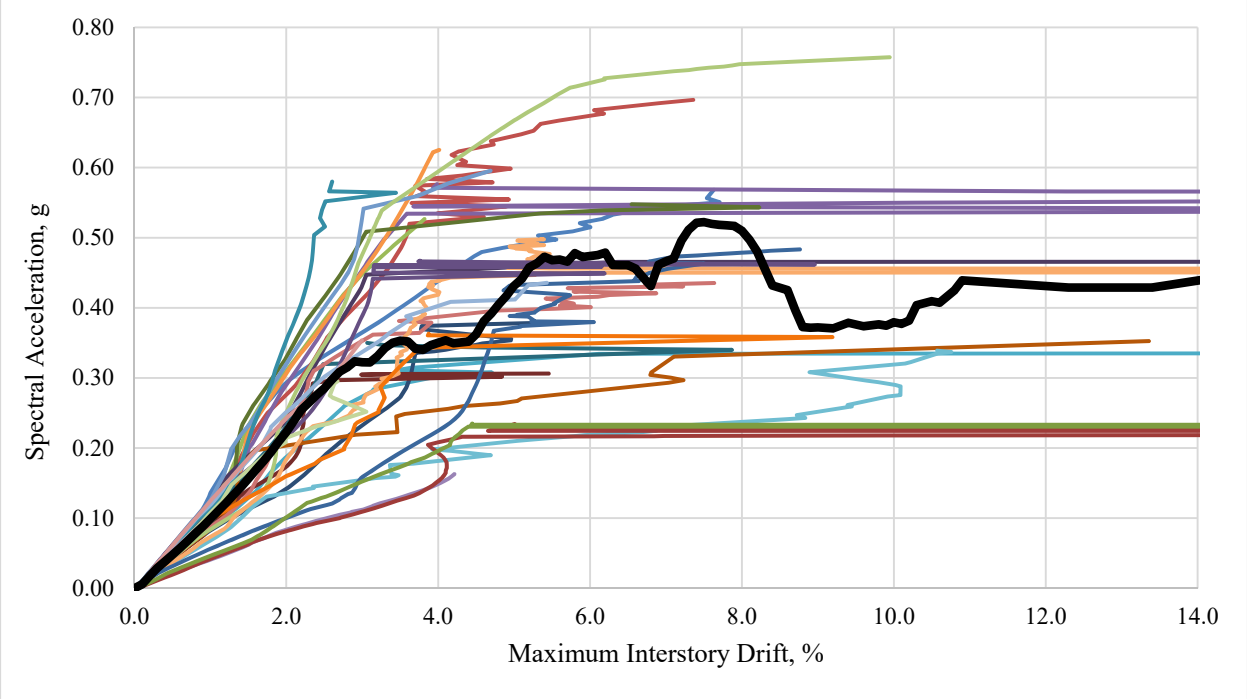


*Figure F-5: Maximum Interstory Drift for PR17M0.66H1.1 Multi-Record IDA Curve Set*

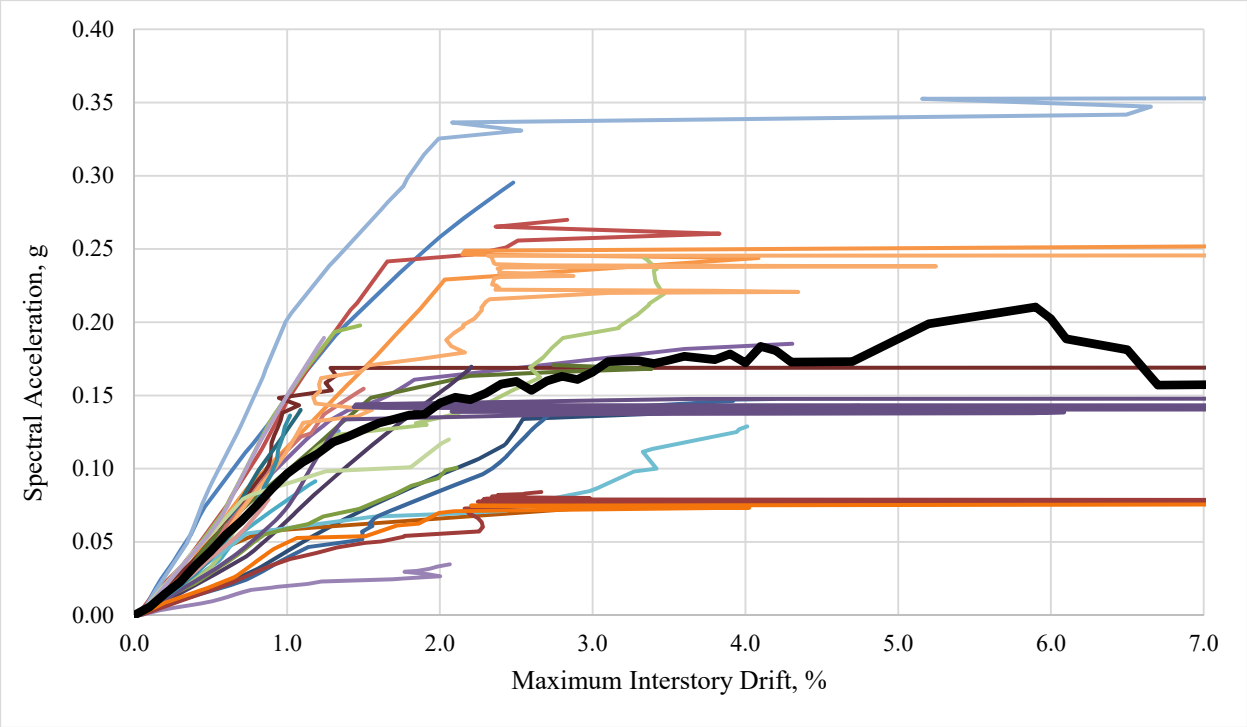


*Figure F-6: Maximum Interstory Drift for PR17M0.33H1.4 Multi-Record IDA Curve Set*

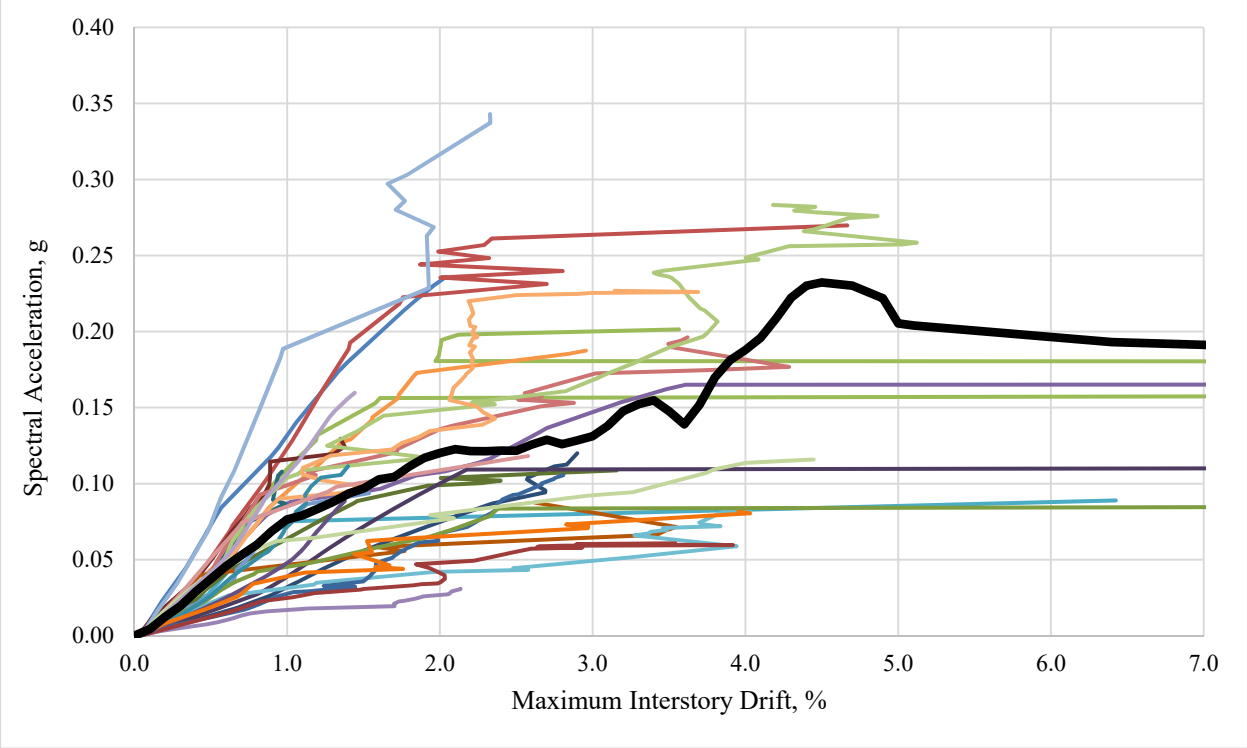


*Figure F-7: Maximum Interstory Drift for PR17M0.33H1.1 Multi-Record IDA Curve Set*

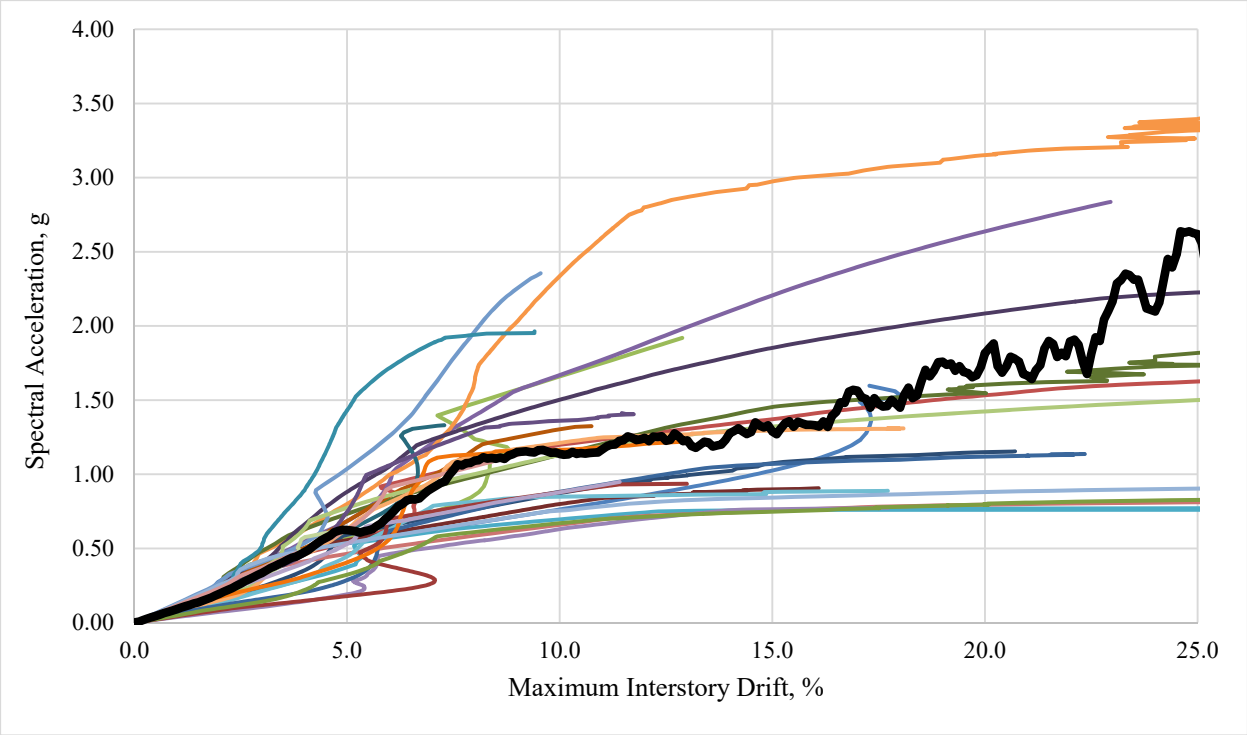


*Figure F-8: Maximum Interstory Drift for PR14M1.0H1.4 Multi-Record IDA Curve Set*

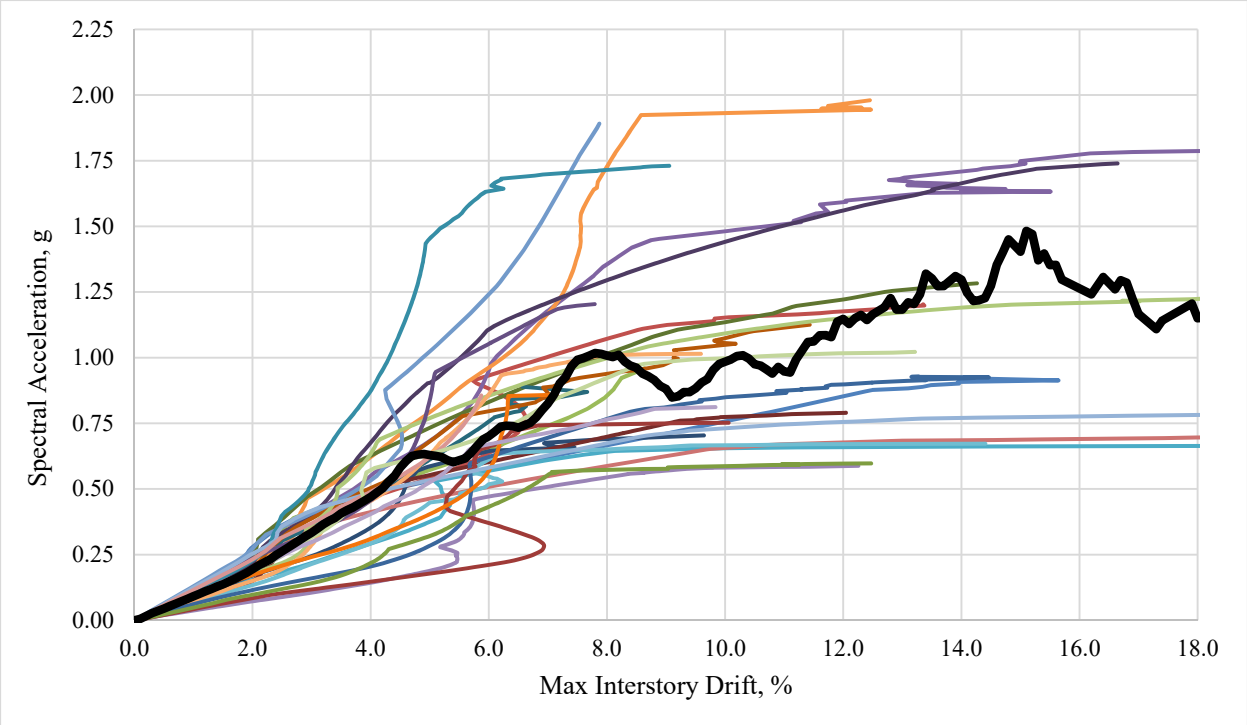


*Figure F-9: Maximum Interstory Drift for PR14M1.0H1.1 Multi-Record IDA Curve Set*

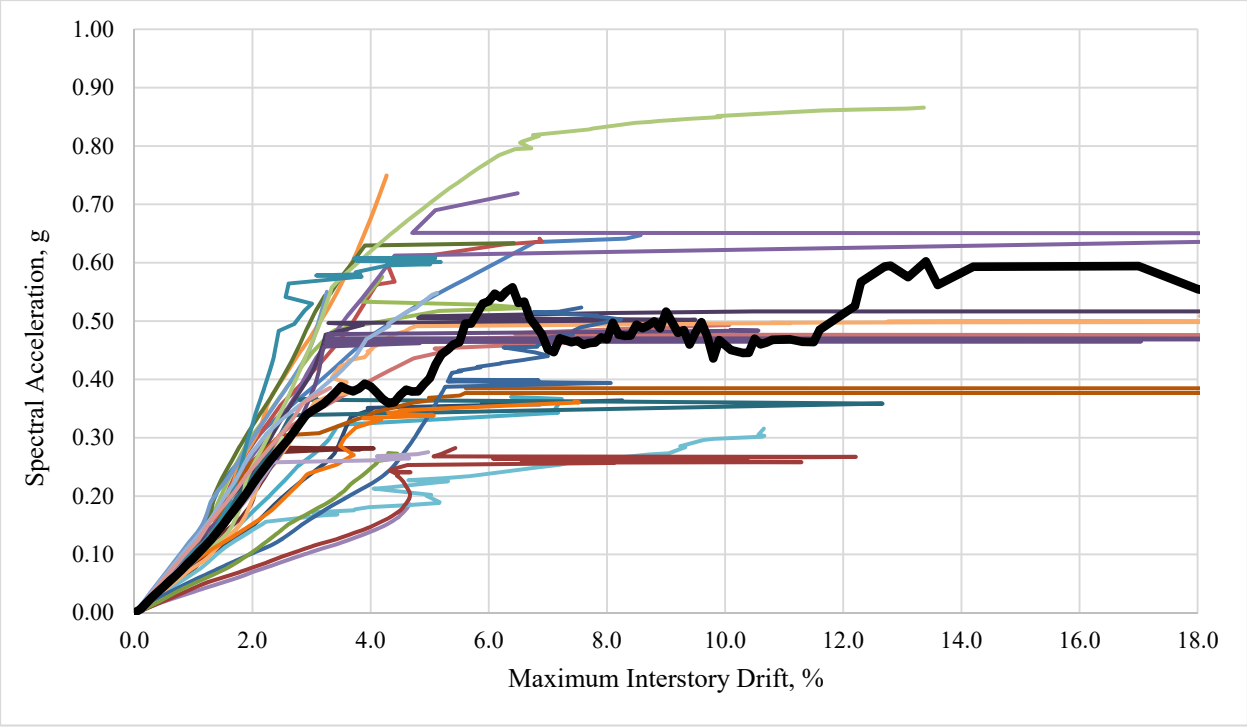


*Figure F-10: Maximum Interstory Drift for PR14M0.66H1.4 Multi-Record IDA Curve Set*

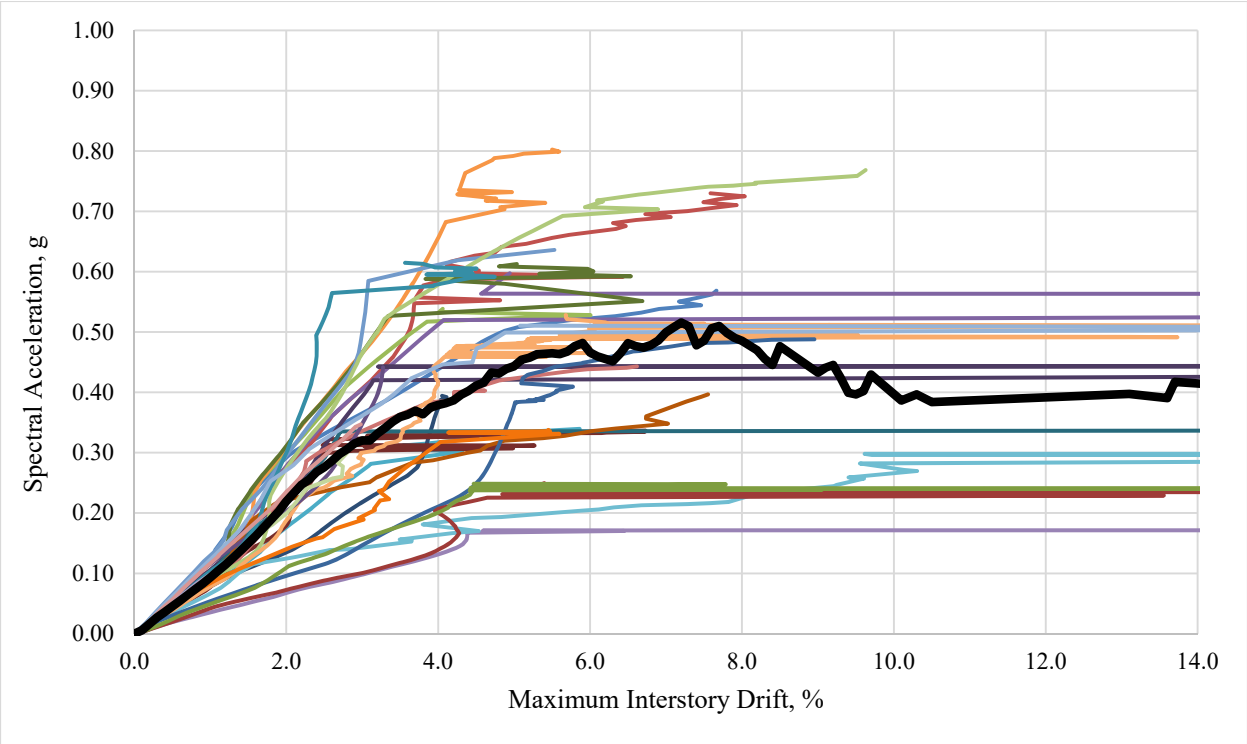


*Figure F-11: Maximum Interstory Drift for PR14M0.66H1.1 Multi-Record IDA Curve Set*

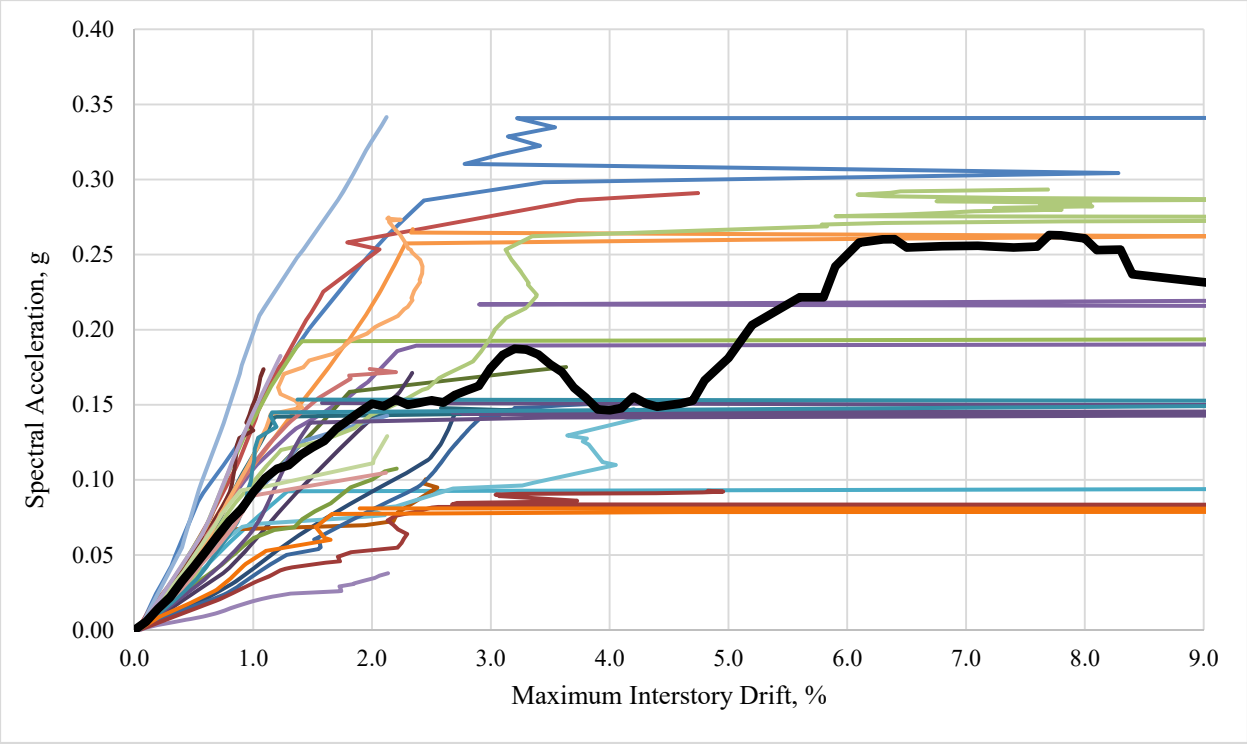


*Figure F-12: Maximum Interstory Drift for PR14M0.33H1.4 Multi-Record IDA Curve Set*

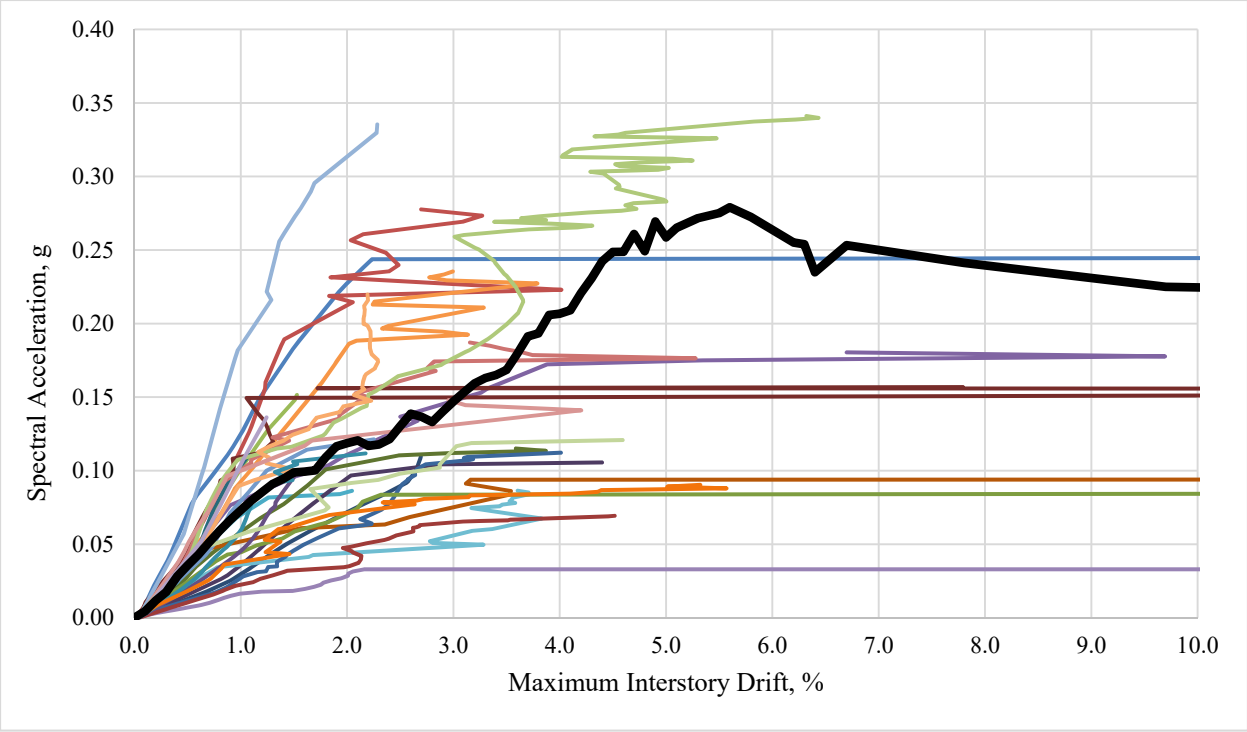


*Figure F-13: Maximum Interstory Drift for PR14M0.33H1.1 Multi-Record IDA Curve Set*

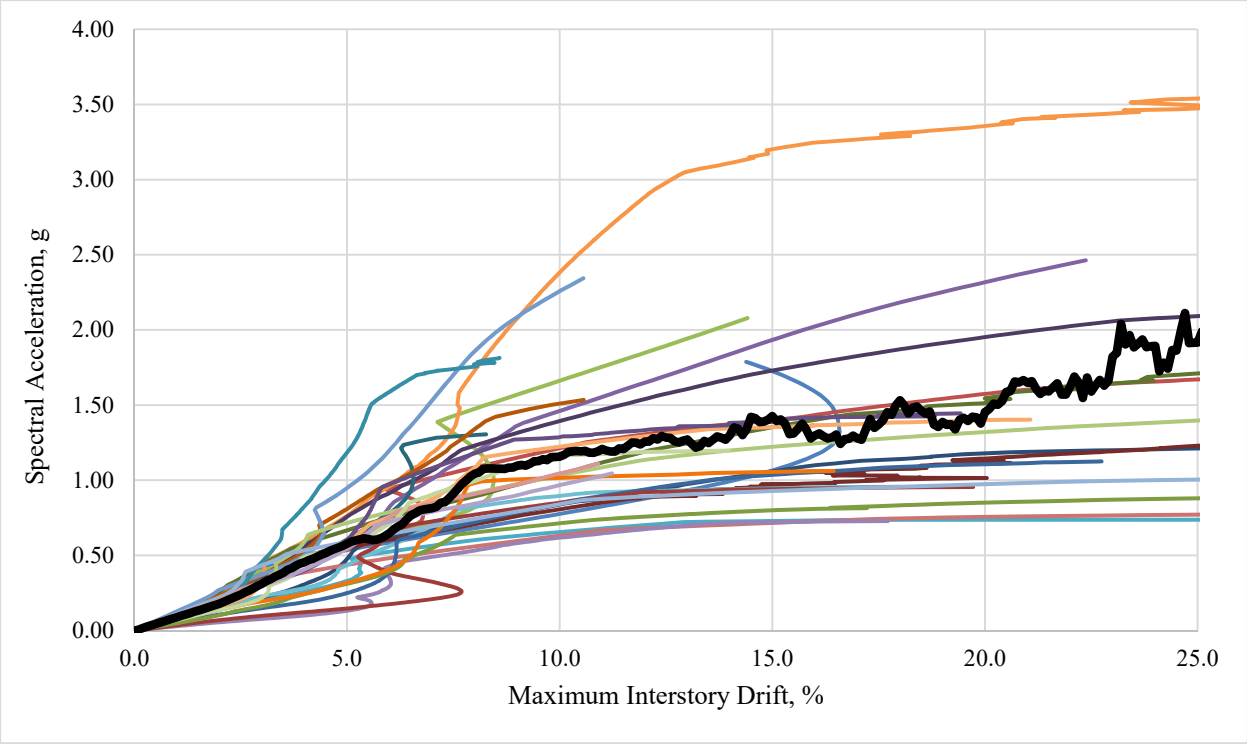


*Figure F-14: Maximum Interstory Drift for PR11M1.0H1.4 Multi-Record IDA Curve Set*

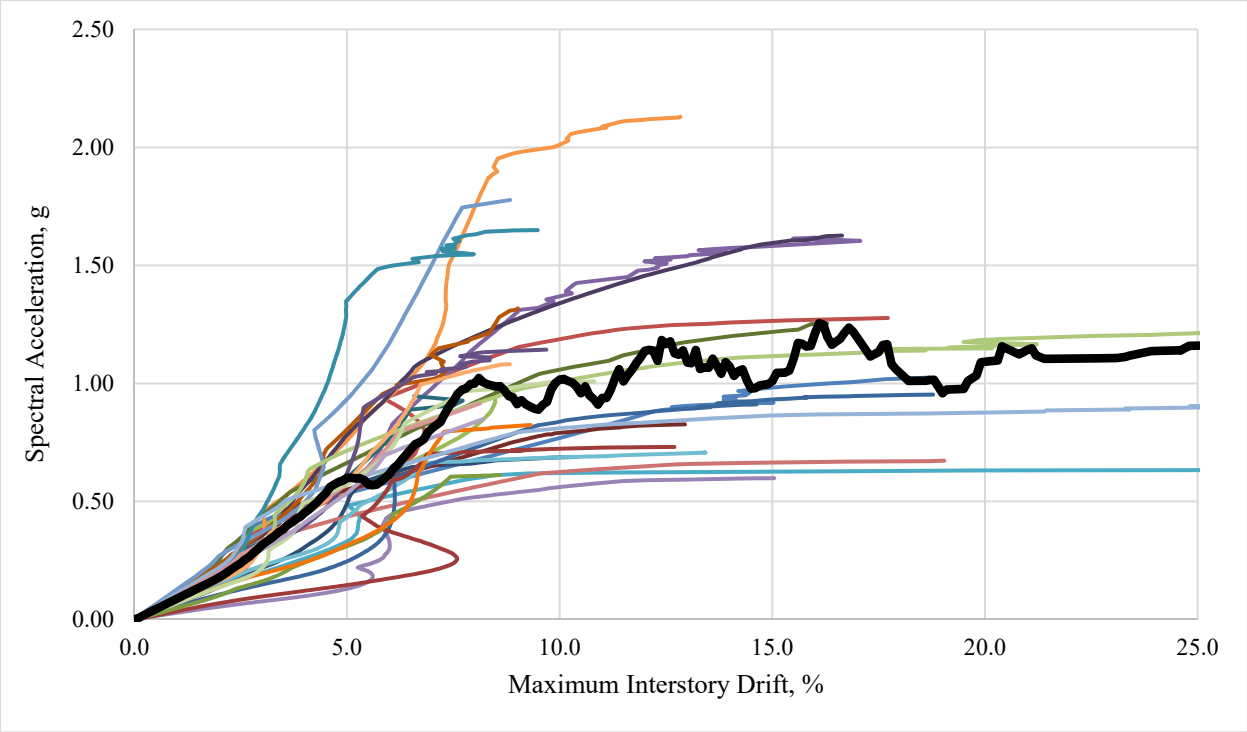


*Figure F-15: Maximum Interstory Drift for PR11M1.0H1.1 Multi-Record IDA Curve Set*

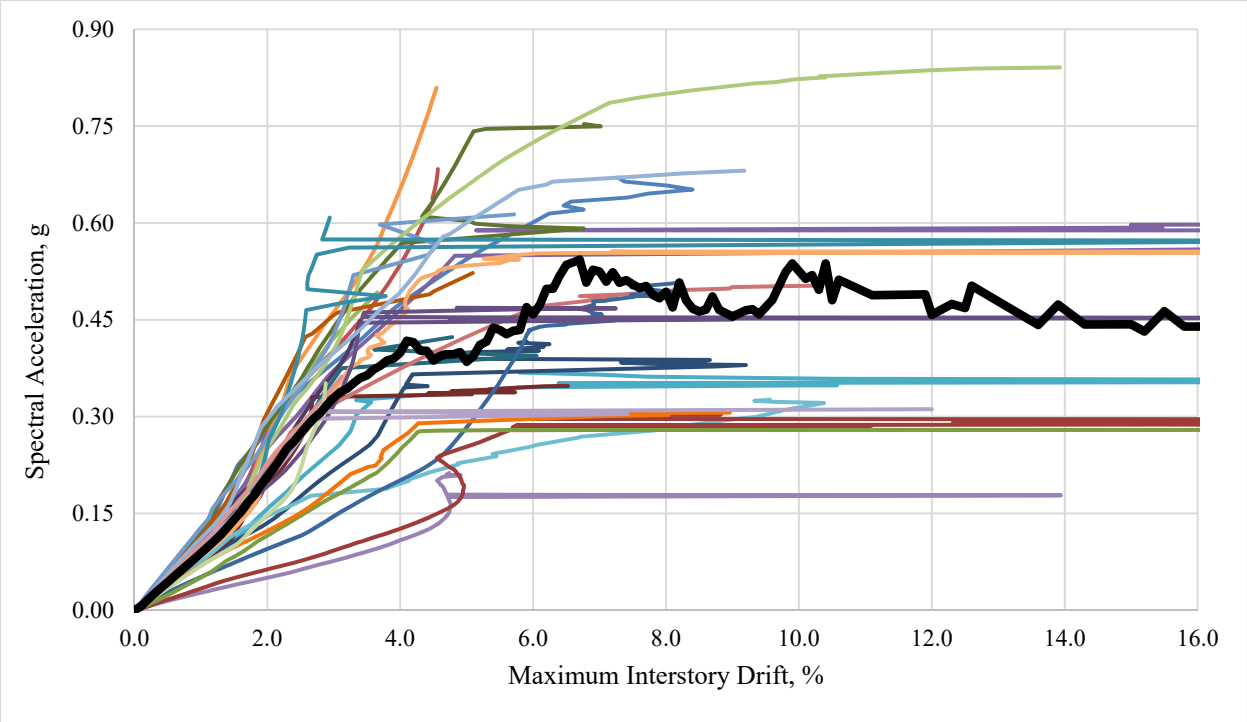


*Figure F-16: Maximum Interstory Drift for PR11M0.66H1.4 Multi-Record IDA Curve Set*

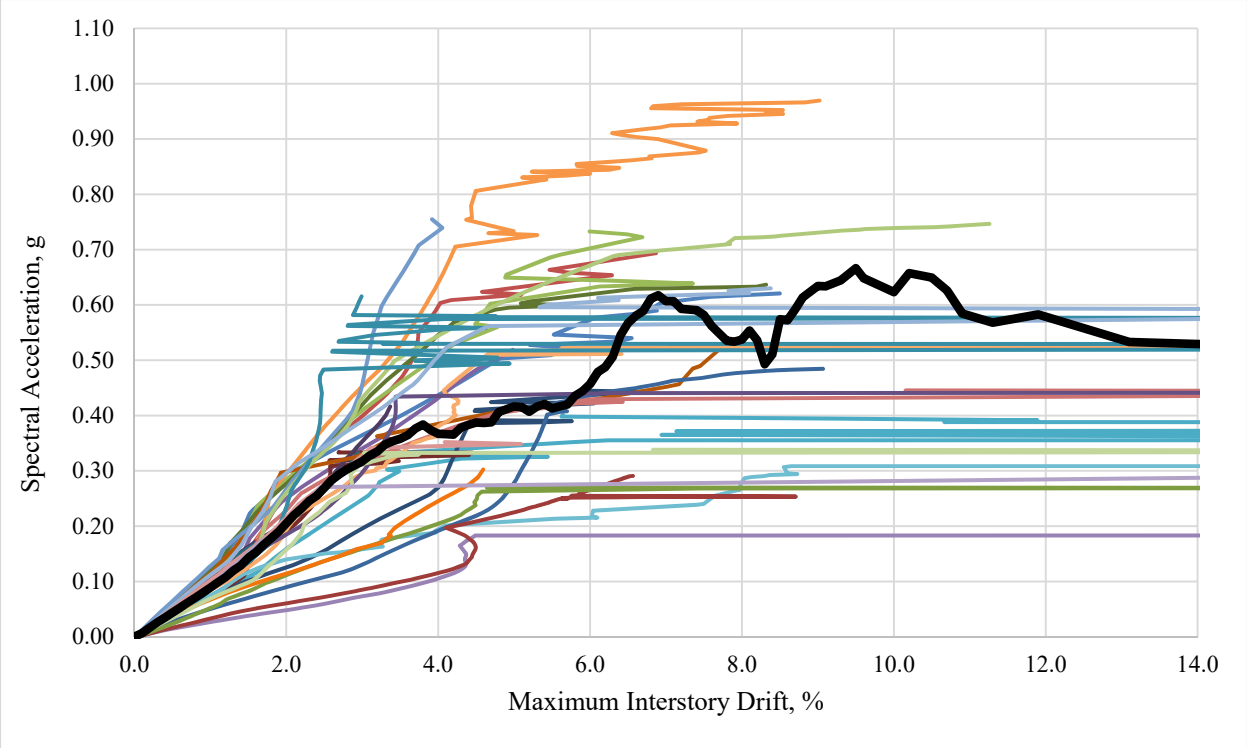


*Figure F-17: Maximum Interstory Drift for PR11M0.66H1.1 Multi-Record IDA Curve Set*

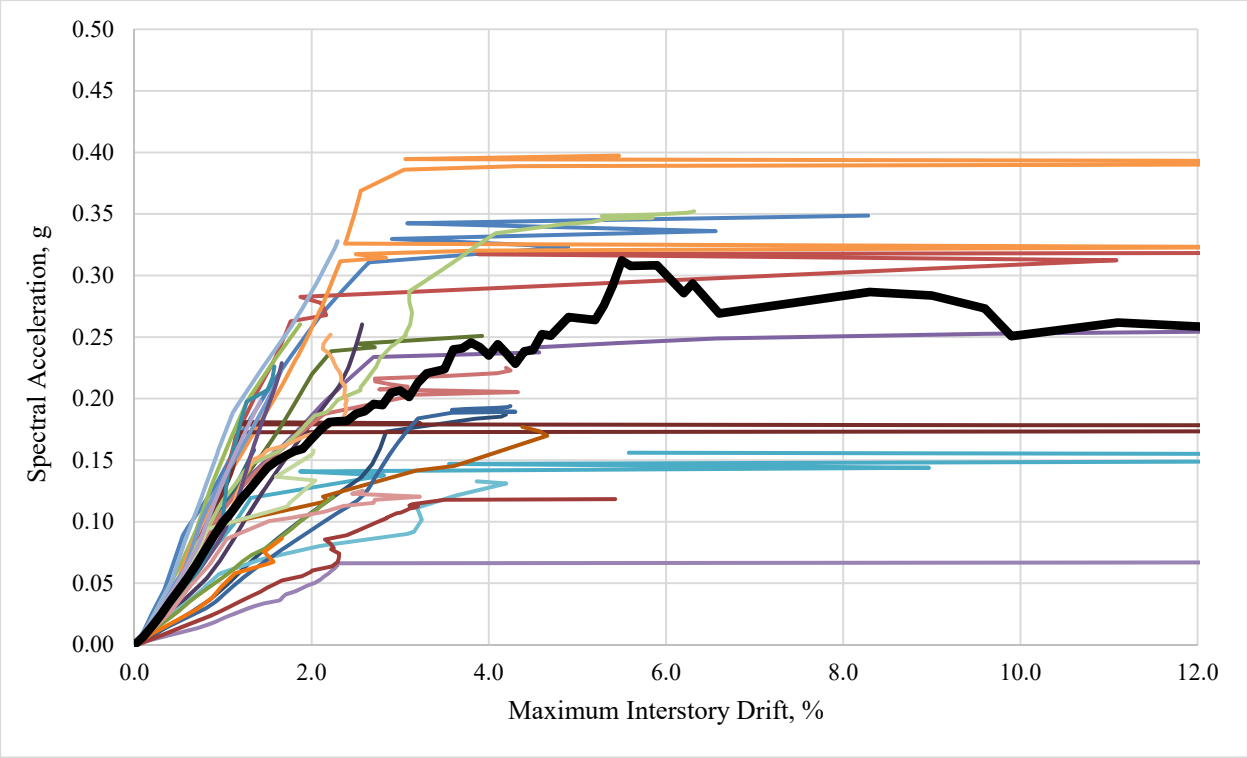


*Figure F-18: Maximum Interstory Drift for PR11M0.33H1.4 Multi-Record IDA Curve Set*

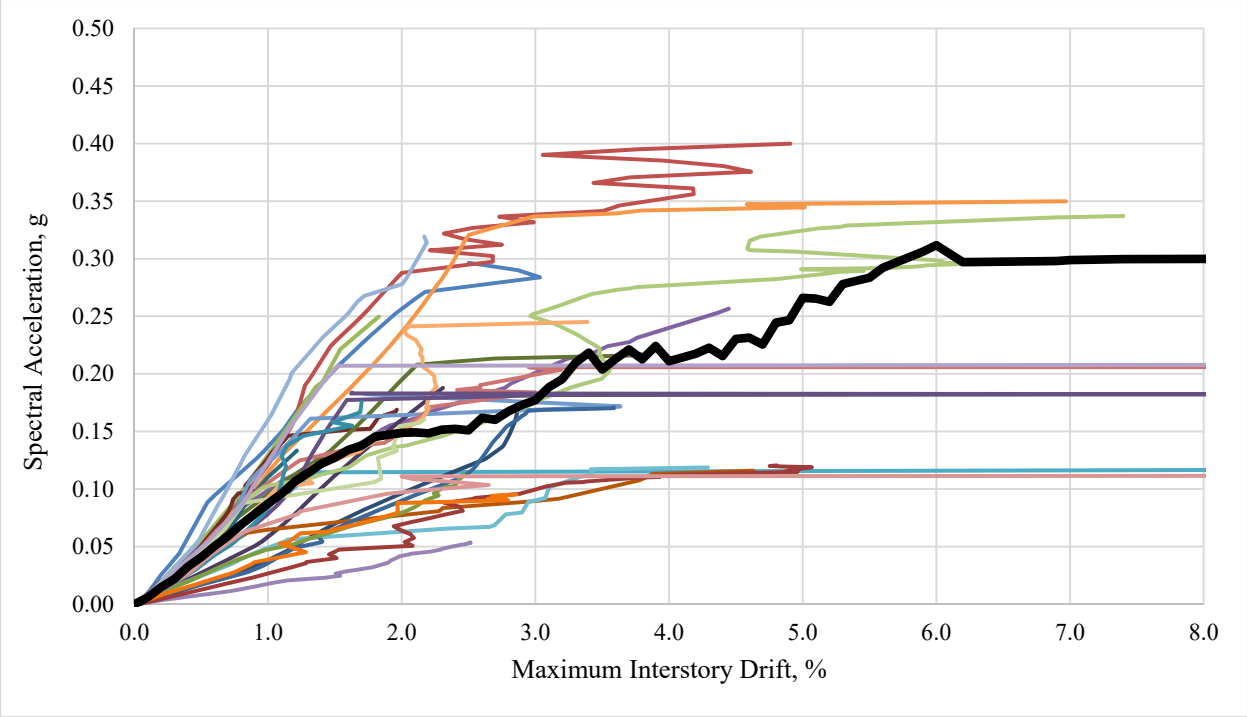


*Figure F-19: Maximum Interstory Drift for PR11M0.33H1.1 Multi-Record IDA Curve Set*

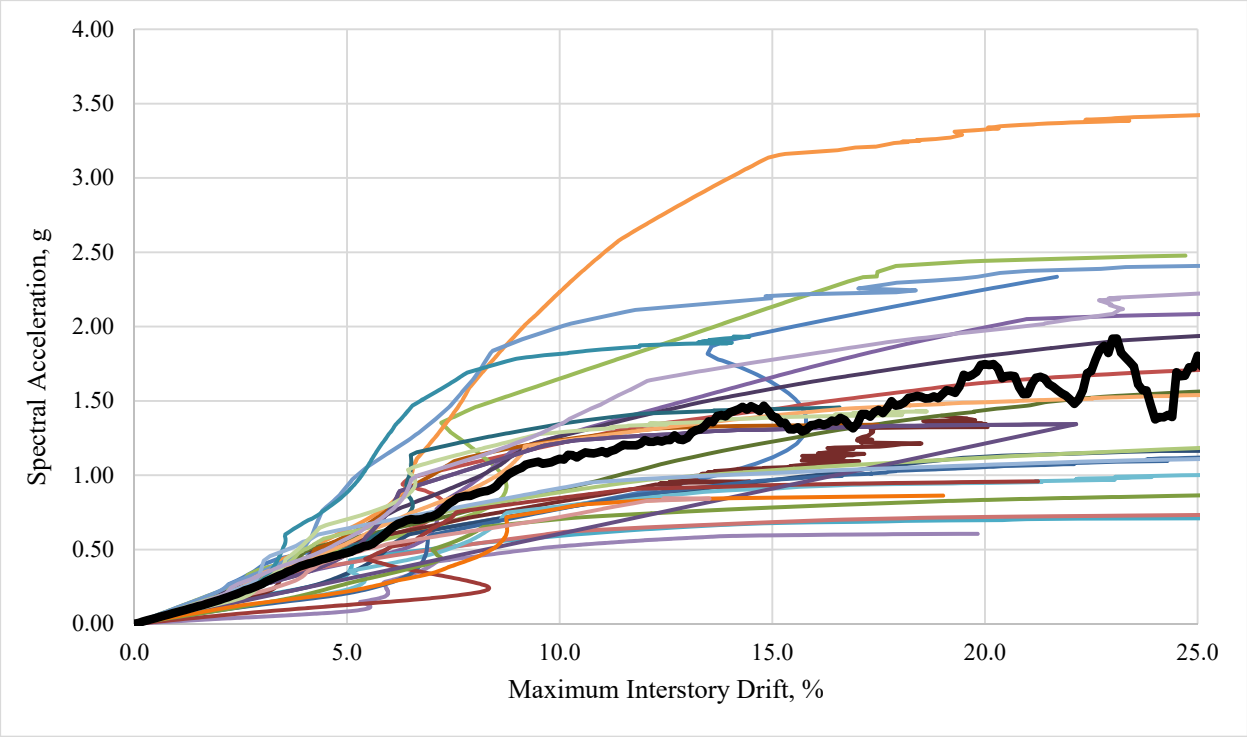


*Figure F-20: Maximum Interstory Drift for PR8M1.0H1.4 Multi-Record IDA Curve Set*

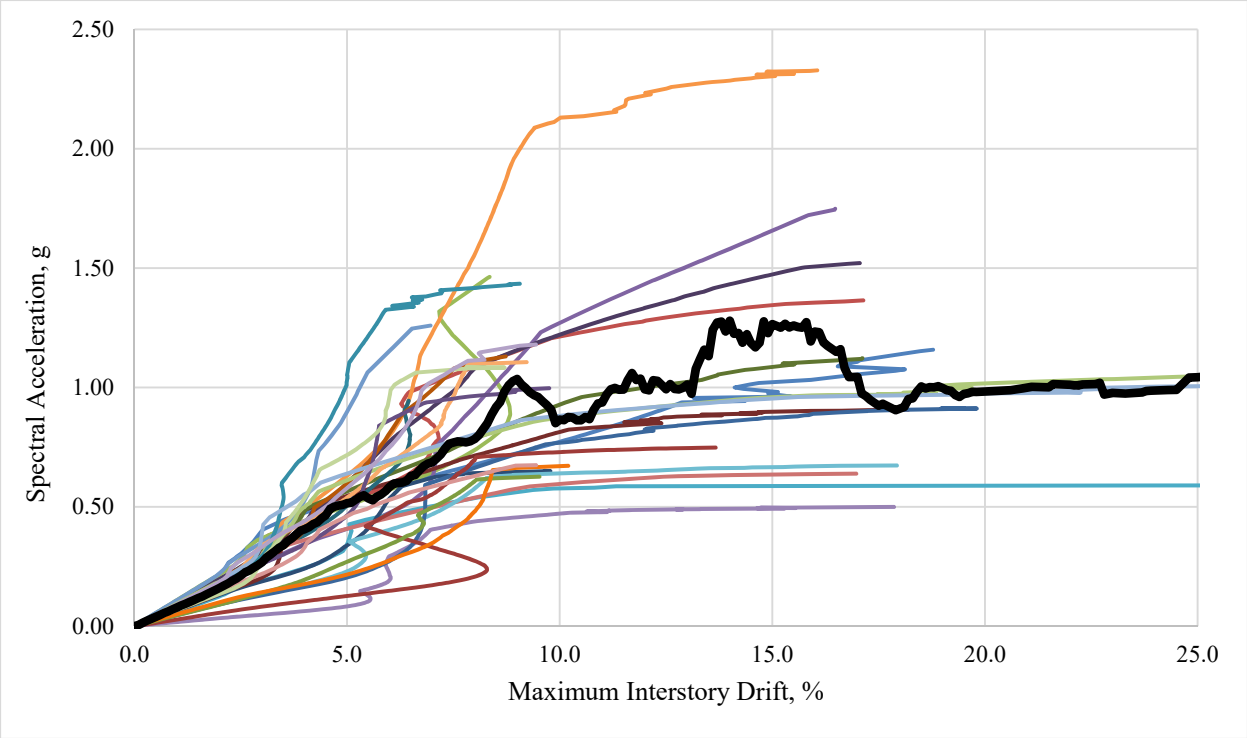


*Figure F-21: Maximum Interstory Drift for PR8M1.0H1.1 Multi-Record IDA Curve Set*

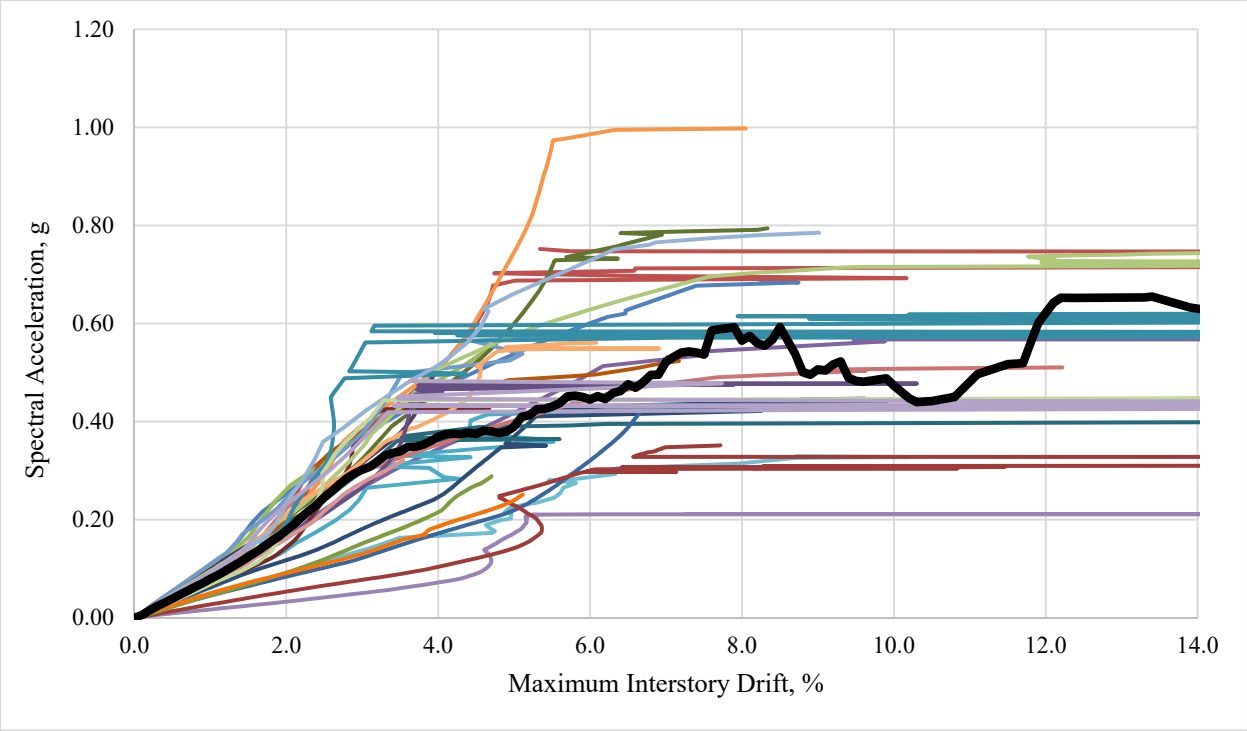


*Figure F-22: Maximum Interstory Drift for PR8M0.66H1.4 Multi-Record IDA Curve Set*

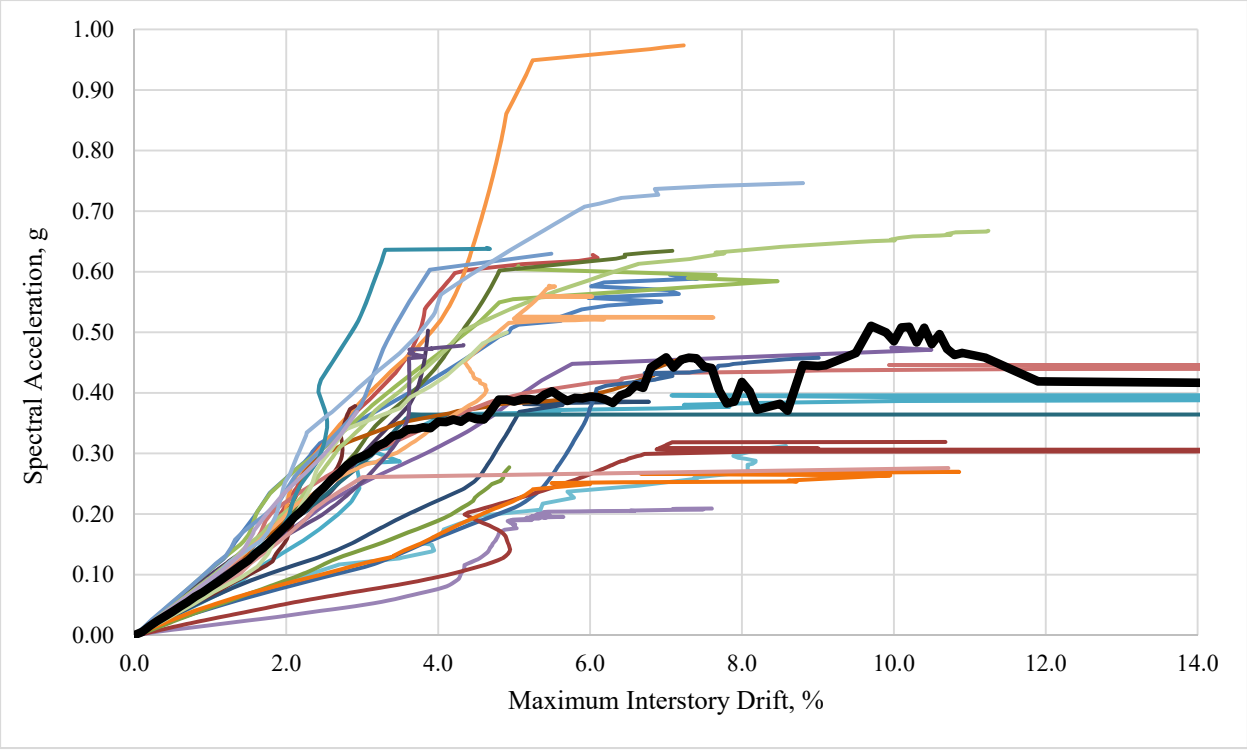


*Figure F-23: Maximum Interstory Drift for PR8M0.66H1.1 Multi-Record IDA Curve Set*

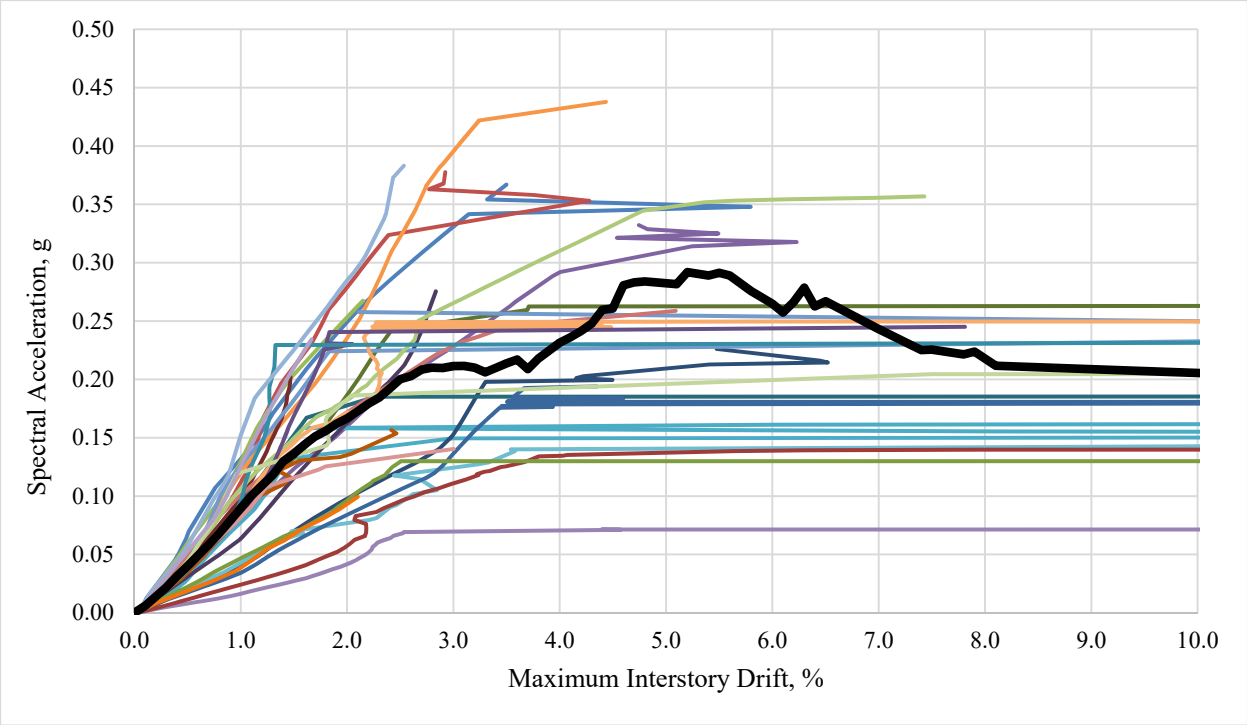


*Figure F-24: Maximum Interstory Drift for PR8M0.33H1.4 Multi-Record IDA Curve Set*

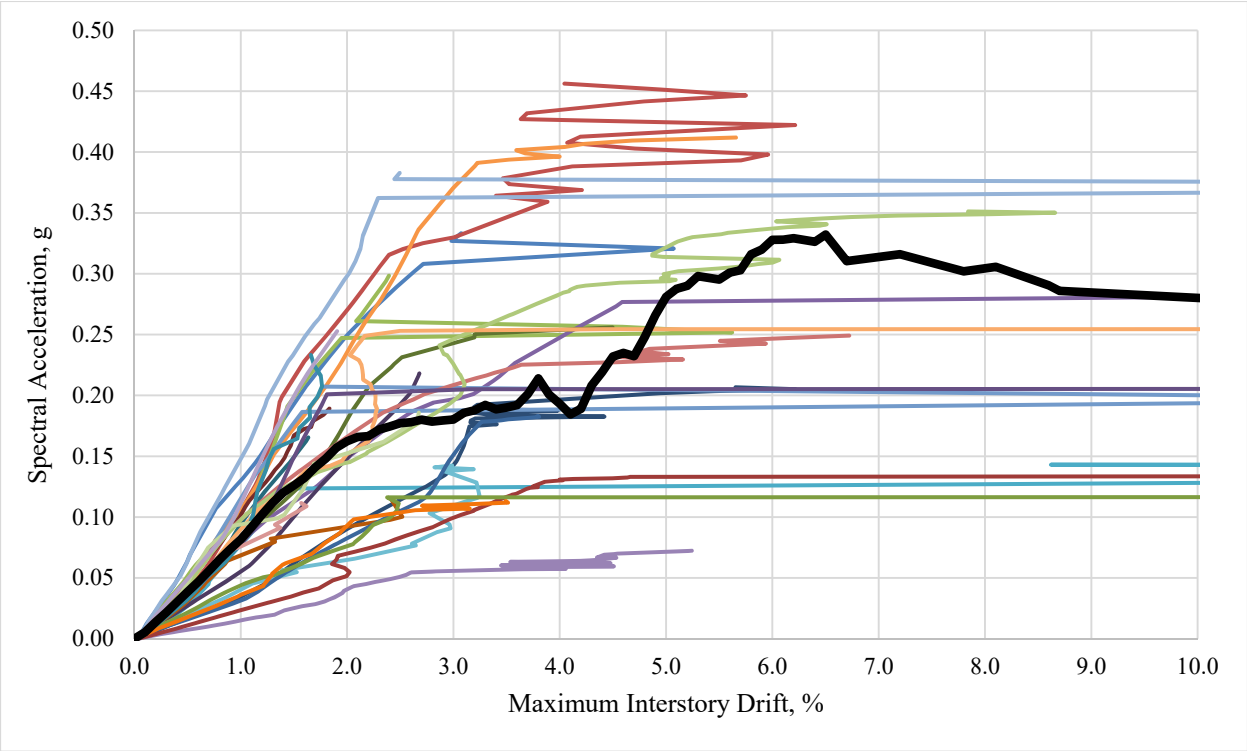


*Figure F-25: Maximum Interstory Drift for PR8M0.33H1.1 Multi-Record IDA Curve Set*

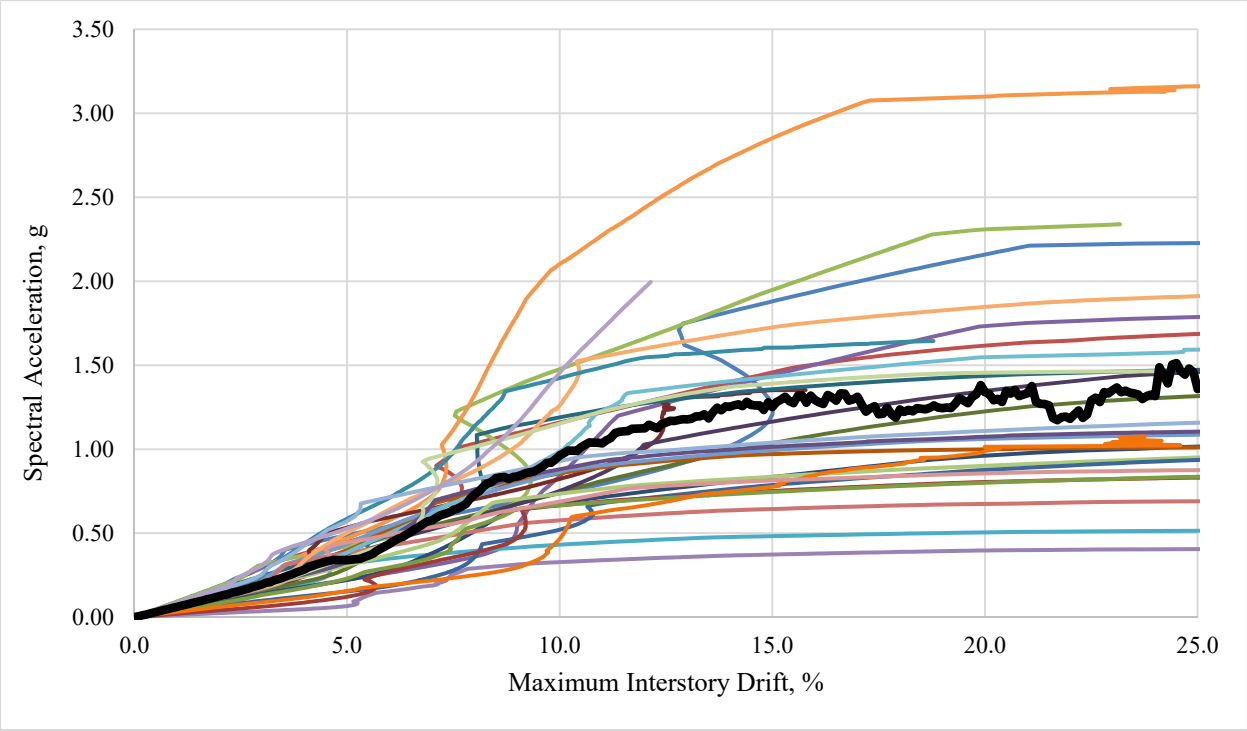


*Figure F-26: Maximum Interstory Drift for PR5M1.0H1.4 Multi-Record IDA Curve Set*

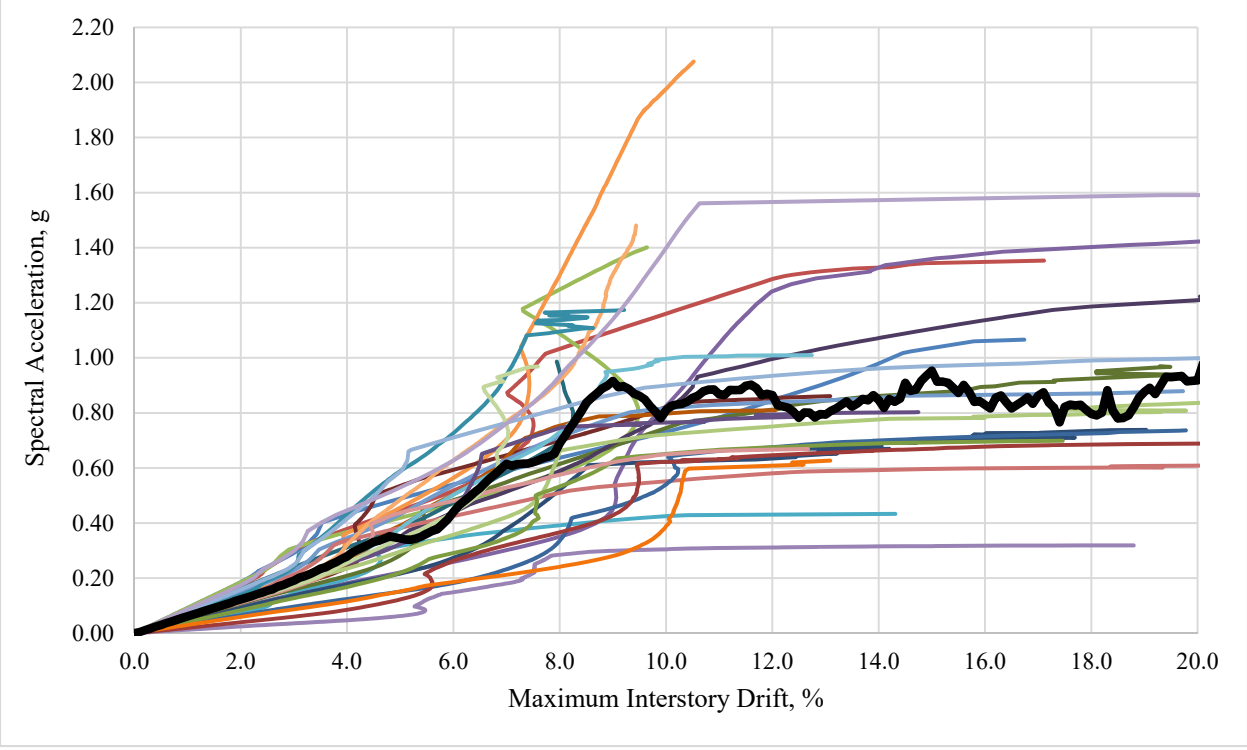


*Figure F-27: Maximum Interstory Drift for PR5M1.0H1.1 Multi-Record IDA Curve Set*

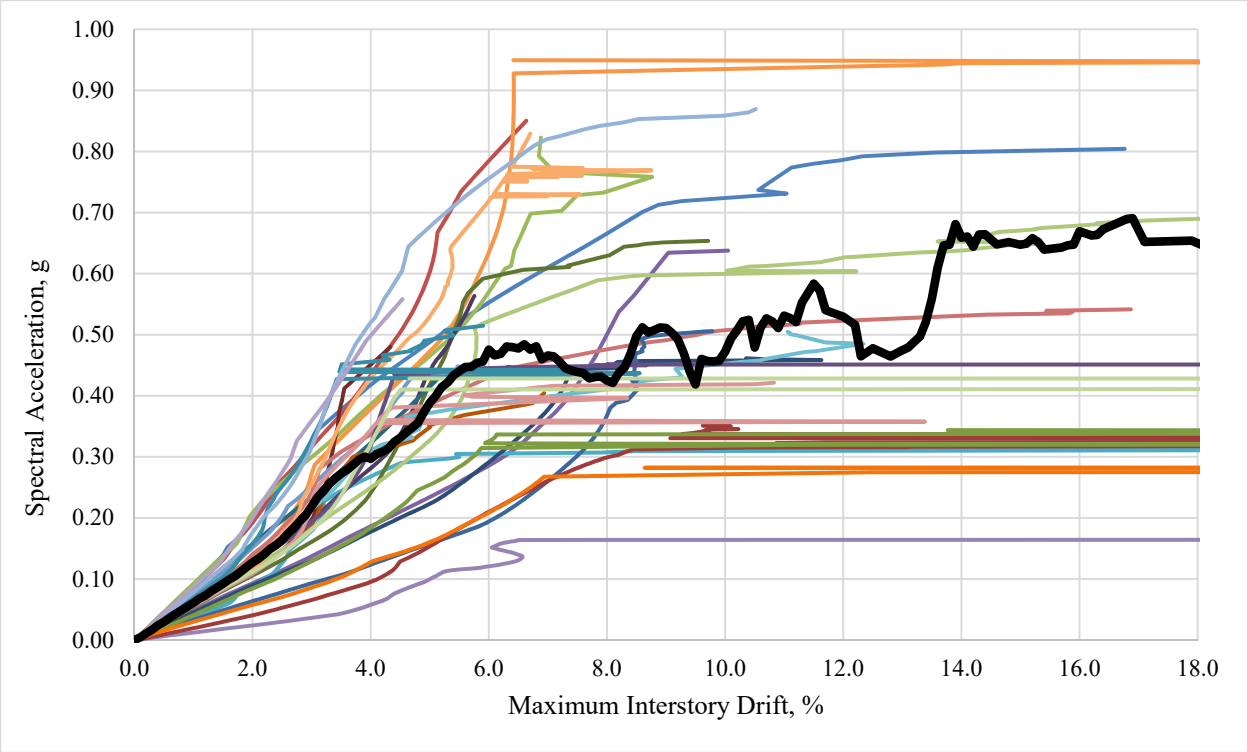


*Figure F-28: Maximum Interstory Drift for PR5M0.66H1.4 Multi-Record IDA Curve Set*

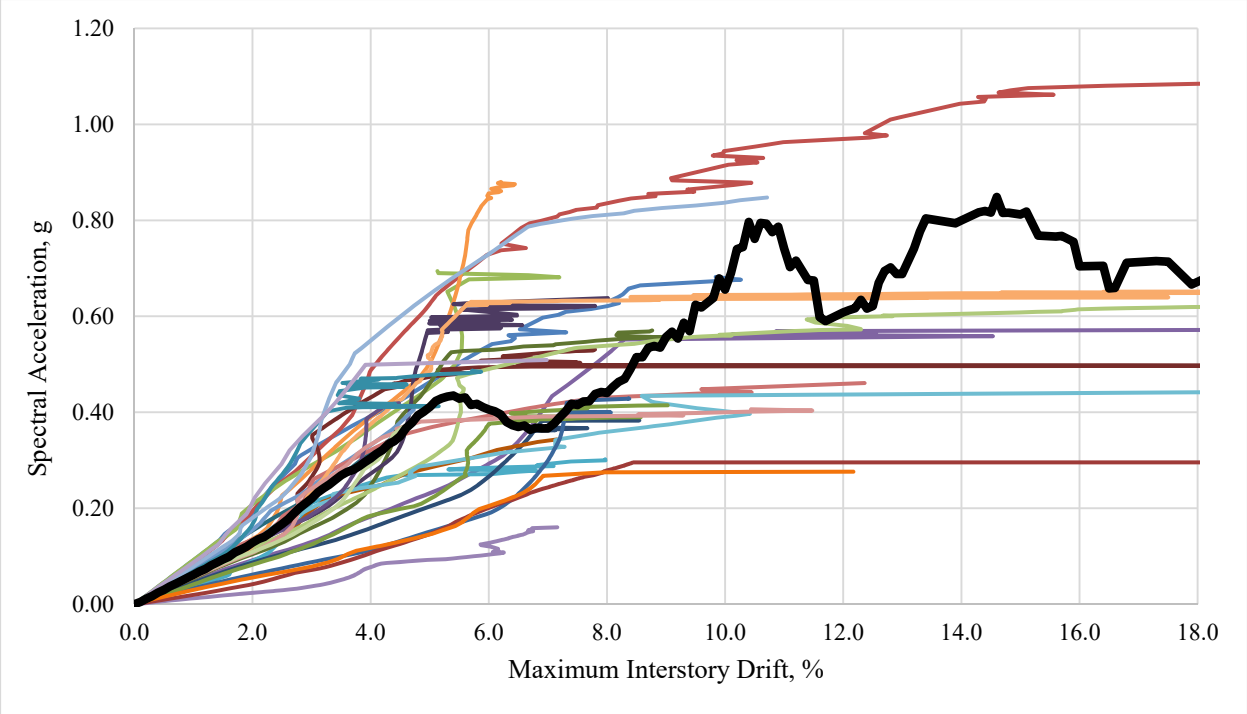


*Figure F-29: Maximum Interstory Drift for PR5M0.66H1.1 Multi-Record IDA Curve Set*

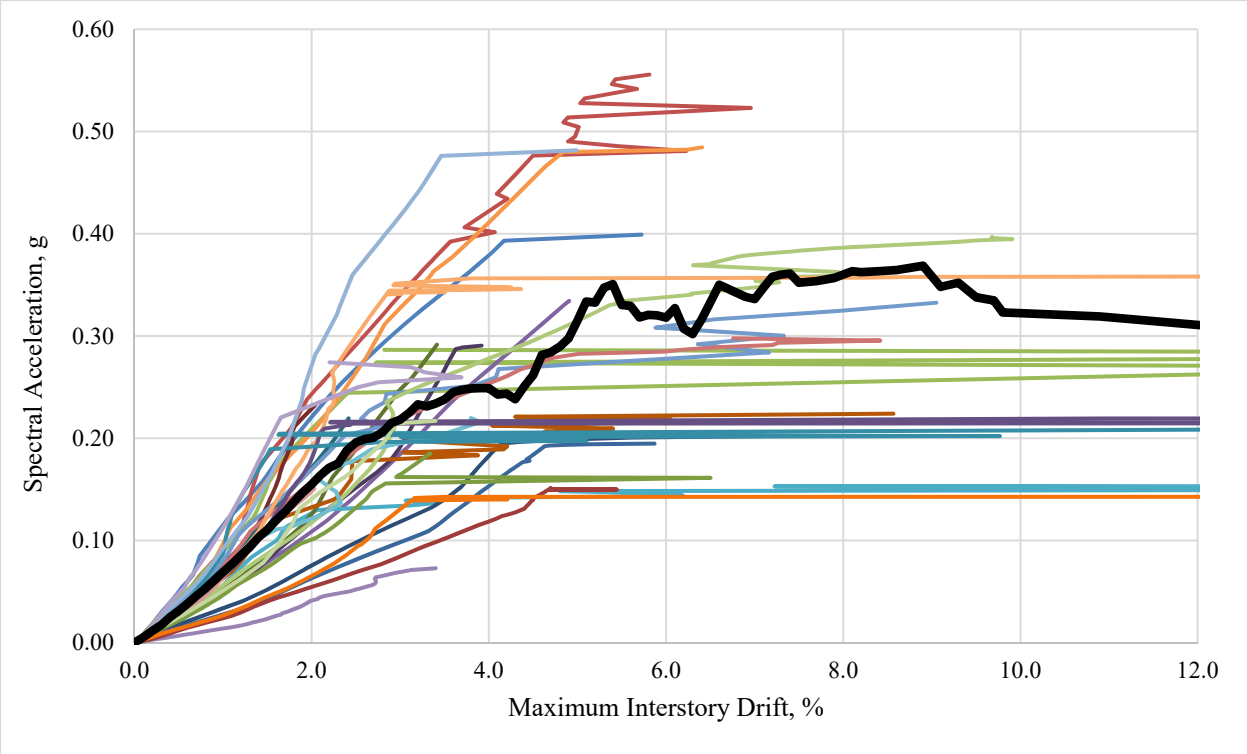


*Figure F-30: Maximum Interstory Drift for PR5M0.33H1.4 Multi-Record IDA Curve Set*

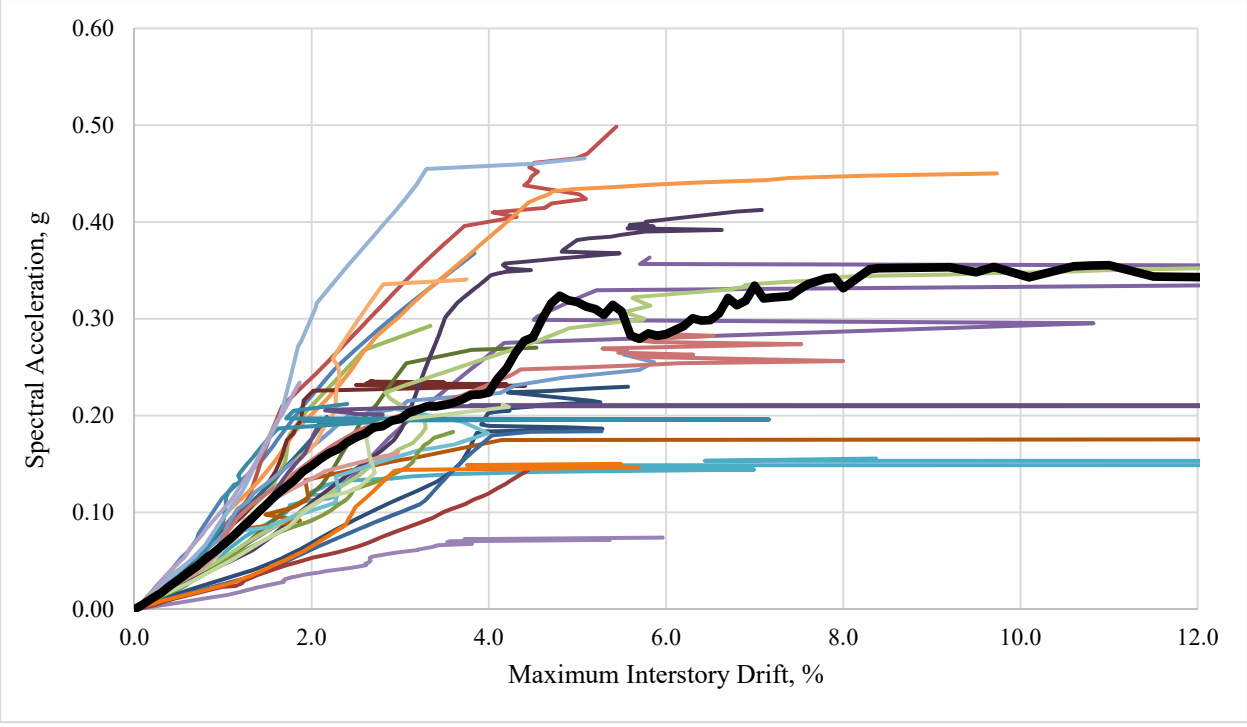


*Figure F-31: Maximum Interstory Drift for PR5M0.33H1.1 Multi-Record IDA Curve Set*

## Appendix G: Maximum Base Shear Multi-Record IDA Curve Sets

This Appendix contains the multi-record IDA curve sets for the maximum base shear DMs for all of the frames.

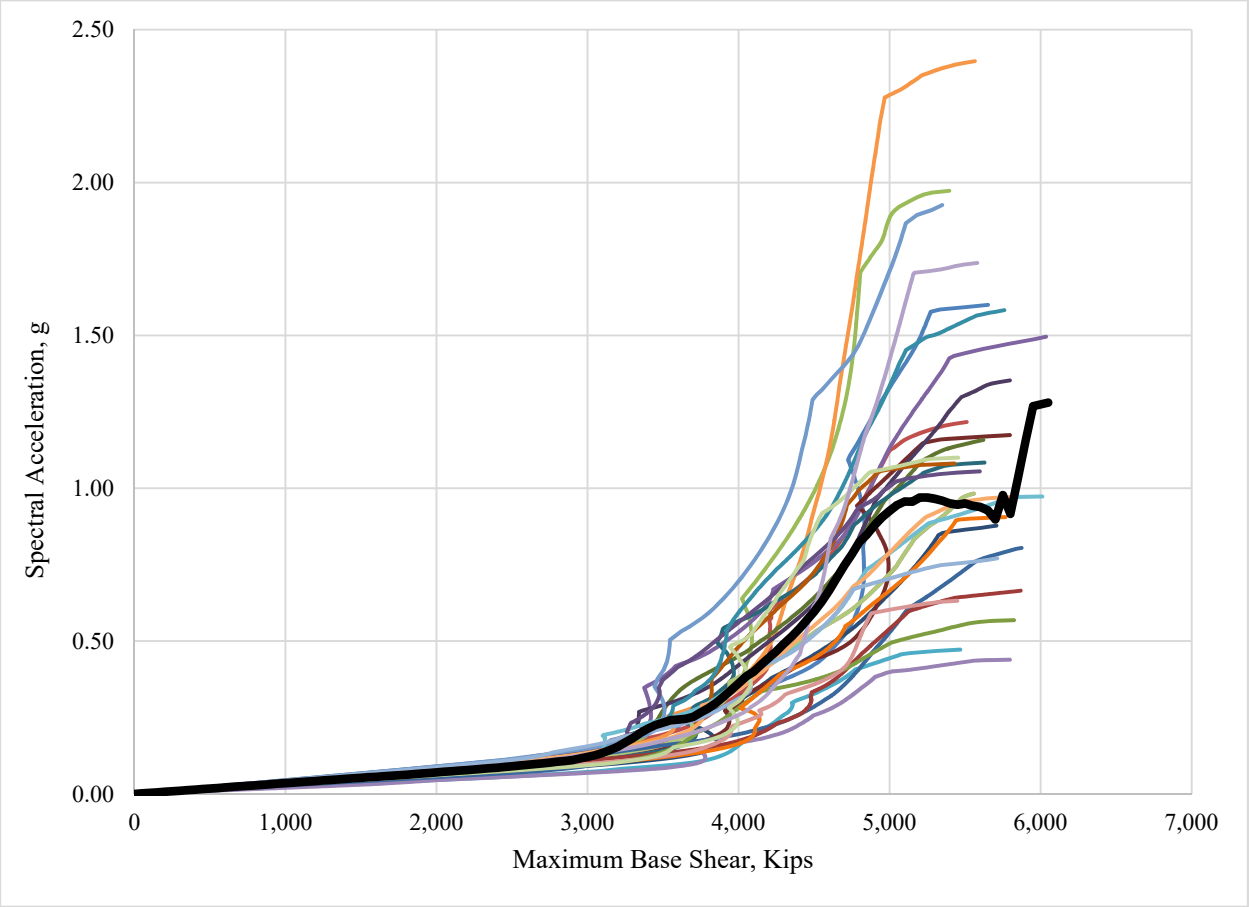


*Figure G-1: Maximum Base Shear for Control Frame Multi-Record IDA Curve Set*

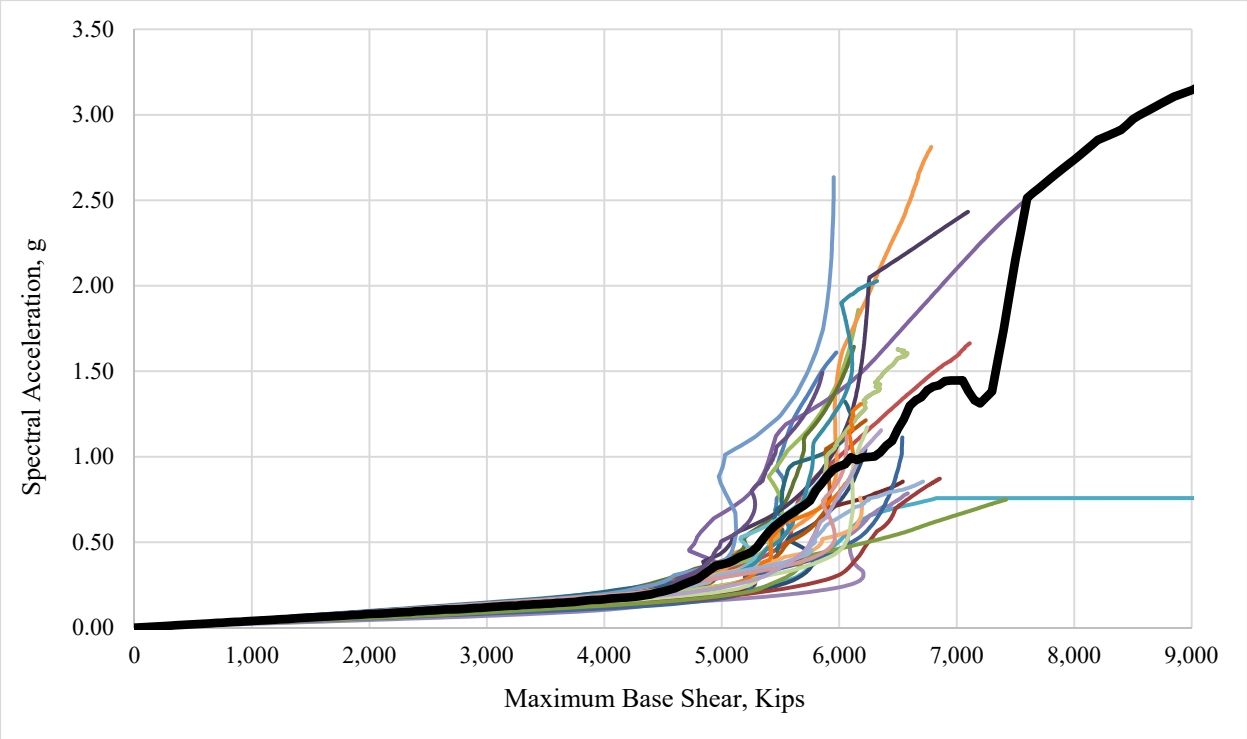


*Figure G-2: Maximum Base Shear for PR17M1.0H1.4 Multi-Record IDA Curve Set*

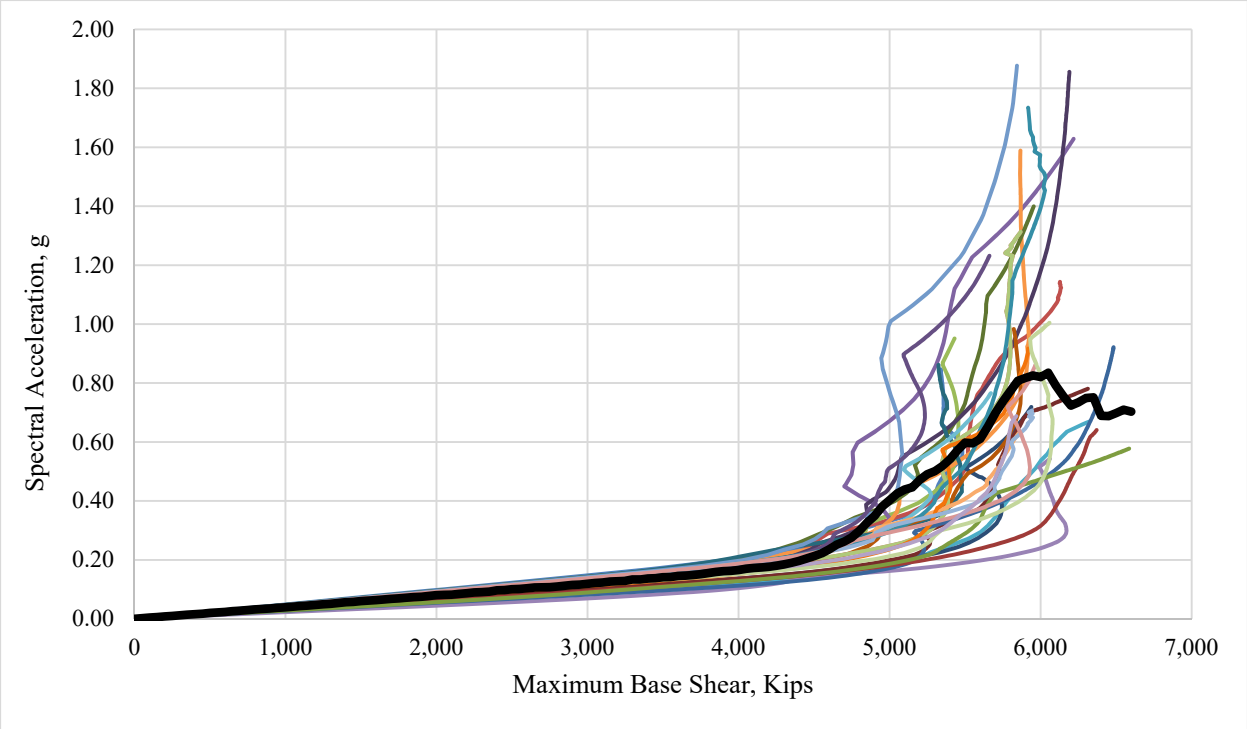


*Figure G-3: Maximum Base Shear for PR17M1.0H1.1 Multi-Record IDA Curve Set*

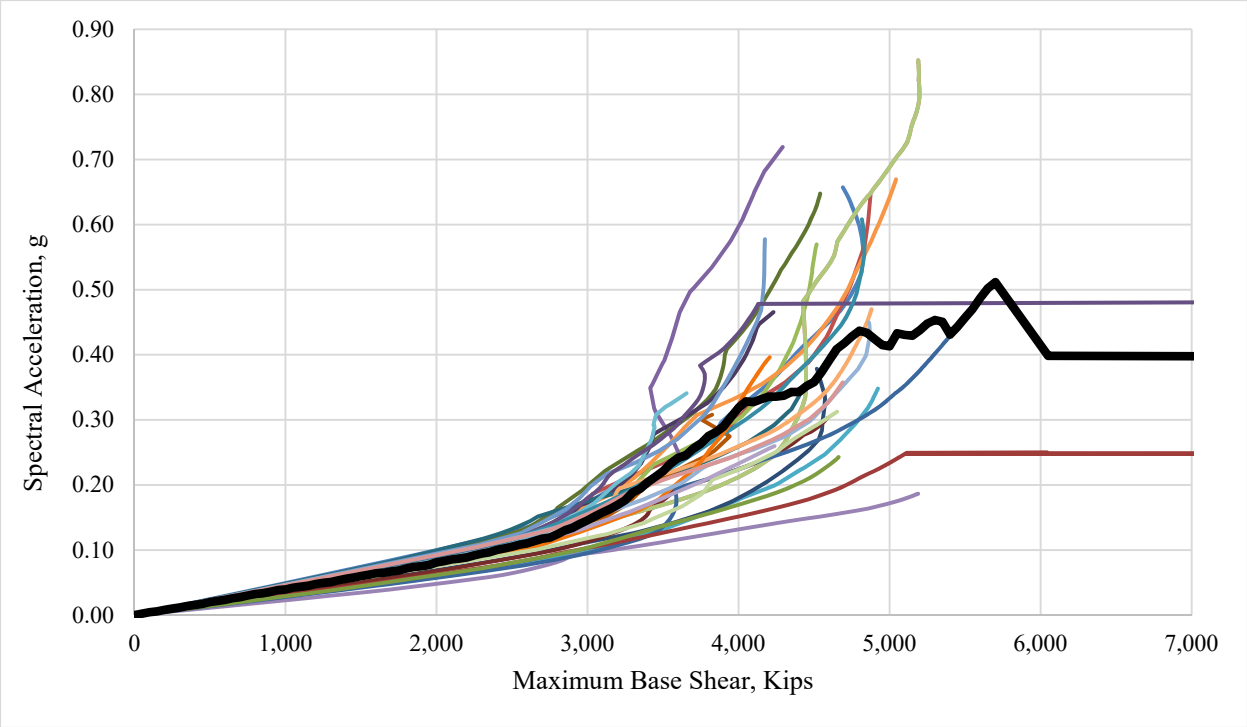


*Figure G-4: Maximum Base Shear for PR17M0.66H1.4 Multi-Record IDA Curve Set*

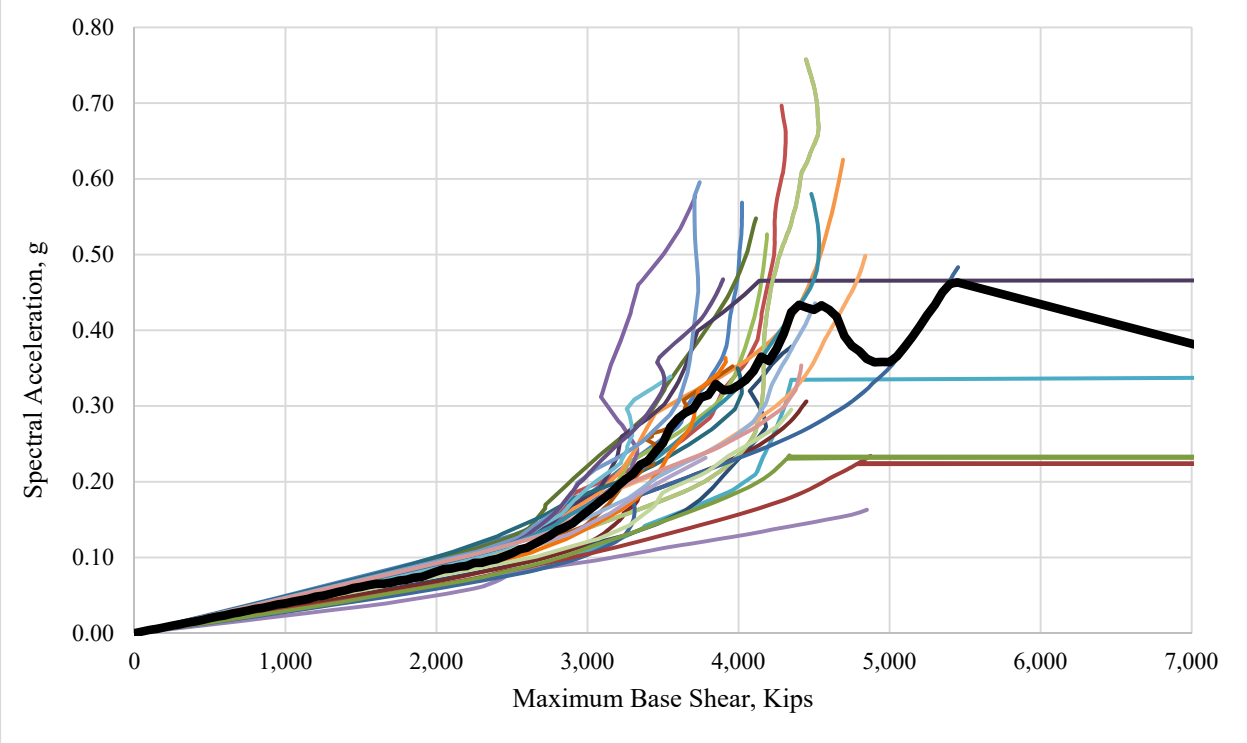


*Figure G-5: Maximum Base Shear for PR17M0.66H1.1 Multi-Record IDA Curve Set*

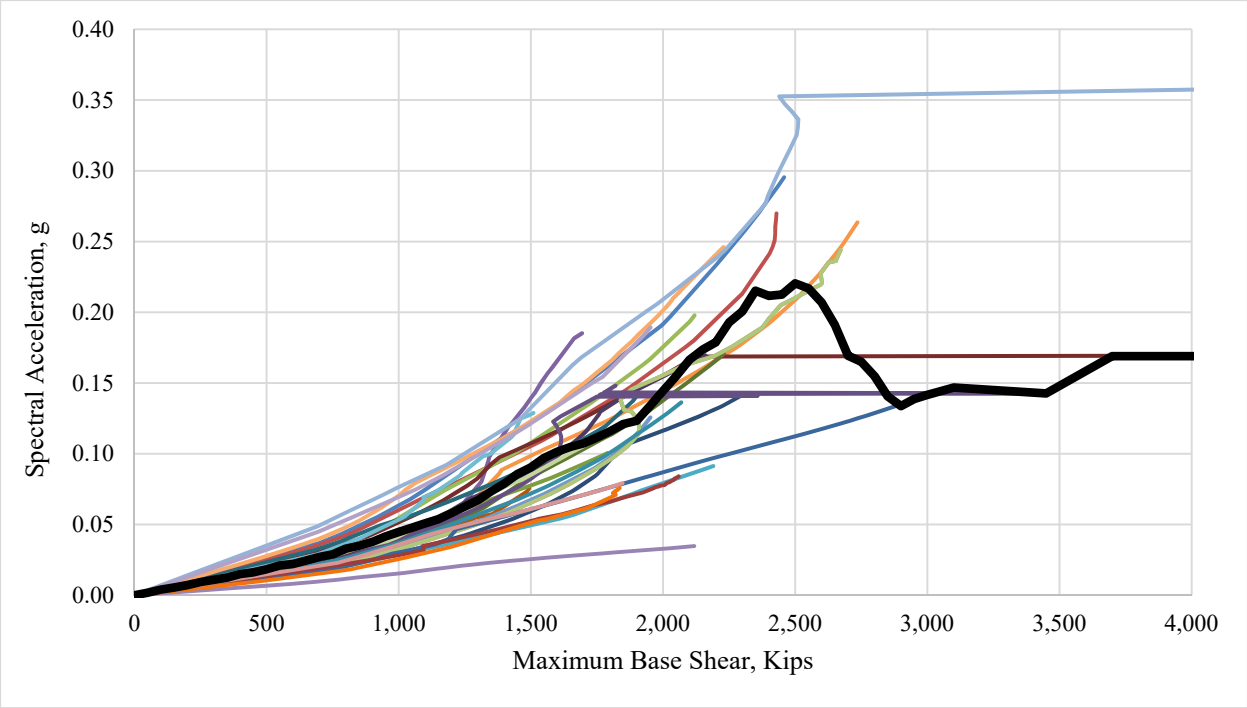


*Figure G-6: Maximum Base Shear for PR17M0.33H1.4 Multi-Record IDA Curve Set*

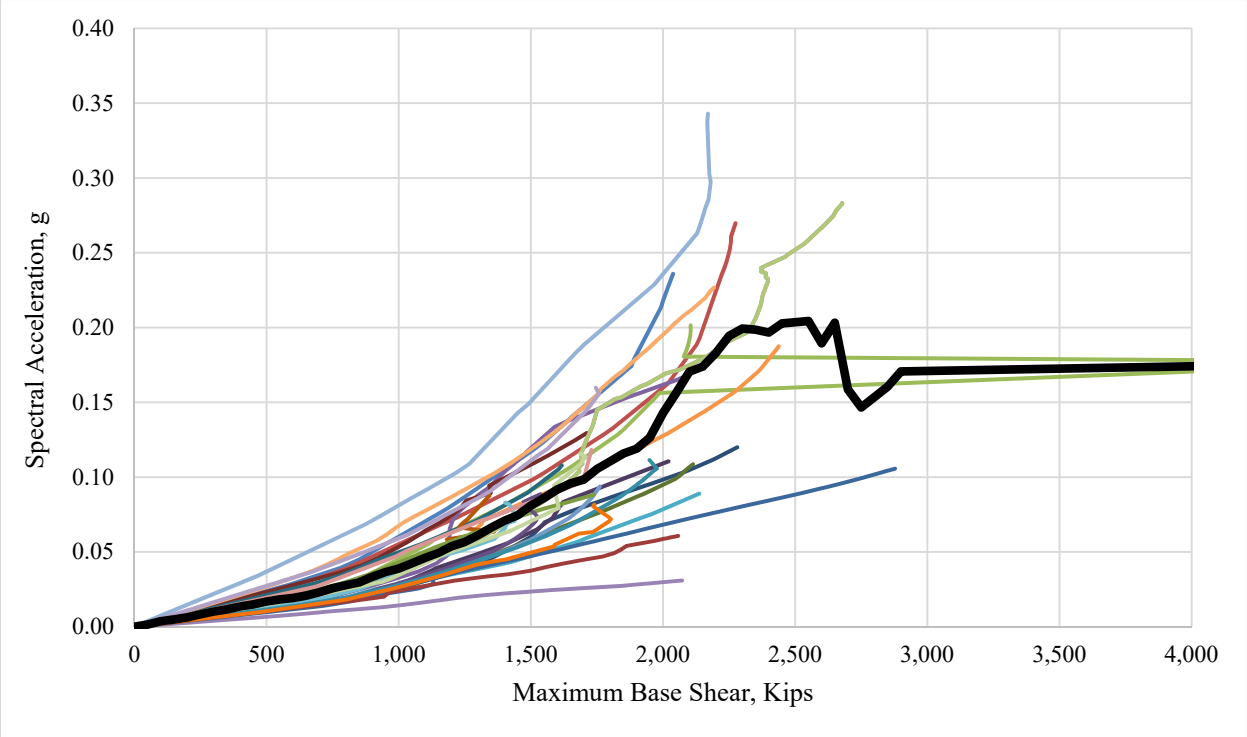


*Figure G-7: Maximum Base Shear for PR17M0.33H1.1 Multi-Record IDA Curve Set*

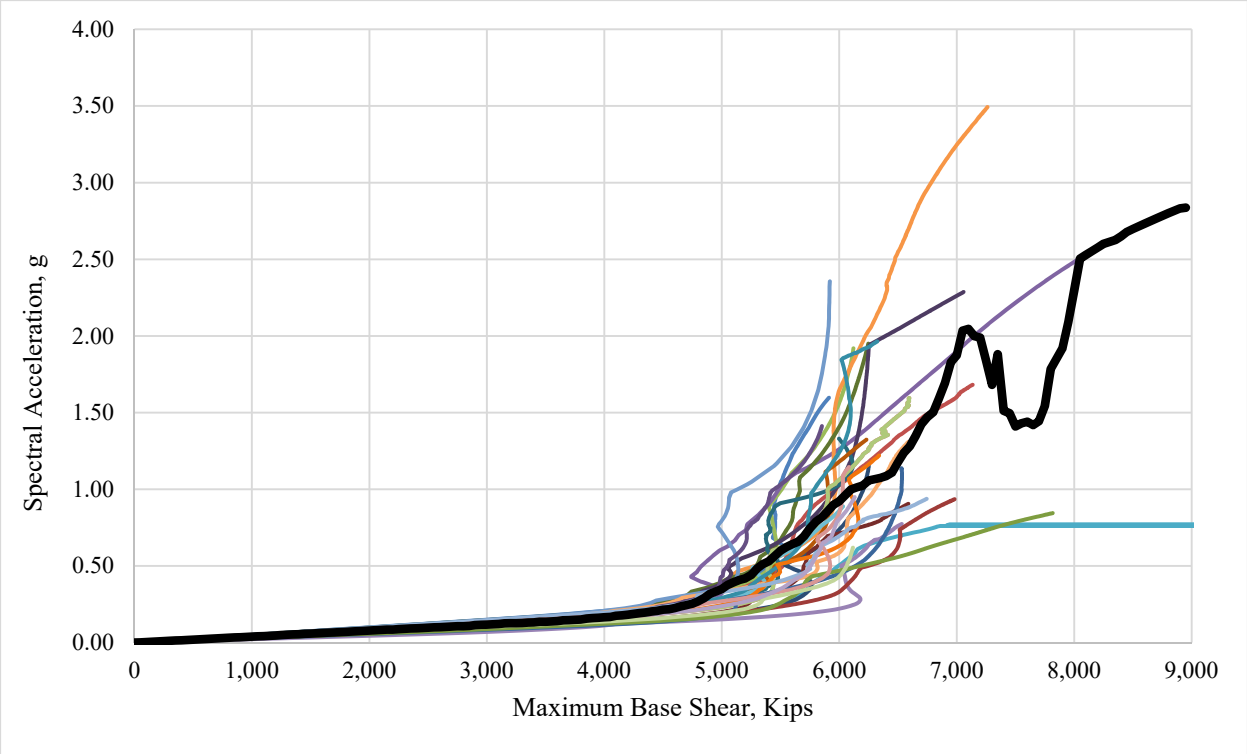


*Figure G-8: Maximum Base Shear for PR14M1.0H1.4 Multi-Record IDA Curve Set*

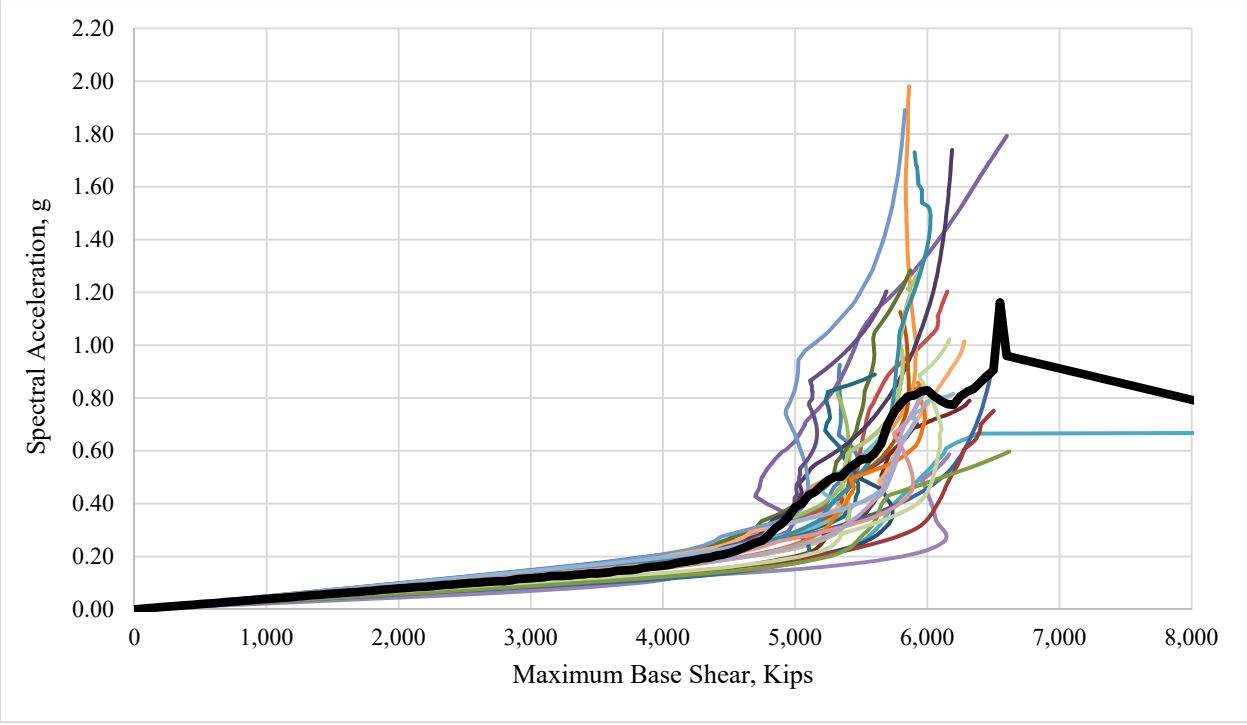


*Figure G-9: Maximum Base Shear for PR14M1.0H1.1 Multi-Record IDA Curve Set*

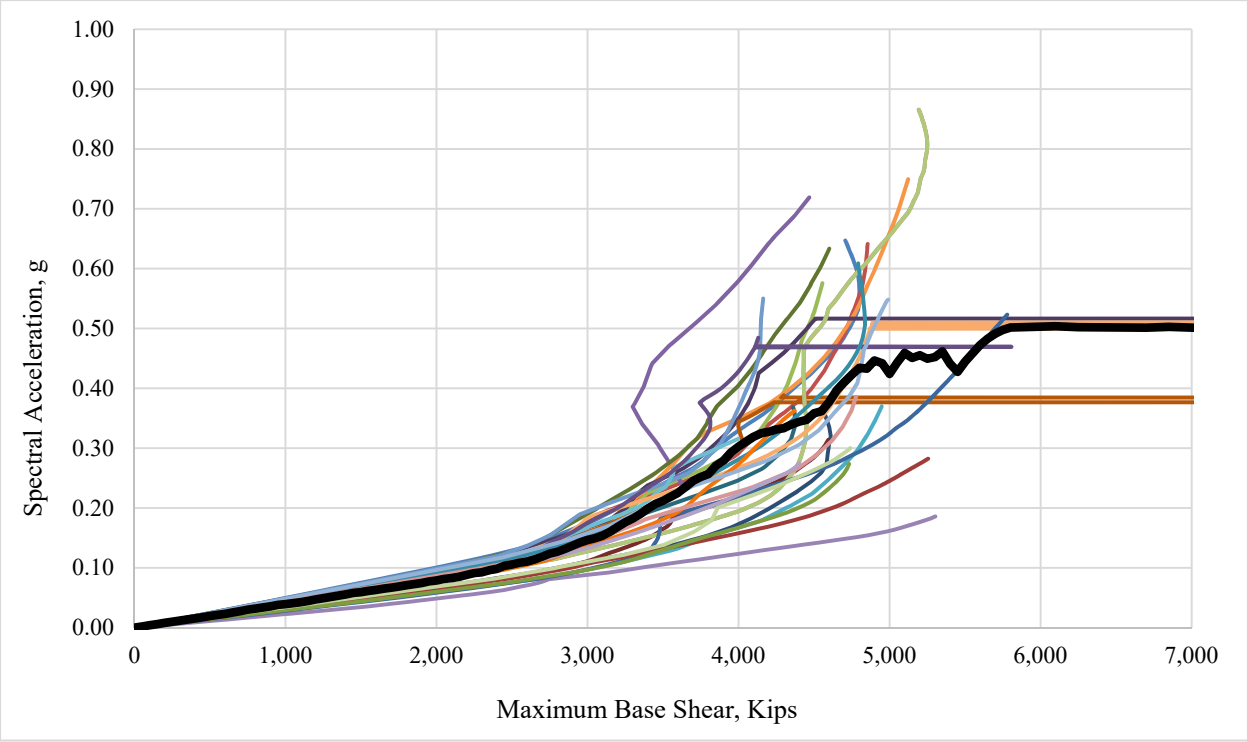


*Figure G-10: Maximum Base Shear for PR14M0.66H1.4 Multi-Record IDA Curve Set*

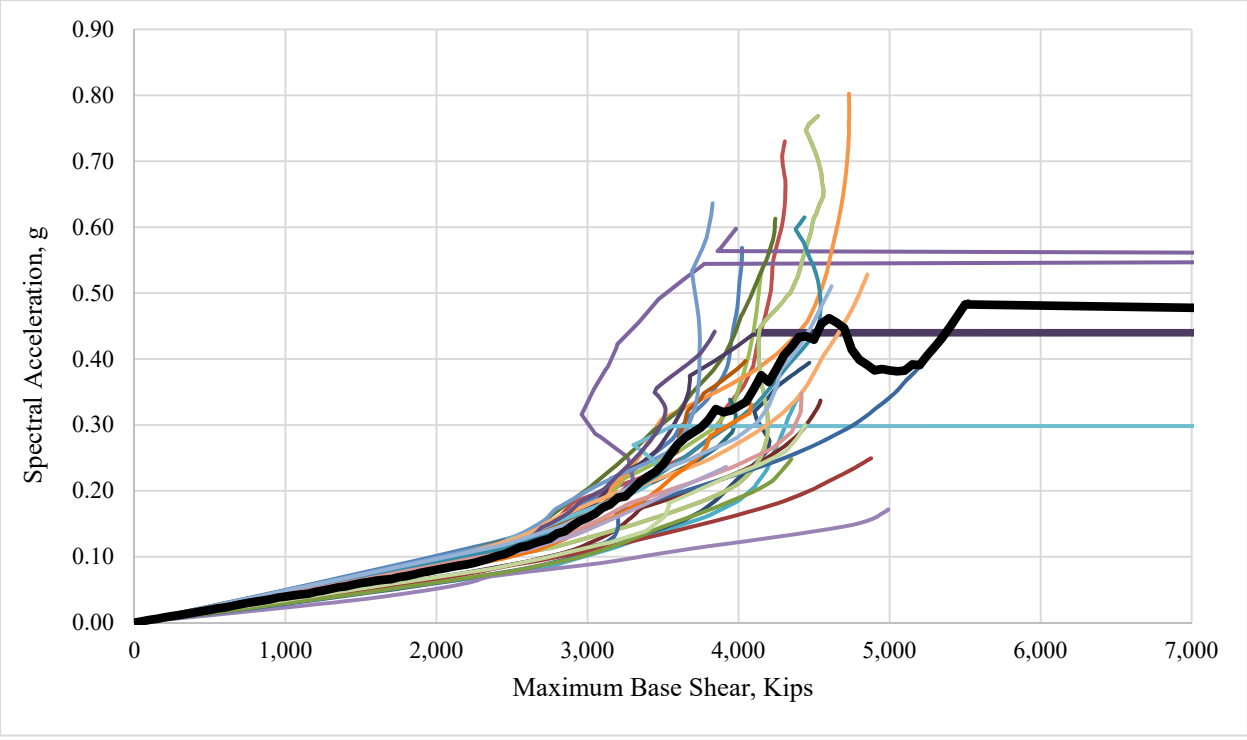


*Figure G-11: Maximum Base Shear for PR14M0.66H1.1 Multi-Record IDA Curve Set*

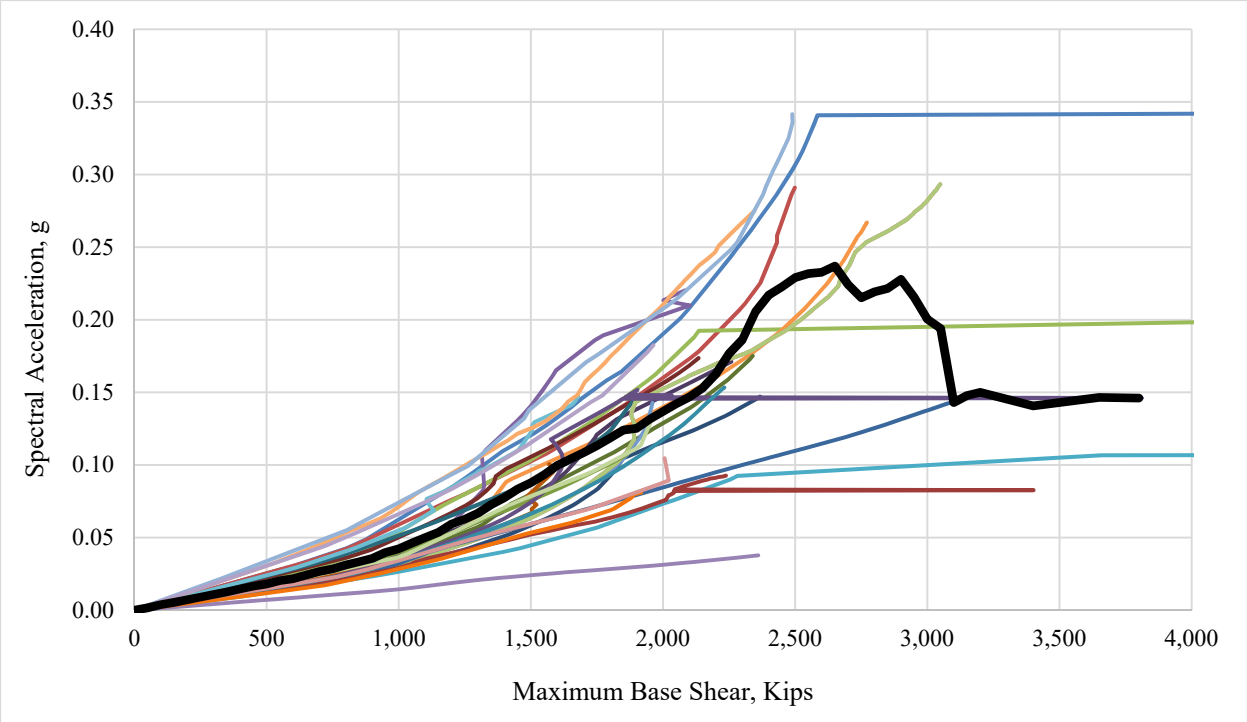


*Figure G-12: Maximum Base Shear for PR14M0.33H1.4 Multi-Record IDA Curve Set*

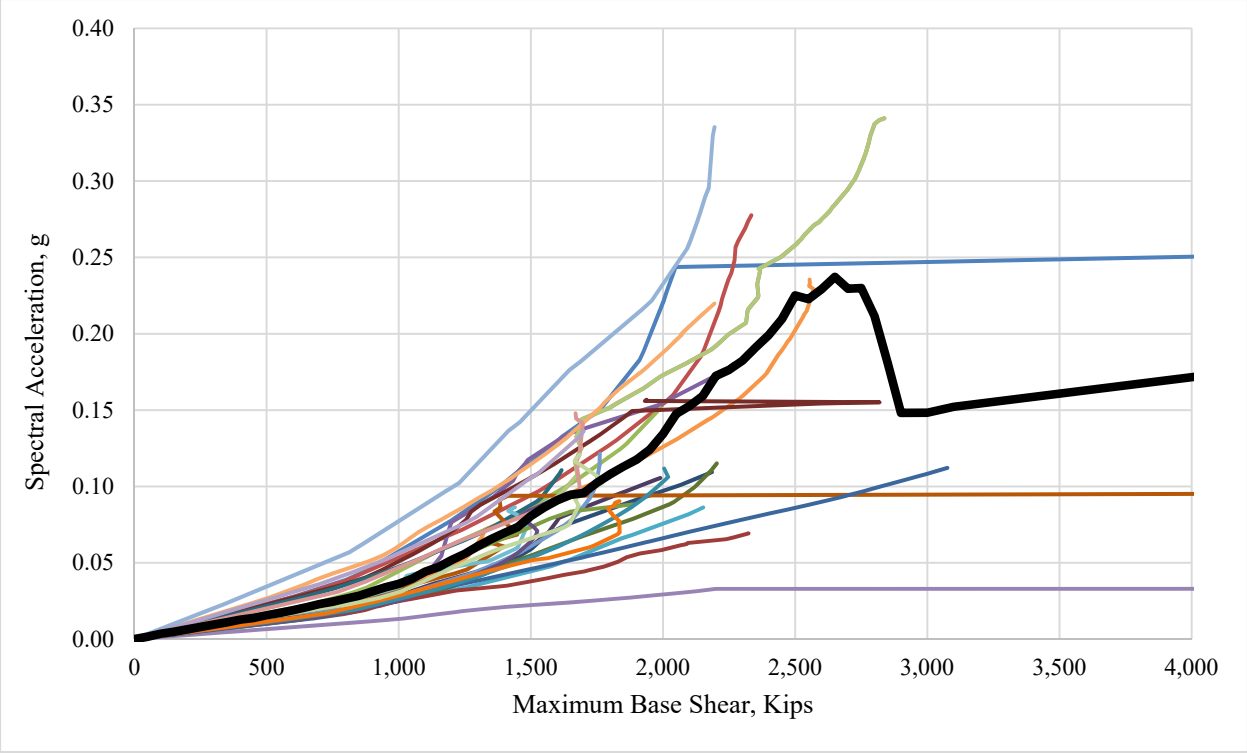


*Figure G-13: Maximum Base Shear for PR14M0.33H1.1 Multi-Record IDA Curve Set*

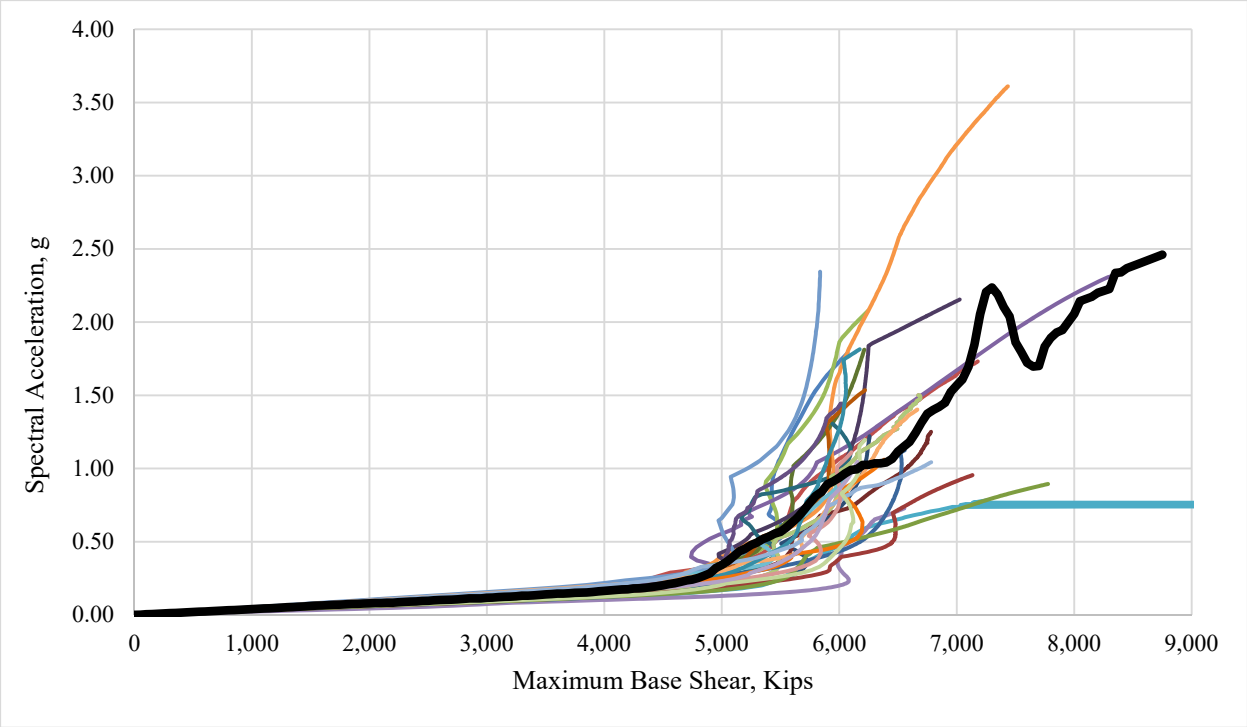


*Figure G-14: Maximum Base Shear for PR11M1.0H1.4 Multi-Record IDA Curve Set*

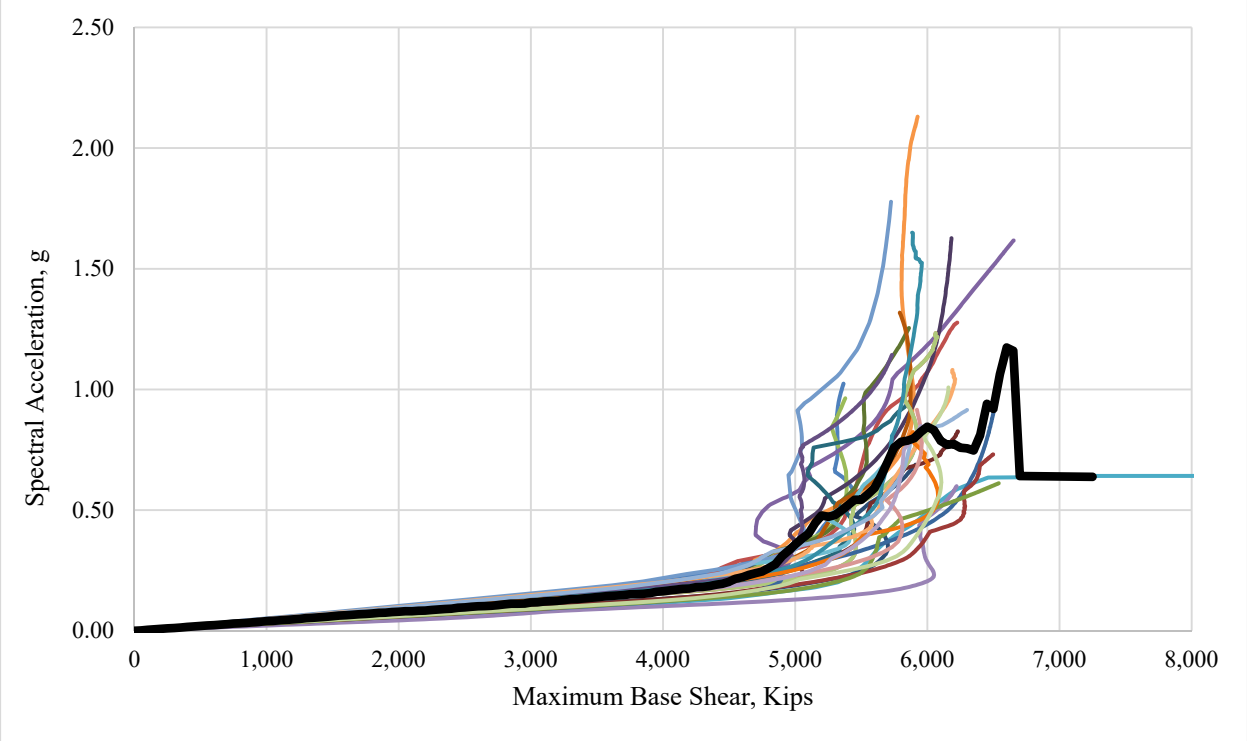


*Figure G-15: Maximum Base Shear for PR11M1.0H1.1 Multi-Record IDA Curve Set*

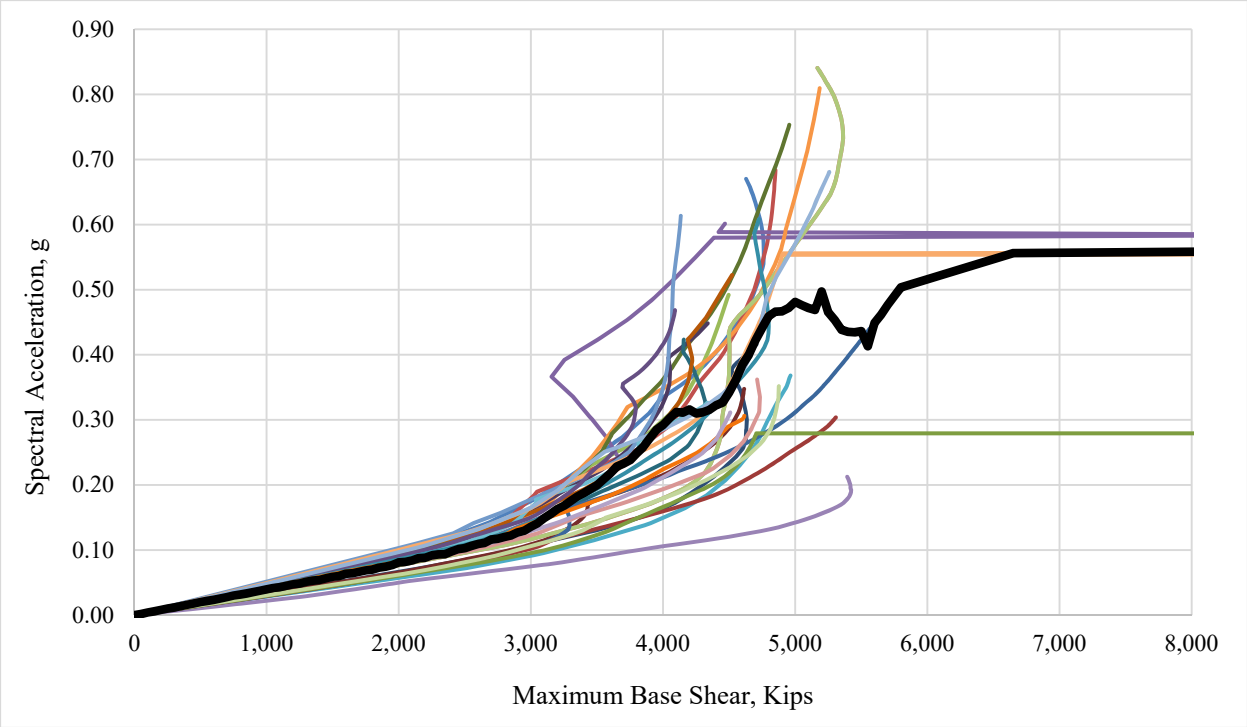


*Figure G-16: Maximum Base Shear for PR11M0.66H1.4 Multi-Record IDA Curve Set*

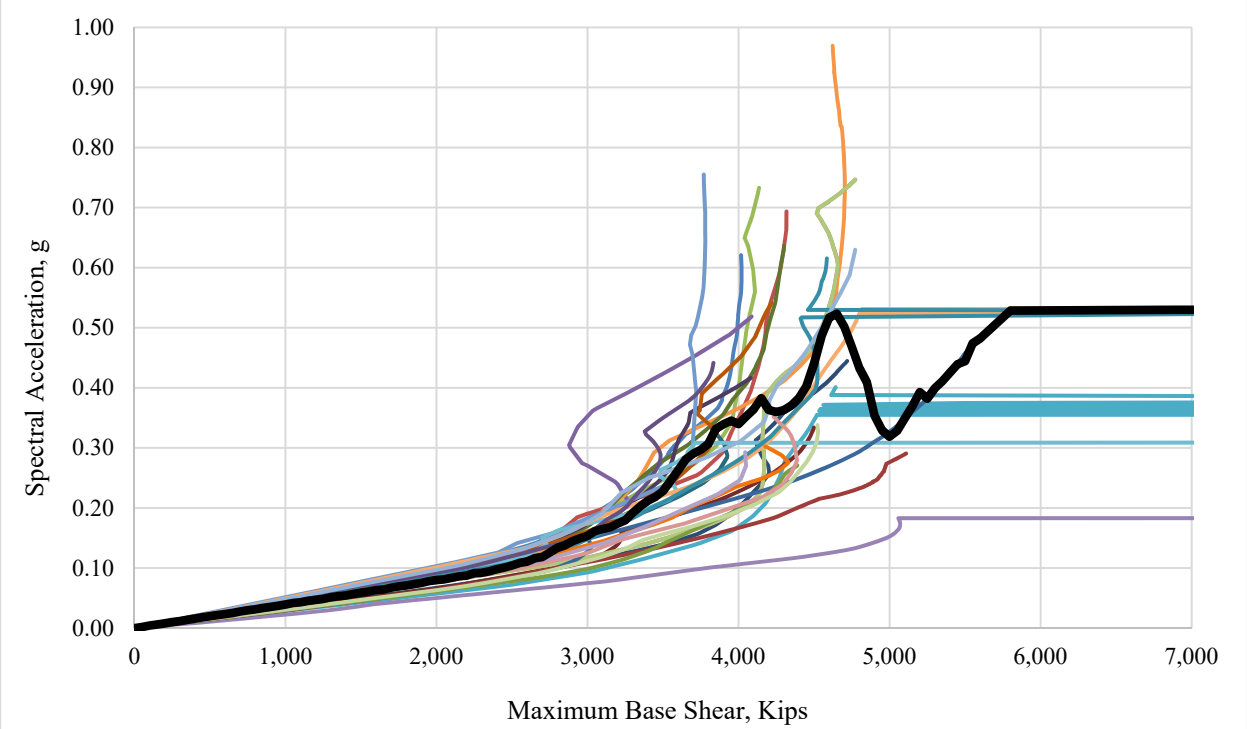


*Figure G-17: Maximum Base Shear for PR11M0.66H1.1 Multi-Record IDA Curve Set*

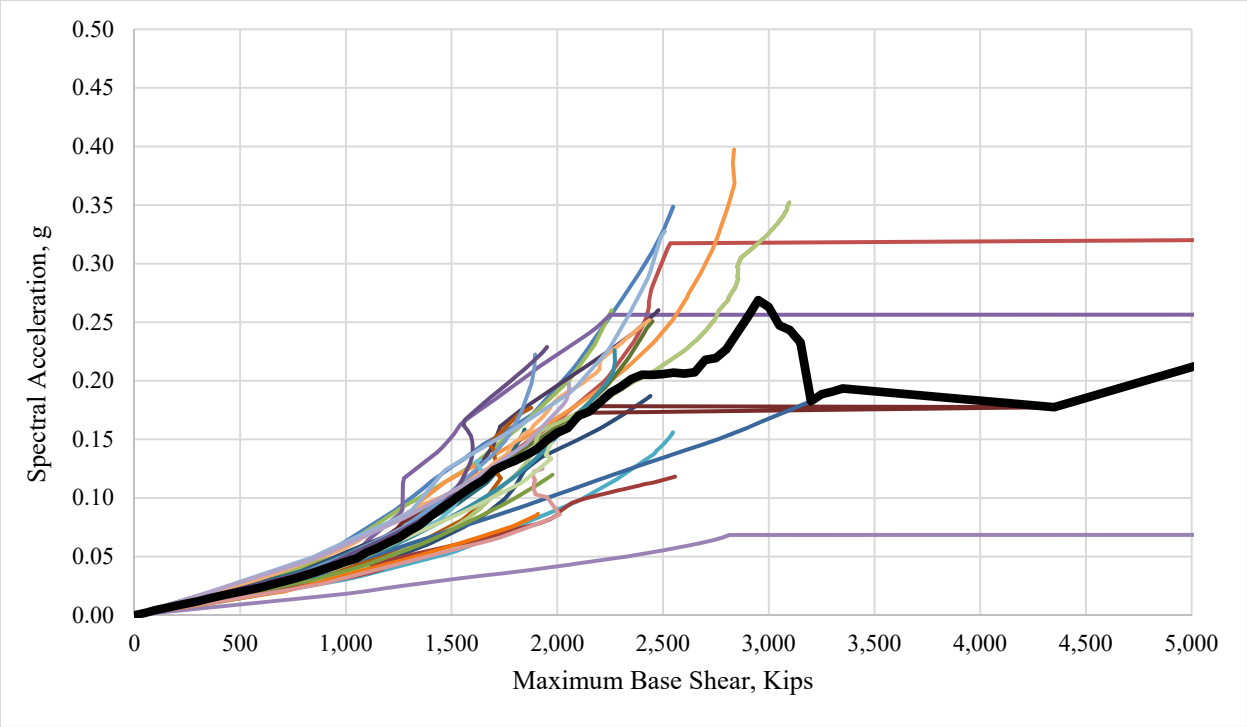


*Figure G-18: Maximum Base Shear for PR11M0.33H1.4 Multi-Record IDA Curve Set*

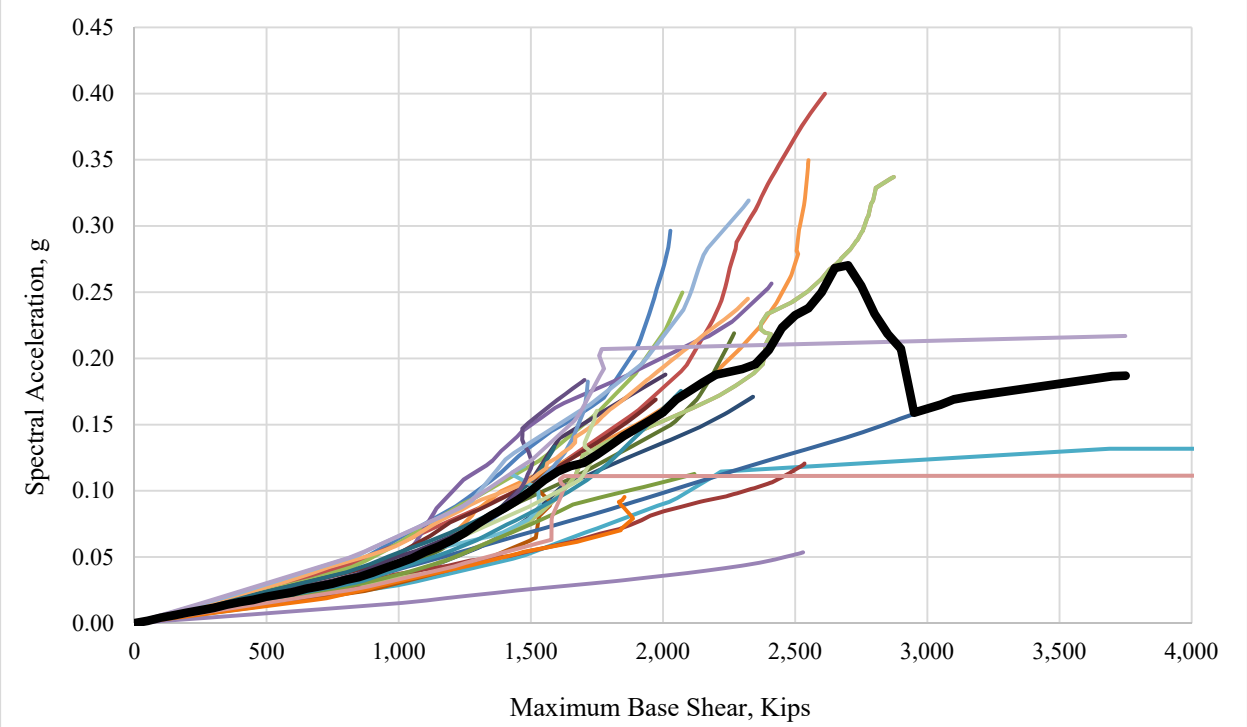


*Figure G-19: Maximum Base Shear for PR11M0.33H1.1 Multi-Record IDA Curve Set*

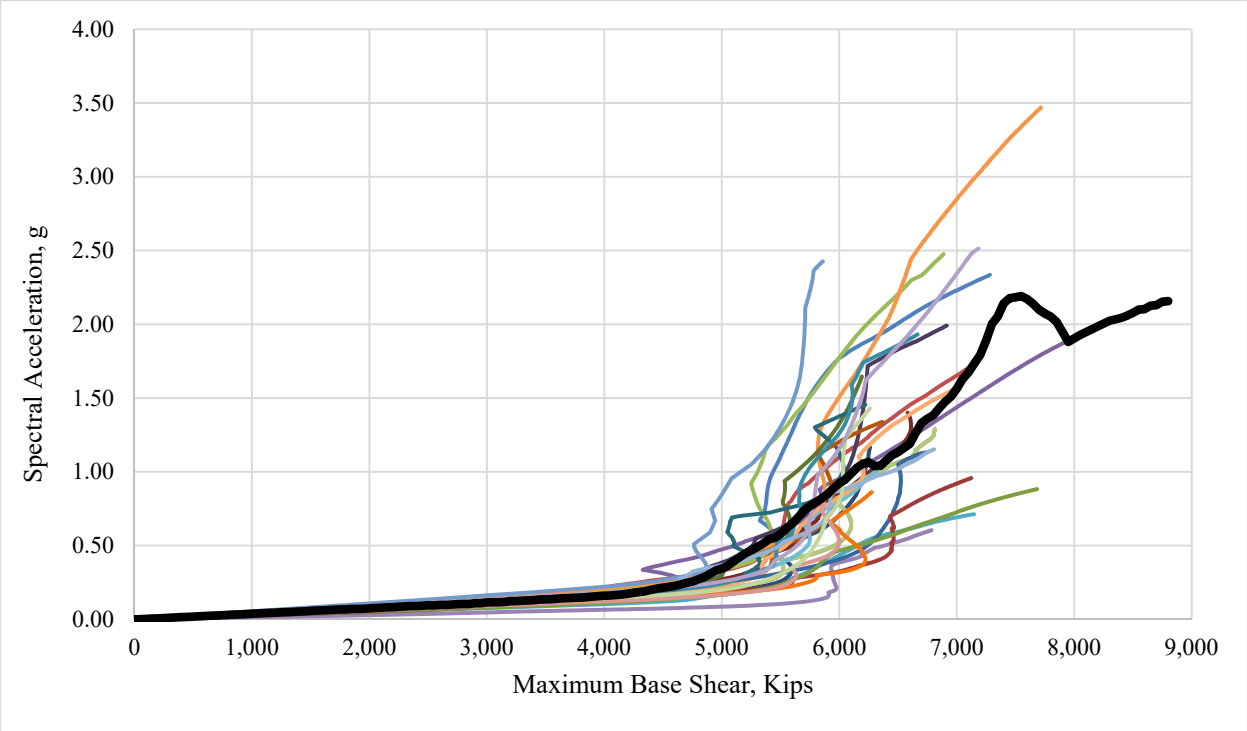


*Figure G-20: Maximum Base Shear for PR8M1.0H1.4 Multi-Record IDA Curve Set*

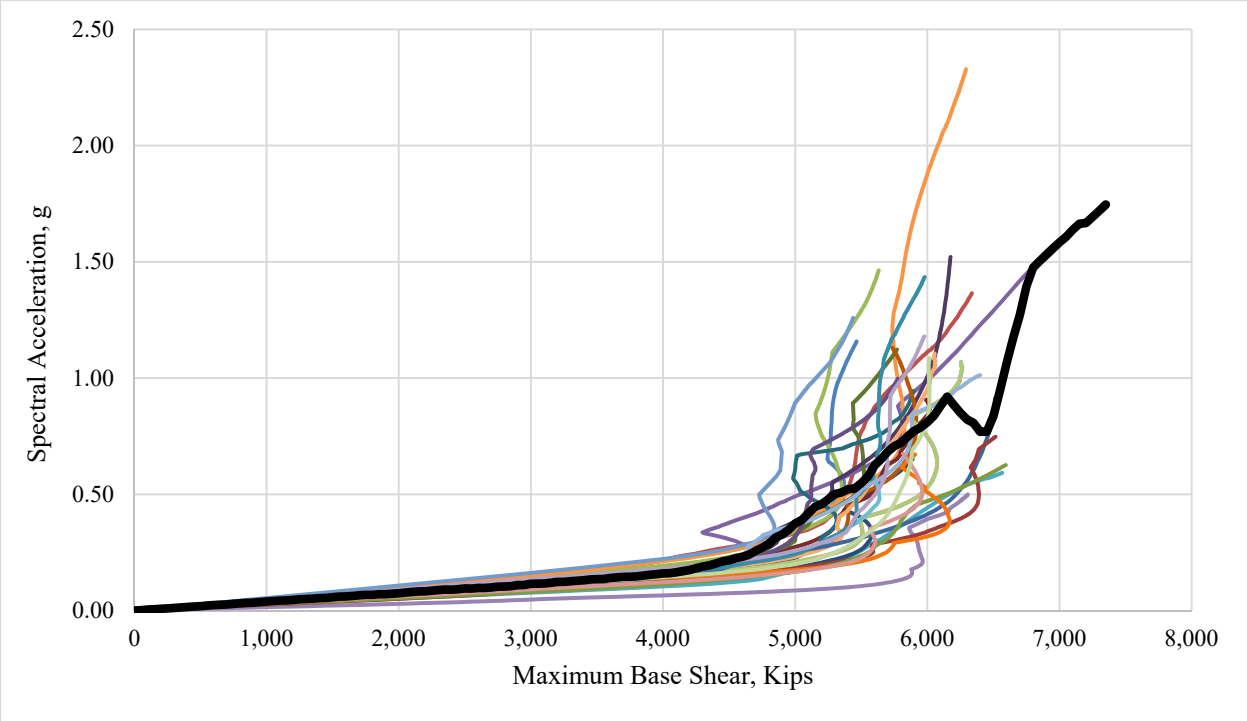


*Figure G-21: Maximum Base Shear for PR8M1.0H1.1 Multi-Record IDA Curve Set*

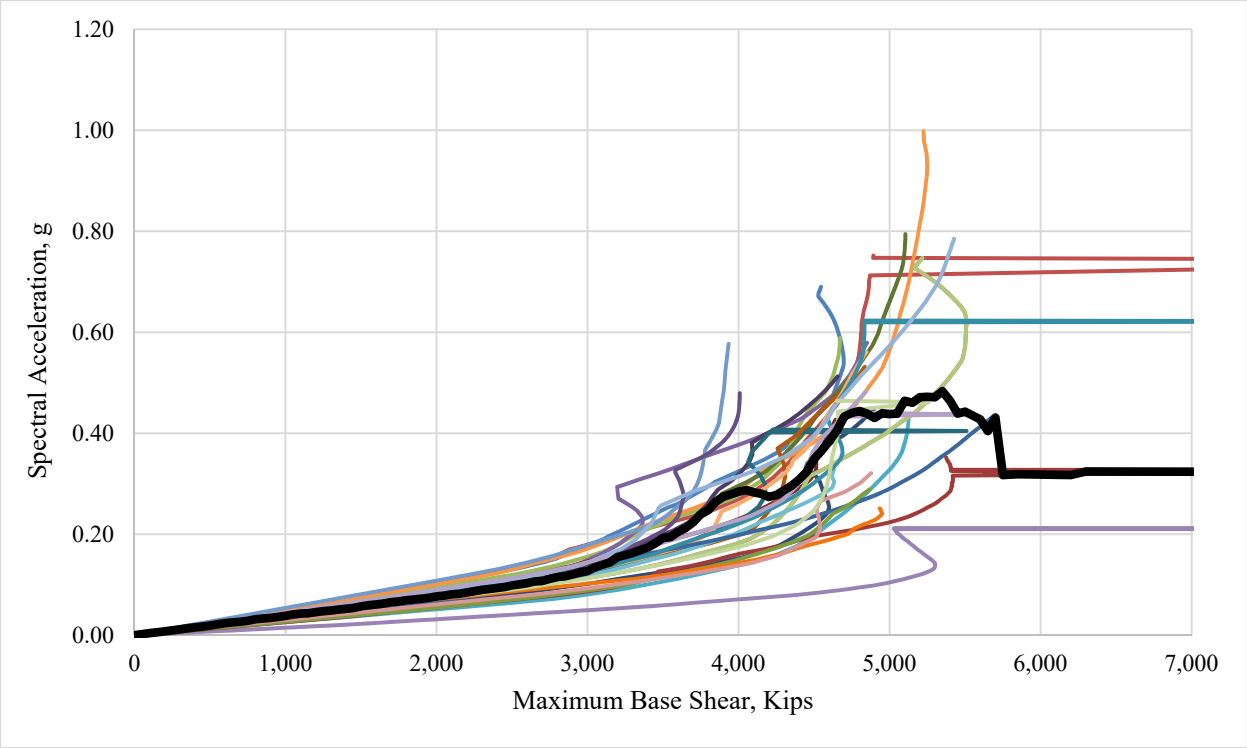


*Figure G-22: Maximum Base Shear for PR8M0.66H1.4 Multi-Record IDA Curve Set*

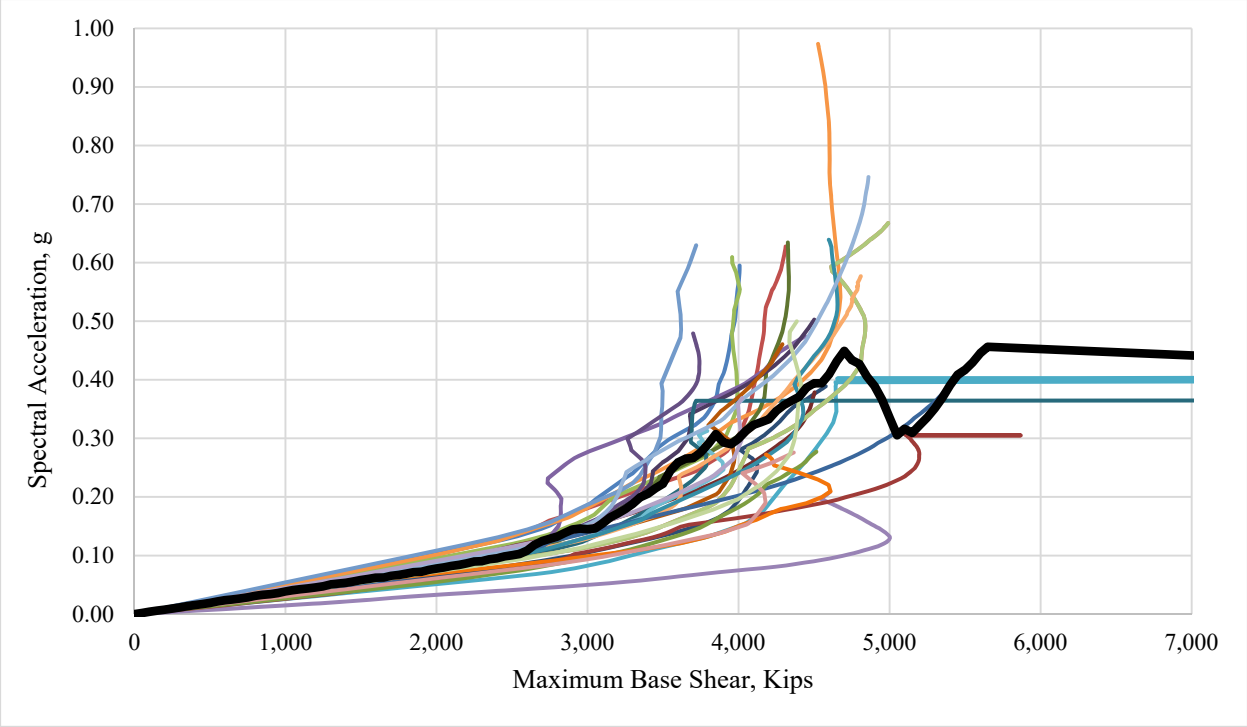


*Figure G-23: Maximum Base Shear for PR8M0.66H1.1 Multi-Record IDA Curve Set*

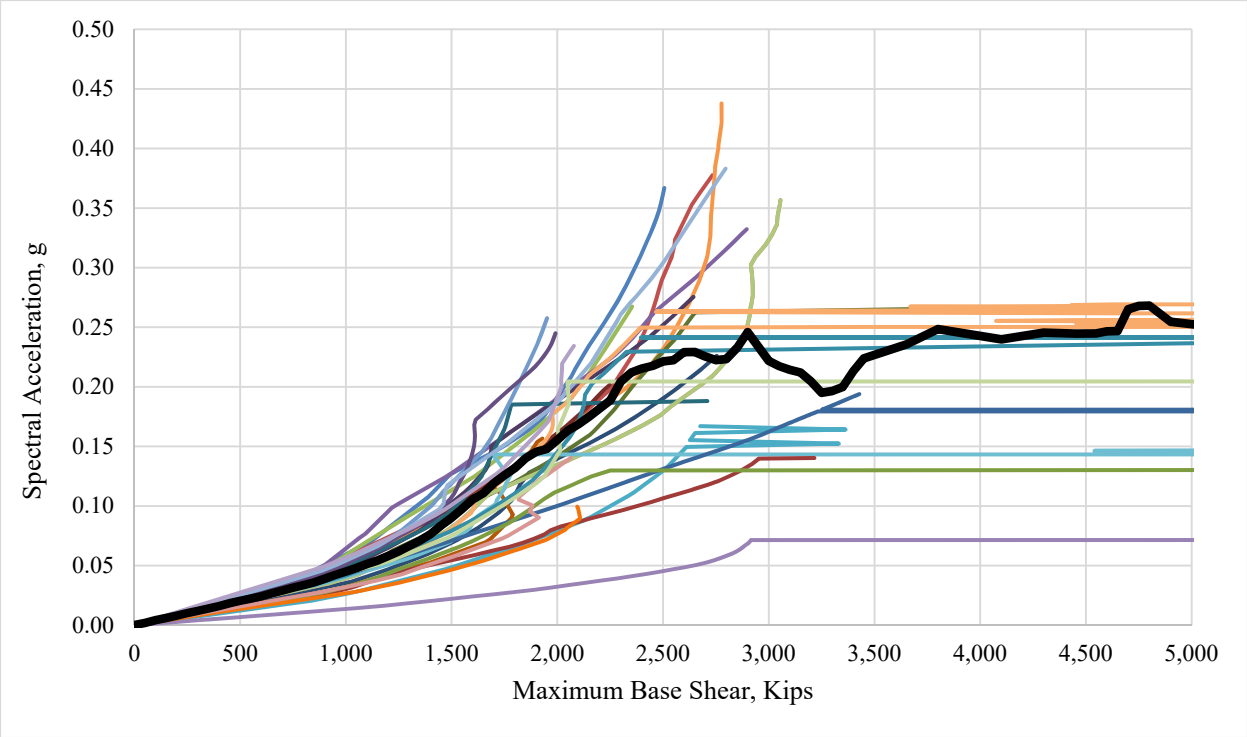


*Figure G-24: Maximum Base Shear for PR8M0.33H1.4 Multi-Record IDA Curve Set*

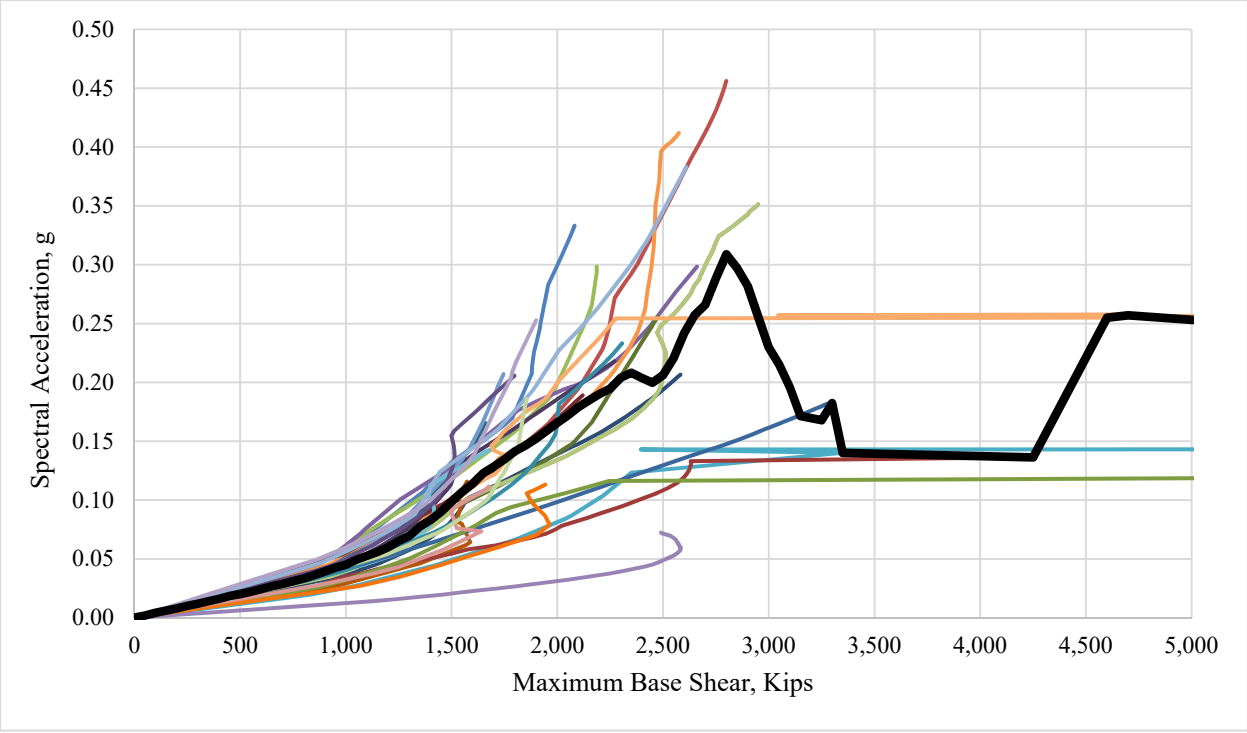


*Figure G-25: Maximum Base Shear for PR8M0.33H1.1 Multi-Record IDA Curve Set*

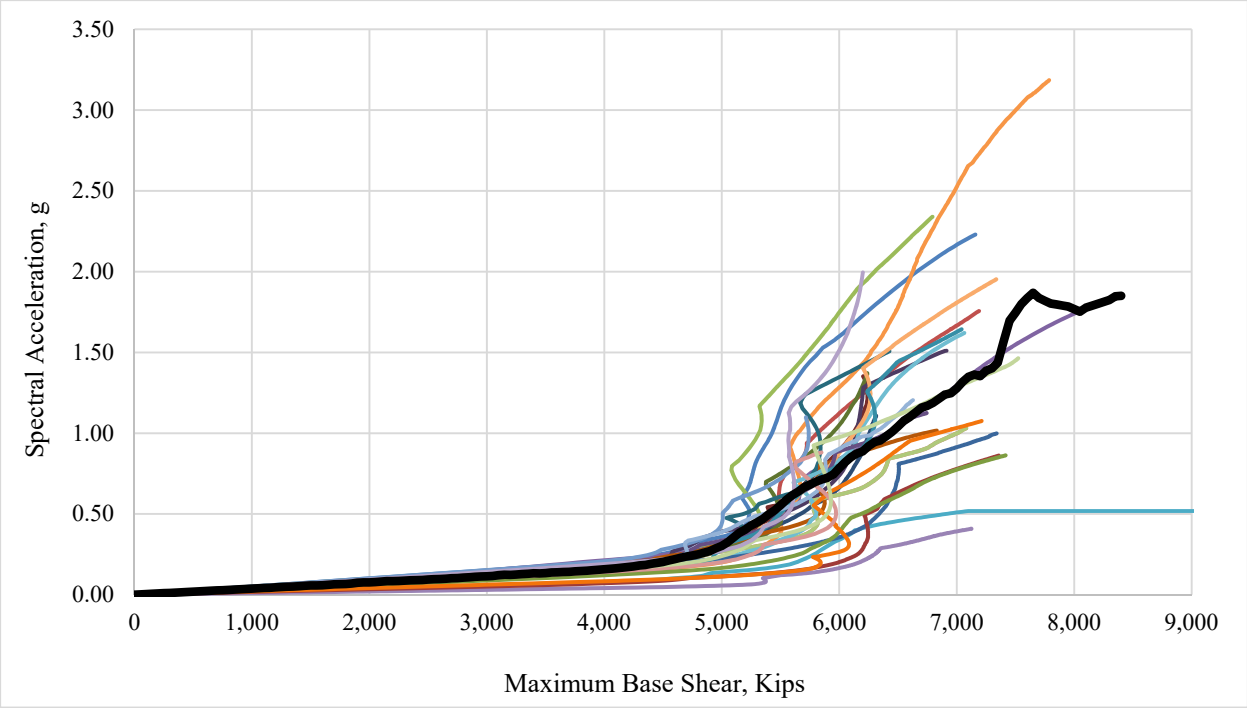


*Figure G-26: Maximum Base Shear for PR5M1.0H1.4 Multi-Record IDA Curve Set*

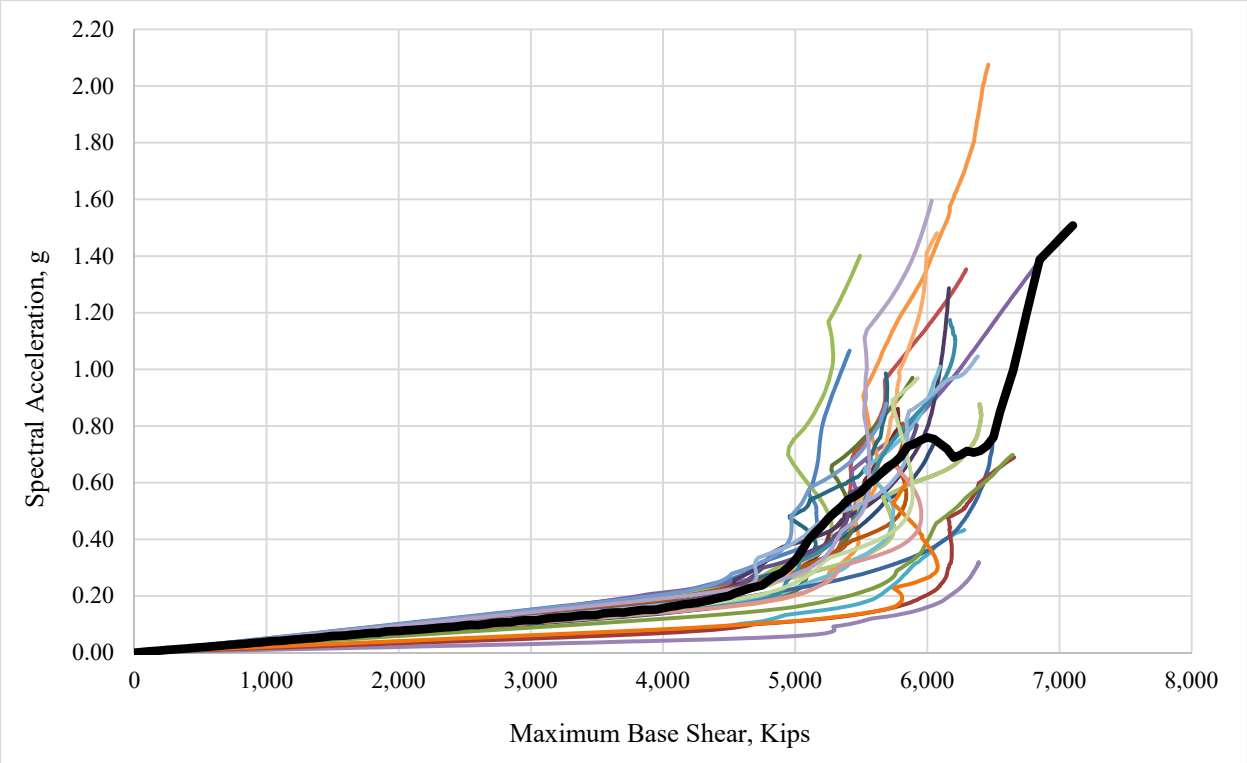


*Figure G-27: Maximum Base Shear for PR5M1.0H1.1 Multi-Record IDA Curve Set*

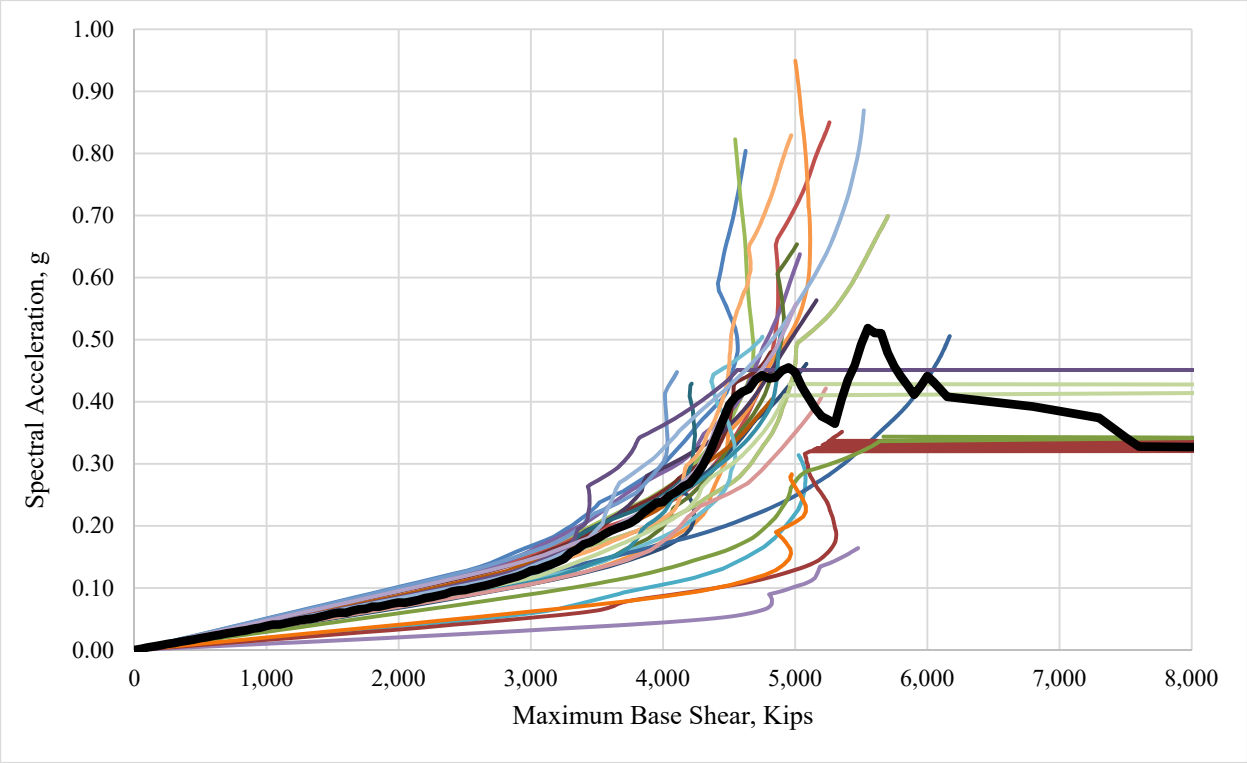


*Figure G-28: Maximum Base Shear for PR5M0.66H1.4 Multi-Record IDA Curve Set*

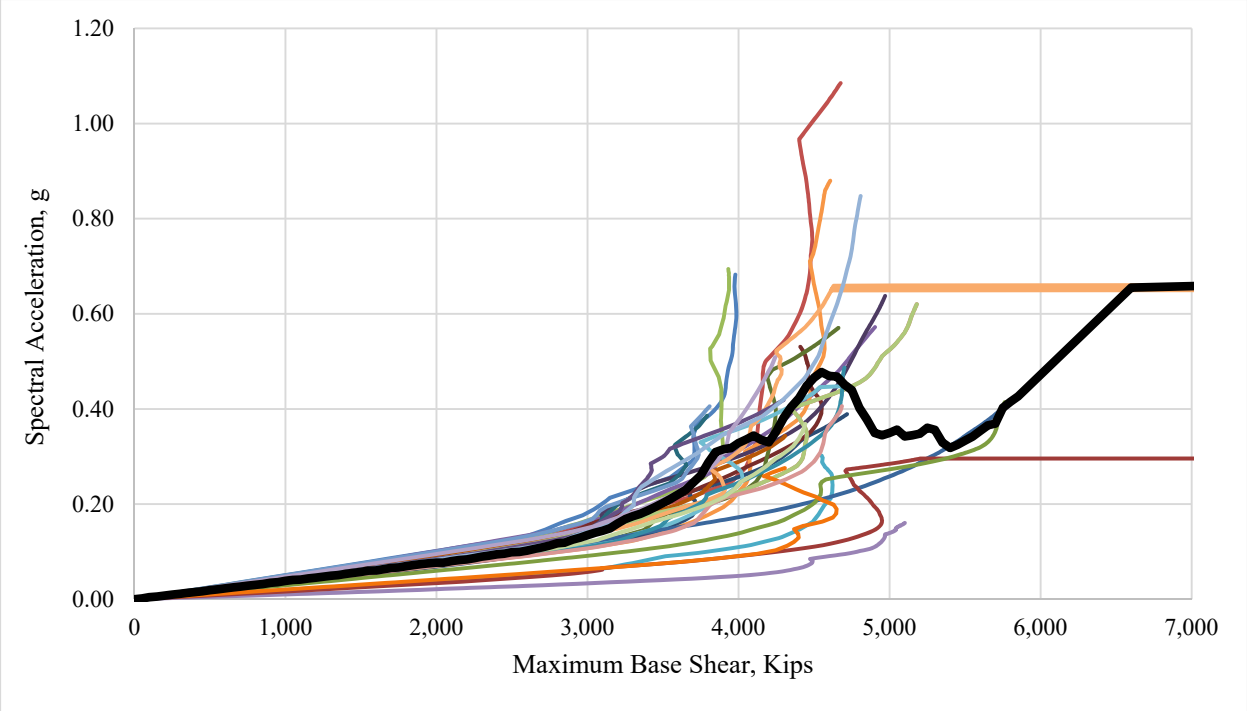


*Figure G-29: Maximum Base Shear for PR5M0.66H1.1 Multi-Record IDA Curve Set*

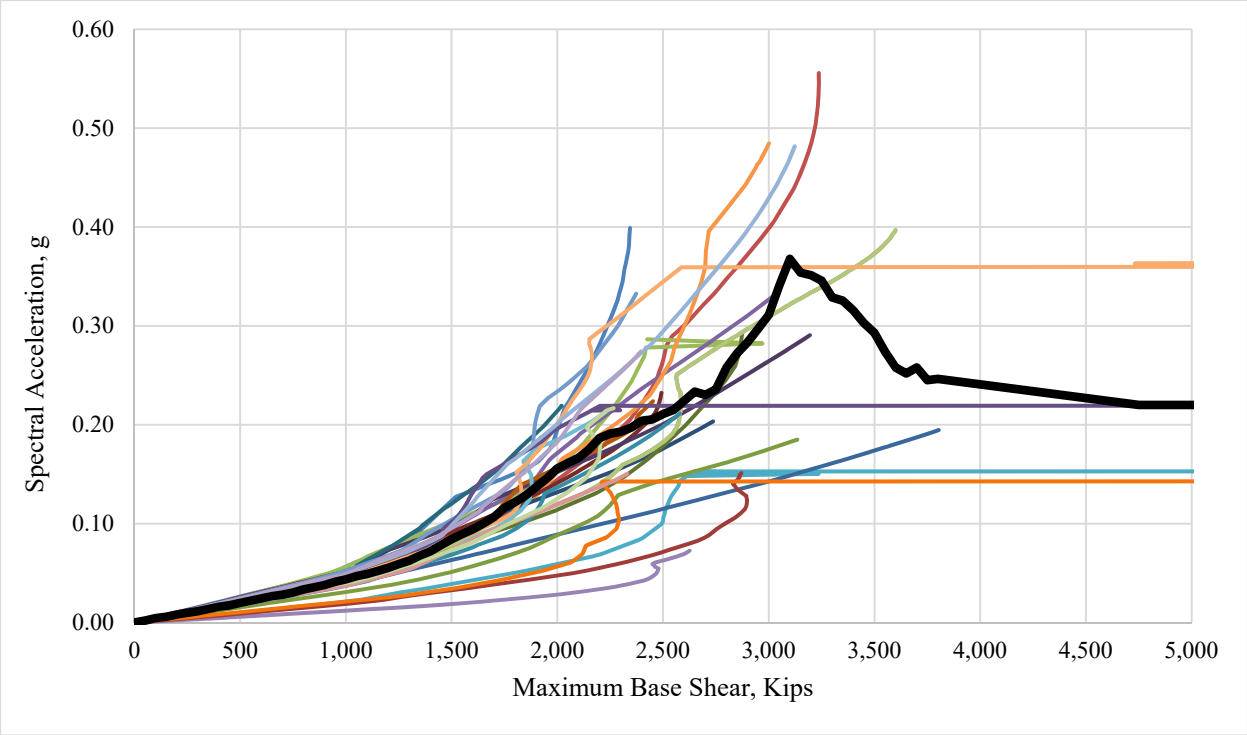


*Figure G-30: Maximum Base Shear for PR5M0.33H1.4 Multi-Record IDA Curve Set*

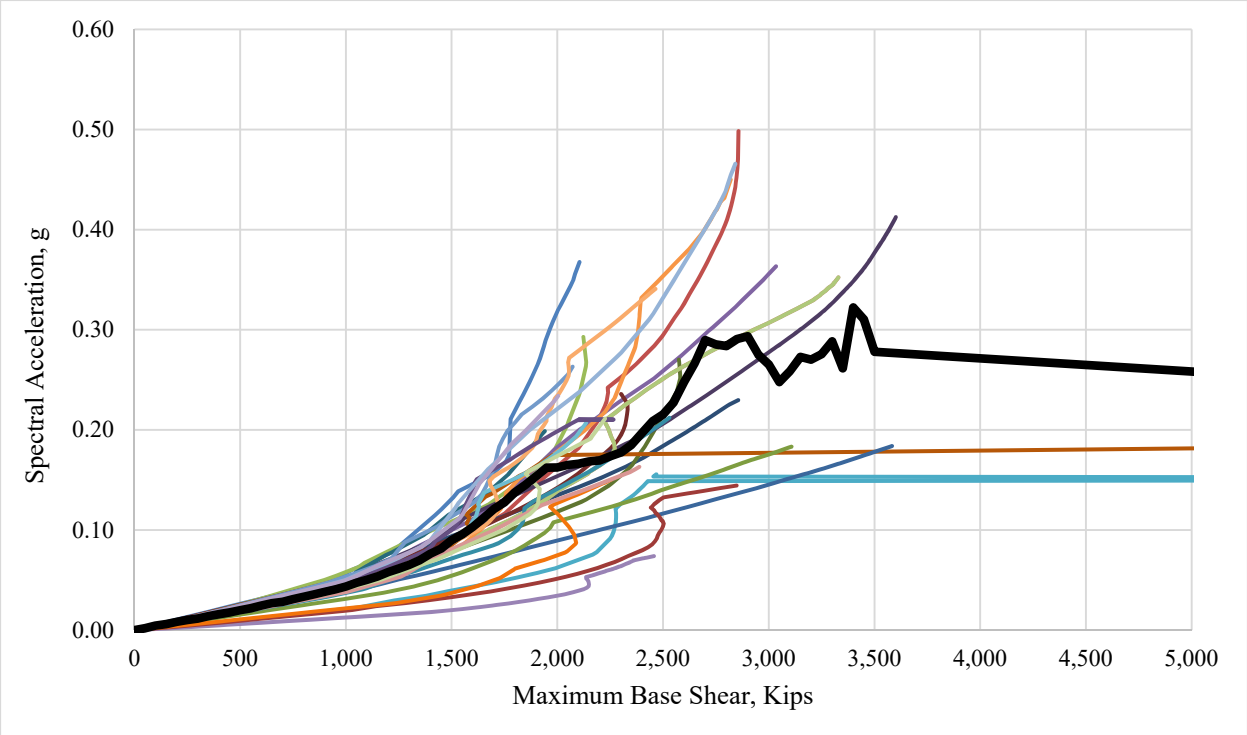


*Figure G-31: Maximum Base Shear for PR5M0.33H1.1 Multi-Record IDA Curve Set*